# Protein Nanoreactors and Native Enzymes for Controlled/Living Radical Polymerization

## Inauguraldissertation

zur
Erlangung der Würde eines Doktors der Philosophie
vorgelegt der
Philosophisch-Naturwissenschaftlichen Fakultät
der Universität Basel

von

**Kasper Renggli**

aus Basel, BS

Basel, 2013

Originaldokument gespeichert auf dem Dokumentenserver der Universität Basel **edoc.unibas.ch**

Dieses Werk ist unter dem Vertrag „Creative Commons Namensnennung-Keine kommerzielle Nutzung-Keine Bearbeitung 3.0 Schweiz“ (CC BY-NC-ND 3.0 CH) lizenziert. Die vollständige Lizenz kann unter **creativecommons.org/licenses/by-nc-nd/3.0/ch/** eingesehen werden.

Genehmigt von der Philosophisch-Naturwissenschaftlichen Fakultät
auf Antrag von

Prof. Dr. Wolfgang Meier
Prof. Dr. Nico Bruns
Prof. Dr. Corinne Vebert

Basel, den 10. Dezember 2013

Prof. Dr. Jörg Schibler
Dekan

**Namensnennung-Keine kommerzielle Nutzung-Keine Bearbeitung 3.0 Schweiz**
(CC BY-NC-ND 3.0 CH)

**Sie dürfen: Teilen** – den Inhalt kopieren, verbreiten und zugänglich machen

**Unter den folgenden Bedingungen:**

**Namensnennung** – Sie müssen den Namen des Autors/Rechteinhabers in der von ihm festgelegten Weise nennen.

**Keine kommerzielle Nutzung** – Sie dürfen diesen Inhalt nicht für kommerzielle Zwecke nutzen.

**Keine Bearbeitung erlaubt** – Sie dürfen diesen Inhalt nicht bearbeiten, abwandeln oder in anderer Weise verändern.

**Wobei gilt:**

- **Verzichtserklärung** – Jede der vorgenannten Bedingungen kann aufgehoben werden, sofern Sie die ausdrückliche Einwilligung des Rechteinhabers dazu erhalten.
- **Public Domain (gemeinfreie oder nicht-schützbare Inhalte)** – Soweit das Werk, der Inhalt oder irgendein Teil davon zur Public Domain der jeweiligen Rechtsordnung gehört, wird dieser Status von der Lizenz in keiner Weise berührt.
- **Sonstige Rechte** – Die Lizenz hat keinerlei Einfluss auf die folgenden Rechte:
  - Die Rechte, die jedermann wegen der Schranken des Urheberrechts oder aufgrund gesetzlicher Erlaubnisse zustehen (in einigen Ländern als grundsätzliche Doktrin des fair use bekannt);
  - Die Persönlichkeitsrechte des Urhebers;
  - Rechte anderer Personen, entweder am Lizenzgegenstand selber oder bezüglich seiner Verwendung, zum Beispiel für Werbung oder Privatsphärenschutz.
- **Hinweis** – Bei jeder Nutzung oder Verbreitung müssen Sie anderen alle Lizenzbedingungen mitteilen, die für diesen Inhalt gelten. Am einfachsten ist es, an entsprechender Stelle einen Link auf diese Seite einzubinden.

**Quelle:** http://creativecommons.org/licenses/by-nc-nd/3.0/ch/ Datum: 10.01.2014

# Table of Contents

This PhD-Thesis is based on the following publications and manuscripts in preparation:

**Chapter 1**

Renggli, K.; Spulber, M.; Pollard, J.; Rother, M.; Bruns, N.: Biocatalytic ATRP: Controlled Radical Polymerizations Mediated by Enzymes. *ACS Symp. Ser.* **2013**, *1144*, 163–171, DOI:10.1021/bk-2013-1144.ch012.

Silva T. B.; Spulber, M.; Kocik, M. K.; Seidi, F.; Charan, H.; Rother, M.; Sigg, S.; Renggli, K.; Kali, G.; Bruns, N.: Hemoglobin and Red Blood Cells Catalyze Atom Transfer Radical Polymerization. *Biomacromolecules* **2013**, *14*, 2703-2712, DOI: 10.1021/bm400556x.

Kali, G.; Silva, T. B.; Sigg, S. J.; Seidi, F.; Renggli, K.; Bruns, N.: ATRPases: Using Nature's Catalysts in Atom Transfer Radical Polymerizations. *ACS Symp. Ser.* **2012**, *1100*, 171–181, DOI: 10.1021/bk-2012-1100.ch011.

Renggli, K.; Urbani, R.; Nussbaumer, M. G.; Pfohl, T.; Bruns, N.: A Chaperonin as Protein Nanoreactor for Atom Transfer Radical Polymerization. *Angew. Chem. Int. Ed.* **2014**, *53*, 1443–1447, DOI: 10.1002/anie.201306798.

Renggli, K.; Baumann, P.; Langowska, K.; Onaca, O.; Bruns, N.; Meier, W.: Selective and Responsive Nanoreactors. *Adv. Funct. Mater.* **2011**, *21*, 1241–1259, DOI: 10.1002/adfm.201001563.

**Chapter 2**

Renggli, K.; Urbani, R.; Nussbaumer, M. G.; Pfohl, T.; Bruns, N.: A Chaperonin as Protein Nanoreactor for Atom Transfer Radical Polymerization. *Angew. Chem. Int. Ed.* **2014**, *53*, 1443–1447, DOI: 10.1002/anie.201306798.

Renggli, K.; Spulber, M.; Pollard, J.; Rother, M.; Bruns, N.: Biocatalytic ATRP: Controlled Radical Polymerizations Mediated by Enzymes. *ACS Symp. Ser.* **2013**, *1144*, 163–171, DOI:10.1021/bk-2013-1144.ch012.

Bruns, N.; Renggli, K.; Seidi, F.; Kali, G.: Atom Transfer Radical Polymerization with Protein-Conjugated Catalysts: Easy Removal of Copper Traces and Controlled Radical Polymerizations in Protein Nanoreactors. *Polym. Prepr. (Am. Chem. Soc., Div. Polym. Chem.)* **2011**, *52*, 521-522.

Silva T. B.; Spulber, M.; Kocik, M. K.; Seidi, F.; Charan, H.; Rother, M.; Sigg, S.; Renggli, K.; Kali, G.; Bruns, N.: Hemoglobin and Red Blood Cells Catalyze Atom Transfer Radical Polymerization. *Biomacromolecules* **2013**, *14*, 2703-2712, DOI: 10.1021/bm400556x.

**Chapter 3**

Renggli, K.; Spulber, M.; Pollard, J.; Rother, M.; Bruns, N.: Biocatalytic ATRP: Controlled Radical Polymerizations Mediated by Enzymes. *ACS Symp. Ser.* **2013**, *1144*, 163–171, DOI:10.1021/bk-2013-1144.ch012.

Kali, G.; Silva, T. B.; Sigg, S. J.; Seidi, F.; Renggli, K.; Bruns, N.: ATRPases: Using Nature's Catalysts in Atom Transfer Radical Polymerizations. *ACS Symp. Ser.* **2012**, *1100*, 171–181, DOI: 10.1021/bk-2012-1100.ch011.

Silva T. B.; Spulber, M.; Kocik, M. K.; Seidi, F.; Charan, H.; Rother, M.; Sigg, S.; Renggli, K.; Kali, G.; Bruns, N.: Hemoglobin and Red Blood Cells Catalyze Atom Transfer Radical Polymerization. *Biomacromolecules* **2013**, *14*, 2703-2712, DOI: 10.1021/bm400556x.

**Chapter 4**

Sigg, S. J.; Seidi, F.; Renggli, K.; Silva, T. B.; Kali, G.; Bruns, N.: Horseradish Peroxidase as a Catalyst for Atom Transfer Radical Polymerization. *Macromol. Rapid Commun.* **2011**, *32*, 1710–1715, DOI: 10.1002/marc.201100349.

**Chapter 5**

Silva T. B.; Spulber, M.; Kocik, M. K.; Seidi, F.; Charan, H.; Rother, M.; Sigg, S.; Renggli, K.; Kali, G.; Bruns, N.: Hemoglobin and Red Blood Cells Catalyze Atom Transfer Radical Polymerization. *Biomacromolecules* **2013**, *14*, 2703-2712, DOI: 10.1021/bm400556x.

**Chapter 6**

Renggli, K.; Baumann, P.; Langowska, K.; Onaca, O.; Bruns, N.; Meier, W.: Selective and Responsive Nanoreactors. *Adv. Funct. Mater.* **2011**, *21*, 1241–1259, DOI: 10.1002/adfm.201001563.

**Chapter 7**

Renggli, K.; Urbani, R.; Nussbaumer, M. G.; Pfohl, T.; Bruns, N.: A Chaperonin as Protein Nanoreactor for Atom Transfer Radical Polymerization. *Angew. Chem. Int. Ed.* **2014**, *53*, 1443–1447, DOI: 10.1002/anie.201306798.

**Chapter 8**

Bruns, N.; Renggli, K.; Lörcher, S.; Pollard, J.; Spulber, M.: Combining Polymers with the Functionality of Proteins. ATRPases, Nanoreactors and Damage Self-Reporting Materials. *Chimia* **2013**, *67*, 777–781, DOI: 10.2533/chimia.2013.777.

Renggli, K.; Baumann, P.; Langowska, K.; Onaca, O.; Bruns, N.; Meier, W.: Selective and Responsive Nanoreactors. *Adv. Funct. Mater.* **2011**, *21*, 1241–1259, DOI: 10.1002/adfm.201001563.

Renggli, K.; Sauter, N.; Nussbaumer, M. G.; Urbani, R.; Pfohl, T.; Bruns, N.: HRP-Mediated ATRP inside Nanoreactors. **2013**, *In Preparation*.

**Chapter 9**

Renggli, K.; Baumann, P.; Langowska, K.; Onaca, O.; Bruns, N.; Meier, W.: Selective and Responsive Nanoreactors. *Adv. Funct. Mater.* **2011**, *21*, 1241–1259, DOI: 10.1002/adfm.201001563.

Renggli, K.; Nussbaumer, M. G.; Walther, M.; Tardy, B.; Sauter, N.; Garni, M.; Hegner, M. U.; Bruns, N.: The Archaeal Chaperonin Thermosome as ATP Triggerable Protein Nanoreactor. **2013**, *In Preparation*.

# Preface

This thesis is the collection of our search for environmently friendlier atom transfer radical polymerization (ATRP) and protein nanoreactors, that was conducted in the group of Nico Bruns and Wolfgang Meier at the University of Basel from October 2009 until November 2013. The thesis is divided into ten chapters where each corresponds to different research projects inspired and influenced by each other. The corresponding current state of the research is also enclosed in each chapter along with a brief introduction in this particular domain. Original publications were rearanged and reformatted so as not to impede the reading flow of the thesis. The experimental data, a full list of publications, as well as a curriculum vitae can be found in the appendices at the end of this thesis.

# 1 General Introduction[1]

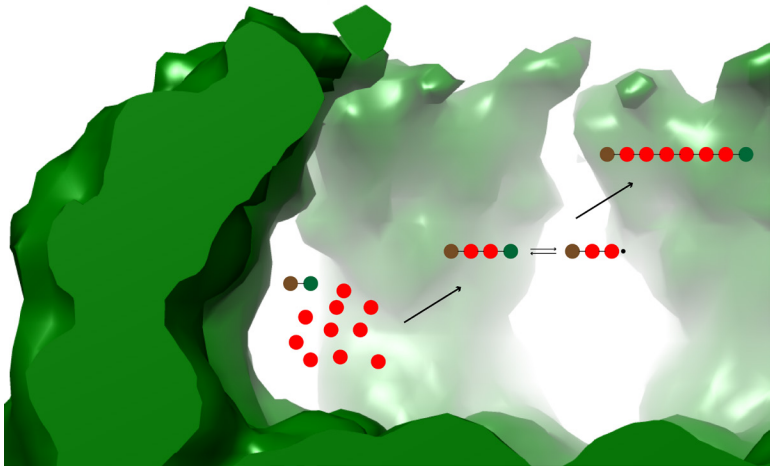

*The advent of controlled radical polymerizations has made polymer science a key discipline for the preparation of nano-, biomedical-, and high tech-materials. Atom transfer radical polymerization (ATRP) is one of the most widely applied controlled radical polymerization. However, an ongoing quest is to develop ATRP reaction conditions that allow reducing the amount of catalyst needed, e.g by confining the reaction into a nanoreactor, or to replace the currently used transition metal complex catalysts with less toxic ones, e.g. enzymes.*

[1] Parts of this chapter were published in: a) K. Renggli, M. Spulber, J. Pollard, M. Rother, N. Bruns, *ACS Symp. Ser.* **2013**, *1144*, 163–171 b) T. B. Silva, M. Spulber, M. K. Kocik, F. Seidi, H. Charan, M. Rother, S. J. Sigg, K. Renggli, G. Kali, N. Bruns, *Biomacromolecules* **2013**, *14*, 2703–2712 c) G. Kali, T. B. Silva, S. J. Sigg, F. Seidi, K. Renggli, N. Bruns, *ACS Symp. Ser.* **2012**, *1011*, 171–181 d) K. Renggli, M. G. Nussbaumer, R. Urbani, T. Pfohl, N. Bruns, *Angew. Chem. Int. Ed.* **2014**, *53*, 1443–1447 e) K. Renggli, P. Baumann, K. Langowska, O. Onaca, N. Bruns, W. Meier, *Adv. Funct. Mater.* **2011**, *21*, 1241–1259.

## 1.1 Radical Polymerization

Radical polymerizations are one of the most widely employed reactions used to synthesize polymers on an industrial scale or in academic labs, principally due to its simplicity and tolerance of functional groups. Products like polystyrene (e.g. Styrofoam), polymethylmethacrylate (Plexiglass), and polyvinylchloride (PVC) are all synthesized on a scale of millions of tons per year worldwide by free radical polymerization, i.e. a chain growth polymerization in which the active, propagating species are radicals. These radicals are highly reactive and readily undergo termination and side reactions that interrupt the growth of a polymer chain.[2] Due to the short life-span of the growing chains, they are active for about 1 s, chemical control of these reactions is poor, giving rise to ill-defined molecular weights and preventing end-group-functionalization of polymer chains.[3] Poor control represents the main drawback of the method, especially when well-defined molecular weights, architectures, sequences of monomers, and functional chain end groups are desired. An example where well-defined molecular weights are desired are block copolymers, e.g. as emulsifiers, as drug-delivery systems, as building blocks for nanostructures, and as materials in solar cells and batteries.[4] The formation of conjugates of polymers and proteins, e.g. for therapeutic applications, relies on the well-defined end-group chemistry of polymers.[5] If control of radical polymerization is achieved, some materials' applications, e.g. self-healing plastics, can be implemented.[6] Over the last two decades, synthesis techniques have been developed that allow a degree of control of radical polymerizations, such as atom transfer radical polymerization (ATRP), reversible addition-fragmentation chain transfer (RAFT) polymerization, and nitroxide-mediated radical polymerization (NMP).[7]

However, radical polymerizations are not limited to man-made processes. Nature uses radical polymerization to produce a variety of biopolymers.[8] The prime example is the synthesis of lignin by an enzyme-catalyzed coupling between aromatic compounds.[9] Lignin's key function is to strengthen wood, and it is the second most

---

2 W. A. Braunecker, K. Matyjaszewski, *Prog. Polym. Sci.* **2007**, *32*, 93–146.

3 a) M. Ouchi, T. Terashima, M. Sawamoto, *Chem. Rev.* **2009**, *109*, 4963–5050 b) W. A. Braunecker, K. Matyjaszewski, *Prog. Polym. Sci.* **2007**, *32*, 93–146.

4 a) K. Renggli, P. Baumann, K. Langowska, O. Onaca, N. Bruns, W. Meier, *Adv. Funct. Mater.* **2011**, *21*, 1241–1259 b) S. Egli, M. G. Nussbaumer, V. Balasubramanian, M. Chami, N. Bruns, C. Palivan, W. Meier, *J. Am. Chem. Soc.* **2011**, *133*, 4476–4483 c) O. Onaca, R. Enea, D. W. Hughes, W. Meier, *Macromol. Biosci.* **2009**, *9*, 129–139 d) K. Kita-Tokarczyk, J. Grumelard, T. Haefele, W. Meier, *Polymer* **2005**, *46*, 3540–3563 e) P. D. Topham, A. J. Parnell, R. C. Hiorns, *J. Polym. Sci. B Polym. Phys.* **2011**, *49*, 1131–1156.

5 a) H.-A. Klok, *Macromolecules* **2009**, *42*, 7990–8000 b) K. L. Heredia, H. D. Maynard, *Org. Biomol. Chem.* **2007**, *5*, 45–53.

6 H. P. Wang, Y. C. Yuan, M. Z. Rong, M. Q. Zhang, *Macromolecules* **2010**, *43*, 595–598.

7 a) K. Matyjaszewski, *Macromolecules* **2012**, *45*, 4015–4039 b) W. A. Braunecker, K. Matyjaszewski, *Prog. Polym. Sci.* **2007**, *32*, 93–146.

8 R. J. P. Williams, E. C. Baughan, R. L. Willson, *Philos. Trans. R. Soc., B* **1985**, *311*, 593–603.

9 R. Hatfield, W. Vermerris, *Plant Physiol.* **2001**, *126*, 1351–1357.

abundant polymer on earth.[10] However, the manner in which Nature controls this polymerization is not fully understood and is a topic of ongoing scientific debate.[11]

Enzymes are environmentally friendly, sustainable, and non-toxic catalysts.[12] They are derived from natural sources, are completely biodegradable (and even edible), and work under mild conditions such as ambient temperature, ambient pressure and in aqueous solution. Moreover, they are highly selective, allowing for desired regio-, stereo-, or chemo-selective transformations. Not surprisingly, enzymes have been extensively used *in vitro* to the benefit of synthetic chemists, and are often considered as green alternatives to conventional catalysts.[13] Indeed, many enzymatic reactions have been exploited for the synthesis of polymers, including polycondensation, ring-opening polymerizations, free radical polymerizations of vinyl-type monomers and the polymerization of aromatic compounds by radical-induced oxidative coupling.[14] However, controlled/living radical polymerizations catalyzed by enzymes remained unknown. Recently our group[15] and di Lena and coworkers[16] discovered concurrently and independently that some metalloproteins can mediate ATRP. These findings represent the first reports of biocatalytic, controlled/living radical polymerization.

Since the middle of the 1990s, controlled/living radical polymerizations such as ATRP have become some of the most widely used polymerization techniques in academic research,[17] applicable to most common monomers such as styrene, and (meth)acrylates.[18] ATRP allows for the synthesis of well-defined polymers with predetermined molecular weights, low molecular weight distributions, complex polymer architectures, as well as polymer chains terminated by functional groups. In ATRP, an organic halide initiator reacts with a low-oxidation-state transition metal catalyst, most commonly complexes of $Cu^{I}$, $Ru^{II}$, and $Fe^{II}$.[19] This results in a high

---

10 W. Boerjan, J. Ralph, M. Baucher, *Annu. Rev. Plant Biol.* **2003**, *54*, 519–546.

11 a) R. Hatfield, W. Vermerris, *Plant Physiol.* **2001**, *126*, 1351–1357 b) W. Boerjan, J. Ralph, M. Baucher, *Annu. Rev. Plant Biol.* **2003**, *54*, 519–546 c) B. Pickel, M.-A. Constantin, J. Pfannstiel, J. Conrad, U. Beifuss, A. Schaller, *Angew. Chem. Int. Ed.* **2009**, *49*, 202–204.

12 F. Hollmann, I. W. C. E. Arends, *Polymers* **2012**, *4*, 759–793.

13 a) S. Kobayashi, A. Makino, *Chem. Rev.* **2009**, *109*, 5288–5353 b) F. Hollmann, I. W. C. E. Arends, *Polymers* **2012**, *4*, 759–793 c) P. Walde, Z. Guo, *Soft Matter* **2011**, *7*, 316–331 d) K. Loos, Ed., *Biocatalysis in Polymer Chemistry*, Wiley-VCH Verlag GmbH & Co. KGaA, **2010**.

14 a) S. Kobayashi, A. Makino, *Chem. Rev.* **2009**, *109*, 5288–5353 b) F. Hollmann, I. W. C. E. Arends, *Polymers* **2012**, *4*, 759–793 c) P. Walde, Z. Guo, *Soft Matter* **2011**, *7*, 316–331 d) K. Loos, Ed., *Biocatalysis in Polymer Chemistry*, Wiley-VCH Verlag GmbH & Co. KGaA, **2010**.

15 a) S. J. Sigg, F. Seidi, K. Renggli, T. B. Silva, G. Kali, N. Bruns, *Macromol. Rapid Commun.* **2011**, *32*, 1710–1715 b) T. B. Silva, M. Spulber, M. K. Kocik, F. Seidi, H. Charan, M. Rother, S. J. Sigg, K. Renggli, G. Kali, N. Bruns, *Biomacromolecules* **2013**, *14*, 2703–2712 c) G. Kali, T. B. Silva, S. J. Sigg, F. Seidi, K. Renggli, N. Bruns, *ACS Symposium Series*, American Chemical Society, Washington, DC, **2012**.

16 a) Y.-H. Ng, F. di Lena, C. L. L. Chai, *Polym. Chem.* **2011**, *2*, 589 b) Y.-H. Ng, F. di Lena, C. L. L. Chai, *Chem. Commun.* **2011**, *47*, 6464–6466.

17 a) K. Matyjaszewski, J. S. Wang, *J. Am. Chem. Soc.* **1995**, *117*, 5614–5615 b) M. Kato, M. Kamigaito, M. Sawamoto, T. Higashimura, *Macromolecules* **1995**, *28*, 1721–1723.

18 a) W. A. Braunecker, K. Matyjaszewski, *Prog. Polym. Sci.* **2007**, *32*, 93–146 b) N. V. Tsarevsky, K. Matyjaszewski, *Chem. Rev.* **2007**, *107*, 2270–2299 c) M. Ouchi, T. Terashima, M. Sawamoto, *Chem. Rev.* **2009**, *109*, 4963–5050 d) F. di Lena, K. Matyjaszewski, *Prog. Polym. Sci.* **2010**, *35*, 959–1021 e) K. Matyjaszewski, *Macromolecules* **2012**, *45*, 4015–4039.

19 a) M. Ouchi, T. Terashima, M. Sawamoto, *Chem. Rev.* **2009**, *109*, 4963–5050 b) F. di Lena, K. Matyjaszewski, *Prog. Polym. Sci.* **2010**, *35*, 959–1021.

oxidation state metal halide complex and an organic radical, which undergoes chain propagation. The halogen atom transfer is an equilibrium reaction, so that the halide is transferred back from the catalyst to the polymer radical. This effectively interrupts chain growth until the dormant, halide-terminated polymer chain is reactivated. By this process, the radical concentration in the reaction mixture at any given time is low; as a result, termination reactions are suppressed. Although ATRP has considerable commercial potential, conventional ATRP has some drawbacks. It is carried out with transition metal complexes as catalysts, most often $Cu^{I}$ complexes. These catalysts are difficult to remove from the polymer product. Due to the (mild) toxicity of transition metal ions and amine ligands, the catalysts interfere with the application of the resulting polymers in biomedical and food grade applications.[20] Moreover, copper ion and amine ligand residues in polymers also represent a problem for technical applications in plastics, as they cause unwanted colouration.[21]

Three approaches have been followed in order to make ATRP environmentally more favorable, i.e. greener and the resulting polymers more compatible with medical and food grade requirements. One approach is the substitution of copper complexes with non-toxic catalysts that are based e.g. on iron ions.[22] However, iron-based ATRP catalysts often have much poorer catalytic properties compared to their copper counterparts. The second approach is to reduce the amount of catalyst required by designing catalysts with higher activity and better performance or by changing the experimental protocol.[23] In particular, the development of techniques such as activators regenerated by electron transfer (ARGET) ATRP, and initiators for continuous activator regeneration (ICAR) ATRP has permitted a reduction in catalyst concentration to the ppm range. In both methods, a reagent (a reducing agent in ARGET, a radical source in ICAR) is added to the reaction mixture in excess, so that inactive, high oxidation state metal complexes that accumulate due to termination reactions are regenerated to their ATRP-active, lower oxidation state, allowing the starting concentration of catalyst to be reduced significantly.[24] The third approach is to remove the catalyst from the polymerization solution at the end of the reaction, e.g. by simple filtration over aluminium oxide columns, scavenging with ion exchange resins, or using Cu-complexes immobilized on solid supports.[25]

---

[20] a) L. Mueller, K. Matyjaszewski, *Macromol. React. Eng.* **2010**, *4*, 180–185 b) N. V. Tsarevsky, K. Matyjaszewski, *Chem. Rev.* **2007**, *107*, 2270–2299.

[21] L. Mueller, K. Matyjaszewski, *Macromol. React. Eng.* **2010**, *4*, 180–185.

[22] a) F. di Lena, K. Matyjaszewski, *Prog. Polym. Sci.* **2010**, *35*, 959–1021 b) M. Ouchi, T. Terashima, M. Sawamoto, *Chem. Rev.* **2009**, *109*, 4963–5050.

[23] a) W. A. Braunecker, K. Matyjaszewski, *Prog. Polym. Sci.* **2007**, *32*, 93–146 b) N. V. Tsarevsky, K. Matyjaszewski, *Chem. Rev.* **2007**, *107*, 2270–2299 c) K. Matyjaszewski, W. Jakubowski, K. Min, W. Tang, J. Huang, W. A. Braunecker, N. V. Tsarevsky, *Proc. Natl. Acad. Sci.* **2006**, *103*, 15309–15314.

[24] W. A. Braunecker, K. Matyjaszewski, *Prog. Polym. Sci.* **2007**, *32*, 93–146.

[25] a) N. V. Tsarevsky, K. Matyjaszewski, *Chem. Rev.* **2007**, *107*, 2270–2299 b) L. Mueller, K. Matyjaszewski, *Macromol. React. Eng.* **2010**, *4*, 180–185.

## 1.2 Nanoreactors

In the macroscopic world, a chemical reactor is a conventional reaction vessel that constrains a chemical reaction within a defined volume. Substrates are fed into reactors through valves or openings, and products are retrieved from the reactor via similar means. Often, a catalyst is present in the reactor to facilitate the reaction. The advantages of chemical reactors include the opportunity to control reaction conditions internally in a precise manner, e.g. by selection of solvents, by setting the temperature, and by speed and mode of agitation. In the micro- and nanoworlds, compartments can be found or generated that also enclose a solvent-filled volume and sequester it from the bulk medium. If a chemical reaction is confined to such a compartment, e.g. by encapsulation of a catalytic species, these compartments can be considered nanoscale reactors.[26] The advantages that arise from such conditions are manifold, but they do not coincide with all of the reasons that macroscopic reactors are usually used. In a nanoreactor, the catalyzed reaction itself might be subject to greater control or selectivity as a result of the confined space available.[27] Furthermore, substrates or intermediates might be enriched inside of the nanoreactor as compared to the outside environment, thereby increasing the catalytic rate.[28] Toxic or unstable substances, e.g. the catalyst or intermediates, may be sequestered from bulk medium, reducing the toxicity of the system or enhancing the stability of the catalyst.[29] Moreover, because of their small size, nanoreactors are ideal vessels for reactions within living tissue in the context of drug-delivery,[30] or immobilized on surfaces as e.g. sensors.[31]

Confined reaction spaces that span various length scales ranging from the macroscopic world down to nanosized structures are found abundantly in biological systems. The controlled and selective exchange of substances across the confining layer is a characteristic hallmark of life. Every organism is a macroscopic entity with a distinct inner volume in which complex chemical transformations occur. This internal volume is separated from the environment by a boundary layer, e.g. the skin. Likewise, cells can be regarded as very complex microreactors. The cell membrane encloses catalytically active species, i.e. enzymes, in a confined volume. It controls access and release of substances into and out of the cell by a variety of pores and active and

---

[26] a) D. M. Vriezema, M. Comellas Aragonès, J. A. A. W. Elemans, J. J. L. M. Cornelissen, A. E. Rowan, R. J. M. Nolte, *Chem. Rev.* **2005**, *105*, 1445–1490 b) M. Uchida, M. T. Klem, M. Allen, P. Suci, M. Flenniken, E. Gillitzer, Z. Varpness, L. O. Liepold, M. Young, T. Douglas, *Adv. Mater.* **2007**, *19*, 1025–1042 c) A. de la Escosura, R. J. M. Nolte, J. J. L. M. Cornelissen, *J. Mater. Chem.* **2009**, *19*, 2274 d) K. T. Kim, S. A. Meeuwissen, R. J. M. Nolte, J. C. M. van Hest, *Nanoscale* **2010**, *2*, 844 e) K. Renggli, P. Baumann, K. Langowska, O. Onaca, N. Bruns, W. Meier, *Adv. Funct. Mater.* **2011**, *21*, 1241–1259 f) M. Marguet, C. Bonduelle, S. Lecommandoux, *Chem. Soc. Rev.* **2013**, *42*, 512.

[27] a) B. Helms, S. J. Guillaudeu, Y. Xie, M. McMurdo, C. J. Hawker, J. M. J. Fréchet, *Angew. Chem.* **2005**, *117*, 6542–6545 b) P. Cotanda, N. Petzetakis, R. K. O'Reilly, *MRS Commun.* **2012**, *2*, 119–126 c) P. B. Zetterlund, *Macromol. Theory Simul.* **2011**, *20*, 660–666 d) P. B. Zetterlund, *Polym. Chem.* **2011**, *2*, 534–549.

[28] M. Kimura, M. Kato, T. Muto, K. Hanabusa, *Macromolecules* **2000**, *33*, 1117–1119.

[29] E. M. Sampson, T. A. Bobik, *J. Bacteriol.* **2008**, *190*, 2966–2971.

[30] P. Tanner, V. Balasubramanian, C. G. Palivan, *Nano Lett.* **2013**, *13*, 2875–2883.

[31] a) M. Grzelakowski, O. Onaca, P. Rigler, M. Kumar, W. Meier, *Small* **2009**, *5*, 2545–2548 b) A. Napoli, M. J. Boerakker, N. Tirelli, R. J. M. Nolte, N. A. J. M. Sommerdijk, J. A. Hubbell, *Langmuir* **2004**, *20*, 3487–3491.

passive mechanisms. Moreover, organelles within cells provide another, smaller level of compartmentalization. Organelles are also equipped with various means to selectively exchange materials with the cytosol. Nature manages to stabilize and protect catalytically active species by separating the reaction space within cells and organelles from the surrounding environment. The reaction conditions, e.g. pH or concentration of certain substrates in the compartments, are controlled in order to influence the course of reactions. Another important feature of Nature's micro- and nanocompartments is spatial control of individual reaction steps in various complex reaction cascades.

When chemical reactions are carried out under man-made conditions, e.g. in organic synthesis, they are often conducted in homogeneous solution. However, Nature's strategy of compartmentalization shows that confining reactions to microscopic or nanoscopic volumes can yield tremendous advantages. Reaction compartments permit the study of the influence of spatial confinement on chemical reactions and provide an opportunity to perform organic synthetic transformations in 'exotic' environments, e.g. biocatalysis in organic solvents[32] or in living cells.[33] Therefore, reaction compartments have attracted much attention recently.[34] Given that their size is most often below 500 nm in diameter, they are referred to as nanoreactors. However, reference to size range is vague and the term is also used for larger structures – some authors speak of microreactors instead.

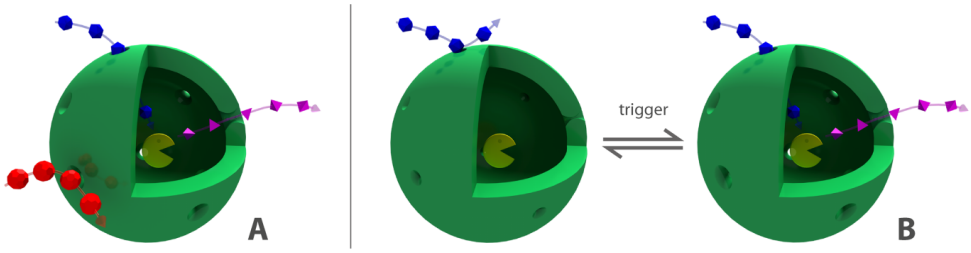


**Figure 1.1** Concept of selective and responsive nanoreactors. a) Selective nanoreactors allow only specific molecules to enter the inner cavity while others are blocked from entering. Selection criteria can be size, charge or hydrophobicity of the diffusing molecules, amongst others. b) Responsive or gated nanoreactors possess pores in the membrane that open or close upon a particular trigger. This trigger can be an external stimulus such a change in pH, the presence of certain reagents, or a change in the local environment of the pores, such as the potential across the shell of the nanoreactor.

32 N. Bruns, J. C. Tiller, *Nano Lett.* **2005**, *5*, 45–48.

33 P. Tanner, V. Balasubramanian, C. G. Palivan, *Nano Lett.* **2013**, *13*, 2875–2883.

34 a) D. M. Vriezema, P. M. L. Garcia, N. S. Oltra, N. S. Hatzakis, S. M. Kuiper, R. J. M. Nolte, A. E. Rowan, J. C. M. van Hest, *Angew. Chem. Int. Ed.* **2007**, *46*, 7378–7382 b) K. Kita-Tokarczyk, J. Grumelard, T. Haefele, W. Meier, *Polymer* **2005**, *46*, 3540–3563 c) A. Mecke, C. Dittrich, W. Meier, *Soft Matter* **2006**, *2*, 751–759 d) T. S. Koblenz, J. Wassenaar, J. N. H. Reek, *Chem. Soc. Rev.* **2008**, *37*, 247–262 e) A. de la Escosura, R. J. M. Nolte, J. J. L. M. Cornelissen, *J. Mater. Chem.* **2009**, *19*, 2274 f) S. F. M. van Dongen, M. Nallani, J. Cornelissen, R. J. M. Nolte, J. C. M. van Hest, *Chem. Eur. J.* **2009**, *15*, 1107–1114 g) P. A. Monnard, M. S. DeClue, H. J. Ziock, *Curr. Nanosci.* **2008**, *4*, 71–87.

We define a nanoreactor as a compartment with a radius of ≤ 100 nm that encloses a volume of solvent in which a chemical reaction occurs (Figure 1.1). Substrates can enter the reactor through the confining layer while products either accumulate inside the nanoreactor or are released into the bulk medium. In most cases the reaction is confined to the nanoreactor because the catalyst is encapsulated there. Selective nanoreactors are considered to be those reaction compartments with a shell that discriminates among molecules, allowing certain molecular species to enter or leave the nanoreactor while others are blocked from entering the cavity (Figure 1.1a). This can be achieved either by means of the intrinsic, semipermeable properties of the boundary layer or by selective pores. While the intrinsic permeability of the confining layer, e.g. a membrane, selects molecules based on size or polarity, pores can also be selective, allowing only a certain kind of molecule with a distinct chemical identity to pass. Some membranes and pores can also change their permeability upon exposure to an external, triggering stimulus, and thus show gated, or switchable behavior (Figure 1.1b).

The most widely studied biomimetic nanocompartments are liposomes, which are vesicular structures formed by lipids in aqueous solution.[35] These vesicles are spherical, self-closing structures with a lipid bilayer membrane that entrap a portion of aqueous phase in their interiors. The formation of these superstructures is based on the self-assembly of defined amphiphilic lipid building blocks in an aqueous system under osmotically-balanced conditions. Hence, liposomes can be employed as carriers by entrapping a hydrophilic cargo in their cavities or a hydrophobic cargo in their membranes. A large variety of liposome-based carrier systems have been developed,[36] especially for drug-delivery purposes, as liposomes are usually safe and biodegradable.[37] Liposomes have also been employed as nanoreactors, e.g. by encapsulating different enzymes in their cavities while retaining their biocatalytic activity.[38] However, liposomes have several drawbacks that hamper their applications. Structural defects and mechanical instability lead to significant leakage.[39] In biomedical applications, the short circulation lifetime of liposomes and their interaction with lipo-proteins is a disadvantage.[40] The fundamental characteristics of liposome

35 Y. Barenholz, *Curr. Opin. Colloid Interface Sci.* **2001**, *6*, 66–77.

36 a) A. Jesorka, O. Orwar, *Annu. Rev. Anal. Chem.* **2008**, *1*, 801–832 b) Y. Barenholz, *Curr. Opin. Colloid Interface Sci.* **2001**, *6*, 66–77.

37 a) P. Goyal, K. Goyal, S. G. Vijaya Kumar, A. Singh, O. P. Katare, D. N. Mishra, *Acta Pharm.* **2005**, *55*, 1–25 b) Y. Malam, M. Loizidou, A. M. Seifalian, *Trends Pharmacol. Sci.* **2009**, *30*, 592–599 c) G. M. El Maghraby, B. W. Barry, A. C. Williams, *Eur. J. Pharm. Sci.* **2008**, *34*, 203–222 d) S. Ganta, H. Devalapally, A. Shahiwala, M. Amiji, *J. Controlled Release* **2008**, *126*, 187–204.

38 A. Jesorka, O. Orwar, *Annu. Rev. Anal. Chem.* **2008**, *1*, 801–832.

39 M. C. Woodle, D. D. Lasic, *Biochim. Biophys. Acta, Biomembr.* **1992**, *1113*, 171–199.

40 Y. Barenholz, *Curr. Opin. Colloid Interface Sci.* **2001**, *6*, 66–77.

nanoreactors as well as their diverse applications have been reviewed extensively elsewhere[41] and are beyond the scope of this thesis.

In addition to liposomes, several other nanovessels have been investigated as potential nanoreactors. These nanoreactors range from swollen domains in polymer networks,[42] to polymer vesicles.[43] All these systems have in common that they enclose a catalyst, most often enzymes, inside a cavity surrounded by a shell or interface. This boundary layer is either selectively permeable for substrates and products, or they encompasse pores that allow for the exchange of matter between the inside and the outside of the nanoreactor. Thus, the activity and the substrate selectivity of the enclosed catalyst in such systems do not only depend on the intrinsic properties of the catalyst, but also on the tailored properties of the nanoreactor.[44] Nature provides intriguing nanovessels with defined pores in the form of protein cages, the best known being ferritin and viral capsids.[45]

---

41 a) A. Jesorka, O. Orwar, *Annu. Rev. Anal. Chem.* **2008**, *1*, 801–832 b) Y. Barenholz, *Curr. Opin. Colloid Interface Sci.* **2001**, *6*, 66–77 c) P. Goyal, K. Goyal, S. G. Vijaya Kumar, A. Singh, O. P. Katare, D. N. Mishra, *Acta Pharm.* **2005**, *55*, 1–25 d) Y. Malam, M. Loizidou, A. M. Seifalian, *Trends Pharmacol. Sci.* **2009**, *30*, 592–599 e) G. M. El Maghraby, B. W. Barry, A. C. Williams, *Eur. J. Pharm. Sci.* **2008**, *34*, 203–222 f) S. Ganta, H. Devalapally, A. Shahiwala, M. Amiji, *J. Controlled Release* **2008**, *126*, 187–204 g) M. C. Woodle, D. D. Lasic, *Biochim. Biophys. Acta, Biomembr.* **1992**, *1113*, 171–199 h) N. Düzgünes, *Liposomes, Part B*, Elsevier, Amsterdam, **2003** h) D. D. Lasic, D. Papahadjopoulos, Eds., *Medical Applications of Liposomes*, Elsevier, Amsterdam, **1998**.

42 a) N. Bruns, J. C. Tiller, *Nano Lett.* **2005**, *5*, 45–48 b) K. Henzler, P. Guttmann, Y. Lu, F. Polzer, G. Schneider, M. Ballauff, *Nano Lett.* **2013**, *13*, 824–828.

43 a) R. J. R. W. Peters, I. Louzao, J. C. M. van Hest, *Chem. Sci.* **2012**, *3*, 335 b) J. Gaitzsch, D. Appelhans, L. Wang, G. Battaglia, B. Voit, *Angew. Chem. Int. Ed.* **2012**, *51*, 4448–4451 c) A. Lu, R. K. O'Reilly, *Curr. Opin. Biotechnol.* **2012**, 1–7.

44 K. Renggli, P. Baumann, K. Langowska, O. Onaca, N. Bruns, W. Meier, *Adv. Funct. Mater.* **2011**, *21*, 1241–1259.

45 a) A. de la Escosura, R. J. M. Nolte, J. J. L. M. Cornelissen, *J. Mater. Chem.* **2009**, *19*, 2274 b) K. Renggli, P. Baumann, K. Langowska, O. Onaca, N. Bruns, W. Meier, *Adv. Funct. Mater.* **2011**, *21*, 1241–1259 c) M. Uchida, M. T. Klem, M. Allen, P. Suci, M. Flenniken, E. Gillitzer, Z. Varpness, L. O. Liepold, M. Young, T. Douglas, *Adv. Mater.* **2007**, *19*, 1025–1042.

## 1.3 Scope of the Thesis

The aim of the present thesis is the generation of new approaches to render atom transfer radical polymerization (ATRP) environmentally friendlier, e.g. by conjugating the ATRP catalyst to proteins that can be removed after polymerization. Furthermore, the conjugation of ATRP catalysts into the cavities of protein cages results in protein nanoreactors, where the catalytic species is enclosed in a confined space. Such nanoreactors could allow the modulation of controlled/living radical polymerization by external triggers.

The first task is to identify potential proteins to be conjugated to ATRP catalysts. Proteins display different functionalities that could enhance the attached ATRP catalyst with additional properties. Dependent on the protein and its desired functionality, an adequate conjugation chemistry has to be determined and the gained protein-catalyst conjugates have to be tested towards ATRP synthesis methods. With an established synthesis route for protein-catalyst conjugates and with a good performing polymerization technique, we will be able to screen for beneficial effects of proteins for ATRP.

Globular proteins could act as handles for the catalyst which enable to precipitate the attached catalyst in order to reduce the final concentration of the transition metal catalyst in polymers synthesized by ATRP. Moreover, the conjugation of ATRP catalyst into the cavities of protein cages could beneficially affect the performance of the polymerization by the space constriction in the nanoreactor.

# 2 Atom Transfer Radical Polymerization with Protein Conjugated Catalysts[46]

*Kasper Renggli, Farzad Seidi, Gergely Kali and Nico Bruns*

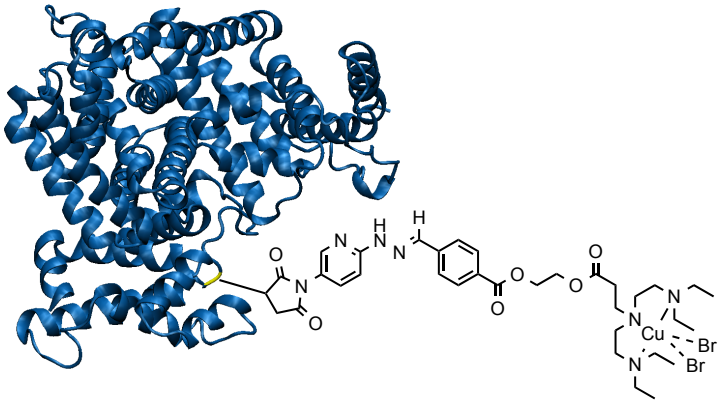


*We report ATRP catalysts conjugated to proteins. By using ARGET ATRP we are able to polymerize NiPAAm and PEGA with a moderate control over the molecular weight and the polydispersity of the polymers. Further, globular proteins serve as a functional handle to remove the attached copper containing catalyst effectively from solution. Such systems allow for the drastic reduction in the residual copper content of polymers synthesized by ATRP in aqueous solution.*

[46] Parts of this chapter were published in: a) K. Renggli, M. G. Nussbaumer, R. Urbani, T. Pfohl, N. Bruns, *Angew. Chem. Int. Ed.* **2014**, *53*, 1443–1447 b) K. Renggli, M. Spulber, J. Pollard, M. Rother, N. Bruns, *ACS Symp. Ser.* **2013**, *1144*, 163–171 c) N. Bruns, K. Renggli, F. Seidi, G. Kali, *Polym. Prepr. (Am. Chem. Soc., Div. Polym. Chem.)* **2011**, *52*, 521–522 d) T. B. Silva, M. Spulber, M. K. Kocik, F. Seidi, H. Charan, M. Rother, S. J. Sigg, K. Renggli, G. Kali, N. Bruns, *Biomacromolecules* **2013**, *14*, 2703–2712.

## 2.1 Introduction

Over the last two decades, synthesis techniques have been developed that allow a degree of control of radical polymerizations, such as atom transfer radical polymerization (ATRP), reversible addition-fragmentation chain transfer (RAFT) polymerization, and nitroxide-mediated radical polymerization (NMP).[47] Each of these methods has its specific strengths and drawbacks. ATRP is one of the most popular controlled/living radical polymerizations because of its great versatility: It is applicable to most vinyl and styrene monomers, tolerates most functional groups, is compatible with proteins and other biomolecules and it results in halide-terminated polymer chains that can be easily converted into a multitude of other functional end-groups.[48] ATRP relies on the reversible deactivation of propagating radicals by transition metal complex catalysts, most often copper(I)-copper(II) redox couples, thus lowering the radical concentration in a reaction and therefore the chances of chain termination, while still producing reactive chain ends.[49] Without a doubt, ATRP and other controlled/living radical polymerizations are amongst the most important recent developments in the field of polymer chemistry and have spurred thousands of scientific publications and a multitude of industrial processes.[50] Polymers prepared by ATRP can be used, e.g., as sealants, lubricants, oil additives, wetting agents, blend compatibilizers, surfactants and pigment stabilizers.[50] However, ATRP also suffers some limitations. The catalysts are tedious to remove from a polymer product, causing unwanted coloration, toxicity and environmental issues.[51] The problem of residual traces of transition metal or amine ligands in final products can hinder biomedical, food-grade, and electronic applications of the polymers. Several recent developments aim to make ATRP more environmentally friendly and the resulting polymers more compatible with biomedical, food grade and electronic requirements. Less toxic iron catalysts are being investigated as alternative to copper-based catalysts[52] and variations of the experimental protocol of ATRP, such as Activators ReGenerated by Electron Transfer (ARGET) and Initiators for Continuous Activator Regeneration (ICAR) ATRP lead to a significant reduction in the concentration of catalysts required for this polymerization.[53]

In order to remove the catalyst from the polymerization solution, several methods have been developed, e.g. simple filtration over aluminium oxide columns, scavenging

---

47 a) K. Matyjaszewski, *Macromolecules* **2012**, *45*, 4015–4039 b) W. A. Braunecker, K. Matyjaszewski, *Prog. Polym. Sci.* **2007**, *32*, 93–146.

48 a) W. A. Braunecker, K. Matyjaszewski, *Prog. Polym. Sci.* **2007**, *32*, 93–146 b) K. Matyjaszewski, *Macromolecules* **2012**, *45*, 4015–4039 c) N. V. Tsarevsky, K. Matyjaszewski, *Chem. Rev.* **2007**, *107*, 2270–2299 d) M. Ouchi, T. Terashima, M. Sawamoto, *Chem. Rev.* **2009**, *109*, 4963–5050 e) K. Matyjaszewski, N. V. Tsarevsky, *Nat. Chem.* **2009**, *1*, 276–288.

49 W. A. Braunecker, K. Matyjaszewski, *Prog. Polym. Sci.* **2007**, *32*, 93–146.

50 K. Matyjaszewski, *Macromolecules* **2012**, *45*, 4015–4039.

51 N. V. Tsarevsky, K. Matyjaszewski, *Chem. Rev.* **2007**, *107*, 2270–2299.

52 a) M. Ouchi, T. Terashima, M. Sawamoto, *Chem. Rev.* **2009**, *109*, 4963–5050 b) F. di Lena, K. Matyjaszewski, *Prog. Polym. Sci.* **2010**, *35*, 959–1021.

53 a) K. Matyjaszewski, *Macromolecules* **2012**, *45*, 4015–4039 b) N. V. Tsarevsky, K. Matyjaszewski, *Chem. Rev.* **2007**, *107*, 2270–2299.

with ion exchange resins, and using Cu-complexes immobilized on solid supports.[54] However, quantitative removal of the metal ions down to concentrations in the parts per billion range remains a difficult task and novel concepts are highly sought after.

We set out to investigate a catalyst system that could be readily purified. We focused on catalysts for ATRP that are conjugated to proteins. The protein acts as a soluble support for the catalyst. However, the biomolecule also provides a good handle to remove the catalyst from the polymerization solution with several of the purification methods known from the toolbox of biochemistry, e.g. precipitation and affinity tags. ATRP catalysts conjugated to proteins not only provide opportunities for effective Cu removal, but also allow conducting ATRP in confined reaction spaces. We will show this concept by using a protein-cage as a nanoreactor for ATRP. In such a nanoreactor, a higher degree of control over the polymerization was achieved compared to the polymerization in aqueous solution (see chapter 7). Using a system with $Cu^{I}$ or $Cu^{II}$ in combination with ascorbate can cause scission of proteins and DNA.[55] By working in an oxygen-free environment this problem can be circumvented.[56] Having only complexed copper or an addition of a chelating agent can reduce or even eliminate the problem since the scission requires free Cu-ions.[57] Thus, conjugating catalysts to proteins with a purification before polymerization presents itself as an elegant solution to this issue.

[54] a) N. V. Tsarevsky, K. Matyjaszewski, *Chem. Rev.* **2007**, *107*, 2270–2299 b) L. Mueller, K. Matyjaszewski, *Macromol. React. Eng.* **2010**, *4*, 180–185.

[55] a) S.-H. Chiou, *Journal of Biochemistry* **1983**, *94*, 1259–1267 b) J. Sereikaite, J. Jachno, R. Santockyte, P. Chmielevski, V.-A. Bumelis, G. Dienys, *Protein J* **2006**, *25*, 369–378.

[56] K. Kim, S. G. Rhee, E. R. Stadtman, *J. Biol. Chem.* **1985**, *260*, 15394–15397.

[57] J. Sereikaite, J. Jachno, R. Santockyte, P. Chmielevski, V.-A. Bumelis, G. Dienys, *Protein J.* **2006**, *25*, 369–378.

## 2.2 Results & Discussion

### 2.2.1 Preparation of Protein Conjugated ATRP Catalysts

Bovine serum albumin (BSA) was used as functional support for ATRP catalysts. BSA is a cheap and remarkably stable protein with a molecular weight of 66.5 kDa and may be referred to as Cohn Fraction V serum albumin (Figure 2.1). Easy and efficient strategies to couple linkers to proteins or peptides can be found in bio-conjugation chemistry where a toolbox of methods is available ranging from click-chemistry to protein/peptide engineering.[58] Typically the proteins are engineered to display a free cysteine or lysine. In peptides the C- or N-terminus is used while recombinant techniques are applied to introduce an unnatural amino acid into the whole protein for site-specific interaction with polymers.[59] BSA displays one free and surface exposed cystein and is therefore an ideal candidate to attach a ligand to complex copper.


**Figure 2.1** Bovin Serum Albumin and its free cystein indicated in red. The structure of BSA (PDB: 3V03)[60] was rendered using the Chimera program.[61]

In order to attach ATRP catalysts to the protein, a ligand bound to a protein-specific linker was synthesized. To this end, 4-formylbenzoic acid was protected to form a dimethoxy acetal. In a one-pot, two-steps synthesis the acetal was esterified with 2-hydroxyethyl acrylate, followed by a Michael-type addition of N,N,N',N'-tetraethyldiethylene triamine (TEDETA) to the double bond of the acrylate. The resulting product was purified by flash chromatography and finally the acetal was cleaved under acidic conditions. The product comprises a tridentate ligand which is

---

58 a) G. T. Hermanson, *Bioconjugate Techniques*, Academic Press, Maryland Heights, **2008** b) R. M. Broyer, G. N. Grover, H. D. Maynard, *Chem. Commun.* **2011**, *47*, 2212–2226.

59 a) L. Wang, P. G. Schultz, *Angew. Chem. Int. Ed.* **2005**, *44*, 34–66 b) E. Baslé, N. Joubert, M. Pucheault, *Chem. Biol.* **2010**, *17*, 213–227 c) A. T. Krueger, B. Imperiali, *ChemBioChem* **2013**, *14*, 788–799.

60 K. A. Majorek, P. J. Porebski, A. Dayal, M. D. Zimmerman, K. Jablonska, A. J. Stewart, M. Chruszcz, W. Minor, *Mol. Immunol.* **2012**, *52*, 174–182.

61 E. F. Pettersen, T. D. Goddard, C. C. Huang, G. S. Couch, D. M. Greenblatt, E. C. Meng, T. E. Ferrin, *J. Comput. Chem.* **2004**, *25*, 1605–1612.

able to complex Cu ions and an aromatic aldehyde (compound **1** in Figure 2.2). The aldehyde moiety can react with heterobifunctional linkers comprising a 6-hydraziniumpyridine functional group. Such linkers are commercially available from SoluLink, CA.

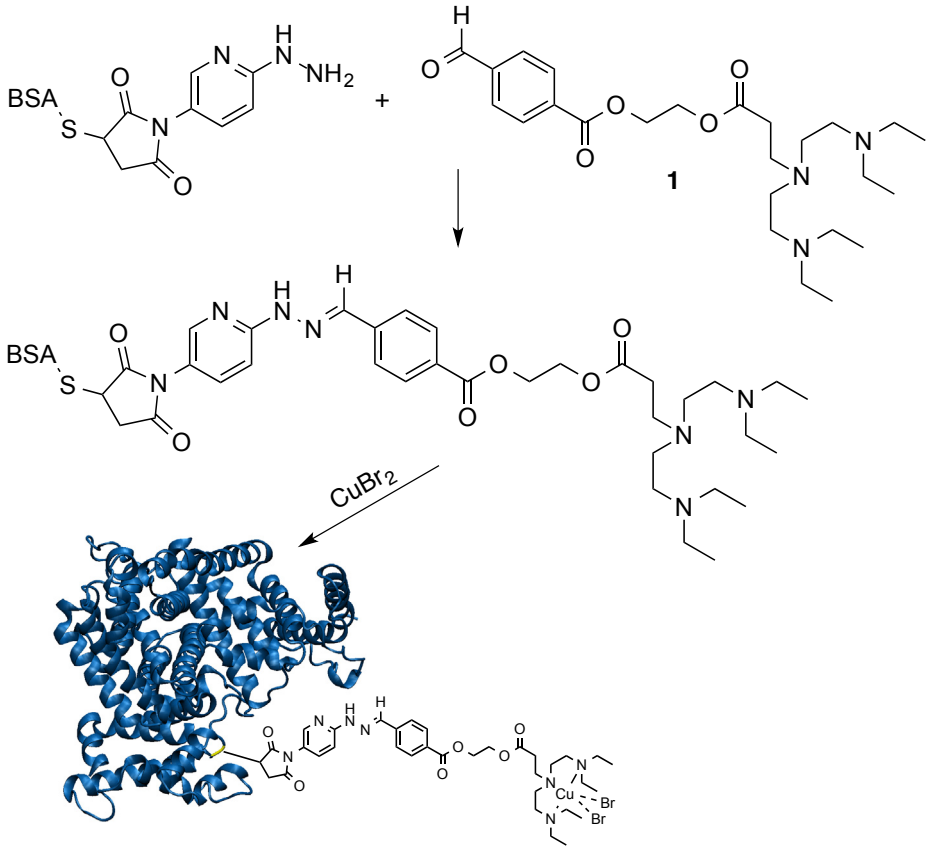


**Figure 2.2** Strategy to covalently attach an ATRP catalyst to albumin from bovine serum. The free cystein of BSA is functionlized using maleimide chemistry. The TEDETA ligand (**1**) forms a stable bis-aryl hydrazone bond that has a distinct absorbtion at 354 nm.

We used a 25-fold excess of 3-N-maleimido-6-hydrazinium hydrochloride (MHPH) to modify the thiol group of the sole surface exposed cysteine on BSA. The 6-hydraziniumpyridine molar substitution ratio (MSR) for BSA was determined by adding an aliquot of a BSA-MHPH sample to a 4-nitrobenzaldehyde solution in buffer. The solution was incubated at 37°C for 1 h and the absorbance at 390 nm for the hydrazone was determined.[62] The MSR for BSA resulted in 0.22 ± 0.01 modified cysteins per BSA (Figure 2.3). This relatively low molecular substitution ratio can be explained by the fact that in commercial BSA preparations, some cysteines are blocked or not surface exposed.

[62] SoluLink Company, *Catalog and Reference Manual* **2008**.

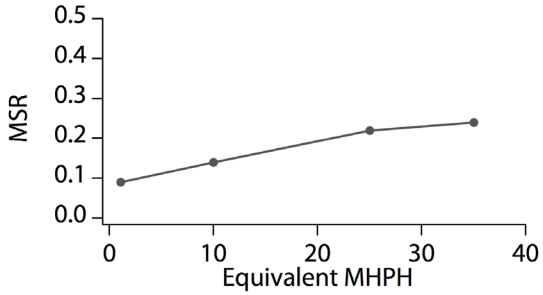


**Figure 2.3** Modification of BSA with MHPH versus the amount of reagent used (relative to surface-exposed thiol groups). A 25-fold excess of MHPH resulted in a MSR of 0.22 ± 0.01 MHPH per BSA.

After modification of BSA with the MHPH-linker, the protein was incubated with an excess of the synthesized TEDETA derivative, upon which a stable bis-aryl hydrazone bond formed. This bond has a specific UV absorption band with a maximum at 354 nm, and thus the number of ligands bound to the proteins could be determined as 0.21 ± 0.01 bis-aryl hydrazone bonds and therefore ligands per BSA (see Figure 2.4).

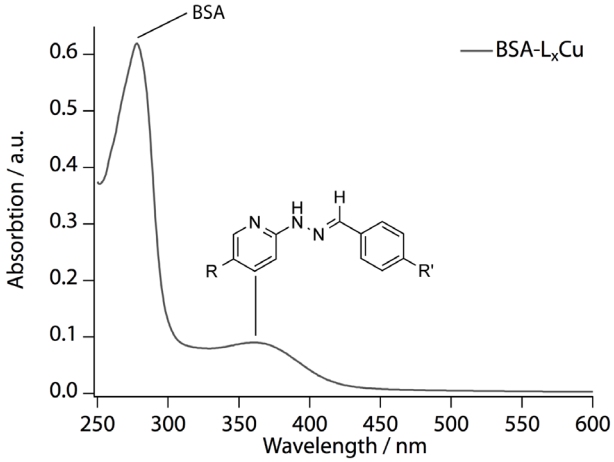


**Figure 2.4** UV/Vis data of BSA-$L_xCu$ reveals a molar substitution ratio of 0.21 ± 0.1 bis-aryl hydrazone bonds (absorbtion at 354 nm) and therefore ligands per BSA.

The protein-ligand conjugate was then used to complex $Cu^{II}$ in an aqueous buffered $CuBr_2$ solution (Figure 2.2). Finally, the unbound copper was removed from the catalysts by size exclusion spin centrifugation. Neutron activation analysis (NAA) of $^{66}Cu$ at 1039.2 keV showed that copper was retained by the protein throughout the purification where the TEDETA ligand was conjugated to the protein, but that native BSA did not bind $Cu^{II}$ (Figure 2.5). Further, NAA confirms that when BSA is functionalized with the ligand (BSA-$L_x$) no trace amounts of copper are introduced to the system.

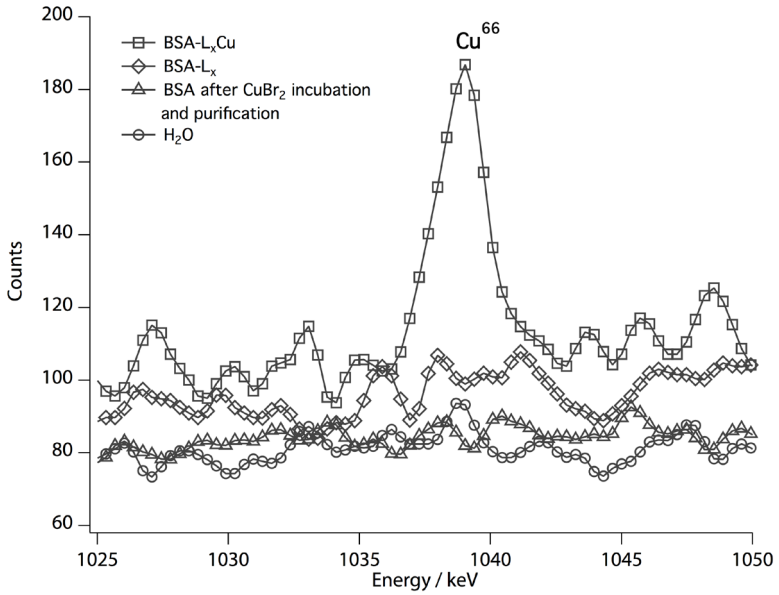


**Figure 2.5** Using neutron activation analysis, it was determined that only the BSA carrying the ligand retained copper, while native BSA after incubation with $CuBr_2$ and purification was copper-free.

The UV/Vis spectrum of BSA-$L_x$Cu after subtraction of the BSA-$L_x$ spectrum shows a broad absorption band at $\lambda > 600$ nm (Figure 2.6). This is characteristic for complexes of $Cu^{II}$ and triamine ligands[63] and also confirms the formation of a BSA-$L_x$Cu complex.

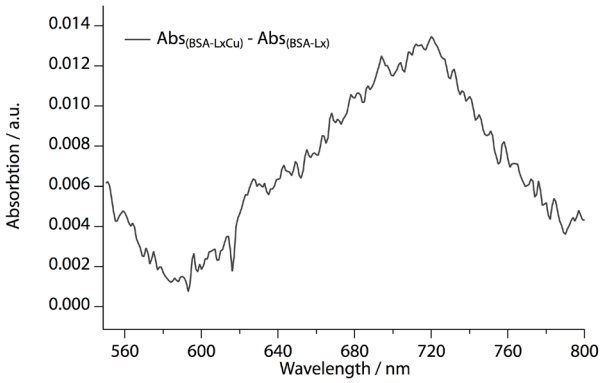


**Figure 2.6** The formation of a copper complex with the BSA-ligand conjugate was also confirmed by UV/Vis spectroscopy, as the typical absorption band for $Cu^{II}$ complexes with a maximum at 720 nm was observed.

[63] B. Kurzak, A. Kamecka, K. Bogusz, J. Jezierska, *Polyhedron* **2008**, *27*, 2952–2958.

In order to determine the structural integrity of BSA upon introduction of the ATRP catalyst, the protein was analyzed by sodium dodecyl sulfate polyacrylamide gel electrophoresis (SDS PAGE; Figure 2.7). The gels diplay the typical absorbtion bands for BSA, whether BSA is modified with an ATRP catalyst or not. Therfore, we can conclude that the protein remains stable after conjugation of the ATRP catalyst.

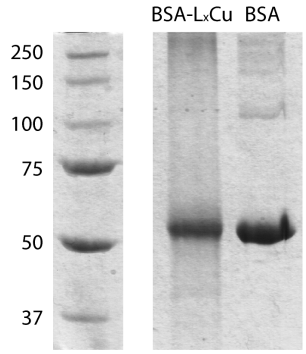


**Figure 2.7** SDS PAGE of BSA-$L_x$Cu shows that BSA is not affected by the conjugation of ligands and the complexation of $Cu^{II}$.

### 2.2.2 ARGET ATRP with Protein-Catalyst Conjugates

Polymerizations were carried out in aqueous solution. To this end, the water-soluble initiator 2-hydroxyethyl-2-bromoisobutyrate (HEBIB), the monomer N-isopropylacrylamide (NiPAAm) and the catalyst were dissolved in aqueous buffer (100 mM sodium acetate, 150 mM NaCl, 80 mM $MgCl_2$, pH 5.2) under Argon atmosphere in molar ratios of [monomer]:[initiator]:[BSA-$L_x$Cu] 67:1:1.5 x $10^{-5}$. The polymerization was initiated by adding the reducing agent ascorbic acid (AscA) to the reaction mixture (ratio [BSA-$L_x$Cu]:[AscA] 1:2.7 x $10^5$; reaction scheme see Figure 2.9). Under these conditions the catalytically active $Cu^I$ species is generated in situ. Moreover, activators (i.e. catalysts) are continuously regenerated by electron transfer, a process named ARGET.[64] After 20 h, the polymerization was stopped by adding non-degassed water and exposing the catalyst to air.

Gel permeation chromatography (GPC) resulted in poly(N-isopropylacrylamide) (pNiPAAm) with an apparent molecular weight $M_n$ of 42600 g $mol^{-1}$ (calibrated against poly(methyl methacrylate)) and a PDI of 1.94 for the ARGET ATRP with BSA-$L_x$Cu (Figure 2.8). This result indicates that the synthesis of pNiPAAm is intrinsically difficult to control in aqueous solution corroberating work previously reported by Millard et al.[65]

---

64 K. Matyjaszewski, *Macromolecules* **2012**, *45*, 4015–4039.

65 P.-E. Millard, N. C. Mougin, A. Böker, A. H. E. Müller, in *Controlled/Living Radical Polymerization: Progress in ATRP, ACS Symp. Ser.*, American Chemical Society, Washington, D.C., U.S.A., **2009**, pp. 127–137.

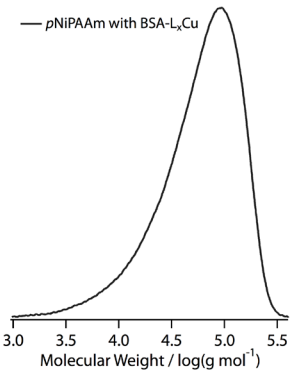


**Figure 2.8** GPC trace of pNiPAAm synthesized by BSA-$L_x$Cu in aqueous buffer.

In addition, we assessed BSA-$L_x$Cu as an ATRP catalyst for a different monomer. We used poly(ethylene glycol) methyl ether acrylate (PEGA), a water soluble monomer with a number average molecular weight of 480 g $mol^{-1}$. The polymerization of PEGA with BSA-$L_x$Cu as catalyst was performed under the same ARGET ATRP conditions used for NiPAAm (reaction schemes see Figure 2.9). GPC analysis of the resulting poly(poly(ethylene glycol) methyl ether acrylate) (pPEGA) displayed a poly(ethylene oxide)-apparent $M_n$ of 119400 g $mol^{-1}$ and a PDI of 3.12.

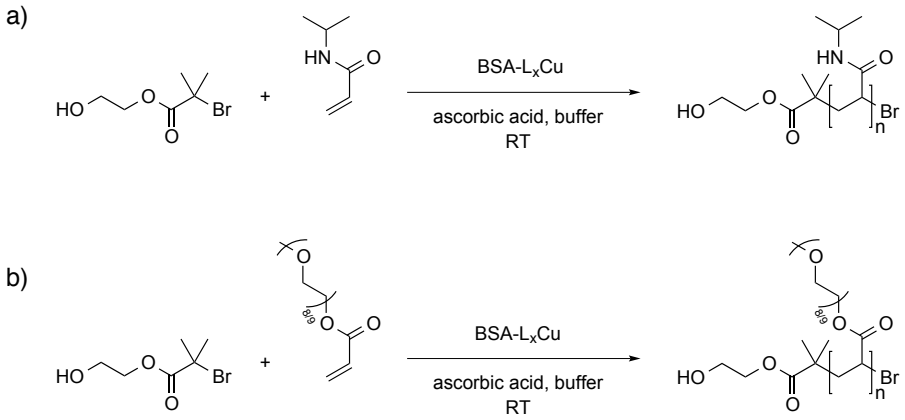


**Figure 2.9** Reaction schemes for the synthesis of a) pNiPAAm in buffer solution b) pPEGA in buffer solution and

### 2.2.3 Copper Removal after Polymerization

The BSA samples were used to analyze the possibility to remove copper from the reaction mixture after polymerization with methods specific for proteins. Two different strategies to remove copper from the resulting polymer solution were explored. In a first approach we used protein precipitation, which is based on altering the solvation potential of the solvent, i.e. lowering the solubility of BSA by the addition of a reagent.

#### 2.2.3.1 Protein-Catalyst Precipitation

Proteins are well known to precipitate in the presence of organic solvent. The ability of BSA to be precipitated by organic solvent was determined with methanol (MeOH), ethanol (EtOH) and formamide as organic co-solvent.

Figures 2.11 and 2.12 show the UV/Vis absortion of BSA at 279 nm versus the percentage of added organic co-solvent. A drop in absorbance is equivalent with a loss of integrity of the protein and therefore precipitation. Surprisingly, BSA turned out to be very robust in organic solvent and showed no drastic change in absorbance for added EtOH or formamide. In the case of MeOH (Figure 2.11), a significant drop with high concentration of MeOH could be observed, indicating that BSA can be precipitated but only with rather harsh conditions. These experiments demonstrated the toughness of BSA towards organic co-solvent but without sufficient precipitation to allow for purification of the desired polymer by filtration.

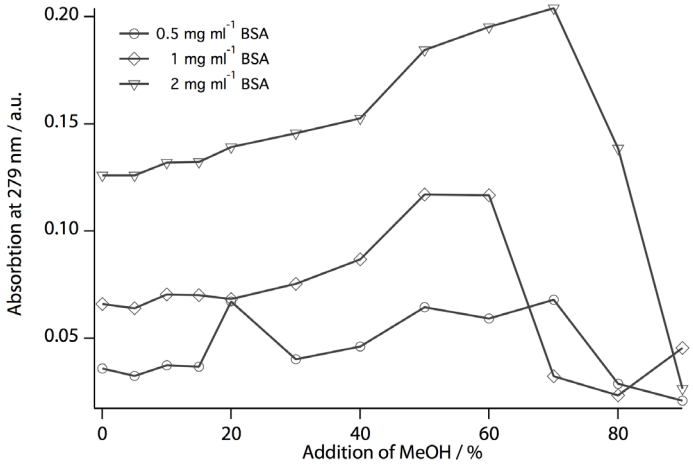


**Figure 2.11** Precipitation of BSA due to MeOH concentrations between 0 and 100%, measured by the absorbtion at 279 nm with UV/Vis spectroscopy.

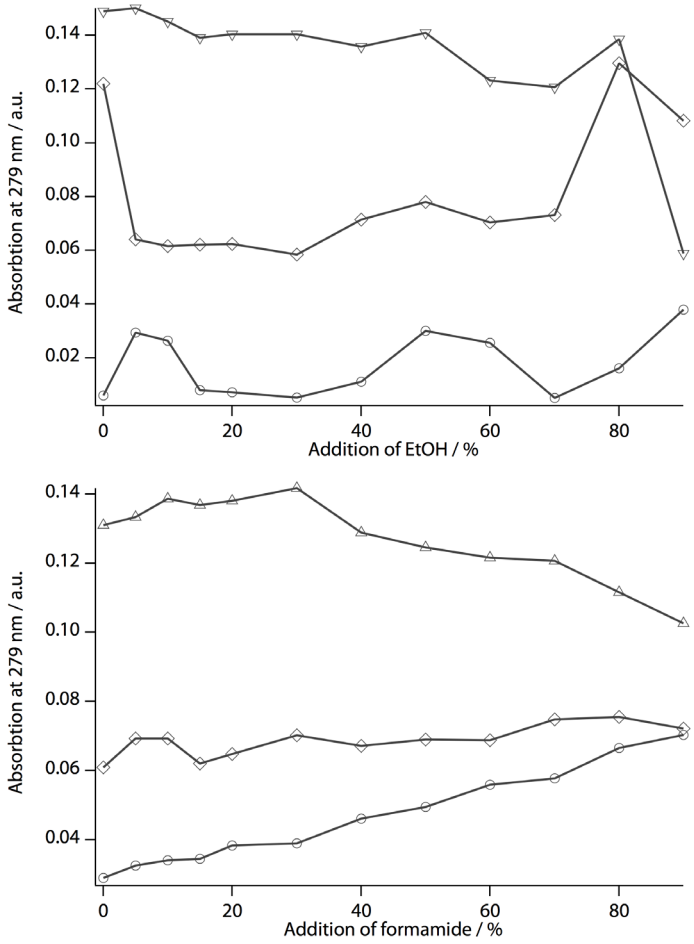


**Figure 2.12** Precipitation of BSA due to organic solvent measured by the absorbtion at 279 nm with UV/Vis spectroscopy. Addition of organic co-solvent between 0 and 100% lead to the conclusion that BSA is extremely stable and is almost soluble in organic solvent.

In order to remove the protein-catalyst conjugate from the final polymer solution we explored alternatives to BSA as a globular protein. We used bovine hemoglobin (Hb), a cheap and abundantly available tetrameric protein with four Fe-containing heme groups.[66] We assessed the precipitation potential of Hb with EtOH as described for BSA. Figure 2.13 shows the UV/Vis absorbtion of Hb at 404 nm, corresponding to the heme group which correlates with the structural stability of the protein. The results indicated, in contrast to BSA, that Hb can be precipitated from solution with the addition of about 60% EtOH.

[66] a) S. N. Vinogradov, L. Moens, *J. Biol. Chem.* **2008**, *283*, 8773–8777 b) O. V. Kosmachevskaya, A. F. Topunov, *Appl. Biochem. Microbiol. (Moscow, Russ. Fed.)* **2009**, *45*, 563–587 c) B. J. Reeder, *Antioxid. Redox Signaling* **2010**, *13*, 1087–1123 d) M. T. Gladwin, J. R. Lancaster, B. A. Freeman, A. N. Schechter, *Nat. Med.* **2003**, *9*, 496–500 e) M. F. Perutz, M. G. Rossmann, A. F. Cullis, H. Muirhead, G. Will, A. C. T. North, *Nature* **1960**, *185*, 416–422 f) J. Everse, N. Hsia, *Free Radic. Biol. Med.* **1997**, *22*, 1075–1099.

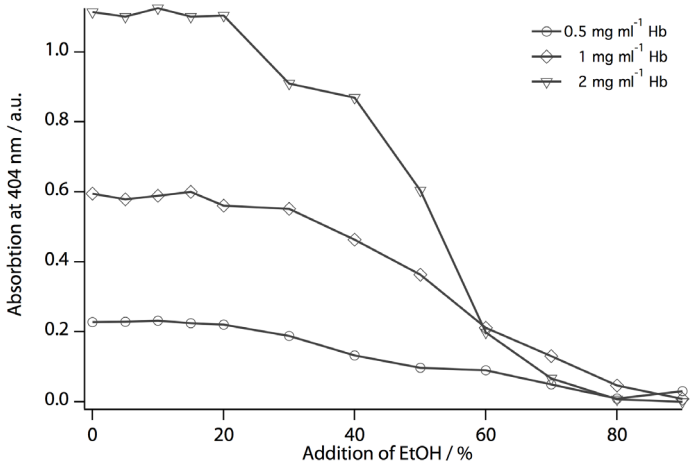


**Figure 2.13** Precipitation of Hb due to organic solvent measured by the absorbtion at 404 nm with UV/Vis spectroscopy. Addition of EtOH between 0 and 100% indicate that Hb can be precipitated with an addition of about 60% EtOH.

After the promising precipitation experiment with native Hb we functionalized Hb without an ATRP ligand. As Hb does not have any cysteins available for modification, we used the linker succinimidyl 6-hydrazinonicotinate acetone hydrazone (HyNic) to target the amino groups of lysine residues. After modification of the protein with the linker, Hb-HyNic was incubated with an excess of the synthesized TEDETA derivative described above, upon which a stable bis-aryl hydrazone bond was formed. The protein-ligand conjugate was then used to complex $Cu^{II}$ in an aqueous buffered $CuBr_2$ solution. Finally, the unbound copper was removed from the catalyst by size exclusion spin chromatography. The resulting Hb-$L_x$Cu was intended to be used to polymerize NiPAAm under ARGET ATRP conditions described for BSA. As this tetrameric Hb protein has four Fe-containing heme groups, we decided to carry out a control reaction with native Hb under the ARGET ATRP conditions that we used to polymerize NiPAAm, but not expecting a polymerization to occur. The aqueous reaction mixture consisted of Hb, monomer, HEBIB as the alkyl bromide initiator and an excess of ascorbic acid. To our surprise, the reaction yielded pNiPAAm, as confirmed by $^1H$ NMR (Figure 2.14). These observations indicated that the protein Hb is responsible for the polymerization. This ability of native enzymes to catalyze ATRP is discussed in chapters 3 to 5. Altough, we obtained exciting new results for Hb, we were still looking for a method to remove copper from a polymer solution and thus focused again to re-evaluate the BSA-$L_x$Cu system.

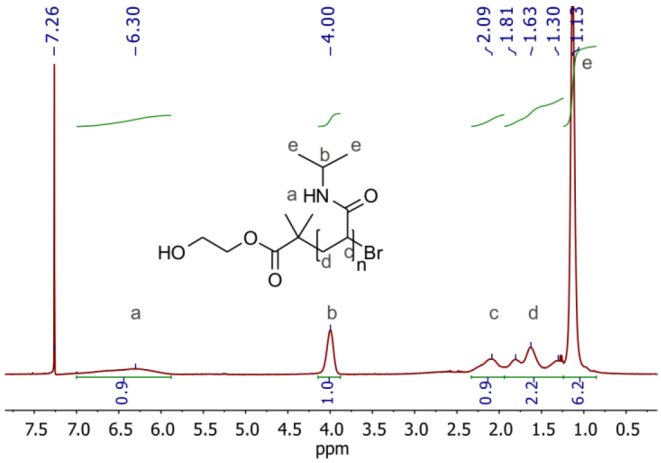


**Figure 2.14** $^{1}$H-NMR spectrum of a purified pNiPAAm sample obtained from a polymerization catalyzed by native Hb. $^{1}$H-NMR (400.1 MHz, $CDCl_3$) δ/ppm = 7.00 - 5.88 (bm, n.1H), 4.14 - 3.88 (bm, n.1H), 2.33 - 1.94 (bm, n.1H), 1.94 - 1.24 (bm, n.2H), 1.24 - 0.88 (bm, n.6H).

Another protein preciptation technique is salting out, whereby the protein undergoes interactions with the salt instead of the water due to increasing salt concentration, exposing the hydrophobic parts of the protein surface. This leads to an aggregation and precipitation of the protein. To this end, BSA was removed from solution by ammonium sulfate precipitation. Compared to the precipitation with organic solvent, the salting out gave better results. We polymerized NiPAAm using BSA-$L_x$Cu as a catalyst for ARGET ATRP with the conditions described above. Moreover, we removed the residual copper after polymerization by precipitation of the protein-catalyst conjugate using an addition of 25% saturated ammonium sulfate solution. Inductively coupled plasma atomic emission spectroscopy (ICP-AES) revealed that 76% of the copper was removed from solution by this technique, reducing the Cu content of the final polymer solution to 24 ± 3 ppb. Matyjaszewsky et al. have shown that ARGET ATRP can be perfomed with Cu catalyst concentrations as low as 50 ppm.[67] This concentration is still approximately $10^3$ times higher than the end-concentration we achieved, which could allow for biomedical and food grade applications.[68]

### 2.2.3.2 Dynabead Removal of Protein-Catalyst Conjugate

In a second approach we used Dynabeads to remove the residual copper from the final polymer solution. Dynabeads are commercially available, uniform, 2.8 µm superparamagnetic beads with recombinant Protein A (approximately 45 kDa) covalently coupled to the surface. We used rabbit IgG anti-BSA antibody to be added to the Dynabeads with Protein A. During a short incubation, the antibody binds to the Dynabeads. The tube was then placed on a magnet, where the beads migrated to the

[67] K. Matyjaszewski, W. Jakubowski, K. Min, W. Tang, J. Huang, W. A. Braunecker, N. V. Tsarevsky, *Proc. Natl. Acad. Sci.* **2006**, *103*, 15309–15314.
[68] N. V. Tsarevsky, K. Matyjaszewski, *Chem. Rev.* **2007**, *107*, 2270–2299.

side of the tube facing the magnet. Next, the supernatant was removed by aspiration. The now bead-bound antibody was used to capture BSA-$L_xCu$ in the final polymer solution. The bound protein-catalyst conjugate was collected on a magnet, utilizing the unique magnetic properties of the Dynabeads, whereas the polymer solution could be removed by aspiration (see Figure 2.15).

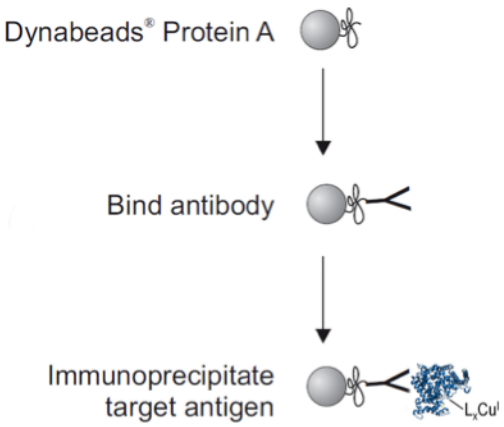


**Figure 2.15** Strategy to remove BSA-$L_xCu$ after polymerization from the product solution to reduce the residual copper in the final polymer. Dynabeads were functionalized with rabbit IgG anti-BSA antibody to capture BSA-$L_xCu$ in solution.

The precipitation of BSA-$L_xCu$ using Dynabeads reduced of the copper concentration by 44%. The Cu content of the final polymer solution was 162 ± 4 ppb, as determined by ICP-AES. This very elegant precipitation solution has the advantage that the catalyst conjugate could be eluted from the antibody and therfore be recycled for additional experiments. However, compared to the copper concentration of the ammonium sulfate precipitated sample, the removal of copper is not as effective.

## 2.3 Conclusions

To the best of our knowledge, we were the first to report ATRP catalysts conjugated to proteins.[69] We assessed BSA and Hb as potential proteins to attach a ligand to complex $Cu^{II}$ by means of bioconjugation chemistry. Hb turned out to polymerize NiPAAm without engineered copper complex and is discussed further in chapters 3 and 5. Although we were not interested to improve the reaction but rather to reduce the residual copper, using ARGET ATRP we were able to polymerize NiPAAm and PEGA with BSA-$L_xCu$ with a moderate control over the molecular weight and the polydispersity of the polymers. Globular proteins could serve as a functional handle to remove the copper containing catalyst effectively from solution. Such systems allow for a drastic reduction in the residual copper content in polymers synthesized by ATRP to ppb levels, either by precipitation or by Dynabead removal.

[69] N. Bruns, K. Renggli, F. Seidi, G. Kali, *Polym. Prepr. (Am. Chem. Soc., Div. Polym. Chem.)* **2011**, *52*, 521–522.

# 3 ATRPases - Native Enzymes for Atom Transfer Radical Polymerization[70]

*The advent of controlled/living radical polymerizations has made polymer science a key discipline for the preparation of nano-, biomedical-, and high tech-materials. Atom transfer radical polymerization (ATRP) is one of the most widely applied controlled/living radical polymerization. However, an ongoing quest is to develop ATRP reaction conditions that allow reducing the amount of catalyst needed, or to replace the currently used transition metal complex catalysts with less toxic ones. Using enzymes as catalysts is a classic strategy in the green chemistry approach, and many enzymatic polymerizations are known. However, controlled/living radical polymerizations that are catalyzed by enzymes or proteins have not been reported until our discovery that the metalloproteins horseradish peroxidase and hemoglobin can polymerize vinyl-monomers under conditions of activators regenerated by electron transfer (ARGET) ATRP.*

[70] Parts of this chapter were published in: a) K. Renggli, M. Spulber, J. Pollard, M. Rother, N. Bruns, *ACS Symp. Ser.* **2013**, *1144*, 163–171 b) G. Kali, T. B. Silva, S. J. Sigg, F. Seidi, K. Renggli, N. Bruns, *ACS Symp. Ser.* **2012**, *1011*, 171–181 c) T. B. Silva, M. Spulber, M. K. Kocik, F. Seidi, H. Charan, M. Rother, S. J. Sigg, K. Renggli, G. Kali, N. Bruns, *Biomacromolecules* **2013**, *14*, 2703–2712 d) S. J. Sigg, F. Seidi, K. Renggli, T. B. Silva, G. Kali, N. Bruns, *Macromol. Rapid Commun.* **2011**, *32*, 1710–1715.

## 3.1 Discovery of ATRPase Activity

In chapter 2 investigations of atom transfer radical polymerization (ATRP) catalysts were described that can be conjugated to proteins, in order to remove the residual copper after polymerization from the final polymer product. In the course of that research we were looking for a cheap and abundantly available protein to test the conjugation chemistry and the polymerization conditions as well as the precipitation ability. Our attention fell on bovine hemoglobin (Hb). As described in section 2.2.3.1, the control reaction with native Hb yielded polymer product, although we were not expecting a polymerization. Under the activators regenerated by electron transfer (ARGET) ATRP conditions native Hb with its four Fe-containing heme groups acted as catalyst for the polymerization of N-isopropylacrylamide (NiPAAm). The overnight reaction yielded a product that precipitated when the aqueous solution was heated above the lower critical solution temperature of poly(N-isopropylacrylamide) (pNiPAAm), i.e., over 32°C, and that redissolved when the solution was cooled back to room temperature. Figure 3.1 shows a typical enzyme-catalyzed (in this case HRP) polymerization of pNiPAAM and the effect of elevated temperature.

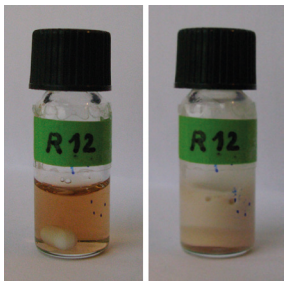


**Figure 3.1** A typical HRP-catalyzed polymerization of NiPAAm under ARGET ATRP conditions after 16 h. Photos were taken at 20°C (left) and at 40°C (right). The brown color of a HRP solution is seen, as well as a precipitate at elevated temperatures. This precipitate is the thermoresponsive polymer pNiPAAm.

To rule out the possibility that the polymerization was catalyzed by impurities on the glassware or in the commercial Hb preparation, we repeated the experiment several times with new glassware, with thoroughly cleaned glassware, and with Hb that was purified by size exclusion diafiltration (MWCO 10000 g $mol^{-1}$) in order to remove all low molecular weight impurities. All reactions yielded pNiPAAm. In contrast, when Hb was omitted from the reaction mixture, no polymer was obtained. Replacing Hb with hemin, the iron(III) proto-porphyrin IX chloride complex of the protein, did not result in any polymerization of NiPAAm either, one reason being that hemin is insoluble in water under acidic conditions.[71] These observations allow us to conclude that, indeed, the protein Hb is responsible for the polymerization. Further control reactions in which either HEBIB or AscA were left out of the reaction mixture yielded

[71] M. J. O'Neil, Ed., in *The Merck Index: an Encyclopedia of Chemicals, Drugs, and Biologicals*, Merck, Whitehouse Station, N.J., U.S.A., **2006**, p. 04644.

no pNiPAAm, indicating that HEBIB and AscA are essential to initiate and drive the polymerization.[72]

In many areas of synthetic chemistry, an environmentally friendly alternative to conventional catalysts is the use of enzymes.[73] Enzymes have been extensively investigated as catalysts for most major polymerization techniques, e.g., polycondensations, ring-opening polymerizations, and free-radical polymerizations.[74] However, Nature's catalysts were not known to mediate controlled/living radical polymerizations, despite the fact that several classes of proteins and enzymes contain transition metal ions at their active sites and therefore could potentially catalyze ATRP. Recently our group[75] and di Lena and coworkers[76] discovered concurrently and independently that some metalloproteins can mediate ATRP and named them ATRPases. These findings represent the first reports of biocatalytic, controlled/living radical polymerization.

---

72 G. Kali, T. B. Silva, S. J. Sigg, F. Seidi, K. Renggli, N. Bruns, *ACS Symp. Ser.*, American Chemical Society, Washington, DC, **2012**.

73 U. T. Bornscheuer, G. W. Huisman, R. J. Kazlauskas, S. Lutz, J. C. Moore, K. Robins, *Nature* **2012**, *485*, 185–194.

74 a) S. Kobayashi, A. Makino, *Chem. Rev.* **2009**, *109*, 5288–5353 b) K. Loos, Ed., *Biocatalysis in Polymer Chemistry*, Wiley-VCH Verlag GmbH & Co. KGaA, **2010**.

75 a) S. J. Sigg, F. Seidi, K. Renggli, T. B. Silva, G. Kali, N. Bruns, *Macromol. Rapid Commun.* **2011**, *32*, 1710–1715 b) G. Kali, T. B. Silva, S. J. Sigg, F. Seidi, K. Renggli, N. Bruns, *ACS Symp. Ser.*, American Chemical Society, Washington, DC, **2012** c) T. B. Silva, M. Spulber, M. K. Kocik, F. Seidi, H. Charan, M. Rother, S. J. Sigg, K. Renggli, G. Kali, N. Bruns, *Biomacromolecules* **2013**, *14*, 2703–2712.

76 a) Y.-H. Ng, F. di Lena, C. L. L. Chai, *Polym. Chem.* **2011**, *2*, 589 b) Y.-H. Ng, F. di Lena, C. L. L. Chai, *Chem. Commun.* **2011**, *47*, 6464–6466.

# 4 Horseradish Peroxidase as Catalyst for Atom Transfer Radical Polymerization[77]

*Severin J. Sigg, Farzad Seidi, Kasper Renggli, Tilana B. Silva, Gergely Kali and Nico Bruns*

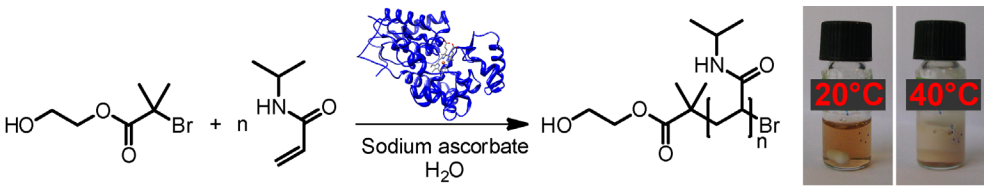


*The hemoprotein horseradish peroxidase (HRP) catalyzes the polymerization of N-isopropyl-acrylamide with an alkyl bromide initiator under conditions of activators regenerated by electron transfer atom transfer radical polymerization (ARGET ATRP) in the absence of any peroxide. This is a novel activity of HRP, which we propose to name ATRPase activity. Bromine-terminated polymers with polydispersity indices (PDIs) as low as 1.44 are obtained. The polymerization follows first order kinetics, but the evolution of molecular weight and the PDI upon increasing conversion deviate from the results expected for an ATRP mechanism. Conversion, $M_n$ and PDI depend on the pH and on the concentration of the reducing agent, sodium ascorbate. HRP is stable during the polymerization and does not unfold or form conjugates.*

[77] This chapter was published in: S. J. Sigg, F. Seidi, K. Renggli, T. B. Silva, G. Kali, N. Bruns, *Macromol. Rapid Commun.* **2011**, *32*, 1710–1715.

## 4.1 Introduction

Hemoproteins such as horseradish peroxidase (HRP; EC 1.11.1.7) have been studied extensively as catalysts for free radical polymerization of vinyl monomer[78] and aromatic compounds,[79] because they catalyze the electron transfer from hydrogen peroxide to a co-substrate, effectively creating radicals that initiate polymerization.[80] HRP is a 44 kDa protein that contains a heme B prosthetic group.[81] Reaction with hydrogen peroxide converts the $Fe^{III}$ resting state of the enzyme to an $Fe^{IV}$ porphyrin radical cation (compound I), which then transfers electrons to substrates along several pathways, including one via an $Fe^{IV}$ species (compound II). HRP-mediated free radical polymerization of vinyl monomers requires peroxide and often a co-substrate, like a β-diketon, as initiator.[82] It has been applied to the polymerization of a whole range of monomers including acrylamide,[83] methacrylates,[84] styrene,[85] and styrene derivatives.[86] Despite this body of literature, catalytic activity of hemoproteins in ATRP was unknown. We propose naming enzymes that exhibit catalytic activity under ATRP conditions as ATRPase, in addition to their conventional names.

## 4.2 Results & Discussion

### 4.2.1 ARGET ATRP of NiPAAm with HRP as ATRP catalyst

In our experiments, the reducing agent was planned to regenerate $Fe^{III}$ in the heme of HRP during the course of the polymerization under ARGET ATRP conditions. In typical experiments, HRP, the initiator 2-hydroxyethyl-2-bromoisobutyrate (HEBIB) and the monomer were dissolved in aqueous buffer under an argon atmosphere. Then, a

---

[78] a) A. Singh, D. L. Kaplan, *J. Polym. Environ.* **2002**, *10*, 85–91 b) A. Singh, D. L. Kaplan, in *Advances in Polymer Science*, Springer-Verlag, Berlin/Heidelberg, **2006**, pp. 211–224 c) F. Hollmann, in *Biocatalysis in Polymer Chemistry* (Ed.: K. Loos), Wiley-VCH Verlag GmbH & Co. KGaA, **2010**, pp. 143–163.

[79] a) M. Reihmann, H. Ritter, in *Advances in Polymer Science*, Springer-Verlag, Berlin/Heidelberg, **2006**, pp. 1–49 b) P. Walde, Z. Guo, *Soft Matter* **2011**, *7*, 316–331.

[80] F. Hollmann, I. W. C. E. Arends, *Polymers* **2012**, *4*, 759–793.

[81] a) A. M. Azevedo, V. C. Martins, D. M. Prazeres, V. Vojinović, J. M. Cabral, L. P. Fonseca, *Biotechnol. Annu. Rev.* **2003**, *9*, 199–247 b) N. C. Veitch, *Phytochemistry* **2004**, *65*, 249–259.

[82] F. Hollmann, I. W. C. E. Arends, *Polymers* **2012**, *4*, 759–793.

[83] a) R. A. Derango, L.-C. Chiang, R. Dowbenko, J. G. Lasch, *Biotechnol. Tech.* **1992**, *6*, 523–526 b) O. Emery, T. Lalot, M. Brigodiot, E. Maréchal, *J. Polym. Sci. A Polym. Chem.* **1997**, *35*, 3331–3333 c) T. Lalot, M. Brigodiot, E. Maréchal, *Polym. Int.* **1999**, *48*, 288–292 d) D. Teixeira, T. Lalot, M. Brigodiot, E. Maréchal, *Macromolecules* **2013**, *32*, 70–72 e) A. Durand, T. Lalot, M. Brigodiot, E. Maréchal, *Polymer* **2001**, *42*, 5515–5521 f) B. Kalra, R. A. Gross, *Green Chem.* **2002**, *4*, 174–178 g) Q. Zhao, J. Sun, H. Ren, Q. Zhou, Q. Lin, *J. Polym. Sci. A Polym. Chem.* **2008**, *46*, 2222–2232 h) R. L. Shogren, J. L. Willett, A. Biswas, *Carbohydr. Polym.* **2009**, *75*, 189–191 i) A. Durand, T. Lalot, M. Brigodiot, E. Marechal, *Polymer* **2000**, *41*, 8183–8192.

[84] a) A. Singh, D. L. Kaplan, *J. Macromol. Sci., Part A: Pure Appl. Chem.* **2004**, *41*, 1377–1386 b) B. Kalra, R. A. Gross, *Biomacromolecules* **2000**, *1*, 501–505 c) R. A. Derango, L.-C. Chiang, R. Dowbenko, J. G. Lasch, *Biotechnol. Tech.* **1992**, *6*, 523–526.

[85] A. Singh, D. Ma, D. L. Kaplan, *Biomacromolecules* **2000**, *1*, 592–596.

[86] a) A. Singh, S. Roy, L. Samuelson, F. Bruno, R. Nagarajan, J. Kumar, V. John, D. Kaplan, *J. Macromol. Sci., Part A: Pure Appl. Chem.* **2001**, *38*, 1219–1230 b) A. Singh, D. L. Kaplan, *Adv. Mater.* **2003**, *15*, 1291–1294.

buffered solution of the reducing agent sodium L-ascorbate was added, and the reaction was stirred at room temperature. Formation of poly(N-isopropylacrylamide) (pNiPAAm) was easily detectable by the precipitate that formed when the solution was heated above the lower critical solution temperature of pNiPAAm (32.5°C; Figure 3.1). $^1$H NMR confirmed the identity of the polymer (Figure 4.1). Gel permeation chromatography (GPC) revealed polymers with monomodal polymer weight distribution. The lowest PDI of 1.44 with a number average molecular weight ($M_n$) of 99900 g mol$^{-1}$ was observed for a reaction at pH 6.0 after 2.5 h (see below). No formation of pNiPAAm was observed in control reactions that lacked enzyme, initiator, or sodium ascorbate. $^1$H COSY NMR of a purified polymer revealed a pair of cross-peaks, which arise from the initiator fragment at the chain start (Figure 4.1).

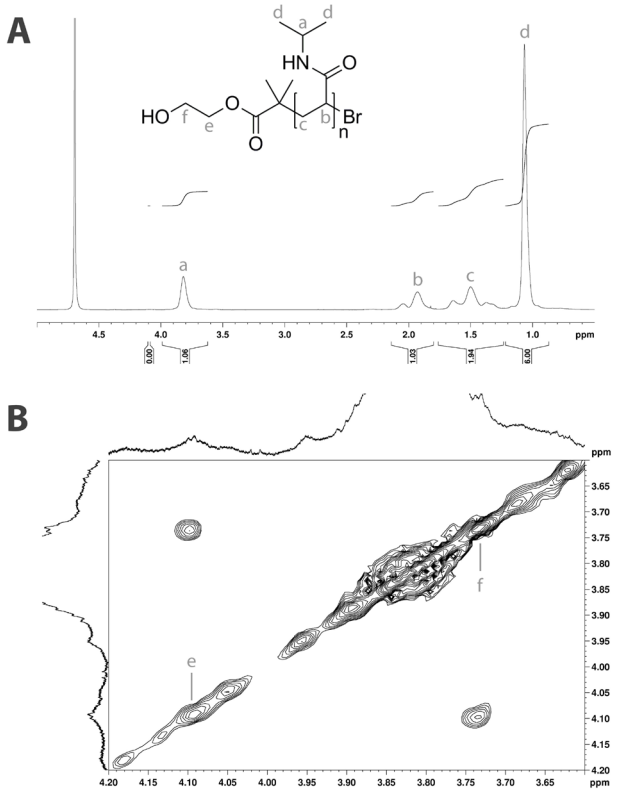


**Figure 4.1** a) $^1$H NMR spectrum and b) $^1$H COSY NMR spectrum of a purified pNiPAAm sample obtained from a polymerization catalyzed by HRP under ARGET ATRP conditions.

The purified pNiPAAm was further analyzed by neutron activation analysis (NAA) for its bromine content: 575 ± 35 mg bromine per gramm polymer were detected (Figure 4.2). With a $M_n$ of 92500 g mol$^{-1}$ (GPC) this concentration translates to 67% of pNiPAAm chains carrying one bromine atom, most probably at their chain end. These results allow us to conclude that HRP reacted with the initiator in order to create a radical species, most probable by an atom transfer of the initiator's bromine to the enzyme. HRP would thus change its oxidation state from $Fe^{III}$ to $Fe^{IV}$. The 2-

hydroxyethyl isobutyrate radical then started polymerization of the monomer. The degree of control in ATRP strongly depends on the ability of the catalyst to transfer the bromine back to the active chain end in order to form the dormant, bromine-terminated polymer species. The more the equilibrium is shifted toward the dormant chain and the reduced catalyst concentration, the more controlled or living is the polymerization.

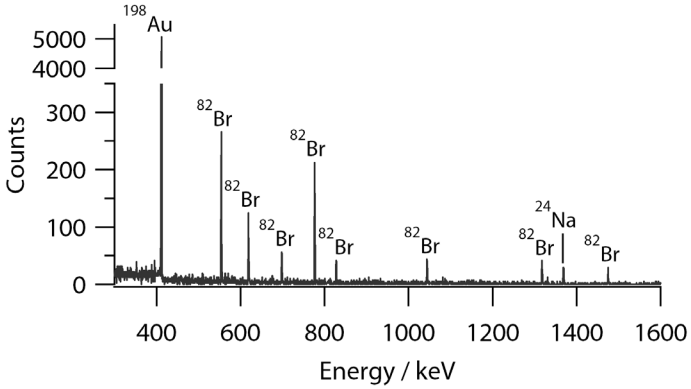


**Figure 4.2** Neutron activation analysis: γ-Spectrum of a purified pNiPAAm sample obtained from a polymerization catalyzed by HRP under ARGET ATRP conditions. The spectrum shows characteristic $^{82}$Br-peaks, as well as the peak of the internal gold standard.

The presence of a significant amount of bromine in the purified polymer proves that the reaction of the active chain toward the dormant species took place. Low PDIs indicate a controlled/living radical polymerization. However, some conditions (e.g., pH 7.5, 16 h reaction time) also yielded poorer PDIs above 2. All obtained polymers have higher molecular weight than expected from the monomer to initiator ratio. This could be due to an initiation catalyzed by HRP, followed by polymerization with some degree of control and chain termination, e.g., by the recombination of two radicals or by a reaction of the polymer radical with the $Fe^{III}$ of another native HRP molecule. HRP in its $Fe^{IV}$ state would then be regenerated to $Fe^{III}$ by reduction with ascorbate. A catalytic chain transfer mechanism can be ruled out, as this would produce double-bond terminated chains, which were not detected in the $^{1}$H NMR spectra. A possible mechanism is shown in Scheme 4.1.

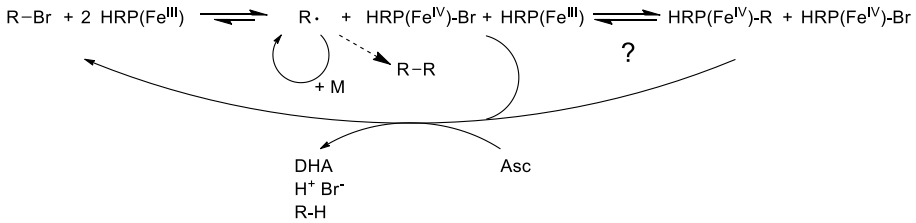


**Scheme 4.1** Putative mechanism of HRP-catalyzed polymerization under ARGET ATRP conditions. (Asc = ascorbate, DHA = dehydroascorbic acid)

As catalytic activity of enzymes can be strongly pH dependent, we systematically varied the pH of the polymerization between pH 5.2 and 10.5 (Figure 4.3). At highest and lowest pH no polymer formation was detected using $^1$H NMR. At intermediate pH, conversions from 3 to 78% were measured after a reaction time of 16 h, with a maximum at pH 7.0. The molecular weight followed a similar trend. Interestingly, PDI was around 1.7 between pH 6.0 and 7.0 and increased significantly in basic reaction conditions. Taking into account that HRP is stable over the analyzed pH range,[87] and that neither the initiator nor the monomer are protonable, these results show that pH influences the activity of HRP differently than its degree of control over the polymerization. Most likely, the rates of the activation reaction of alkyl bromides as well as the deactivation and termination reaction of radicals vary independently with the electrostatic potential distribution on the enzyme, and the redox potential of the heme. As the polymerization at pH 6.0 yielded polymers with a relative low PDI and a molecular weight closest to the theoretically expected value, all further reactions were performed at this pH.

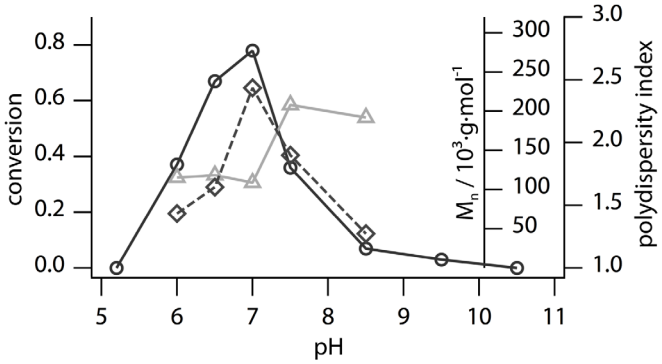


**Figure 4.3** Influence of pH on conversion (○), molecular weight (◊), and PDI (Δ) in HRP-catalyzed polymerizations of NiPAAm under ARGET ATRP conditions. (Ratio of HEBIB:NiPAAm:HRP 1:68:0.034; ratio ascorbate:HRP 33:1; reaction time: 16 h)

The concentration of ascorbate was also found to influence the polymerization reaction (Figure 4.4). The conversion increased linearly with increasing ascorbate concentration, while PDI and $M_n$ values increased and decreased, respectively. If deactivation reactions of radicals happened frequently during the polymerization, HRP accumulated in the non-active $Fe^{IV}$ form. The reducing agent would then have been necessary to regenerate the native oxidation state and thus to increase conversion. An initiation by sodium ascorbate alone can be ruled out, due to the fact that no polymer is formed in the abscence of HEBIB and that NMR of purified polymers showed no signals charateristic of ascorbate or its derivatives.

[87] D. Schomburg, M. Salzmann, D. Stephan, *Enzyme Handbook 7*, Springer, **1993**.

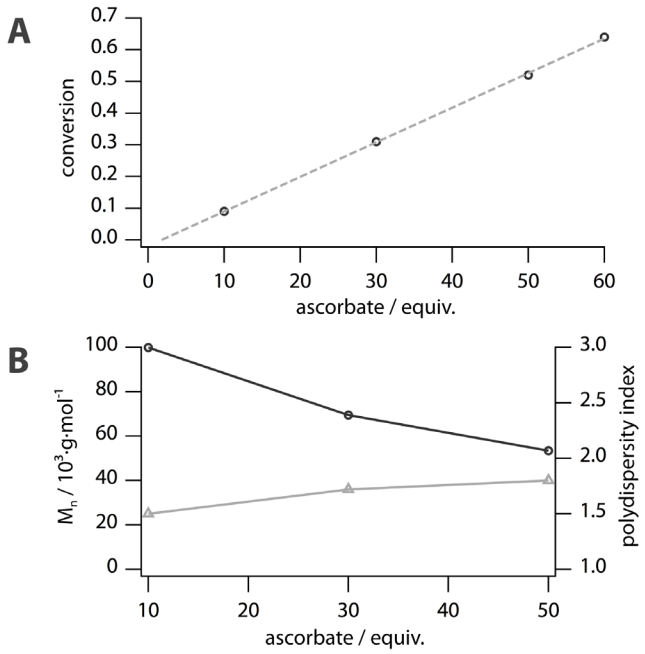


**Figure 4.4** Influence of reducing agent/enzyme ratio on the HRP-catalyzed polymerization of NiPAAm under ARGET ATRP conditions. A) Conversion, B) molecular weight (○) and PDI (Δ) as a function of equivalents sodium ascorbate. (Ratio of HEBIB:NiPAAm:HRP 1:68:0.034; pH 6.0; reaction time: 16 h)

In order to gain further insight into the mechanism of the HRP-mediated polymerization, the reaction kinetics and the evolution of the molecular weight and molecular weight distribution were followed by $^1$H NMR and by GPC for a polymerization at pH 6.0 (Figure 4.5). One characteristic of controlled/living radical polymerizations is that they follow first order kinetics, which results in a linear correlation between reaction time and the negative natural logarithm of the conversion. Indeed, the corresponding graph shows a linear range from initiation to about 7 h reaction time. At longer reaction times, the reaction slowed down and the polymerization came to a stop at a conversion of 48% after 24 h, possibly due to the depletion of ascorbate. The number average molecular weight of the polymer was 99900 g mol$^{-1}$ at the first time point and then decreased with increasing conversion. However, the total signal intensity in the GPC increased with conversion. The PDI was 1.44 at the beginning and increased during the course of the polymerization. These findings are not in agreement with the typical ATRP mechanism that results in a proportional increase of $M_n$ with conversion and constant or slightly decreasing PDIs.[88] A detailed inspection of the GPC traces (Figure 4.5c) reveals that, at the beginning of the reaction, quite large and relatively narrowly distributed polymers were formed. In the course of the reaction, these chains did not grow significantly. More chains of the

[88] K. Matyjaszewski, W. Jakubowski, K. Min, W. Tang, J. Huang, W. A. Braunecker, N. V. Tsarevsky, *Proc. Natl. Acad. Sci.* **2006**, *103*, 15309–15314.

similar length formed in addition to some shorter chains. These shorter chains were responsible for lowering the average molecular weight and broadening the molecular weight distribution. Whether they were bromine terminated and would grow further or whether they were irreversibly terminated cannot be distinguished by GPC. The maximum chain length appears to be determined by the precise reaction conditions. One possible explanation would be that the accessibility of the enzyme's active site depends on the length of the polymer chain, with a lower probability of longer chains to reach the active site, possibly with an upper size limit. Another possibility could be that HRP itself acts as a chain termination agent by the addition of the radical of the growing chain to an HRP in its resting $Fe^{III}$ state. As the HRP was subsequently reduced back to its native redox state, this would have resulted in a catalytic chain termination that yielded H-terminated polymer chains.

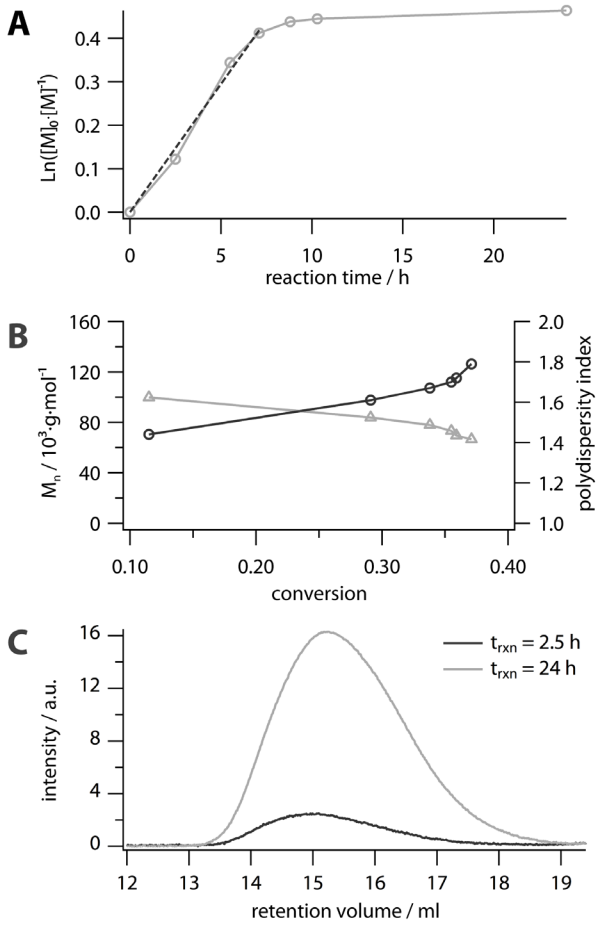


**Figure 4.5** a) Kinetic plot, b) molecular weight (Δ) and PDI (○) as a function of conversion, and c) selected GPC traces of a HRP-catalyzed polymerization of NiPAAm under ARGET ATRP conditions. (Ratio of HEBIB:NiPAAm:HRP 1:68:0.034; ratio ascorbate:HRP 33:1; pH 6.0)

### 4.2.2 Biochemical Characterization of HRP Before and After Polymerization

A catalyst is defined as a reactant which is not consumed during the reaction (and which accelerates a reaction). From the data presented above, it cannot be derived if HRP acts as a catalyst in the polymerization. Several reactions are plausible that could permanently alter the structure of HRP. These include unfolding and denaturation, which could also lead to the dissociation of the heme from the protein, the permanent trapping of the iron in an oxidation state other than the native $Fe^{III}$, and the formation of HRP-polymer conjugates. Therefore, several biochemical methods were applied to characterize the HRP before and after the polymerization (Figure 4.6).

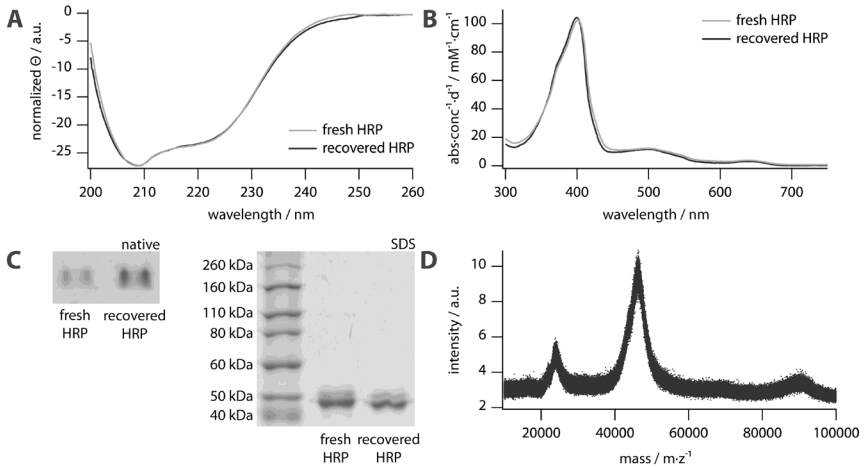


**Figure 4.6** Characterization of HRP before (grey) and after (black) a polymerization of NiPAAm under ARGET ATRP conditions at pH 6.0 for 16 h. a) Circular dichroism spectra, b) UV/Vis spectra, c) native and SDS gel electrophoresis. d) MALDI-TOF mass spectrum of recycled HRP shows the molecular ion peak of $HRP^{+}$ at m $z^{-1}$ 44000, $HRP^{2+}$ at m $z^{-1}$ 22000, HRP $dimer^{+}$ at m $z^{-1}$ 88000 and HRP $trimer^{2+}$ weak at m $z^{-1}$ 66000.

Circular dichroism (CD) spectroscopy is sensitive to the secondary structure of proteins. The CD spectra of native HRP and HRP purified from the polymerization mixture are typical for an α-helix-rich protein and do not show any significant differences to untreated HRP, indicating that the HRP did not unfold. The UV/Vis spectra of the two samples are very similar and have Soret maxima between 400 and 402 nm, and two smaller maxima at 499 and 643 nm, respectively. Such spectra correspond to HRP in its $Fe^{III}$ resting state.[89] The presence of compound II, compound III, or ferrous-HRP can be ruled out, as they possess Soret maxima between 415 and 437 nm.[90] Thus, HRP is in its native oxidation state before and after polymerization.

[89] W. E. Blumberg, J. Peisach, B. A. Wittenberg, J. B. Wittenberg, *J. Biol. Chem.* **1968**, *243*, 1854–1862.

[90] a) J. B. Wittenberg, R. W. Noble, B. A. Wittenberg, E. Antonini, M. Brunori, J. Wyman, *J. Biol. Chem.* **1967**, *242*, 626–634 b) W. E. Blumberg, J. Peisach, B. A. Wittenberg, J. B. Wittenberg, *J. Biol. Chem.* **1968**, *243*, 1854–1862.

Formation of HRP-polymer conjugates, either by termination of a polymer chain with an HRP molecule or by grafting of a pNiPAAm chain from a radical on the enzyme, would result in an increase in the enzyme's molecular weight. SDS and native gel electrophoresis did not show any difference in the molecular mass of the two samples. Mass spectrometry analysis of the HRP after polymerization showed the typical molecular mass of 44 kDa of native HRP. We therefore conclude that no enzyme-polymer conjugates formed during the polymerization. Overall, the characterization of the HRP showed that the enzyme is not altered under ARGET ATRP conditions, proving that HRP acts as a catalyst.

## 4.3 Conclusion

Horseradish peroxidase (HRP) catalyzes the polymerization of NiPAAm under aqueous ARGET ATRP conditions with an organobromine initiator in the absence of any peroxide. This is a novel enzymatic activity. Peroxidases were previously known to catalyze polymerizations in the presence of hydrogen peroxide and other peroxides. The HRP mediated polymerization under ARGET ATRP conditions yielded polymers with relative low, albeit not excellent PDIs down to 1.44 and number average molecular weights between 50000 and 220000 g $mol^{-1}$. Signals from the initiator were detected in the NMR spectra of a purified polymer sample, and the sample was shown to contain a significant amount of bromine.

We assume that several reactions compete with each other: the initiation by atom transfer of a bromine from the initiator (and from dormant chains) to the HRP, the radical chain propagation, the deactivation toward the dormant species in an ATRP equilibrium, a termination reaction with a second HRP molecule and other radical termination reactions such as recombination. As control over the radical polymerization is not perfect, we further assume that the ATRP equilibrium is shifted toward the radical site. Sodium ascorbate plays a crucial role and regenerates atom transfer inactive HRP. However, in this first report we did not quantify the individual rate constants or the ATRP equilibrium constant. Also, enzymatic reactions might follow a mechanism completely different from well-understood reactions in organic or polymer chemistry. To elucidate the exact mechanism of HRP mediated polymerization under ARGET ATRP conditions and to identify the parameters that can increase the controlled/living character of the polymerization is part of our ongoing research. Nevertheless, HRP is catalytically active in this polymerization and can therefore be called an ATRPase. As HRP is non-toxic and compatible with food-grade packaging, polymers synthesized with this protein will not have the toxicity problems encountered in conventional ATRP-based polymers. ATRPases might become a green alternative to conventional ATRP catalysts. Finally, we are also aware of the fact that a possible *in vivo* formation of radicals by the reaction of organohalogen compounds with peroxidases and related enzymes might be an explanation for the toxicity of many halogenated organic compounds and may be part of yet undiscovered metabolic pathways.

# 5 Hemoglobin and Red Blood Cells Catalyze Atom Transfer Radical Polymerization[91]

*Tilana B. Silva, Mariana Spulber, Marzena K. Kocik, Farzad Seidi, Himanshu Charan, Martin Rother, Severin J. Sigg, Kasper Renggli, Gergely Kali and Nico Bruns*

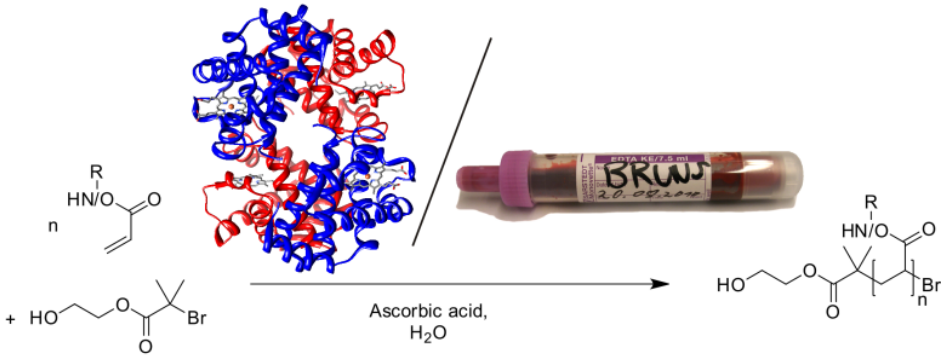


Hemoglobin (Hb) is a promiscuous protein that not only transports oxygen, but also catalyzes several biotransformations. A novel in vitro catalytic activity of Hb is described. Bovine Hb and human erythrocytes were found to display ATRPase activity, i.e., they catalyzed the polymerization of vinyl monomers under conditions typical for atom transfer radical polymerization (ATRP). N-isopropylacrylamide (NiPAAm), poly(ethylene glycol) methyl ether acrylate (PEGA), and poly(ethylene glycol) methyl ether methacrylate (PEGMA) were polymerized using organobromine initiators and the reducing agent ascorbic acid in acidic aqueous solution. In order to avoid chain transfer from polymer radicals to Hb's cysteine residues, the accessible cysteines were blocked by a reaction with a maleimide. The formation of polymers with bromine chain ends, relatively low polydispersity indices (PDI), first order kinetics and an increase in the molecular weight of poly(poly(ethylene glycol) methyl ether acrylate) (pPEGA) and poly(poly(ethylene glycol) methyl ether methacrylate) (pPEGMA) upon conversion indicate that control of the polymerization by Hb occurred via reversible atom transfer between the protein and the growing polymer chain. For pPEGA and pPEGMA, the reactions proceeded with a good to moderate degree of control. Sodium dodecyl sulfate (SDS) gel electrophoresis, circular dichroism spectroscopy, and time-resolved ultraviolet/visible (UV/Vis) spectroscopy revealed that the protein was stable during polymerization, and only underwent minor conformational changes. As Hb and erythrocytes are readily available, environmentally friendly, and nontoxic, their ATRPase activity is a useful tool for synthetic polymer chemistry. Moreover, this novel activity enhances the understanding of Hb's redox chemistry in the presence of organobromine compounds.

[91] This chapter was published in: T. B. Silva, M. Spulber, M. K. Kocik, F. Seidi, H. Charan, M. Rother, S. J. Sigg, K. Renggli, G. Kali, N. Bruns, *Biomacromolecules* **2013**, *14*, 2703–2712.

## 5.1 Introduction

Hemoglobin (Hb) is the main component of red blood cells of vertebrates. Perhaps the most commonly known function of the protein (even to the layman) is its capacity to bind and transport oxygen. This makes Hb essential for many life forms.[92] Not surprisingly, Hb is one of the most widely investigated proteins. Since its discovery and the exploration of its primary functions in the middle of the 19th century,[93] countless papers have been published describing its physiological role and its biochemistry.[94] Over the years, knowledge has emerged that Hb is a promiscuous protein that can play many more roles other than solely carrying oxygen. The iron-containing heme protein is also directly and indirectly involved in the transport of $CO_2$ and can react with, bind to, and transport many other gaseous molecules, such as NO, $H_2S$, or CO.[95] Moreover, Hb is a redox enzyme with a distinct pseudoperoxidase activity *in vitro* and *in vivo*, because its iron can cycle between oxidation states II, III, and IV.[96] Hb not only catalyzes the conversion of different inorganic peroxides, such as $H_2O_2$[97] and sodium perborate,[98] but also of various alkyl peroxides and lipid hydroperoxides.[99] Examples for Hb's peroxidase activity are the forensic luminol test for blood,[100] oxidation of pyrogallol,[101] or bisphenol A[102] by $H_2O_2$ and the initiation of polymerization of aniline induced by $H_2O_2$.[103] Hb is also known to react with

---

92 a) A. I. Alayash, F. D'Agnillo, P. W. Buehler, *Expert Opin. Biol. Ther.* **2007**, *7*, 665–675 b) C. Natanson, S. J. Kern, P. Lurie, S. M. Banks, S. M. Wolfe, *JAMA, J. Am. Med. Assoc.* **2008**, *299*, 2304–2312 c) F. E. Lui, R. Kluger, *ChemBioChem* **2010**, *11*, 1816–1824.

93 a) F. L. Hünefeld, *Der Chemismus in Der Thierischen Organisation*, F. a. Brockhaus, Leipzig, **1840** b) F. Hoppe-Seyler, *Med. Chem. Untersuch.* **1866**, *1*, 133–140.

94 a) S. N. Vinogradov, L. Moens, *J. Biol. Chem.* **2008**, *283*, 8773–8777 b) O. V. Kosmachevskaya, A. F. Topunov, *Appl. Biochem. Microbiol. (Moscow, Russ. Fed.)* **2009**, *45*, 563–587 c) B. J. Reeder, *Antioxid. Redox Signaling* **2010**, *13*, 1087–1123 d) M. T. Gladwin, J. R. Lancaster, B. A. Freeman, A. N. Schechter, *Nat. Med.* **2003**, *9*, 496–500 e) M. F. Perutz, M. G. Rossmann, A. F. Cullis, H. Muirhead, G. Will, A. C. T. North, *Nature* **1960**, *185*, 416–422 f) J. Everse, N. Hsia, *Free Radic. Biol. Med.* **1997**, *22*, 1075–1099.

95 a) O. V. Kosmachevskaya, A. F. Topunov, *Appl. Biochem. Microbiol. (Moscow, Russ. Fed.)* **2009**, *45*, 563–587 b) B. J. Reeder, *Antioxid. Redox Signaling* **2010**, *13*, 1087–1123 c) M. T. Gladwin, J. R. Lancaster, B. A. Freeman, A. N. Schechter, *Nat. Med.* **2003**, *9*, 496–500.

96 a) O. V. Kosmachevskaya, A. F. Topunov, *Appl. Biochem. Microbiol. (Moscow, Russ. Fed.)* **2009**, *45*, 563–587 b) B. J. Reeder, *Antioxid. Redox Signaling* **2010**, *13*, 1087–1123 c) J. Everse, N. Hsia, *Free Radic. Biol. Med.* **1997**, *22*, 1075–1099.

97 a) J. Everse, N. Hsia, *Free Radic. Biol. Med.* **1997**, *22*, 1075–1099 b) A. I. Alayash, R. P. Patel, R. E. Cashon, *Antioxid. Redox Signaling* **2001**, *3*, 313–327.

98 T. I. Quickenden, P. D. Cooper, *Luminescence* **2001**, *16*, 251–253.

99 a) O. V. Kosmachevskaya, A. F. Topunov, *Appl. Biochem. Microbiol. (Moscow, Russ. Fed.)* **2009**, *45*, 563–587 b) B. J. Reeder, *Antioxid. Redox Signaling* **2010**, *13*, 1087–1123 c) A. I. Alayash, R. P. Patel, R. E. Cashon, *Antioxid. Redox Signaling* **2001**, *3*, 313–327.

100 a) T. I. Quickenden, P. D. Cooper, *Luminescence* **2001**, *16*, 251–253 b) W. Specht, *Angew. Chem.* **1937**, *50*, 155–164R. A. Zweidinger, L. T. Lytle, C. G. Pitt, *J. Forensic Sci.* **1973**, *18*, 296–302.

101 C. Huang, H. Bai, C. Li, G. Shi, *Chem. Commun.* **2011**, *47*, 4962–4964.

102 T. Tang, H. Fan, S. Ai, R. Han, Y. Qiu, *Chemosphere* **2011**, *83*, 255–264.

103 a) X. Hu, Y. Y. Zhang, K. Tang, G. L. Zou, *Synth. Met.* **2005**, *150*, 1–7 b) X. Hu, K. Tang, S. G. Liu, Y. Y. Zhang, G. L. Zou, *React. Funct. Polym.* **2005**, *65*, 239–248 c) X. Hu, X. S. Shu, X. W. Li, S. G. Liu, Y. Y. Zhang, G. L. Zou, *Enzyme Microb. Technol.* **2006**, *38*, 675–682.

organobromine compounds,[104] and many halocarbons have toxic effects on red blood cells.[105] However, the mechanisms involved in these reactions have only been elucidated in some instances: Bromomalononitrile reacts in a noncatalytic redox reaction to yield the corresponding alkane, bromide ions, and oxidized Hb, i.e., methemoglobin.[106] The reductive dehalogenation reaction proceeds via radicals that are thought to be quenched by reaction with another Hb. On the other hand, polyhalogenated compounds such as $CF_3CHBrCl$ and $BrCCl_3$ react with the prosthetic group of Hb to form modified heme[107] and protein-bound heme adducts.[108] Despite this variety of reactions involving Hb and its availability in large quantities at low cost, this protein has not found widespread use as a catalyst or reagent in the field of synthetic chemistry. The main technological interest resides in its potential use as a blood substitute,[109] or its application as a redox-active component on electrodes of sensing devices.[110]

## 5.2 Results & Discussion

We discovered the ability of bovine Hb and of human erythrocytes to act as ATRPase in the polymerizations of the monomers N-isopropylacrylamide (NiPAAm), poly(ethylene glycol) methyl ether acrylate (PEGA), and poly(ethylene glycol) methyl ether methacrylate (PEGMA) in aqueous solution with 2-hydroxyethyl-2-bromoisobutyrate (HEBIB) or 2-bromopropionitrile (BPN) as water-soluble initiators. The reactions were performed under ARGET ATRP conditions with ascorbic acid (AscA) as the reducing agent. No peroxides are needed to drive this reaction, and its mechanism differs substantially from any previously reported catalytic activity of Hb. Our discovery of Hb's ATRPase activity is described in chapter 3.

---

[104] a) R. S. Wade, C. E. Castro, *J. Am. Chem. Soc.* **1973**, *95*, 231–234 b) E. W. Bartnicki, N. O. Belser, C. E. Castro, *Biochemistry* **1978**, *17*, 5582–5586 c) R. Tolando, S. Cazzaro, R. Ferrara, M. Rezzadore, M. Manno, *Biochem. Pharmacol.* **1995**, *49*, 233–241 d) J. T. Kindt, A. Woods, B. M. Martin, R. J. Cotter, Y. Osawa, *J. Biol. Chem.* **1992**, *267*, 8739–8743 e) Y. Osawa, C. S. Fellows, C. A. Meyer, A. Woods, J. A. Castoro, R. J. Cotter, C. L. Wilkins, R. J. Highet, *J. Biol. Chem.* **1994**, *269*, 15481–15487.

[105] F. J. Hidalgo, R. Zamora, A. L. Tappel, *Toxicol. Lett.* **1990**, *52*, 191–199.

[106] a) R. S. Wade, C. E. Castro, *J. Am. Chem. Soc.* **1973**, *95*, 231–234 b) E. W. Bartnicki, N. O. Belser, C. E. Castro, *Biochemistry* **1978**, *17*, 5582–5586.

[107] R. Tolando, S. Cazzaro, R. Ferrara, M. Rezzadore, M. Manno, *Biochem. Pharmacol.* **1995**, *49*, 233–241.

[108] a) J. T. Kindt, A. Woods, B. M. Martin, R. J. Cotter, Y. Osawa, *J. Biol. Chem.* **1992**, *267*, 8739–8743 b) Y. Osawa, C. S. Fellows, C. A. Meyer, A. Woods, J. A. Castoro, R. J. Cotter, C. L. Wilkins, R. J. Highet, *J. Biol. Chem.* **1994**, *269*, 15481–15487.

[109] a) A. I. Alayash, F. D'Agnillo, P. W. Buehler, *Expert Opin. Biol. Ther.* **2007**, *7*, 665–675 b) C. Natanson, S. J. Kern, P. Lurie, S. M. Banks, S. M. Wolfe, *JAMA, J. Am. Med. Assoc.* **2008**, *299*, 2304–2312 c) F. E. Lui, R. Kluger, *ChemBioChem* **2010**, *11*, 1816–1824.

[110] a) S. Garabagiu, G. Mihailescu, *J. Electroanal. Chem.* **2011**, *659*, 196–200 b) Y. Wu, S. Hu, *Microchim. Acta* **2007**, *159*, 1–17 c) K. Charradi, C. Forano, V. Prevot, A. Ben Haj Amara, C. Mousty, *Langmuir* **2009**, *25*, 10376–10383.

### 5.2.1 Chain Transfer to the Cysteins of Hb and Suppression of this Side Reaction

The polymerizations catalyzed by Hb resulted in a brown solid when lyophilized (Figure 5.1). An additional purification step designed to remove all free Hb from the final polymerization product (redissolving in THF, followed by filtration over a plug of aluminum oxide and removal of the solvent), did not change the color of the product. PNiPAAm itself is a white solid, so that the color must derive from residual Hb. Furthermore, GPC revealed a bimodal molecular weight distribution of the polymer (Figure 5.1). The thiol group of surface-exposed cysteines in proteins can act as a chain transfer agent in radical polymerizations.[111] Bovine Hb has one cysteine residue on each of its two β-subunits.[112] These residues are located in conformational plastic domains and are accessible for reagents, as they react with maleimides.[113] Hence, Hb's cysteine residues could play the role of a chain transfer agent. Chain transfer would result in the formation of H-terminated pNiPAAm chains and Hb−pNiPAAm conjugates. This would explain the observation of the brown polymer, as made above. SDS gel electrophoresis confirmed this hypothesis, as it showed the presence of a smeared band at high molecular weights, indicative of protein−polymer conjugates (Figure 5.1).

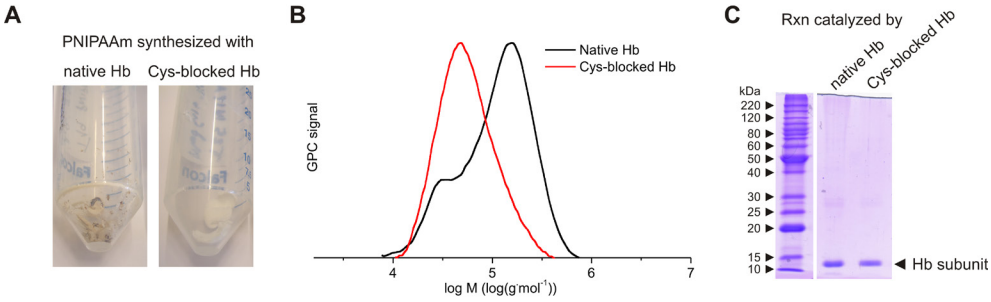


**Figure 5.1** Comparison of pNiPAAm obtained from polymerizations catalyzed by native Hb or Cys-blocked Hb under ARGET ATRP conditions. a) Photographs of purified polymers, b) GPC traces, c) SDS electrophoresis gel of polymerization mixtures. Experimental conditions: Ratio of HEBIB/NiPAAm/Asc/Hb 1:77:3:0.015.

In order to suppress chain transfer to the Hb, the cysteines on the protein were blocked by reaction with N-(2-hydroxyethyl)maleimide (HEMI). This reagent reacts with thiols in a Michael-type addition, resulting in thioether bonds that are not prone to attack by free radicals. All accessible cysteines were modified, as determined by Ellman's tests. The UV/Vis and the CD spectra of the Cys-blocked Hb do not show significant differences to the spectra of native Hb (Figure 5.2). These findings allow us

[111] A. Valdebenito, P. Espinoza, E. A. Lissi, M. V. Encinas, *Polymer* **2010**, *51*, 2503–2507.
[112] E. Reischl, A. L. Dafre, J. L. Franco, D. Wilhelm Filho, *Comp. Biochem. Physiol., Part C: Toxicol. Pharmacol.* **2007**, *146*, 22–53.
[113] Y. Zhang, V. S. Bhatt, G. Sun, P. G. Wang, A. F. Palmer, *Bioconjugate Chem.* **2008**, *19*, 2221–2230.

to conclude that the modification of the Hb did not alter the protein's structure. Polymerization of NiPAAm with Cys-blocked Hb yielded white products with monomodal molecular weight distributions (Figure 5.1). A typical sample had a number average molecular weight ($M_n$) of 45800 g $mol^{-1}$ and a polydispersity index (PDI) of 1.48 (GPC), while with native Hb yielded a polymer with a $M_n$ of 70200 g $mol^{-1}$ and a PDI of 1.80. Moreover, no polymer-protein conjugates were detected in SDS gel electrophoresis (Figure 5.1). Thus, chain transfer occurred with native Hb, but not with Hb in which cysteines were chemically blocked. As chain transfer is an unwanted reaction in ATRP, further reactions were carried out with Cys-blocked Hb.

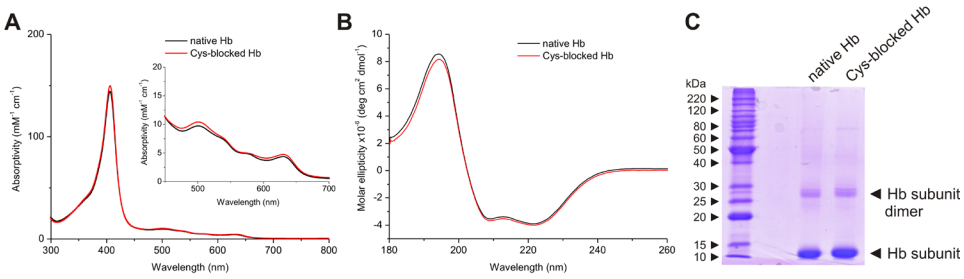


**Figure 5.2** Characterization of native Hb and Cys-blocked Hb. a) UV/Vis spectra, b) circular dichroism spectra, c) SDS gel electrophoresis.

### 5.2.2 Effect of pH on the ATRPase Activity of Cys-Blocked Hb

Since any catalytic activity of proteins are pH dependent, the polymerization of NiPAAm with Cys-blocked Hb was carried out within a pH range of 1.5 to 7.6. At pH 1.5 and pH 7.6 no polymer formed during a reaction time of 24 h, whereas polymerization occurred from pH 3.2 to 5.8 with a maximum conversion of 66% at pH 4.0. The conversion of polymerizations conducted at pH $\geq$ 4.5 varied considerably between multiple runs and were not reproducible. Furthermore, a color change from brown to green was observed for these reactions. This color change may be due to heme-to-protein covalent bond formation between a porphyrin radical and a radical on a nearby amino acid,[114] or due to the conversion of one of the pyrrole rings in the heme to pyrroline.[114] Such degradation of Hb's redox centers can explain the low and inconsistent conversions observed at these pH values. At pH 3.2 and 4.0, the reaction mixtures retained their brown color, and conversion of multiple runs was similar. Interestingly, the pH of reactions carried out with AscA in unbuffered water is 3.7. By chance, this pH is close to the optimal conditions (with respect to conversion) determined by systematic variation of pH. In conclusion, the polymerization catalyzed by Hb has a pH optimum in acidic conditions. To keep the reaction conditions as simple as possible, all further polymerizations were carried out in pure water with in situ acidification by the reducing agent, AscA.

[114] B. J. Reeder, *Antioxid. Redox Signaling* **2010**, *13*, 1087–1123.

### 5.2.3 Proof that Br-Transfer is Involved in ATRPase Activity

To provide evidence for Br-atom transfer involvement in the mechanism of the polymerization, a NiPAAm polymerization catalyzed by Cys-blocked Hb was quenched after 45 min. The resulting polymer was purified by passage through neutral aluminum oxide, followed by extensive dialysis in order to remove all traces of bromine ions and nonreacted initiator. The bromine content of the polymer was determined to be 300 ± 11 µg $g^{-1}$ by NAA. Combining this number with $M_n$ = 95400 g $mol^{-1}$ (PDI = 1.47) from GPC reveals that approximately 36% of polymer chains carry one bromine atom, most likely at their chain end. Additional evidence for Br-terminated chain ends came from a chain extension experiment. The purified polymer was used as a macroinitiator for conventional ATRP of NiPAAm in water, using a TEDETA copper(I)bromide complex as catalyst. The reaction was stopped after 24 h, and the molecular weight as well as the PDI of the polymer was determined by GPC (Figure 5.3). Compared to the macroninitiator, the $M_n$ of the pNiPAAm increased to 121700 g $mol^{-1}$, while the molecular weight distribution became broader, resulting in an increase in the PDI to 1.83. These are clear indications that further chain growth occurred in the second polymerization and confirms the presence of Br-terminated chain ends in the pNiPAAm obtained from the protein-catalyzed polymerization. The increase in PDI indicates that not all chains were able to initiate the chain extension polymerization, which fits the NAA results of nonquantitative bromination. A nonquantitative chain end functionalization is most probably due to side and termination reactions that compete with the ATRP equilibrium during the Hb-catalyzed polymerization, such as the reaction of radicals with a Hb($Fe^{II}$) species.

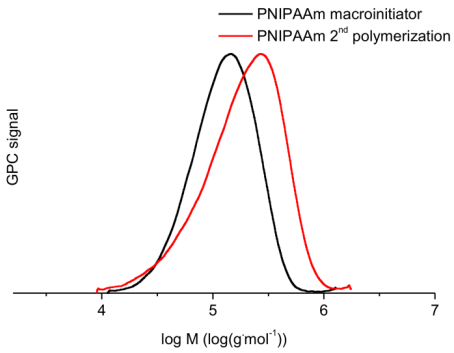


**Figure 5.3** GPC traces of a chain extension experiment. A polymerization of NiPAAm catalyzed by Cys-blocked Hb under ARGET ATRP conditions yielded a polymer that was used as a macroinitiator for a second polymerization of NIPAAm catalyzed by a conventional ATRP catalyst. Experimental conditions for the preparation of the pNiPAAm macroinitiator: Ratio of HEBIB/NiPAAm/AscA/Hb 1:79:1:0.008.

### 5.2.4 Kinetic Investigations

In order to gain insight into the mechanism of the polymerizations catalyzed by Cys-blocked Hb, kinetics as well as the evolution of molecular weight and PDI were followed by $^1$H NMR and GPC, respectively. First order kinetics is one of the premises of ATRP. A high degree of control of the polymerization manifests itself in a linear increase in molecular weight with conversion and low PDIs.[115] The semilogarithmic plot of $\ln([M]_0/[M])$ versus reaction time of NiPAAm polymerization is linear up to a reaction time of approximately 4 h (73% conversion) (Figure 5.4a). This proves that the polymerizations followed first order kinetics and indicates that the radical concentration was constant during the first hours of the reaction.

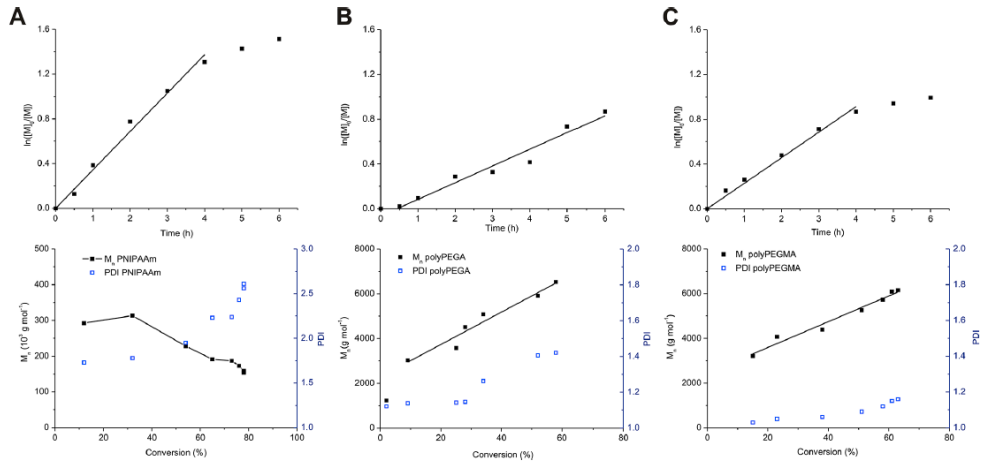


**Figure 5.4** Kinetic investigations of polymerizations catalyzed by Cys-blocked Hb under ARGET ATRP conditions. a) NiPAAm, b) PEGA, and c) PEGMA. Kinetic plots, and the evolution of molecular weight and PDI as a function of conversion are shown. Experimental conditions: a) ratio of HEBIB/NiPAAm/AscA/Hb 1:79:1:0.008, b) ratio of HEBIB/PEGA/AscA/Hb 1:78:3:0.007, c) ratio of HEBIB/PEGMA/AscA/Hb 1:75:1.5:0.008.

At longer reaction times, the polymerizations stopped. However, such a reaction could be restarted by the further addition of AscA (Figure 5.5), indicating that the polymerization stopped due to depletion of reducing agent and not due to irreversible inactivation of the biocatalyst. The second, restarted reaction also followed first-order kinetics, as indicated by a linear slope in the semilogarithmic plot. GPC revealed that, at the beginning of the reaction, pNiPAAm of rather high molecular weight ($M_n$ = 292500 g mol$^{-1}$) and a PDI of 1.73 formed (Figure 5.4a).

[115] N. V. Tsarevsky, K. Matyjaszewski, *Chem. Rev.* **2007**, *107*, 2270–2299.

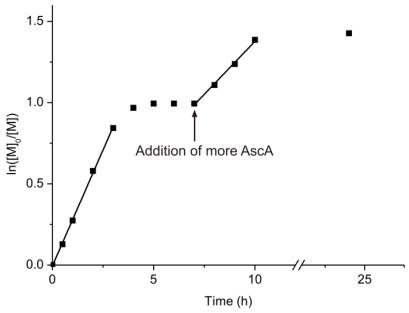


**Figure 5.5** Kinetic plot of a polymerization of NiPAAm catalyzed by Cys-blocked Hb under ARGET ATRP conditions. An additional degased aliquot of AscA (20 mg dissolved in 2 ml of water) was added to the reaction mixture after 7 h. Initial experimental conditions: Ratio of HEBIB/NiPAAm/AscA/Hb 1:78:1:0.008.

While the reaction still proceeded, more of these polymer chains formed, but also shorter chains that caused the average molecular weight to drop and the molecular weight distribution to broaden. The evolution of $M_n$ and PDI with conversion during the polymerization of NiPAAm suggests a low degree of control over the polymerization due to the presence of irreversible chain termination reactions,[116] e.g., caused by a low deactivation efficiency, or by reaction of a growing polymer radical with an Hb subunit in its $Fe^{II}$ state.

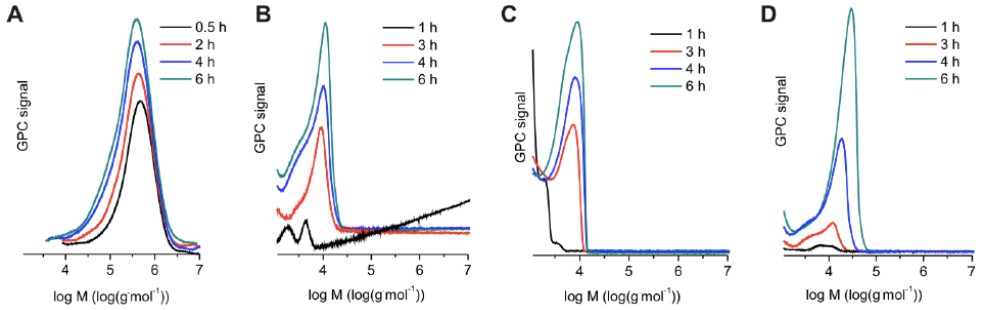


**Figure 5.6** a-b) Selected GPC traces of kinetic experiments in Figure 5.4: a) NiPAAm, b) PEGA, c) PEGMA. d) Selected GPC traces of the kinetic in Figure 5.9 (As monomer and polymer were not separated prior to GPC measurements during kinetic experiments, the non-reacted monomers PEGA and PEGMA give rise to a GPC signal below log M ≈ 3.2).

NiPAAm is well-known to be difficult to polymerize in a controlled/living way by means of ATRP in aqueous solution.[117] Therefore, polymerizations were also carried out with the monomers PEGA and PEGMA (Figure 5.4b, c). Both monomers

[116] M. Teodorescu, K. Matyjaszewski, *Macromolecules* **1999**, *32*, 4826–4831.
[117] a) G. Masci, L. Giacomelli, V. Crescenzi, *Macromol. Rapid Commun.* **2004**, *25*, 559–564 b) P.-E. Millard, N. C. Mougin, A. Böker, A. H. E. Müller, in *ACS Symp. Ser.*, American Chemical Society, Washington DC, **2009**, pp. 127–137.

polymerized with first order kinetics, however, the acrylate only reacted after an induction period of approximately 30 min. The molecular weights of both polymers increased linearly with conversion up to PS-apparent $M_n$ of 6150-6530 g $mol^{-1}$. The polydisperties were relative low: The PDI of PEGA rose from 1.14 at the beginning of the polymerization to 1.42 at 58% conversion, while the PDI of PEGMA stayed below 1.17 throughout the reaction. These findings show that the polymerization of PEGA and PEGMA was controlled/living by Cys-blocked hemoglobin. The increase in PDI at higher conversions suggests, however, that the degree of control is not perfect. The GPC traces show shoulders at lower molecular weight (Figure 5.6), indicating that chain termination reactions occurred.

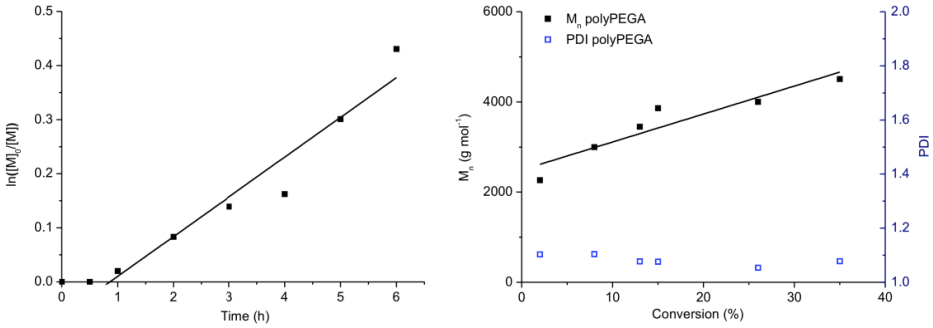


**Figure 5.7** Kinetic investigations of a BPN-initiated polymerization of PEGA catalyzed by Cys-blocked Hb under ARGET ATRP conditions. The kinetic plot, and the evolution of molecular weight and PDI as a function of conversion are shown. Experimental conditions: Ratio of BPN/PEGA/AscA/Hb 1:74:1:0.007.

The induction time observed in polymerizations of PEGA could be due to slow initiation. However, PEGA polymerizations that were initiated with the more reactive initiator 2-bromopropionitrile (BPN)[118] also showed this lag phase (Figure 5.7). It is therefore likely that the Hb needs to undergo some structural changes caused by interactions between protein, monomer, and polymer before it efficiently mediates the polymerization of PEGA. The BPN-initiated polymerization resulted in first-order kinetics, an increase in molecular weight with conversion, and the PDI stayed below 1.11.

### 5.2.5 Polymerizations Catalyzed by Erythrocytes

As Hb was found to be a catalyst for polymerizations under ARGET ATRP conditions, the question arose as to whether a similar polymerization could be catalyzed by fresh erythrocytes. To this end, red blood cells were obtained according to standard hospital procedures from blood samples of the Corresponding Author. Oxygen was then removed from the erythrocytes by treatment with argon, and the cells were added to reaction mixtures of HEBIB, AscA, and NiPAAm or PEGA, respectively, in water. Analytical samples of the NiPAAm polymerization were taken

[118] W. Tang, K. Matyjaszewski, *Macromolecules* **2007**, *40*, 1858–1863.

after 2 and 4 h. After 24 h, the mixture was probed for the presence of pNiPAAm by heating above 32ºC. A precipitate formed and redissolved when the mixture was cooled to room temperature, indicating that indeed pNiPAAm had been formed. Figure 5.8 provides photographic documentation of such an experiment. $^{1}$H NMR showed a conversion of 40% after 2 h, 78% after 4 h and full conversion after 24 h. The polymer was purified from the reaction mixture, yielding a brown solid after lyophilization. SDS electrophoresis confirmed the presence of polymer-protein conjugates along with unmodified Hb (Figure 5.8). GPC analysis revealed pNiPAAm with a $M_n$ of 55100 g mol$^{-1}$ and a PDI of 2.09 after 2 h. With increasing reaction time, $M_n$ decreased to 23900 g mol$^{-1}$, and the PDI increased to 3.48 at full conversion (Figure 5.8). A full kinetic was recorded for the erythrocyte-catalyzed polymerization of PEGA (Figure 5.9). The polymerization proceeded to 58% conversion within 4 h, after which it slowed down. It roughly followed first-order kinetics. In the course of the reaction the molecular weight of pPEGA increased linearly to a $M_n$ of 9240 g mol$^{-1}$. However, the PDI also increased from 1.18 at 1 h reaction time to 1.68 at 6 h, indicating a lower degree of control in the later stages of this polymerization.

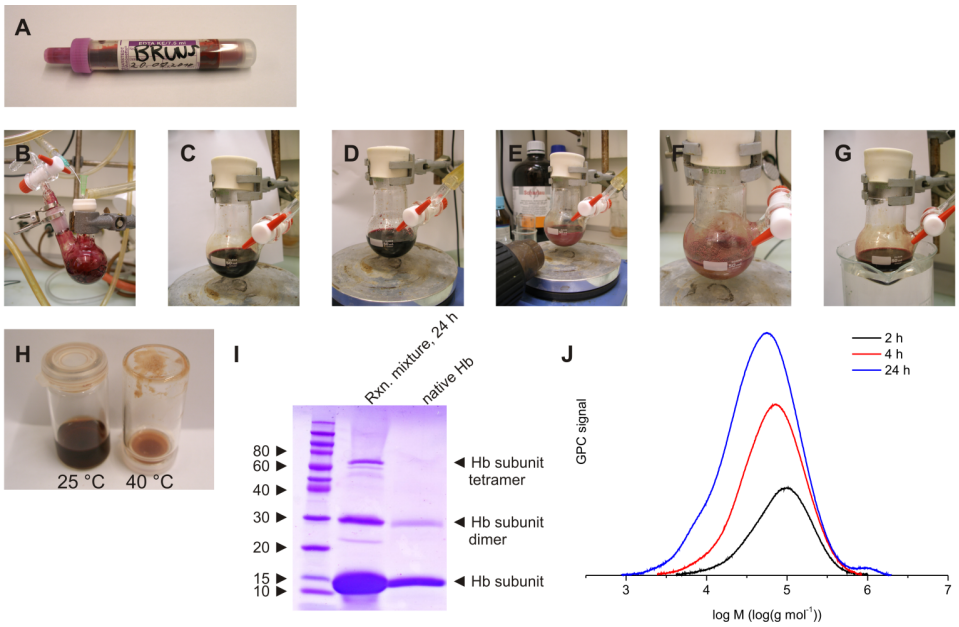


**Figure 5.8** Polymerization of NiPAAm under ARGET ATRP conditions using human erythrocytes as catalyst. a-h) Photographic documentation: a) Fresh sample of erythrocytes from the corresponding author, b) deoxygenation of erythrocytes by purging with argon, c) reaction mixture at the beginning of the polymerization, d) reaction mixture after overnight stirring, e) a precipitate formed upon gentle heating of the reaction mixture, indicating the presence of pNiPAAm, f) precipitate at approx. 40°C, g) upon cooling to room temperature, the precipitate dissolved, h) reaction mixture after filtration through a plug of neutral aluminium oxide, i) SDS gel electrophoresis of reaction mixture and native Hb, j) evolution of GPC traces during polymerization ($t_{rxn}$ = 2 h: $M_n$ = 55100 g mol$^{-1}$, PDI = 2.09, conversion = 40%; $t_{rxn}$ = 4 h: $M_n$ = 39900 g mol$^{-1}$, PDI = 2.37, conversion = 78%; $t_{rxn}$ = 24 h: $M_n$ = 23900 g mol$^{1}$, PDI = 3.48, conversion = 100%).

Both polymerizations show that red blood cells are able to catalyze polymerizations of vinyl-type monomers under ARGET ATRP conditions. The erythrocytes exhibited some control over the radical polymerization in the case of PEGA, but a lack of control in the case of NiPAAm. Moreover, protein-polymer conjugates were also formed. The lower degree of control compared to Cys-blocked Hb is not surprising, considering that crude erythrocyte samples contain many other molecules and proteins apart from Hb that could interfere with ATRP, e.g., by providing thiols that react with radicals. Furthermore, human Hb has six cysteine residues[119] that were not blocked with appropriate reagents. Nevertheless, the polymerizations with erythrocytes suggest that dehalogenation reactions that result in radical formation might also happen under anaerobic conditions *in vivo*.

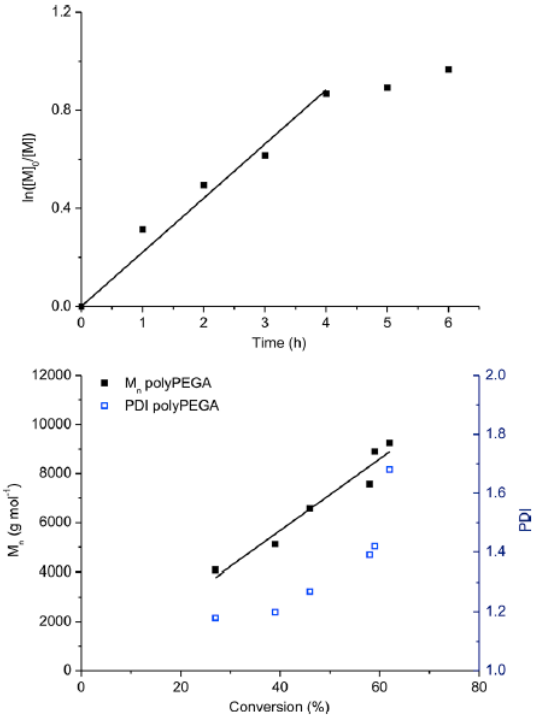


**Figure 5.9** Kinetic investigation of the polymerization of PEGA catalyzed by erythrocytes under ARGET ATRP conditions. The kinetic plot and the evolution of molecular weight and PDI as a function of conversion are shown. Experimental conditions: ratio of HEBIB/PEGA/AscA 1:78:3, 2 ml erythrocytes.

[119] E. Reischl, A. L. Dafre, J. L. Franco, D. Wilhelm Filho, *Comp. Biochem. Physiol., Part C: Toxicol. Pharmacol.* **2007**, *146*, 22–53.

### 5.2.6 Characterization of Hb Before, During, and After the Polymerization

If Hb acts as a catalyst in ARGET ATRP, it should be stable during the reaction and not suffer structural degradation. Reports in the literature show that some organohalides denaturate Hb,[120] while Hb is also reported to be structurally stable in the presence of other alkyl halides.[121] The heme is prone to attack by radicals;[122] however, covalent modifications to the heme do not necessarily impede catalytic activity of hemeproteins.[123] ARGET ATRP at pH 3.7 did not cause the protein to precipitate. As discussed above, SDS gel electrophoresis revealed that the Cys-blocked Hb subunits did not change in molecular weight during the reaction (Figure 5.1c), i.e., the protein did not form conjugates with polymers. CD spectroscopy was used to probe the secondary structure of the protein. The CD spectra of Cys-blocked Hb and of a protein sample that was recovered from a typical polymerization run of NiPAAm are presented in Figure 5.10a. Both far-UV spectra resemble each other and are typical of proteins rich in α-helices. However, the recovered Hb has slightly lower ellipticity. Thus, the overall structure of Hb was conserved during the polymerization, but minor changes occurred that decrease the helix content of the protein in favor of an irregular structure. Apart from these structural rearrangements, Cys-blocked Hb is stable under the acidic ARGET ATRP conditions.

---

120 R. S. Wade, C. E. Castro, *J. Am. Chem. Soc.* **1973**, *95*, 231–234.

121 a) R. S. Wade, C. E. Castro, *J. Am. Chem. Soc.* **1973**, *95*, 231–234 b) E. W. Bartnicki, N. O. Belser, C. E. Castro, *Biochemistry* **1978**, *17*, 5582–5586.

122 a) R. Tolando, S. Cazzaro, R. Ferrara, M. Rezzadore, M. Manno, *Biochem. Pharmacol.* **1995**, *49*, 233–241 b) J. T. Kindt, A. Woods, B. M. Martin, R. J. Cotter, Y. Osawa, *J. Biol. Chem.* **1992**, *267*, 8739–8743 c) Y. Osawa, C. S. Fellows, C. A. Meyer, A. Woods, J. A. Castoro, R. J. Cotter, C. L. Wilkins, R. J. Highet, *J. Biol. Chem.* **1994**, *269*, 15481–15487.

123 a) B. J. Reeder, *Antioxid. Redox Signaling* **2010**, *13*, 1087–1123 b) K. P. Moore, S. G. Holt, R. P. Patel, D. A. Svistunenko, W. Zackert, D. Goodier, B. J. Reeder, M. Clozel, R. Anand, C. E. Cooper, et al., *J. Biol. Chem.* **1998**, *273*, 31731–31737.

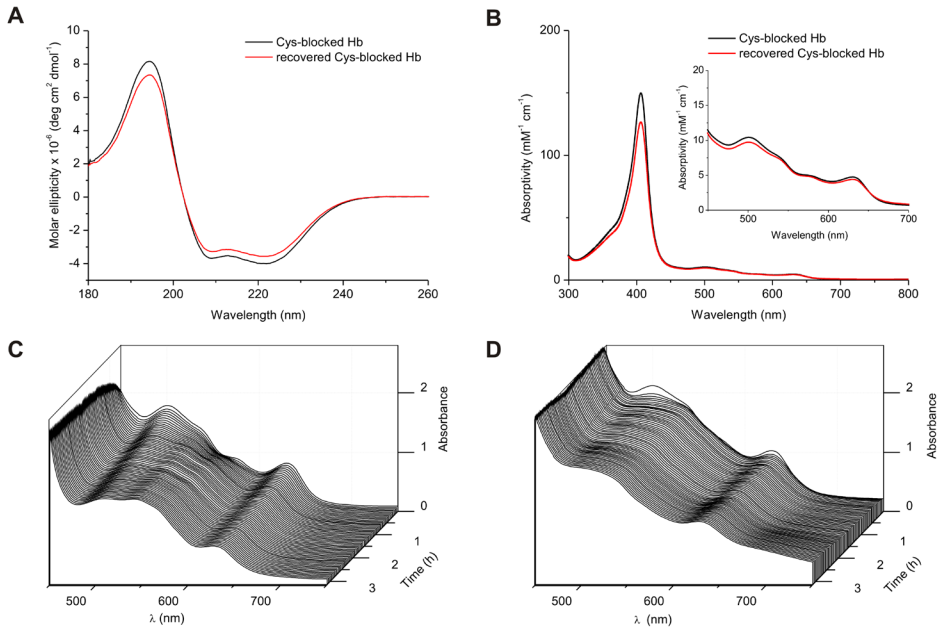


**Figure 5.10** Characterization of Cys-blocked Hb before, during and after a polymerization of NiPAAm under ARGET ATRP conditions. a) Circular dichroism spectra, b) UV/Vis spectra, c) Time dependent Vis spectra of Cys-blocked Hb during a reduction with AscA in the absence of initiator and monomer. The first spectrum was recorded after the addition of AscA. Spectra were recorded every 45 s. Experimental conditions: Ratio of AscA/Hb 1:0.03, pH 3.7. d) Time dependent Vis spectra of Cys-blocked Hb during a polymerization of NiPAAm under ARGET ATRP conditions. The first spectrum was recorded after the addition of AscA. Spectra were recorded every 45 s. Experimental conditions: Ratio of HEBIB/NiPAAm/AscA/Hb 1:79:1:0.008.

UV/Vis spectroscopy allows a determination of the oxidation state of the Fe in Hb.[124] Furthermore, it has been used to assess whether and how radicals covalently alter the structure of the heme,[125] lead to heme-to-protein cross-links,[126] or lead to the formation of hemichromes.[127] The spectrum of Cys-blocked Hb before polymerization

[124] a) B. J. Reeder, *Antioxid. Redox Signaling* **2010**, *13*, 1087–1123 b) W. G. Zijlstra, A. Buursma, *Comp. Biochem. Physiol., Part B: Biochem. Mol. Biol.* **1997**, *118*, 743–749 c) C. C. Winterbourn, in *Methods in Enzymology* (Eds.: L. Packer, A.N. Glazer), Academic Press, San Diego, CA, USA, **1990**, pp. 265–272.

[125] a) B. J. Reeder, *Antioxid. Redox Signaling* **2010**, *13*, 1087–1123 b) R. Tolando, S. Cazzaro, R. Ferrara, M. Rezzadore, M. Manno, *Biochem. Pharmacol.* **1995**, *49*, 233–241 c) J. T. Kindt, A. Woods, B. M. Martin, R. J. Cotter, Y. Osawa, *J. Biol. Chem.* **1992**, *267*, 8739–8743 d) Y. Osawa, C. S. Fellows, C. A. Meyer, A. Woods, J. A. Castoro, R. J. Cotter, C. L. Wilkins, R. J. Highet, *J. Biol. Chem.* **1994**, *269*, 15481–15487.

[126] a) B. J. Reeder, *Antioxid. Redox Signaling* **2010**, *13*, 1087–1123 b) J. T. Kindt, A. Woods, B. M. Martin, R. J. Cotter, Y. Osawa, *J. Biol. Chem.* **1992**, *267*, 8739–8743.

[127] a) C. C. Winterbourn, in *Methods in Enzymology* (Eds.: L. Packer, A.N. Glazer), Academic Press, San Diego, CA, USA, **1990**, pp. 265–272 b) M. Minetti, C. Mallozzi, G. Scorza, M. D. Scott, F. A. Kuypers, B. H. Lubin, *Arch. Biochem. Biophys.* **1993**, *302*, 233–244 c) W. Kaca, R. I. Roth, K. D. Vandegriff, G. C. Chen, F. A. Kuypers, R. M. Winslow, J. Levin, *Biochemistry* **1995**, *34*, 11176–11185.

(Figure 5.10) shows a maximum of the Soret band at 406 nm, two minor maxima at 500 and 630 nm, and two shoulders at 538 and 576 nm. This corresponds to the typical absorption pattern of methemoglobin.[128] This is not surprising, because lyophilized hemoglobin is readily oxidized in air, and the commercial preparation of Hb was therefore predominantly methemoglobin.

In order to follow the oxidation state changes during the polymerization, reactions were run with Cys-blocked Hb in a sealed, argon-filled cuvette in a UV/Vis spectrometer. While the Soret band was too intense to be monitored, the visible range of the spectrum could be followed over time. When Cys-blocked Hb was treated with AscA in the absence of monomer and organo-bromide initiator, a spectrum evolved with a peak at 627 nm and a broad absorption band comprising peaks at 509 and 541 nm (Figure 5.10c). Such a spectrum is characteristic of intermediate hemoglobin, a valency hybrid in which the α-chains are in the $Fe^{III}$ state and the β-chains in the $Fe^{II}$ state ($\alpha^{III}\beta^{II}$).[129] Indeed, methemoglobin has been reported to be reduced by ascorbic acid to this species.[130] The evolution of Cys-blocked Hb's spectrum during ARGET ATRP showed different results. In Figure 5.10d, the first three hours of a polymerization are reported at intervals of 45 s, while Figure 5.11 shows the evolution of spectra over a period of 13 h at intervals of 4 min. During the first 4.5 min of the reaction, the maximum at 500 nm transformed into a broad adsorption band with a shoulder at 536 nm. The maxima at 627 nm became less pronounced. This spectrum was dominant during the initial hours of the polymerization. Most likely, it resulted from the combined presence of $\alpha^{III}\beta^{II}$ and methemoglobin: Initially, methemoglobin was reduced by AscA but, at the same time, organobromine compounds are efficient oxidizing agents for reduced Hb.[131] Thus, the reaction of $\alpha^{III}\beta^{II}$ with organo-bromine initiator and Br-terminated dormant polymer chains yielded methemoglobin, which was converted back to $\alpha^{III}\beta^{II}$ by transfer of Br to the polymer radical, or by reduction with AscA. After 4-6 hours of polymerization (c.f. Figure 5.11), the shoulder at 536 nm disappeared, and a spectrum with an adsorption band at 510 nm, and two minor bands at 627 and 686 nm evolved.

---

[128] a) B. J. Reeder, *Antioxid. Redox Signaling* **2010**, *13*, 1087–1123 b) W. G. Zijlstra, A. Buursma, *Comp. Biochem. Physiol., Part B: Biochem. Mol. Biol.* **1997**, *118*, 743–749.

[129] A. Tomoda, M. Takeshita, Y. Yoneyama, *J. Biol. Chem.* **1978**, *253*, 7415–7419.

[130] a) A. Tomoda, M. Takeshita, Y. Yoneyama, *J. Biol. Chem.* **1978**, *253*, 7415–7419 b) A. Tomoda, A. Tsuji, S. Matsukawa, M. Takeshita, Y. Yoneyama, *J. Biol. Chem.* **1978**, *253*, 7420–7423.

[131] a) W. A. Braunecker, K. Matyjaszewski, *Prog. Polym. Sci.* **2007**, *32*, 93–146 b) E. W. Bartnicki, N. O. Belser, C. E. Castro, *Biochemistry* **1978**, *17*, 5582–5586.

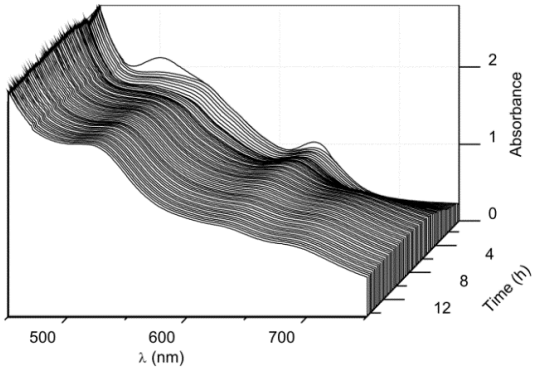


**Figure 5.11** Time dependent Vis spectra of a NiPAAm polymerization catalyzed by Cys-blocked Hb under ARGET ATRP conditions. Experimental conditions: Ratio of HEBIB/NiPAAm/AscA/Hb 1:79:1:0.008. The first spectrum was recorded after the addition of AscA. Spectra were recorded every 4 min.

This reaction time corresponds to the time at which the polymerization stopped (Figure 5.11). Unfortunately, it was not possible to assign the spectra of this Hb unambiguously to a known derivative of Hb. However, a UV/Vis spectrum of Cys-blocked Hb that was purified at the end of a typical polymerization and exposed to air shows the characteristics of methemoglobin, albeit with a slightly reduced molar Soret absorption (Figure 5.10b). The presence of the Soret band proves that the heme groups were not destroyed by radical-induced cleavage of the porpyhrin ring. The Soret band's position at 406 nm and the absence of a shoulder at longer wavelengths, a feature of the spectrum of $\alpha^{III}\beta^{II}$,[132] indicate that all iron was in a $Fe^{III}$ oxidation state. Thus, the concentration of $\alpha^{III}\beta^{II}$ decreased during the reaction, and Hb accumulated in a ferric state that resulted in a methemoglobin-like species after purification. Moreover, the spectrum indicates that the recovered Hb neither contained hemichromes nor did it have heme-to-protein cross-links, as these species have other distinctive absorption patterns in the visible region.[133] The formation of covalently modified prosthetic hemes cannot be ruled out, because some are reported to have a methemoglobin-like absorption spectrum.[134] This could also account for the lower Soret adsorptivity of the recovered protein.

[132] A. Tomoda, M. Takeshita, Y. Yoneyama, *J. Biol. Chem.* **1978**, *253*, 7415–7419.

[133] a) B. J. Reeder, *Antioxid. Redox Signaling* **2010**, *13*, 1087–1123 b) J. T. Kindt, A. Woods, B. M. Martin, R. J. Cotter, Y. Osawa, *J. Biol. Chem.* **1992**, *267*, 8739–8743 c) C. C. Winterbourn, in *Methods in Enzymology* (Eds.: L. Packer, A.N. Glazer), Academic Press, San Diego, CA, USA, **1990**, pp. 265–272 d) M. Minetti, C. Mallozzi, G. Scorza, M. D. Scott, F. A. Kuypers, B. H. Lubin, *Arch. Biochem. Biophys.* **1993**, *302*, 233–244 e) W. Kaca, R. I. Roth, K. D. Vandegriff, G. C. Chen, F. A. Kuypers, R. M. Winslow, J. Levin, *Biochemistry* **1995**, *34*, 11176–11185.

[134] R. Tolando, S. Cazzaro, R. Ferrara, M. Rezzadore, M. Manno, *Biochem. Pharmacol.* **1995**, *49*, 233–241.

### 5.2.7 Mechanistic Discussion

In summary, the experimental results allow us to draw the following, putative mechanistic picture of the Hb-catalyzed polymerization (Scheme 5.2). The reaction starts with methemoglobin being reduced to intermediate hemoglobin by AscA. Then, $\alpha^{III}\beta^{II}$ activates the alkylbromide initiator yielding Hb-iron(III)bromide and an alkyl radical. This radical starts the chain propagation. The presence of bromine-terminated polymers proves that Hb can transfer Br back to the organo radical, yielding a dormant polymer chain and Hb-iron(II). Thus, an ATRP equilibrium between dormant species and activated, propagating radical species evolves. With the monomers PEGA and PEGMA, the deactivation is efficient enough to allow a good to moderate degree of control of the polymerization. Hb-iron(III) species accumulate due to termination reactions of polymer radicals, and due to the reaction of radicals with Hb-iron(II). The activating species $\alpha^{III}\beta^{II}$ is regenerated through the reduction of Hb-iron(III) by the excess of AscA, until the reducing agent is consumed. As the oxidation of deoxyhemoglobin to methemoglobin by alkyl-bromides is known to be an axial inner sphere process,[135] it is likely that the redox reactions involved in the Hb-catalyzed polymerization follow an inner-sphere electron transfer.

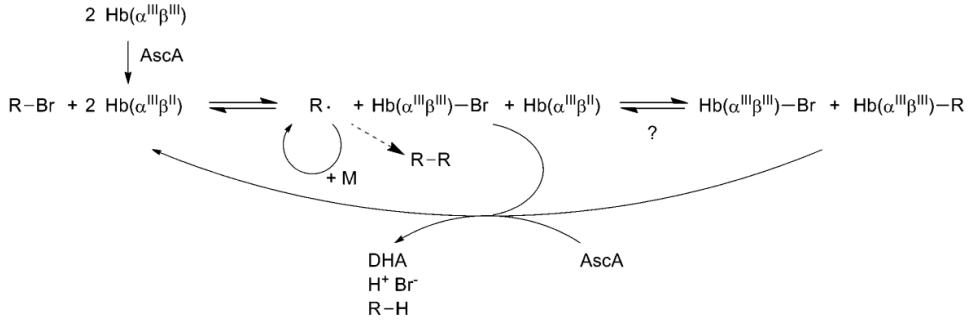


**Scheme 5.2** Possible mechanism of Hb-Catalyzed Polymerization under ARGET ATRP Conditions.

## 5.3 Conclusion

Bovine Hb and human erythrocytes were found to be catalysts for the polymerization of vinyl-type monomers under ARGET ATRP conditions, using alkyl bromides as an initiators and the reducing agent AscA. Therefore, Hb is an ATRPase. The kinetics of the polymerization were of first order, and the reaction yielded partially bromine-terminated polymers with relative low polydispersity indices. Moreover, the polymerization of PEGA and PEGMA resulted in an increase in molecular weight with conversion. These are signs of a controlled/living character of the reaction. The mechanism of the polymerization, although not yet fully elucidated, resembles the redox and atom transfer reactions encountered in conventional ARGET ATRP.

[135] a) R. S. Wade, C. E. Castro, *J. Am. Chem. Soc.* **1973**, *95*, 231–234 b) E. W. Bartnicki, N. O. Belser, C. E. Castro, *Biochemistry* **1978**, *17*, 5582–5586.

The reversible interplay of dehalogenation and halogenation reactions involved in the ATRPase activity of hemoglobin is a novel aspect in the wide and rich landscape of functions and reactions associated with this protein. Moreover, ATRPase activity of Hb and other suitable enzymes complement the existing repertoire of biocatalytic polymerizations, being the first examples of native enzymes that are able to catalyze controlled/living radical polymerizations. From a technological point of view, the newly discovered ATRPase activity of Hb and erythrocytes could provide a green, nontoxic, and even edible alternative to conventional ATRP catalysts, especially if the catalytic performance of the protein is further increased. An entire plethora of biocatalyst engineering methods, such as directed evolution, rational design, immobilization, and the use of enzymes in organic solvents, stands ready to achieve this goal. Apart from revealing a useful synthetic activity of Hb for *in vitro* biotransformations, our findings have significance beyond polymer sciences. The possibility that certain reactions of the polymerase activity of hemoglobin and of erythrocytes could happen *in vivo*, in particular the reversible, catalytic creation of radicals from halogenated small- and macro-molecules, might lead to a deeper understanding of the toxicity of organohalogen compounds and their metabolic pathways.

# 6 Nanoreactors[136]

*Kasper Renggli, Patric Baumann, Karolina Langowska, Ozana Onaca, Nico Bruns and Wolfgang Meier*

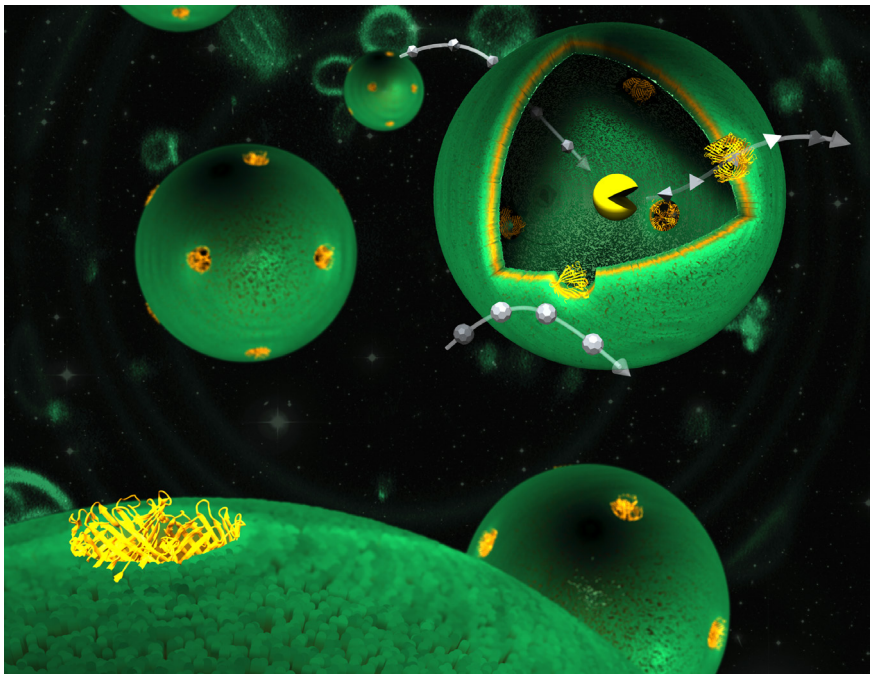

*Chemical reactions can be confined to nanoscale compartments by encapsulating catalysts in hollow nano-objects. Such reaction compartments effectively become nanoreactors when substrate and product are exchanged between bulk solution and cavity. In this chapter, natural nanoreactors that include protein-based bacterial microcompartments, protein cages, and viruses are discussed. Our work focuses on the group II chaperonin thermosome from the archaea Thermoplasma acidophilum as protein nanoreactor for atom transfer radical polymerization in aqueous solution. Nanoreactors hold promise for applications ranging from selective and size-constrained organic synthesis to biomedical advances (e.g. artificial organelles, biosensing) and as analytical tools to study reaction mechanisms.*

[136] This chapter was published as part of: K. Renggli, P. Baumann, K. Langowska, O. Onaca, N. Bruns, W. Meier, *Adv. Funct. Mater.* **2011**, *21*, 1241–1259.

## 6.1 Introduction

Confined reaction spaces that span various length scales ranging from the macroscopic world down to nanosized structures are found abundantly in biological systems. The controlled and selective exchange of substances across the confining layer is a characteristic hallmark of life. Every organism is a macroscopic entity with a distinct inner volume in which complex chemical transformations occur. This internal volume is separated from the environment by a boundary layer, e.g. the skin. Likewise, cells can be regarded as very complex microreactors. The cell membrane encloses catalytically active species, i.e. enzymes, in a confined volume. It controls access and release of substances into and out of the cell by a variety of pores and active and passive mechanisms. Moreover, organelles within cells provide another, smaller level of compartmentalization. Organelles are also equipped with various means to selectively exchange materials with the cytosol. Nature manages to stabilize and protect catalytically active species by separating the reaction space within cells and organelles from the surrounding environment. Furthermore, the reaction conditions, e.g. pH or concentration of certain substrates in the compartments, are controlled in order to influence the course of reactions. Another important feature of Nature's micro- and nanocompartments is spatial control of individual reaction steps in various complex reaction cascades.

## 6.2 Nature's Nanoreactor

Most of the compartmental boundaries of cells and cellular organelles are lipid-based membranes. However, a variety of protein-based compartments have attracted great attention recently.[137] Cage-like proteins such as ferritins or chaperonins provide cavities that can sequester metal oxides or partially unfolded proteins from the cytosol. Protein-based compartments of bacteria and archea provide isolated environments within cells that do not possess membrane-enclosed organelles. Viruses, on the other hand, protect their genetic material outside the context of a typical cell by enclosure inside a cavity formed by a protein coat of virus particles.

Protein containers consist of multiple copies of individual protein subunits that self-assemble into structures that are often highly symmetric (Figure 6.1). Only one or a few different protein building blocks are necessary to create structures that comprise between 14 and several thousand individual subunits. The structures span a broad scope of shapes and sizes, ranging from the spherical DNA-binding protein of starved cells (Dps) with a diameter of 9 nm,[138] to the carboxysomes, polyhedral proteinaceous shells with a diameter of 80 nm to 150 nm,[139] to viral capsids with diameters between

[137] a) A. de la Escosura, R. J. M. Nolte, J. J. L. M. Cornelissen, *J. Mater. Chem.* **2009**, *19*, 2274 b) C. M. Niemeyer, *Angew. Chem. Int. Ed.* **2001**, *40*, 4128–4158 c) S. Kang, T. Douglas, *Science* **2010**, *327*, 42–43 d) M. Uchida, M. T. Klem, M. Allen, P. Suci, M. Flenniken, E. Gillitzer, Z. Varpness, L. O. Liepold, M. Young, T. Douglas, *Adv. Mater.* **2007**, *19*, 1025–1042.

[138] M. Uchida, M. T. Klem, M. Allen, P. Suci, M. Flenniken, E. Gillitzer, Z. Varpness, L. O. Liepold, M. Young, T. Douglas, *Adv. Mater.* **2007**, *19*, 1025–1042.

[139] S. Q. Cheng, Y. Liu, C. S. Crowley, T. O. Yeates, T. A. Bobik, *BioEssays* **2008**, *30*, 1084–1095.

18 nm and 500 nm.[140] Examples of rod-shaped containers are the tobacco mosaic virus, with dimensions of 18 nm to 300 nm, and the M23 bacteriophage, with a diameter of 6.5 nm and a length of 860 nm.[140]

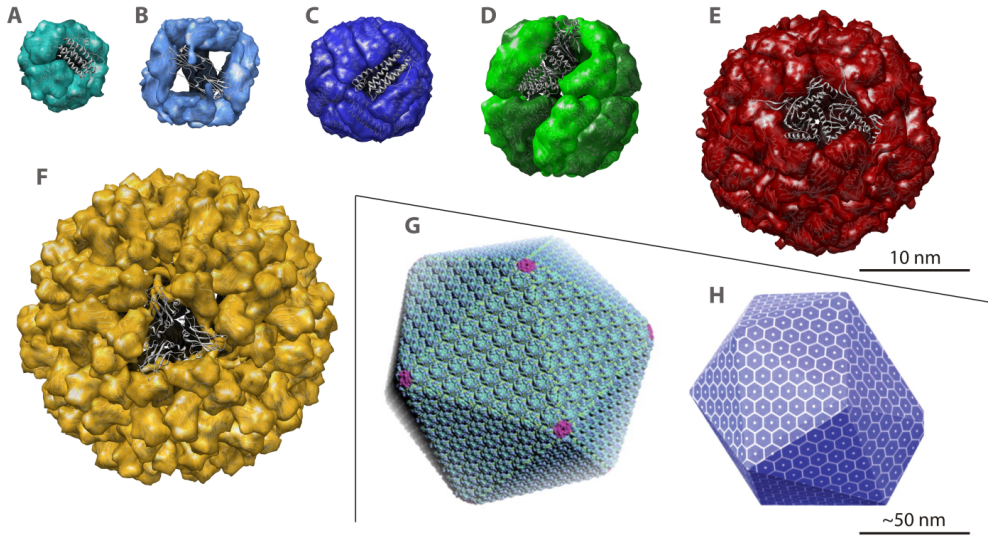


**Figure 6.1** Structures and models of some nanoreactors found in Nature: Protein cages, a virus, and microbial protein microcompartments. a) DNA-binding protein from starved cells (Dps) (PDB: 1QGH),[141] b) small heat-shock protein (sHSP) (PDB: 1SHS),[142] c) apoferritin (PDB: 1DAT),[143] d) thermosome (THS) (PDB: 1A6D),[144] e) encapsulin (PDB: 3DKT),[145] f) cowpea chlorotic mottle virus (CCMV) (PDB: 1CWP),[146] g) proposed model of carboxysome,[147] h) proposed model of ethanolamine utilization (Eut) microcompartment.[148] Structures of a-g were rendered using the Chimera program,[149] models in g and h are reproduced from [147] and from [148], respectively, with permission from AAAS.

[140] a) T. Douglas, M. Young, *Science* **2006**, *312*, 873–875 b) M. Fischlechner, E. Donath, *Angew. Chem. Int. Ed.* **2007**, *46*, 3184–3193.
[141] A. Ilari, S. Stefanini, E. Chiancone, D. Tsernoglou, *Nat. Struct. Biol.* **2000**, *7*, 38–43.
[142] K. K. Kim, R. Kim, S.-H. Kim, *Nature* **1998**, *394*, 595–599.
[143] B. Gallois, B. L. d'Estaintot, M. A. Michaux, A. Dautant, T. Granier, G. Precigoux, J. A. Soruco, F. Roland, O. Chavas-Alba, A. Herbas, et al., *JBIC, J. Biol. Inorg. Chem.* **1997**, *2*, 360–367.
[144] L. Ditzel, J. Lowe, D. Stock, K. O. Stetter, H. Huber, R. Huber, S. Steinbacher, *Cell* **1998**, *93*, 125–138.
[145] M. Sutter, D. Boehringer, S. Gutmann, S. Guenther, D. Prangishvili, M. J. Loessner, K. O. Stetter, E. Weber-Ban, N. Ban, *Nat. Struct. Mol. Biol.* **2008**, *15*, 939–947.
[146] J. A. Speir, S. Munshi, G. Wang, T. S. Baker, J. E. Johnson, *Structure* **1995**, *3*, 63–78.
[147] S. Tanaka, C. A. Kerfeld, M. R. Sawaya, F. Cai, S. Heinhorst, G. C. Cannon, T. O. Yeates, *Science* **2008**, *319*, 1083–1086.
[148] S. Tanaka, M. R. Sawaya, T. O. Yeates, *Science* **2010**, *327*, 81–84.
[149] S. Litvinchuk, Z. Lu, P. Rigler, T. D. Hirt, W. Meier, *Pharm. Res.* **2009**, *26*, 1711–1717.

Protein-based cages have attracted the attention of scientists as potential nanoreactors because of their extensive size-range. Moreover, these biological entities often possess the capacity to gate access to their cavities in a precise way. As more and more structures are resolved, protein cages are being seen as offering the unique opportunity for site-selective modification by chemical conjugation or by using genetic engineering techniques. Many protein cages are remarkably stable, despite the fact that they are self-assembled structures with, often, no covalent linkage between subunits. As an example, ferritin is stable to 85°C[150] and to 6 M guanidine at pH 7.[151] Thus, protein cages have the potential for use as nanoreactors in technical applications or under normal lab conditions. Stability can be further increased by chemical modifications e.g. by PEGylation, by genetic engineering or by using protein cages derived from organisms that live in extreme environments, such as hydrothermal deep sea vents or hot springs.[152]

The protein shell encloses one or (in the case of chaperonins) two central cavities with primarily hydrophilic walls. Static and gated pores in the shell allow access to the cavities. These gaps of a defined size are formed at the interface between subunits. The diameters of the 'static' pores range from 0.4 nm in ferritin[153] to approximately 3 nm in the small heat-shock protein (sHSP).[154] These pores are big enough to allow water, ions, low molecular weight molecules, and small polymers to enter and leave the protein container. Larger molecules, however, are not able to pass through the pores. Thus, these pores act as a size-exclusion gate. Furthermore, some of the pores are lined by charged amino acid residues, rendering them selectively permeable to charged molecules. Protein shells are not static or rigid vessels, but rather flexible entities that react to variations in their external environments.

However, the catalytic species are usually too large to be enclosed through the pores in the protein shell. A method to encapsulate and release these macromolecules and into the cavity of protein containers is the reversible assembly/disassembly of the protein containers from/into subunits. Some RNA plant viruses exhibit such behavior.[155] This can be exploited to load a virion *in vitro* with guest molecules such as proteins,[156] inorganic nanoparticles,[157] and anionic polymers.[158] CCMV disassembles

---

150 S. Stefanini, S. Cavallo, C.-Q. Wang, P. Tataseo, P. Vecchini, A. Giartosio, E. Chiancone, *Arch. Biochem. Biophys.* **1996**, *325*, 58–64.

151 I. Listowsky, G. Blauer, S. Englard, J. J. Betheil, *Biochemistry* **1972**, *11*, 2176–2182.

152 M. Uchida, M. T. Klem, M. Allen, P. Suci, M. Flenniken, E. Gillitzer, Z. Varpness, L. O. Liepold, M. Young, T. Douglas, *Adv. Mater.* **2007**, *19*, 1025–1042.

153 B. Gallois, B. L. d'Estaintot, M. A. Michaux, A. Dautant, T. Granier, G. Precigoux, J. A. Soruco, F. Roland, O. Chavas-Alba, A. Herbas, et al., *JBIC, J. Biol. Inorg. Chem.* **1997**, *2*, 360–367.

154 a) K. K. Kim, R. Kim, S.-H. Kim, *Nature* **1998**, *394*, 595–599 b) K. K. Kim, H. Yokota, S. Santoso, D. Lerner, R. Kim, S.-H. Kim, *J. Struct. Biol.* **1998**, *121*, 76–80.

155 J. E. Johnson, J. A. Speir, *J. Mol. Biol.* **1997**, *269*, 665–675.

156 M. Comellas Aragonès, H. Engelkamp, V. I. Claessen, N. A. J. M. Sommerdijk, A. E. Rowan, P. C. M. Christianen, J. C. Maan, B. J. M. Verduin, J. J. L. M. Cornelissen, R. J. M. Nolte, *Nat. Nanotechnol.* **2007**, *2*, 635–639.

157 a) T. Douglas, M. Young, *Science* **2006**, *312*, 873–875 b) A. de la Escosura, M. Verwegen, F. D. Sikkema, M. Comellas Aragonès, A. Kirilyuk, T. Rasing, R. J. M. Nolte, J. J. L. M. Cornelissen, *Chem. Commun.* **2008**, 1542–1544.

into protein dimers and RNA when exposed to pH above 7.5. After purification of the protein subunits and adjustment of the pH to 5.0, the virion self-assembles into empty or, in the presence of cargo, cargo-filled viral capsids.[159] Another example of reversible assembly/disassembly is ferritin, which disassembles at pH 2 and reassembles at pH 7.[160]

### 6.2.1 Protein-Based Microbial Microcompartments

Although the biological role of many protein containers is either the storage or transport of cargo, e.g. in the case of ferritin and viruses, some examples are known whereby substrates enter the confined volume, encounter a catalytically active species and are converted to products that subsequently leave the cage. Thus, Nature uses hollow protein assemblies as nanoreactors in much the same sense as envisaged by us. Furthermore, there is some evidence that access to the cavity of the cages is selective or even gated.[161] Prime examples for Nature's gated nanoreactors are bacterial microcompartments that function as protein-based organelles in otherwise non-compartmentalized bacterial cells.[162] Typically, a few thousand proteins form a shell with a polyhedral shape and a diameter between 80 nm to 150 nm that contain several different enzymes. Carboxysomes are such microcompartments.[163] They are found in all cyanobacteria and some chemoautotrophs and enhance $CO_2$ fixation by encapsulating the sequential metabolic enzymes carbonic anhydrase and ribulose-1,5-bisphosphate carboxylase-oxygenase (RuBisCO). The shell of the carboxysome is thought to be a diffusion barrier to the intermediate metabolite, $CO_2$, thus increasing the local substrate concentration for the $CO_2$-converting RuBisCO. Ethanolamine utilization (Eut) microcompartments[164] and propandiol utilization (Pdu) microcompartments[165] are found in bacteria such as *E. coli* and *S. enterica*. They sequester metabolizing enzymes that convert ethanolamine into ethanol or 1,2-propanediol into propionyl-CoA, respectively. The metabolic intermediates acetaldehyde or propionaldehyde are consumed before they can escape the shell and

---

158 a) F. D. Sikkema, M. Comellas Aragonès, R. G. Fokkink, B. J. M. Verduin, J. J. L. M. Cornelissen, R. J. M. Nolte, *Org. Biomol. Chem.* **2007**, *5*, 54–57 b) Y. Hu, R. Zandi, A. Anavitarte, C. M. Knobler, W. M. Gelbart, *Biophys. J.* **2008**, *94*, 1428–1436.

159 a) A. de la Escosura, R. J. M. Nolte, J. J. L. M. Cornelissen, *J. Mater. Chem.* **2009**, *19*, 2274 b) J. E. Johnson, J. A. Speir, *J. Mol. Biol.* **1997**, *269*, 665–675.

160 B. Webb, J. Frame, Z. Zhao, M. L. Lee, G. D. Watt, *Arch. Biochem. Biophys.* **1994**, *309*, 178–183.

161 a) S. Q. Cheng, Y. Liu, C. S. Crowley, T. O. Yeates, T. A. Bobik, *BioEssays* **2008**, *30*, 1084–1095 b) S. Tanaka, M. R. Sawaya, T. O. Yeates, *Science* **2010**, *327*, 81–84.

162 a) S. Kang, T. Douglas, *Science* **2010**, *327*, 42–43 b) S. Q. Cheng, Y. Liu, C. S. Crowley, T. O. Yeates, T. A. Bobik, *BioEssays* **2008**, *30*, 1084–1095 c) S. Tanaka, C. A. Kerfeld, M. R. Sawaya, F. Cai, S. Heinhorst, G. C. Cannon, T. O. Yeates, *Science* **2008**, *319*, 1083–1086.

163 a) T. O. Yeates, C. A. Kerfeld, S. Heinhorst, G. C. Cannon, J. M. Shively, *Nat. Rev. Microbiol.* **2008**, *6*, 681–691 b) S. Tanaka, C. A. Kerfeld, M. R. Sawaya, F. Cai, S. Heinhorst, G. C. Cannon, T. O. Yeates, *Science* **2008**, *319*, 1083–1086.

164 a) S. Q. Cheng, Y. Liu, C. S. Crowley, T. O. Yeates, T. A. Bobik, *BioEssays* **2008**, *30*, 1084–1095 b) S. Tanaka, M. R. Sawaya, T. O. Yeates, *Science* **2010**, *327*, 81–84.

165 a) S. Q. Cheng, Y. Liu, C. S. Crowley, T. O. Yeates, T. A. Bobik, *BioEssays* **2008**, *30*, 1084–1095 b) C. S. Crowley, M. R. Sawaya, T. A. Bobik, T. O. Yeates, *Structure* **2008**, *16*, 1324–1332.

thus are prevented from being released into the cytosol at toxic levels.[166] Furthermore, volatile aldehydes are not lost as a carbon source to the bacteria by diffusion across the cell-membrane.[167]

Smaller protein-based microcompartments that enclose enzymes or are themselves catalytically active have been identified and their structures characterized. These include the 24 nm diameter encpasulin from *Th. maritioma*,[168] *B. subtilis* lumazine synthase,[169] the eukaryotic pyruvate dehydrogenase complex,[170] and 2-hydroxy-pentadienoic acid hydratase from *E. coli*.[171] They possess pores in their shells, but it remains to be determined whether these pores selectively control or even gate substrate access to the biocatalysts in a way other than by imposing a size restriction on the molecules capable of entering and leaving the compartment. Furthermore, bacterial microcompartments and the smaller enzymatically active protein compartments have not been used as nanoreactors *in vitro* thus far.

### 6.2.2 Protein Cages

In contrast to protein microcompartments, protein cages have been applied as nanoreactors in a non-biological context. Ferritins were the first protein cages used as catalysts[172] for *in vitro* reactions and continue to be the most widely explored protein-based nanoreactors.[173] Members of the family of ferritins are found in all realms of life. Their biological function is to sequester and store iron in a soluble, bioavailable, and safe form.[174] Ferritins are spherical cages 12 nm in diameter, composed of 24

---

166 a) E. M. Sampson, T. A. Bobik, *J. Bacteriol.* **2008**, *190*, 2966–2971 b) M. R. Rondon, R. Kazmierczak, J. C. Escalantesemerena, *J. Bacteriol.* **1995**, *177*, 5434–5439 c) M. R. Rondon, A. R. Horswill, J. C. Escalantesemerena, *J. Bacteriol.* **1995**, *177*, 7119–7124.

167 J. T. Penrod, J. R. Roth, *J. Bacteriol.* **2006**, *188*, 2865–2874.

168 M. Sutter, D. Boehringer, S. Gutmann, S. Guenther, D. Prangishvili, M. J. Loessner, K. O. Stetter, E. Weber-Ban, N. Ban, *Nat. Struct. Mol. Biol.* **2008**, *15*, 939–947.

169 K. Ritsert, R. Huber, D. Turk, R. Ladenstein, K. Schmidt-Baese, A. Bacher, *J. Mol. Biol.* **1995**, *253*, 151–167.

170 Z. H. Zhou, D. B. McCarthy, C. M. O'Connor, L. J. Reed, J. K. Stoops, *Proc. Natl. Acad. Sci.* **2001**, *98*, 14802–14807.

171 M. G. Montgomery, A. R. Coker, I. A. Taylor, S. P. Wood, *J. Mol. Biol.* **2010**, *396*, 1379–1391.

172 V. V. Nikandrov, C. K. Grätzel, J. E. Moser, M. Grätzel, *J. Photochem. Photobiol., B* **1997**, *41*, 83–89.

173 a) V. V. Nikandrov, C. K. Grätzel, J. E. Moser, M. Grätzel, *J. Photochem. Photobiol., B* **1997**, *41*, 83–89 b) I. Kim, H.-A. Hosein, D. R. Strongin, T. Douglas, *Chem. Mater.* **2002**, *14*, 4874–4879 c) D. Ensign, M. Young, T. Douglas, *Inorg. Chem.* **2004**, *43*, 3441–3446 d) Y. Shin, A. Dohnalkova, Y. Lin, *J. Phys. Chem. C* **2010**, *114*, 5985–5989 e) T. Ueno, M. Suzuki, T. Goto, T. Matsumoto, K. Nagayama, Y. Watanabe, *Angew. Chem. Int. Ed.* **2004**, *43*, 2527–2530 f) M. Suzuki, M. Abe, T. Ueno, S. Abe, T. Goto, Y. Toda, T. Akita, Y. Yamada, Y. Watanabe, *Chem. Commun.* **2009**, 4871–4873 g) S. Abe, J. Niemeyer, M. Abe, Y. Takezawa, T. Ueno, T. Hikage, G. Erker, Y. Watanabe, *J. Am. Chem. Soc.* **2008**, *130*, 10512–10514 h) J. Niemeyer, S. Abe, T. Hikage, T. Ueno, G. Erker, Y. Watanabe, *Chem. Commun.* **2008**, 6519–6521 i) S. Abe, K. Hirata, T. Ueno, K. Morino, N. Shimizu, M. Yamamoto, M. Takata, E. Yashima, Y. Watanabe, *J. Am. Chem. Soc.* **2009**, *131*, 6958–6960 j) Z. Varpness, C. Shoopman, J. W. Peters, M. Young, T. Douglas, *ACS Symp. Ser.* **2008**, *986*, 263–272.

174 a) N. D. Chasteen, P. M. Harrison, *J. Struct. Biol.* **1999**, *126*, 182–194 b) X. Liu, E. C. Theil, *Acc. Chem. Res.* **2005**, *38*, 167–175 c) E. C. Theil, X. S. Liu, T. Tosha, *Inorg. Chim. Acta* **2008**, *361*, 868–874 d) P. Arosio, R. Ingrassia, P. Cavadini, *Biochim. Biophys. Acta, Gen. Subj.* **2009**, *1790*, 589–599.

subunits.[175] A hydrated ferric oxide (or phosphate) forms within their 8 nm-diameter cavity. They possess eight pores with a diameter of 0.4 nm and a constriction of 0.33 nm. They were long considered static, but experimental evidence has shifted this thinking to possibly active or gated pores.[176] A local unfolding of the pores due to heat or to low concentration of chaotropes (such as 1 mM urea or guanidine) results in an opening of the pores.[177] This increases the accessibility of the iron core to chelating agents that facilitate release of $Fe^{2+}$ from the ferritin.

Here, we will highlight examples where ferritins have been used as nanoreactors in the sense described above. As their natural role is the mineralization of iron, they have also been used extensively to prepare inorganic nanoparticles inside their cavities. The use of ferritins as templates for inorganic nanoparticle synthesis is beyond the scope of this thesis and was reviewed recently.[178] A natural step beyond preparing ferritins with inorganic cores was to employ them as catalysts. Ferritin, with its native and/or reconstituted oxyhydroxide ferrihydrite core, was shown to catalyze the photoreduction of cytochrome C and viologens,[179] as well as to reduce an aqueous chromium(VI) species to chromium(III)[180] and copper(II) to copper(0)[181] while being illuminated with UV- or visible light, respectively. As cytochrome C and viologen are too big to enter the pores, electron transfer was proposed to occur through the protein shell. In the case of Cr, mechanistic uncertainties remain as to whether the substrates entered the ferritin or not while the $Cu^0$ particles formed inside the protein cage. More recently, Au-Ag alloy nanoparticles formed inside apo-ferritin, i.e., a ferritin deprived of its native core, were used to catalyze the reduction of 4-nitrophenol to corresponding 4-aminophenol in the presence of $NaBH_4$.[182] However, putative selective properties of the pores with respect to substrates were not investigated in these works. These properties were first described by Watanabe and coworkers, who used ferritin encapsulating Pd nanoclusters as size-selective hydrogenation catalysts.[183] To this end, $Pd^{II}$ ions were concentrated at the interior of apo-ferritin, i.e., a ferritin deprived of its native core, and reduced chemically to form Pd particles of 2.0 ± 0.3 nm diameter. The reactivity of the resulting catalyst to various olefins such as acrylamide and *tert*-butyl acrylamide roughly correlated with the volume of the olefins, indicating that the pores discriminate among substrate sizes. In subsequent work, the authors improved catalytic performance by using Au-Pd alloy nanoparticles and Au-Pd core-shell nanoparticles generated

---

175 a) B. Gallois, B. L. d'Estaintot, M. A. Michaux, A. Dautant, T. Granier, G. Precigoux, J. A. Soruco, F. Roland, O. Chavas-Alba, A. Herbas, et al., *JBIC, J. Biol. Inorg. Chem.* **1997**, *2*, 360–367 b) D. M. Lawson, P. J. Artymiuk, S. J. Yewdall, J. M. A. Smith, J. C. Livingstone, A. Treffry, A. Luzzago, S. Levi, P. Arosio, et al, *Nature* **1991**, *349*, 541–544.

176 a) X. Liu, E. C. Theil, *Acc. Chem. Res.* **2005**, *38*, 167–175 b) P. Arosio, R. Ingrassia, P. Cavadini, *Biochim. Biophys. Acta, Gen. Subj.* **2009**, *1790*, 589–599.

177 X. Liu, W. Jin, E. C. Theil, *Proc. Natl. Acad. Sci. U. S. A.* **2003**, *100*, 3653–3658.

178 M. Uchida, M. T. Klem, M. Allen, P. Suci, M. Flenniken, E. Gillitzer, Z. Varpness, L. O. Liepold, M. Young, T. Douglas, *Adv. Mater.* **2007**, *19*, 1025–1042.

179 V. V. Nikandrov, C. K. Grätzel, J. E. Moser, M. Grätzel, *J. Photochem. Photobiol., B* **1997**, *41*, 83–89.

180 I. Kim, H.-A. Hosein, D. R. Strongin, T. Douglas, *Chem. Mater.* **2002**, *14*, 4874–4879.

181 D. Ensign, M. Young, T. Douglas, *Inorg. Chem.* **2004**, *43*, 3441–3446.

182 Y. Shin, A. Dohnalkova, Y. Lin, *J. Phys. Chem. C* **2010**, *114*, 5985–5989.

183 T. Ueno, M. Suzuki, T. Goto, T. Matsumoto, K. Nagayama, Y. Watanabe, *Angew. Chem. Int. Ed.* **2004**, *43*, 2527–2530.

inside of the ferritin.[184] Furthermore, noncovalent coordination of Pd(allyl) complexes onto the interior surface of genetically engineered apo-ferritin yielded active species that catalyzed the Suzuki coupling reaction between 4-iodoaniline and phenylboronic acid to yield 4-phenylaniline.[185] A similar approach allowed incorporation of various ferrocene derivatives into apo-ferritin. However, no organic reaction was catalyzed using these potential catalysts.[186] In further work by the Watanabe group, Rh(norbornadiene) was complexed onto the metal-complexing sites of apo-ferritin.[187] These systems catalyzed the polymerization of phenylacetylene inside the confined volume of the cage, yielding polymers of restricted molecular weight and a narrower molecular weight distribution compared to a free Rh complex (inside cage: $M_w/M_n$ = 2.1 to 2.6 vs. free catalyst $M_w/M_n$ = 21.4). The polymers were extracted from the protein shell by disassembling the ferritin into individual subunits at pH 2. The selectivity of the pores was investigated by using derivatives of phenylacelytene as monomers. While a monomer carrying an amino group as a substituent was polymerized, phenlyacetylenes bearing carboxylic acid or phosphonic acid groups were not polymerized, indicating that anionic monomers are hindered from entering the pores, which are lined with a negative electrostatic potential.

Young, Douglas, and coworkers investigated several protein cages, namely ferritin,[188] small heat-shock protein (sHSP) from *M. jannaschii*,[189] and DNA binding protein from starved cells (Dps) of *L. innocua*[190] as hosts for the formation of platinum nanoclusters that are able to catalyze hydrogen formation. Dps is a mini-ferritin that protects DNA during starvation from oxidative damage by accumulating iron atoms in its cavity. In comparison to ferritin, it is smaller and composed of only 12 subunits. The cage has an outer diameter of 9 nm and an inner diameter of 5 nm.[191] Hydrophilic pores 0.8 nm in diameter along the three-fold axis are lined with negatively charged residues and allow access to the cavity. sHSP is a chaperone that assembles from 24 subunits into a 12 nm cage.[192] The interior cavity of 6.5 nm diameter is accessible through eight trigonal and six square-planer pores, their edges being 3 nm and 1.7 nm long, respectively. Thus, these pores are considerably larger than those of ferritins and Dps, presumably allowing for easier access to and egress from the cage. The Pt nanoclusters inside the cages efficiently catalyzed the reduction of $H^+$ to $H_2$ when this reaction was coupled to a light-activated photosystem outside of the nanoreactor. The

---

184 M. Suzuki, M. Abe, T. Ueno, S. Abe, T. Goto, Y. Toda, T. Akita, Y. Yamada, Y. Watanabe, *Chem. Commun.* **2009**, 4871–4873.

185 S. Abe, J. Niemeyer, M. Abe, Y. Takezawa, T. Ueno, T. Hikage, G. Erker, Y. Watanabe, *J. Am. Chem. Soc.* **2008**, *130*, 10512–10514.

186 J. Niemeyer, S. Abe, T. Hikage, T. Ueno, G. Erker, Y. Watanabe, *Chem. Commun.* **2008**, 6519–6521.

187 S. Abe, K. Hirata, T. Ueno, K. Morino, N. Shimizu, M. Yamamoto, M. Takata, E. Yashima, Y. Watanabe, *J. Am. Chem. Soc.* **2009**, *131*, 6958–6960.

188 Z. Varpness, C. Shoopman, J. W. Peters, M. Young, T. Douglas, *ACS Symp. Ser.* **2008**, *986*, 263–272.

189 Z. Varpness, J. W. Peters, M. Young, T. Douglas, *Nano Lett.* **2005**, *5*, 2306–2309.

190 S. Kang, J. Lucon, Z. B. Varpness, L. Liepold, M. Uchida, D. Willits, M. Young, T. Douglas, *Angew. Chem. Int. Ed.* **2008**, *47*, 7845–7848.

191 A. Ilari, S. Stefanini, E. Chiancone, D. Tsernoglou, *Nat. Struct. Biol.* **2000**, *7*, 38–43.

192 K. K. Kim, R. Kim, S.-H. Kim, *Nature* **1998**, *394*, 595–599.

photocatalytic oxidation of simple organic compounds such as EDTA by ruthenium trisbypiridine was coupled to hydrogen formation via methyl viologen. This mediator had to cycle in and out of the cage.[193] In a slightly simpler reaction, a photosystem based on an Ir complex was used as a mediator-less photocatalyst in conjunction with the Pt clutser.[194] Here, the photocatalyst was assumed to cycle in and out of the cage. The initial catalytic activity of the Pt clusters inside sHsp and ferritin nanoreactors was better than the initial activity obtained for protein-free Pt particles, illustrating the enhancement of catalytic performance due to the protein nanoreactor, possibly by isolating and protecting the clusters from agglomeration.[195] Although three different protein cages were used, only the catalytic performance of the sHsp and the ferritin system were compared under identical conditions.[196] Hydrogen production rates are higher for the Pt-ferritin than for Pt-sHsp. This finding was attributed to the smaller size of Pt nanoparticles in ferritin compared with the particles in sHsp. Thus, it remains to be seen whether the size of the pores has an influence on the reaction.

Chaperonins are very promising candidates as nanoreactors because of their built-in lids that gate large openings. Archaeal thermosomes (THS) are self-assembled spheres approximately 15.8 nm in diameter in their closed conformation. The sphere is formed of two stacked, eight-membered rings that each enclose an ovaloid cavity with inner diameters of 5.4 and 8.6 nm.[197] Each cavity can hold globular proteins up to 50 kDa[197] and can be accessed through approximately 8-10 nm wide pores when THS is in an open state.[198] Our group used a covalent linker strategy to entrap proteins that diffused through the open gate into the thermosome of *Th. acidophilum*.[199] Two different fluorescent proteins were encapsulated simultaneously into the two cavities of the cage, as proven by their ability to carry out a fluorescence resonance energy transfer (FRET). The strategy is generic and allows for the encapsulation of a variety of proteins, including enzymes such as horseradish peroxidase (HRP). The enzymes were catalytically active inside the THS. Moreover, given that the function of THS *in vivo* is to refold denatured proteins, the cage stabilized the guest to thermal degradation, increasing the half-live of the enhanced yellow fluorescent protein and of HRP at 70°C by up to 2.3-times.[200]

---

193 a) Z. Varpness, C. Shoopman, J. W. Peters, M. Young, T. Douglas, *ACS Symp. Ser.* **2008**, *986*, 263–272 b) Z. Varpness, J. W. Peters, M. Young, T. Douglas, *Nano Lett.* **2005**, *5*, 2306–2309.

194 S. Kang, J. Lucon, Z. B. Varpness, L. Liepold, M. Uchida, D. Willits, M. Young, T. Douglas, *Angew. Chem. Int. Ed.* **2008**, *47*, 7845–7848.

195 Z. Varpness, J. W. Peters, M. Young, T. Douglas, *Nano Lett.* **2005**, *5*, 2306–2309.

196 Z. Varpness, C. Shoopman, J. W. Peters, M. Young, T. Douglas, *ACS Symp. Ser.* **2008**, *986*, 263–272.

197 L. Ditzel, J. Lowe, D. Stock, K. O. Stetter, H. Huber, R. Huber, S. Steinbacher, *Cell* **1998**, *93*, 125–138.

198 a) G. Schoehn, M. Hayes, M. Cliff, A. R. Clarke, H. R. Saibil, *J. Mol. Biol.* **2000**, *301*, 323–332 b) J. Zhang, M. L. Baker, G. F. Schröder, N. R. Douglas, S. Reissmann, J. Jakana, M. Dougherty, C. J. Fu, M. Levitt, S. J. Ludtke, et al., *Nature* **2010**, *463*, 379–383 c) C. R. Booth, A. S. Meyer, Y. Cong, M. Topf, A. Sali, S. J. Ludtke, W. Chiu, J. Frydman, *Nat. Struct. Mol. Biol.* **2008**, *15*, 746–753.

199 N. Bruns, K. Pustelny, L. M. Bergeron, T. A. Whitehead, D. S. Clark, *Angew. Chem. Int. Ed.* **2009**, *48*, 5666–5669.

200 a) N. Bruns, D. S. Clark, *in preparation* b) N. Bruns, D. S. Clark, *Chimia* **2011**, *65*, 245–249.

### 6.2.3 Viruses

Despite the vast library of known viral protein cages,[201] only two capsids have been used to date as an *in vitro*-nanoreactor. The work by Nolte and coworkers on the cowpea chlorotic mottle virus (CCMV) as a single-enzyme nanoreactor is a beautiful example of the opportunities that emerge when such systems are explored.[202] The capsid of CCMV has an outer diameter of 28 nm. It consists of 180 coat proteins that enclose a cavity of 18 nm in diameter. As mentioned above, it reversibly disassembles at low pH. Furthermore, CCMV undergoes pH-dependant swelling that is accompanied by an opening of pores. The virus was loaded with the horseradish peroxidase by disassembly/reassembly of the capsid in the presence of enzyme. The experimental protocol ensured that the reassembled virion contained either one or no enzyme molecule, thus permitting the study of single enzyme kinetics. The peroxidase was used to catalyze the oxidation of a non-fluorescent substrate added to the surrounding solution, into a fluorescent product inside of the nanoreactor. The product diffused from the virus into solution through pores. By measuring the diffusion rate of the fluorophores as a function of pH with fluorescence correlation spectroscopy, it was shown that the diffusion rate of the product increased by a factor of 2-3 above pH 5.7, which was attributed to the opening of pores. Indeed, the pore size is known to be small at low pH and increases to a diameter of approximately 2 nm at pH > 6.5.[203] In subsequent work, the group developed a method to encapsulate a controlled number of protein molecules inside of CCMV via interactions of coiled-coil peptide domains.[204] Enhanced green fluorescent protein (eGFP) was used as the guest, but the method also lends itself to the encapsulation of active enzymes. The second, very recent, approach by Douglas and coworkers encapsulates alcohol dehydrogenase D into the cavity of the bacteriophage P22.[205] By changing to different morphological states of P22 and thereby altering the volume of the cavities, they demonstrated a change in the overall activity of the encapsulated enzyme.

---

[201] M. Uchida, M. T. Klem, M. Allen, P. Suci, M. Flenniken, E. Gillitzer, Z. Varpness, L. O. Liepold, M. Young, T. Douglas, *Adv. Mater.* **2007**, *19*, 1025–1042.

[202] M. Comellas Aragonès, H. Engelkamp, V. I. Claessen, N. A. J. M. Sommerdijk, A. E. Rowan, P. C. M. Christianen, J. C. Maan, B. J. M. Verduin, J. J. L. M. Cornelissen, R. J. M. Nolte, *Nat. Nanotechnol.* **2007**, *2*, 635–639.

[203] J. A. Speir, S. Munshi, G. Wang, T. S. Baker, J. E. Johnson, *Structure* **1995**, *3*, 63–78.

[204] I. J. Minten, L. J. A. Hendriks, R. J. M. Nolte, J. J. L. M. Cornelissen, *J. Am. Chem. Soc.* **2009**, *131*, 17771–17773.

[205] D. P. Patterson, P. E. Prevelige, T. Douglas, *ACS Nano* **2012**, *6*, 5000–5009.

# 7 A Chaperonin as Protein Nanoreactor for Atom Transfer Radical Polymerization[206]

*Kasper Renggli, Martin G. Nussbaumer, Raphael Urbani, Thomas Pfohl and Nico Bruns*

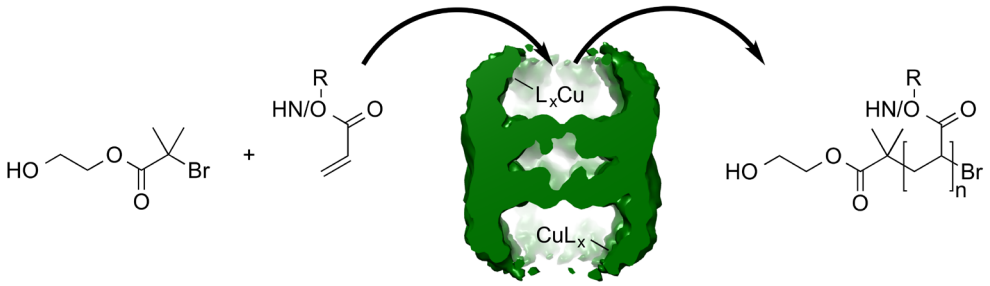


*The group II chaperonin thermosome (THS) from the archaea Thermoplasma acidophilum is reported as nanoreactor for atom transfer radical polymerization (ATRP). A copper catalyst was entrapped into the THS in order to confine the polymerization into this protein cage. THS possesses pores that are wide enough to release polymers into solution. The nanoreactor favourably influenced the polymerization of N-isopropyl acrylamide and poly(ethylene glycol) methyl ether acrylate.*

[206] This chapter was published as part of: K. Renggli, M. G. Nussbaumer, R. Urbani, T. Pfohl, N. Bruns, *Angew. Chem. Int. Ed.* **2014**, *53*, 1443–1447.

## 7.1 Introduction

We introduced the above mentioned thermosome (THS), a group II chaperonin from the archaea *Thermoplasma acidophilum*,[207] as a nanoreactor for polymerization reactions. THS is a hexadecameric protein complex that consists of eight α- and eight β- subunits. In its closed conformation is a spherical protein cage about 16 nm in diameter that encloses two cavities of approx. 130 $nm^3$ each (Figure 7.1a).[208] It provides a folding chamber to refold denatured proteins and can cycle between open and closed states by the consumption of ATP.[207] The advantage of using THS as a nanoreactor compared to other established nanoreactor systems is that the chaperonin, when in its open conformation, possesses pores that are large enough to allow macromolecules to enter and leave the cavities (Figure 7.1b).[209] Thus, it should be an ideal nanoreactor to synthesize polymers in its interior with the possibility to release the formed macromolecule into solution.

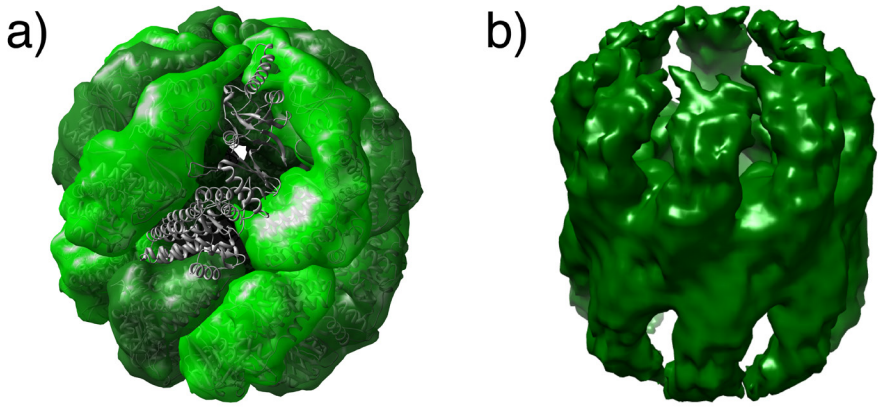


**Figure 7.1** Structure of THS a) Representation of THS in its closed conformation.[208] b) Cryo-electron microscopy (cyro-EM) density map of a thermosome in its open conformation (Data from *Methanococcus maripaludis* in its wild-type open conformation,[210] since no structural data of the THS in this conformation is available in the databases. This structure is in good agreement with the cyro-EM data of the THS.[211])

The chaperonin confines the chemical reaction into a defined volume. On the macroscopic scale, this is important to control and modulate the reaction through parameters such as the temperature, stirring, and feeding rates of substrates. If,

---

207 M. G. Bigotti, A. R. Clarke, *Arch. Biochem. Biophys.* **2008**, *474*, 331–339.

208 L. Ditzel, J. Lowe, D. Stock, K. O. Stetter, H. Huber, R. Huber, S. Steinbacher, *Cell* **1998**, *93*, 125–138.

209 a) L. Ditzel, J. Lowe, D. Stock, K. O. Stetter, H. Huber, R. Huber, S. Steinbacher, *Cell* **1998**, *93*, 125–138 b) M. G. Bigotti, A. R. Clarke, *Arch. Biochem. Biophys.* **2008**, *474*, 331–339 c) N. Bruns, K. Pustelny, L. M. Bergeron, T. A. Whitehead, D. S. Clark, *Angew. Chem. Int. Ed.* **2009**, *48*, 5666–5669.

210 J. Zhang, M. L. Baker, G. F. Schröder, N. R. Douglas, S. Reissmann, J. Jakana, M. Dougherty, C. J. Fu, M. Levitt, S. J. Ludtke, et al., *Nature* **2010**, *463*, 379–383.

211 G. Schoehn, E. Quaite-Randall, J. L. Jiménez, A. Joachimiak, H. R. Saibil, *J. Mol. Biol.* **2000**, *296*, 813–819.

however, a reaction is confined in a vessel with dimensions on the nanoscale, i.e. into a yocto liter volume of the THS, the course of a chemical reaction can be influenced in unique ways.[212] Reaction rates can be enhanced by bringing substrate and catalyst in close proximity,[213] side reactions can be suppressed by limiting the number of reactive species that encounter each other,[214] the reactor can act as a template that defines the size of the formed products,[215] and the nanoreactor can provide a cavity to influence single chain folding of synthetic polymers.[216] Furthermore, reactions can be carried out in environments where the reaction would normally not occur, such as biocatalysis in organic solvents[217] or in living cells.[218] Nanoreactors also offer the possibility to investigate reactions on the single molecule level in order to gain insight into reaction mechanisms and catalysis.[219]

In the field of polymer synthesis, atom transfer radical polymerization (ATRP) has proven to be one of the most versatile and successful controlled/living radical polymerization techniques, as it tolerates the presence of numerous functional groups, biomacromolecules, and reaction media.[220] As discussed in chapter 1, it enables synthesis of polymers with a good control over the molecular weight, narrow molecular weight distribution, and advanced architectures. Polymers synthesized by ATRP have been used as building blocks for nanostructures,[221] to form protein-polymer

---

[212] a) D. M. Vriezema, P. M. L. Garcia, N. S. Oltra, N. S. Hatzakis, S. M. Kuiper, R. J. M. Nolte, A. E. Rowan, J. C. M. van Hest, *Angew. Chem. Int. Ed.* **2007**, *46*, 7378–7382 b) M. Uchida, M. T. Klem, M. Allen, P. Suci, M. Flenniken, E. Gillitzer, Z. Varpness, L. O. Liepold, M. Young, T. Douglas, *Adv. Mater.* **2007**, *19*, 1025–1042 c) A. de la Escosura, R. J. M. Nolte, J. J. L. M. Cornelissen, *J. Mater. Chem.* **2009**, *19*, 2274 d) K. Renggli, P. Baumann, K. Langowska, O. Onaca, N. Bruns, W. Meier, *Adv. Funct. Mater.* **2011**, *21*, 1241–1259 e) K. T. Kim, S. A. Meeuwissen, R. J. M. Nolte, J. C. M. van Hest, *Nanoscale* **2010**, *2*, 844 f) M. Marguet, C. Bonduelle, S. Lecommandoux, *Chem. Soc. Rev.* **2012**, *42*, 512.

[213] T. Terashima, A. Nomura, M. Ouchi, M. Sawamoto, *Macromol. Rapid Commun.* **2012**, *33*, 833–841.

[214] B. Helms, S. J. Guillaudeu, Y. Xie, M. McMurdo, C. J. Hawker, J. M. J. Fréchet, *Angew. Chem.* **2005**, *117*, 6542–6545.

[215] a) R. McHale, J. P. Patterson, P. B. Zetterlund, R. K. O'Reilly, *Nat. Chem.* **2012**, *4*, 491–497 b) M. Okuda, Y. Suzumoto, K. Iwahori, S. Kang, M. Uchida, T. Douglas, I. Yamashita, *Chem. Commun.* **2010**, *46*, 8797.

[216] a) J.-F. Lutz, M. Ouchi, D. R. Liu, M. Sawamoto, *Science* **2013**, *341,* 1238149 b) O. Altintas, C. Barner-Kowollik, *Macromol. Rapid Commun.* **2012**, *33*, 958–971.

[217] N. Bruns, J. C. Tiller, *Nano Lett.* **2005**, *5*, 45–48.

[218] P. Tanner, V. Balasubramanian, C. G. Palivan, *Nano Lett.* **2013**, *13*, 2875–2883.

[219] a) M. Comellas Aragonès, H. Engelkamp, V. I. Claessen, N. A. J. M. Sommerdijk, A. E. Rowan, P. C. M. Christianen, J. C. Maan, B. J. M. Verduin, J. J. L. M. Cornelissen, R. J. M. Nolte, *Nat. Nanotechnol.* **2007**, *2*, 635–639 b) S.-H. Shin, H. Bayley, *J. Am. Chem. Soc.* **2005**, *127*, 10462–10463.

[220] a) W. A. Braunecker, K. Matyjaszewski, *Prog. Polym. Sci.* **2007**, *32*, 93–146 b) K. Matyjaszewski, *Macromolecules* **2012**, *45*, 4015–4039.

[221] a) E. Cabane, V. Malinova, W. Meier, *Macromol. Chem. Phys.* **2010**, *211*, 1847–1856 b) Y.-C. Lin, S.-W. Kuo, *Polym. Chem.* **2012**, *3*, 882.

conjugates,[222] and in drug-delivery systems.[223] Synthesis in aqueous media has also been successfully demonstrated.[224] Working in pure water still presents a challenge as the polymerization is often fast and side reactions tend to play a more important role than in other reaction media.[225] Confining the reaction space within the small volume of a nanoreactor should increase the degree of control over the polymerization and increase the end-functionality of the products.[226] Further, the reaction rate can be increased in comparison to homogenous systems.[227]

[222] a) R. M. Broyer, G. N. Grover, H. D. Maynard, *Chem. Commun.* **2011**, *47*, 2212–2226 b) M. A. Gauthier, H.-A. Klok, *Chem. Commun.* **2008**, 2591 c) M. A. Gauthier, H.-A. Klok, *Polym. Chem.* **2010**, *1*, 1352 d) K. Renggli, N. Bruns, *ACS Symp. Ser.*, American Chemical Society, Washington, DC, **2010 e)** H.-A. Klok, *Macromolecules* **2009**, *42*, 7990–8000.

[223] a) A. Schallon, C. V. Synatschke, V. Jérôme, A. H. E. Müller, R. Freitag, *Biomacromolecules* **2012**, *13*, 3463–3474 b) J. Wang, J. Zhang, S. Yu, W. Wu, X. Jiang, *ACS Macro Lett.* **2013**, *2*, 82–85 c) D. C. Forbes, M. Creixell, H. Frizzell, N. A. Peppas, *Eur. J. Pharm. Biopharm.* **2013**, *84*, 472–478.

[224] a) W. A. Braunecker, K. Matyjaszewski, *Prog. Polym. Sci.* **2007**, *32*, 93–146 b) K. Matyjaszewski, *Macromolecules* **2012**, *45*, 4015–4039 c) M. Sawamoto, M. Kamigaito, *Macromol. Symp.* **2002**, *177*, 17–24 d) P. B. Zetterlund, Y. Kagawa, M. Okubo, *Chem. Rev.* **2008**, *108*, 3747–3794 e) X. S. Wang, R. A. Jackson, S. P. Armes, *Macromolecules* **2000**, *33*, 255–257 f) S. Averick, A. Simakova, S. Park, D. Konkolewicz, A. J. D. Magenau, R. A. Mehl, K. Matyjaszewski, *ACS Macro Lett.* **2011**, *1*, 6–10 g) M. F. Cunningham, *Prog. Polym. Sci.* **2008**, *33*, 365–398 h) N. V. Tsarevsky, K. Matyjaszewski, *Chem. Rev.* **2007**, *107*, 2270–2299.

[225] a) N. V. Tsarevsky, K. Matyjaszewski, *Chem. Rev.* **2007**, *107*, 2270–2299 b) P.-E. Millard, N. C. Mougin, A. Böker, A. H. E. Müller, in *Controlled/Living Radical Polymerization: Progress in ATRP, ACS Symp. Ser.*, American Chemical Society, Washington, DC, USA, **2009**, pp. 127–137.

[226] a) P. B. Zetterlund, *Macromol. Theory Simul.* **2011**, *20*, 660–666 b) P. B. Zetterlund, *Polym. Chem.* **2011**, *2*, 534.

[227] P. Cotanda, N. Petzetakis, R. K. O'Reilly, *MRS Commun.* **2012**, *2*, 119–126.

## 7.2 Results & Discussion

### 7.2.1 Preparation of THS-$L_xCu$

A proposed strategy to sequester ATRP into a protein nanoreactor is to conjugate initiators to protein cages.[228] However, this grafting-from approach does not allow for a continuous production of polymers since only one polymer chain per protein-bound initiator is formed and the chain is covalently attached to the protein. In order to use THS as a nanoreactor for ATRP, we therefore chose to entrap an ATRP catalyst into the THS and start chain growth from soluble initiators that diffuse into the THS, i.e. they would not be covalently bound to the protein. Thus, polymer chains that form in the protein cage are able to leave the cavity and make room for further chains to grow.

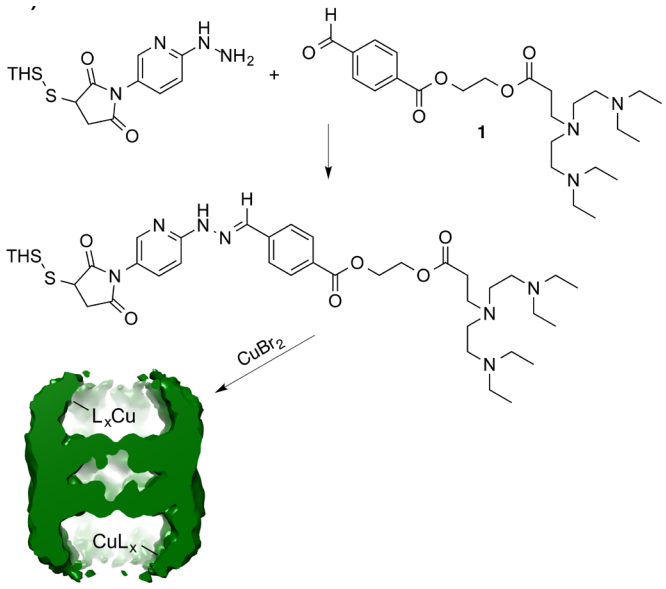


**Figure 7.2** Coupling strategy to covalently bind a TEDETA derived ligand (**1**) into the cavities of THS. This ligand is used to complex $Cu^{II}$ resulting in a protein-catalyst conjugate, i.e. a nanoreactor for ATRP.

A catalyst was conjugated into the cavities of the THS using bis-aryl hydrazone linker chemistry, similar to our previously reported method to entrap fluorescent proteins into THS.[229] To this end, a THS mutant that displays one free cysteine residue on the inside surface of each β-subunit was expressed in *E. coli* BL21 (DE3) Codon Plus-RIL. Fermentations in nutrient rich Terrific Broth medium were carried out at 30°C. Purification of THS with a 1:1 ratio of both subunits was performed in three chromatography steps. An anion-exchange chromatography to capture the THS from

[228] J. Lucon, S. Qazi, M. Uchida, G. J. Bedwell, Ben LaFrance, P. E. Prevelige Jr, T. Douglas, *Nat. Chem.* **2012**, *4*, 781–788.

[229] N. Bruns, K. Pustelny, L. M. Bergeron, T. A. Whitehead, D. S. Clark, *Angew. Chem. Int. Ed.* **2009**, *48*, 5666–5669.

the cell lysate was followed by size-exclusion chromatography to remove low molecular mass assemblies and single subunits. The remaining cell sample was further purified by a second, high-resolution anion-exchange chromatography to yield fully assembled $\alpha_8/\beta_8$ THS.[230] The corresponding fractions were identified by SDS-PAGE and native gel electrophoresis (Figure 7.3c and d), which resulted in proteins with 960 kDa in mass.

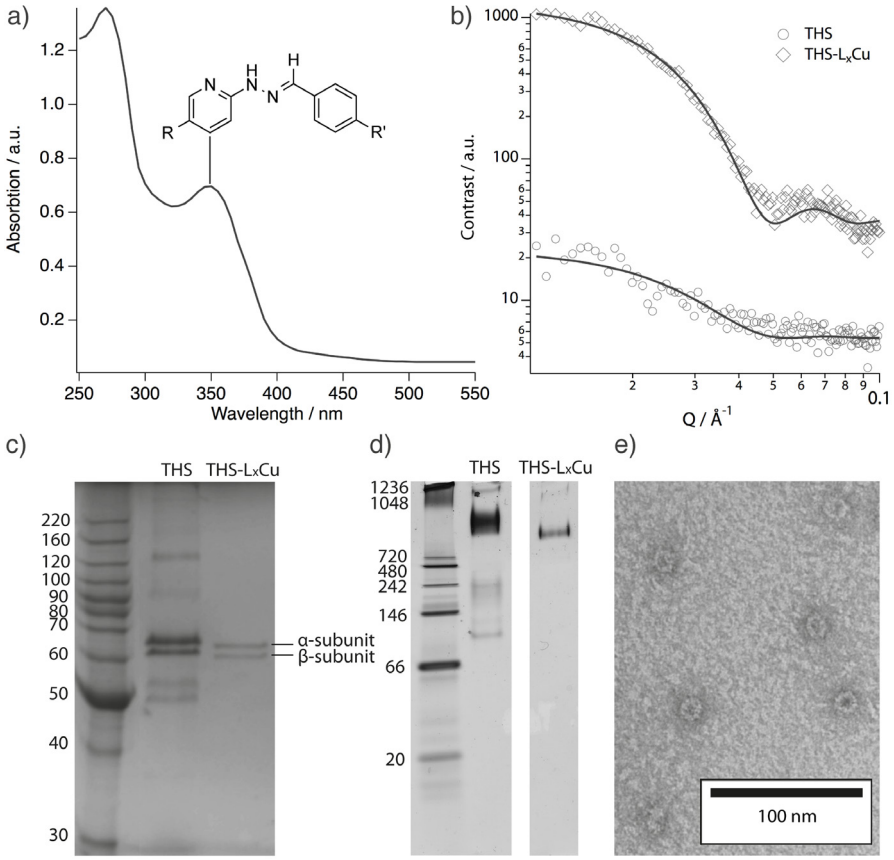


**Figure 7.3** Characterization of THS-$L_x$Cu. a) UV/Vis data reveals a molar substitution ratio of 3.9 ± 0.1 bis-aryl hydrazone bonds and therefore ligands per THS. b) SAXS data of THS-$L_x$Cu in comparison to non-modified THS shows a higher contrast induced by the electron-dense copper that is bound to the ligand in the THS. c) SDS gel electrophoresis of the THS-$L_x$Cu, d) native gel electrophoresis, and e) TEM images of THS-$L_x$Cu show that the cage structure of the THS is not affected by the conjugation of ligands and the complexation of $Cu^{II}$.

The β-subunit displaying a free cystein residue was completely modified with a 25-fold excess (with respect to thiol groups) of 3-maleimido-6-hydraziniumpyridine hydrochloride (MHPH) as determined by UV/Vis spectroscopy. After purification, the modified THS was reacted with (**1**), a derivative of the ligand *N*,*N*,*N*′,*N*′-

[230] N. Bruns, K. Pustelny, L. M. Bergeron, T. A. Whitehead, D. S. Clark, *Angew. Chem. Int. Ed.* **2009**, *48*, 5666–5669.

tetraethyldiethylene triamine (TEDETA) featuring an aromatic aldehyde moiety (Figure 7.2). The reaction yielded a stable bis-aryl hydrazone bond between the protein and the ligand.[231] The formation of this linker is traceable by UV/Vis spectroscopy, as it has a characteristic absorption band with a maximum at 354 nm. Figure 7.3a shows the UV/Vis spectrum of the conjugate. The typical adsorption band of proteins with a maximum at 280 nm as well as the band of the bis-aryl hydrazone link are clearly observable. The deconvolution of this spectrum allows calculation of the average number of bis-aryl hydrazone bonds and therefore ratio of ligands per THS to be 3.9 ± 0.1.

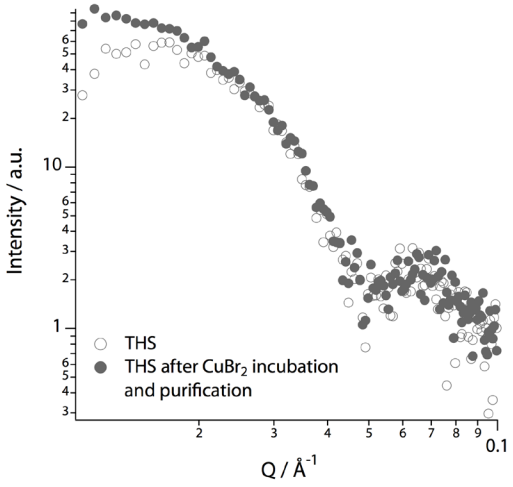


**Figure 7.4** Comparison of SAXS data of non-modified THS and non-modified THS that was incubated with $CuBr_2$ and purified by the steps as performed for the THS with engineered ligand. The data show no differences in shape and therefore indicates that copper is not complexed at the THS itself.

The attached ligand was used to complex $Cu^{II}$ ions, followed by purification of the modified THS (THS-$L_xCu$) by size exclusion spin centrifugation. The linker can only have formed inside the THS due to the location of the engineered cysteine residues. Therefore, the TEDETA-Cu complex must be entrapped in the cavity of the chaperonin. This was confirmed by small angle X-ray scattering (SAXS) measurements. THS-$L_xCu$ showed an increased contrast compared to the non-modified THS (Figure 7.3b). This indicates that the former is a nano-object with higher electron density than the THS alone, i.e. the engineered THS contained copper ions. The fit resulted in a diameter of 17.2 nm for THS-$L_xCu$, which is in agreement with the diameter of the protein in the apo state.[232] Therefore, it can be concluded that the

[231] a) G. T. Hermanson, *Bioconjugate Techniques*, Academic Press, Maryland Heights, **2008** b) A. Grotzky, T. Nauser, H. Erdogan, A. D. Schlüter, P. Walde, *J. Am. Chem. Soc.* **2012**, *134*, 11392–11395.

[232] a) G. Schoehn, E. Quaite-Randall, J. L. Jiménez, A. Joachimiak, H. R. Saibil, *J. Mol. Biol.* **2000**, *296*, 813–819 b) M. Nitsch, J. Walz, D. Typke, M. Klumpp, L. O. Essen, W. Baumeister, *Nat. Struct. Biol.* **1998**, *5*, 855–857.

electron rich copper ions reside in the inner cavities of the THS. In order to elucidate whether the THS alone, i.e. without a TEDETA ligand, also binds copper, non-modified THS was incubated in a $CuBr_2$ solution and purified as described above. The comparison of SAXS data of this sample with data of THS that had not been exposed to $Cu^{II}$ shows no difference in shape (Figure 7.4). This indicates that copper is not complexed by the THS itself.

The SAXS data give a first indication that THS maintains its structural integrity upon introduction of the ATRP catalyst. In order to further prove this, the protein cage was analyzed by sodium dodecyl sulfate polyacrylamide gel electrophoresis (SDS PAGE) and by native PAGE (Figure 7.3c and d). Both gels show the same bands for THS, independent of their modification with the ATRP catalyst. Furthermore, transmission electron microscopy (TEM) images of the protein-catalyst conjugate show spherical objects approx. 16 nm in diameter, which are typical for fully assembled THS (Figure 7.3e).[233] Thus, the overall structure of THS appears to not be affected by the encapsulated ATRP catalyst.

### 7.2.2 Polymerization of NiPAAm with THS-$L_x$Cu

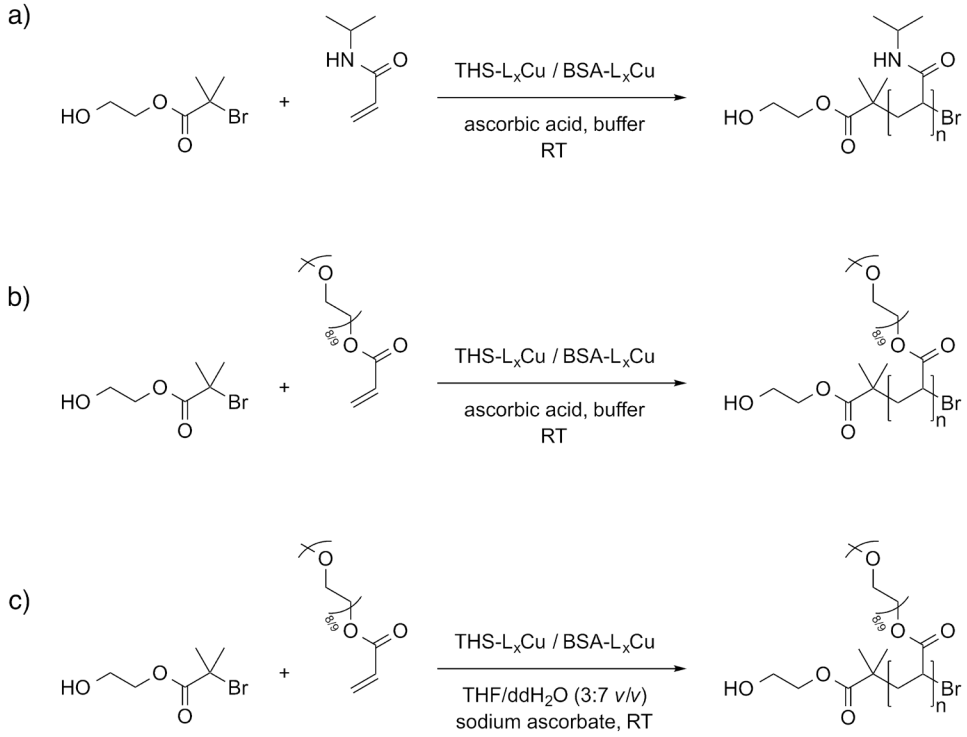


**Figure 7.5** Reaction schemes for the synthesis of a) pNiPAAm in buffer solution b) pPEGA in buffer solution and c) pPEGA in a $ddH_2O$/THF (7:3 *v*/*v*) solution mixture under ARGET ATRP conditions.

[233] a) G. Schoehn, E. Quaite-Randall, J. L. Jiménez, A. Joachimiak, H. R. Saibil, *J. Mol. Biol.* **2000**, *296*, 813–819 b) M. Nitsch, J. Walz, D. Typke, M. Klumpp, L. O. Essen, W. Baumeister, *Nat. Struct. Biol.* **1998**, *5*, 855–857 c) M. G. Bigotti, A. R. Clarke, *J. Mol. Biol.* **2005**, *348*, 13–26.

Polymerizations were conducted by adding THS-$L_x$Cu to an aqueous buffered solution (100 mM sodium acetate, 150 mM NaCl, 80 mM $MgCl_2$, pH 5.2) of the water-soluble initiator 2-hydroxyethyl-2-bromoisobutyrate (HEBIB) and the monomer N-isopropylacrylamide (NiPAAm) in molar ratios of [Monomer]:[Initiator]:[THS-$L_x$Cu] 67:1:1.5 x $10^{-5}$ under argon atmosphere (reaction scheme see Figure 7.5). An excess of ascorbic acid (AscA) (ratio [THS-$L_x$Cu]:[AscA] 1:2.7 x $10^{-5}$) was added to reduce $Cu^{II}$ in situ to its catalytically active form THS-$L_xCu^{I}$ and to regenerate $Cu^{II}$ that could accumulate during the polymerization, according to the activators regenerated by electron transfer (ARGET) ATRP method.[234] The polymerization was stopped after 20 hours by exposure to ambient air and addition of non-deoxygenated buffer solution. Polymerizations were performed using the THS nanoreactor in its apo state, i.e. in the absence of ATP. In this state both lids of the protein cage are open.[235] Thus, any macromolecules that are synthesized within the THS can leave the cavities after polymerization.

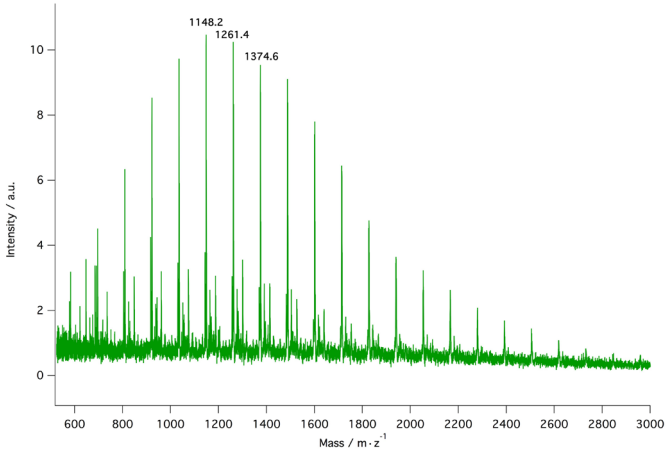


**Figure 7.6** MALDI-ToF MS data of pNiPAAm synthesized with THS-$L_x$Cu in aqueous buffer.

Poly(N-isopropyl acrylamide) (pNiPAAm) was separated from the protein cage by size exclusion spin centrifugation (100k MWCO) leaving the THS in the supernatant while the polymer could be collected from the flow-through. Matrix assisted laser desorption/ionization time of flight mass spectrometry (MALDI-ToF MS) of the latter showed a series of signals spaced 113.2 m $z^{-1}$, with a number average molecular weight of 1500 g $mol^{-1}$ and a polydispersity index (PDI) of 1.11 (Figure 7.6). As the molecular weight of the monomer is 113.16 g $mol^{-1}$, this data shows that the reaction yielded pNiPAAm. The low PDI indicates that the polymerization proceeded with a good degree of control. Peak analysis of the MALDI-ToF MS spectra reveals a

234 K. Matyjaszewski, *Macromolecules* **2012**, *45*, 4015–4039.

235 a) J. Zhang, M. L. Baker, G. F. Schröder, N. R. Douglas, S. Reissmann, J. Jakana, M. Dougherty, C. J. Fu, M. Levitt, S. J. Ludtke, et al., *Nature* **2010**, *463*, 379–383 b) M. G. Bigotti, A. R. Clarke, *Arch. Biochem. Biophys.* **2008**, *474*, 331–339.

repeating set of peaks separated from adjacent sets by the monomer molecular weight of 113.16 Da. Under the applied MALDI-ToF MS conditions, adducts with three different ions $H^+$, $Na^+$ and $K^+$ and the polymer are formed. A detailed analysis of the attributed peaks and a comparison to the calculated values is shown in Figure 7.7.

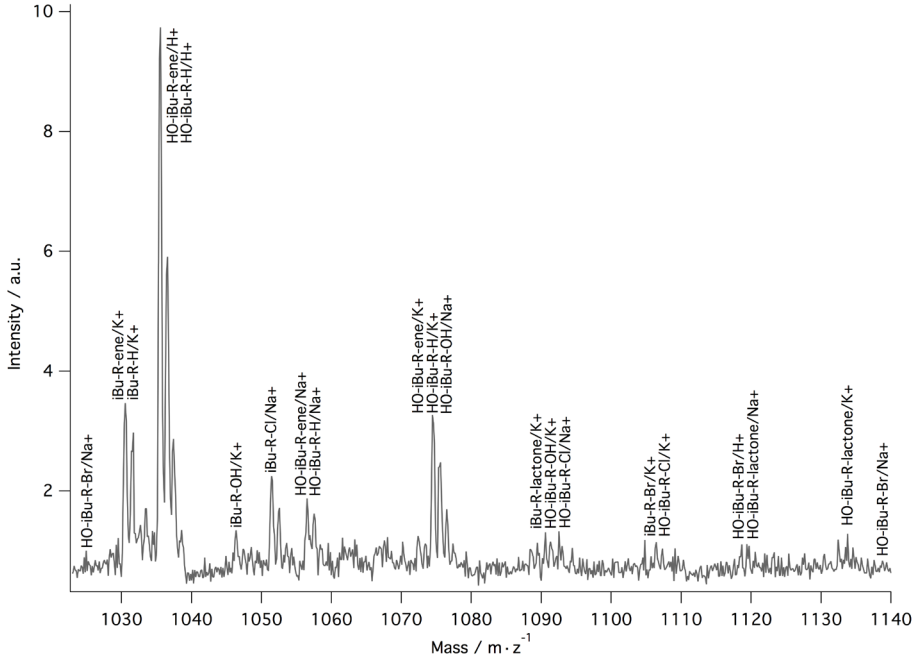


**Figure 7.7** The Figure shows a zoom of the main spectra (Figure 7.6) being a repeating set of peaks starting with HO-iBu-R-Br/$Na^+$ where R = $(NiPAAm)_n$. In the chosen MALDI-ToF MS conditions, adducts of the polymer with three different ions $H^+$, $Na^+$ and $K^+$ are formed. In addition, the peaks correspond to chains bearing a hydroxyethyl isobutyrate (HO-iBu) or due to the acidic conditions of MALDI-ToF MS sample preparation an isobutyric acid (iBu) residue from the initiator at one end and an H, ene, OH, Br, Cl or a lactone residue at the other chain end. Although in radical polymerization -H or unsaturated analogue -ene end groups might be the result of a disproportionation during the reaction, halogen-terminated polymers products tend to yield -H, -ene, -OH and -lactone end groups next to the halogens in mass spectrometric measurements.[236] These end groups are presumed to be generated during the ionization process in the MS rather than by poor control over the polymerization reaction. We also observe chloride terminated polymers next to the bromine termination. This is expected due to the presence of $MgCl_2$ and NaCl in the buffer that was used for the polymerization.

To set our findings into perspective, polymerizations were conducted under the same conditions, but with the ATRP catalyst conjugated to the outside of a globular protein, bovine serum albumin (BSA), instead of the protein nanoreactor, as described in chapter 2. The synthesis of NiPAAm was performed under ARGET ATRP conditions with BSA-$L_xCu$ as catalyst. Gel permeation chromatography (GPC)

[236] a) Y. Xia, X. Yin, N. A. Burke, H. D. Stöver, *Macromolecules* **2005**, *38*, 5937–5943 b) F. Ganachaud, M. J. Monteiro, R. G. Gilbert, M.-A. Dourges, S. H. Thang, E. Rizzardo, *Macromolecules* **2000**, *33*, 6738–6745.

determined pNiPAAm with an apparent molecular weight $M_n$ of 42600 g mol$^{-1}$ (calibrated against poly(methyl methacrylate)) and a PDI of 1.94 (GPC trace see Figure 2.8). By comparing the two different catalytic systems, THS as protein nanoreactor versus the globular protein BSA, we can draw the conclusion that the synthesized polymers are substantially shorter and have a lower PDI if produced in the nanoreactor. This indicates that the synthesis of pNiPAAm, which is intrinsically difficult to control in aqueous solution,[237] benefits from the confined reaction space and exerts greater control over the polymerization. Further, the lower $M_n$ indicates that the polymer synthesis is slower (e.g. due to diffusion limitations) and stops at shorter chain lengths. This is most probably due to either the space constriction within the cavities of the THS nanoreactor or the diffusion of polymer chain out of the nanoreactor. A reason for the low degree of control with the BSA-$L_x$Cu may derive from the very low concentration of catalyst in the system. This can be neglected in the THS since the growing polymer chain stays in close proximity to the catalyst inside of the nanoreactor.

### 7.2.3 Polymerization of PEGA with THS-$L_x$Cu

The scope of THS as nanoreactor for polymerizations was further explored by conducting the experiments with a different monomer. Poly(ethylene glycol) methyl ether acrylate (PEGA) with a number average molecular weight of 480 g mol$^{-1}$ was polymerized with THS-$L_x$Cu under the same ARGET ATRP conditions used for pNiPAAm, yielding poly(Poly(ethylene glycol) methyl ether acrylate ) (pPEGA) with a poly(ethylene oxide)-apparent $M_n$ of 14700 g mol$^{-1}$ and a PDI of 1.95, as analyzed by GPC (reaction schemes see Figure 7.5). In comparison, the BSA-conjugated catalyst produced pPEGA with apparent $M_n$ of 119400 g mol$^{-1}$ and a PDI of 3.12. In addition, the polymerization of PEGA with THS-$L_x$Cu was run in the presence of ATP. By the hydrolysis of ATP the THS cycles between open and closed states.[238] The reaction resulted in pPEGA with an apparent $M_n$ of 17500 g mol$^{-1}$ and a PDI of 2.50. As the addition of ATP had no beneficial effect on the polymerization, the following reactions were carried out without ATP.

Addition of organic co-solvents to aqueous ATRP can result in better performance of a given catalyst, since side reactions, e.g. disproportionation of the ATRP activator, loss of the halide ligand by the ATRP deactivator as well as fast chain propagation are suppressed, thus resulting in better-controlled polymerizations.[239] Therefore, PEGA was also polymerized in a 7:3 *v*/*v* mixture of double distilled water (dd$H_2O$) and THF, using THS-$L_x$Cu as catalyst (reaction schemes see Figure 7.5). The product of this experiment resulted in an apparent $M_n$ of 1400 g mol$^{-1}$ and a PDI of 1.06 (Figure 7.8). BSA-$L_x$Cu yielded pPEGA with an apparent $M_n$ of 14900 g mol$^{-1}$ and a PDI of 1.84. The PDI and the average molecular weight of pPEGA synthesized in the presence of

[237] P.-E. Millard, N. C. Mougin, A. Böker, A. H. E. Müller, in *Controlled/Living Radical Polymerization: Progress in ATRP, ACS Symp. Ser.*, American Chemical Society, Washington, D.C., U.S.A., **2009**, pp. 127–137.
[238] M. G. Bigotti, A. R. Clarke, *Arch. Biochem. Biophys.* **2008**, *474*, 331–339.
[239] N. V. Tsarevsky, K. Matyjaszewski, *Chem. Rev.* **2007**, *107*, 2270–2299.

organic co-solvent are lower compared to the ones obtained without co-solvents. In addition, these experiments confirm that reactions carried out in nanoreactors yield a narrower distribution of polymers.

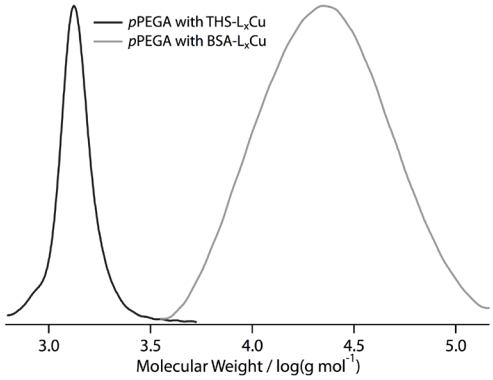


**Figure 7.8** Comparison of GPC traces from pPEGA synthesized with THS-$L_x$Cu or with BSA-$L_x$Cu in a dd$H_2O$/THF (7:3 *v*/*v*) mixture.

For the ATRP to be confined into the THS, the protein cage has to be stable during the polymerization. The most harsh reaction condition was the one with THF as co-solvent. It was therefore assessed whether or not the THS retained its structure in a typical PEGA polymerization in this water/THF mixture. For that purpose a sample of the reaction mixture after polymerization was characterized by gel electrophoresis and TEM. SDS and native PAGE (Figure 7.9a and b) show the distinct bands of the two subunits and of the fully assembled THS without residues of degraded protein. Moreover, TEM (Figure 7.9c) indicates that the shape and size of the protein cage remains intact. Thus, the protein cage was stable under these reaction conditions.

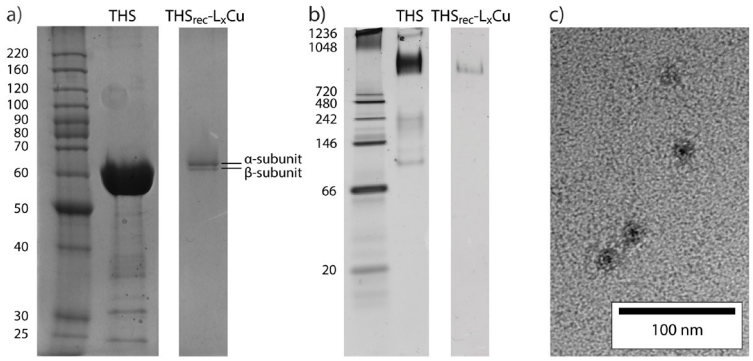


**Figure 7.9** Characterization of THS-$L_x$Cu after the polymerization in a 7:3 *v*/*v* mixture of water and THF. a) SDS gel electrophoresis, b) native gel electrophoresis and c) TEM images of THS-$L_x$Cu recovered after polymerization ($THS_{rec}$-$L_x$Cu). The data allows the conclusion that THS remains stable during polymerization and retains its structure.

A set of control reactions was carried out to ensure that only the Cu-TEDETA complex in the THS bears copper that is catalytically active in ATRP. Non-modified THS was incubated with $CuBr_2$ solution. Then, size exclusion spin centrifugation was used to remove the unbound copper. The resulting THS was used to polymerize NiPAAm and PEGA under the conditions described above. The reactions did not yield polymer products as checked by $^1H$ NMR and GPC. These experiments, in combination with the SAXS data discussed above (Figure 7.4), indicate that copper ions are not complexed by the protein. Further, we assessed whether the bis-aryl hydrazone linker could complex copper ions in an ATRP-active form. For this purpose an analogue of the BSA-$L_x$ was produced that incorporated the linker, but no TEDETA ligand. BSA was modified with MHPH, followed by reaction with methyl 4-formylbenzoate (4FB) (Figure 7.10). The modified protein BSA-4FB was mixed with $CuBr_2$ solution. After size exclusion spin centrifugation it was used as a catalyst for ARGET ATRP of NiPAAm with the same reaction conditions as described above. The polymerization with BSA-4FB did not yield any polymer as checked by $^1H$ NMR and GPC. This control reaction with BSA-4FB indicates that, even though copper ions might be complexed by the linker, only TEDETA in combination with copper ions results in complexes that are able to catalyze ATRP. This underscores the necessity for conjugating a suitable Cu-binding ligand into the THS in order to obtain an ATRP catalyst inside of the protein cage.

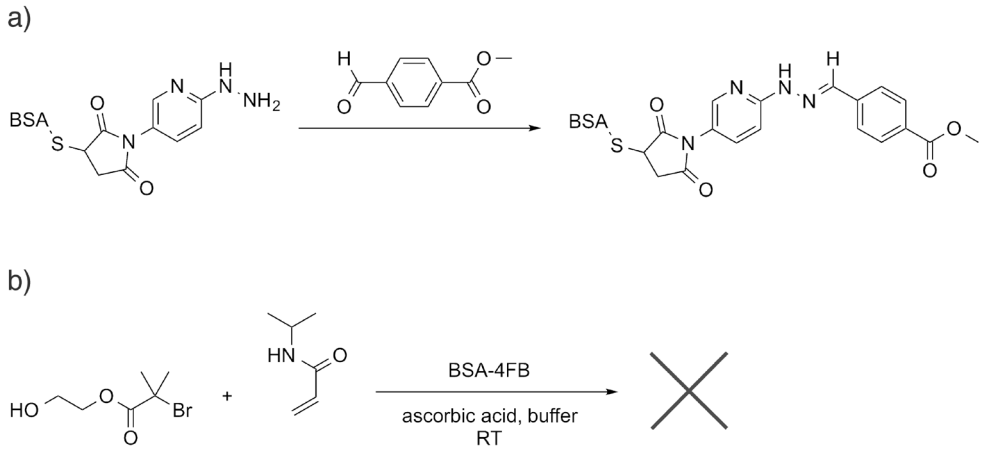


**Figure 7.10** Reaction with BSA-4FB. a) BSA-MHPH was modified with methyl 4-formylbenzoate to yield BSA-4FB b) Reaction scheme for the synthesis of pNiPAAm with BSA-4FB in buffer solution under ARGET ATRP conditions.

## 7.3 Conclusion

We introduced the chaperonin THS as a nanoreactor and conducted ATRP in the protein cage by binding an ATRP catalyst to the inner cavities of the protein. THS is particularly appealing for this application as it has pores that are large enough to allow macromolecules to enter and leave the cavities. The synthesized polymers are therefore released into the surrounding solution without having to disassemble the protein cage into its subunits. We showed that the confined space within the nanoreactor results in polymers with a narrower molecular weight distribution compared to a system where the catalyst is conjugated to a globular protein. Such a positive effect on the polymerization is most probably due to the proximity of the ATRP reagents and is consistent with simulations of other nanoreactor systems.[240]

Protein nanoreactors could influence polymerizations in some unique ways, e.g. by imparting selectivity for certain monomers, or by modulating the rate of the polymerization through triggers that close and open pores in the protein wall. As chaperonins are Nature's folding chambers, they could beneficially affect the folding of (block)copolymers when sequestered single polymer chains are synthesized within their cavity. In addition, the use of protein nanoreactors could enable mechanistic studies of ATRP on a single molecule level.

[240] P. B. Zetterlund, *Polym. Chem.* **2011**, *2*, 534.

# 8 Incorporation of ATRPases into Protein Nanoreactors[241]

*Kasper Renggli, Nora Sauter, Martin G. Nussbaumer, Raphael Urbani, Mohamed Chami, Thomas Pfohl and Nico Bruns*

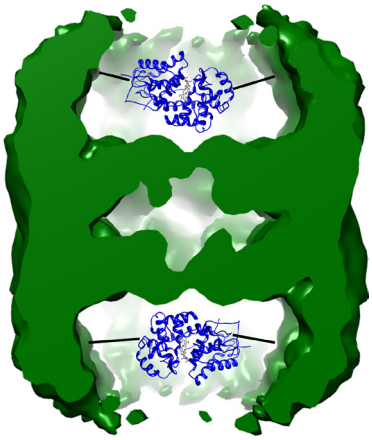

*In a first experimental approach we demonstrated the incorporation of ATRPases, i.e. horseradish peroxidase, into the cavities of the chaperonin thermosome. The resulting nanoreactor was used to polymerize PEGA under ARGET ATRP conditions in a mixture of 7:3 v/v water and THF under an argon atmosphere. The resulting polymers benefit from the confined space of the nanoreactor.*

[241] Parts of this chapter were published in: a) N. Bruns, S. Lörcher, K. Makyla, K. Renggli, M. Spulber, *Chimia* **2013**, *67*, 777–781 b) K. Renggli, P. Baumann, K. Langowska, O. Onaca, N. Bruns, W. Meier, *Adv. Funct. Mater.* **2011**, *21*, 1241–1259.

## 8.1 Introduction

Nanoreactors provide a confined reaction space with dimensions on the nanoscale.[242] Chemical reactions are confined to these yocto liter volumes when catalysts are enclosed into the nanoreactors. Compartmentalization and confinement of reactions into defined reaction spaces is a very common principle in nature. For example, cells and organelles provide microscopic reaction space, while in lipid vesicles, the iron-storage protein ferritin and bacterial protein microcompartments are examples of nanoscale reaction compartments. In addition, the confinement of reactions into nanoscale reaction volumes offers several advantages for technological applications and enhanced synthetic chemistry.[243] For example, side reactions can be suppressed, as the confined volume brings reagent and catalysts into closer spatial proximity.[244] Moreover, the selectivity of a reaction can be altered by controlling the type of substrates which can permeate into the nanoreactor.[245] Also, a nanoreactor provides a protective shell that shields the enclosed catalyst from degrading agents outside of the nanoreactor, therefore allowing it to function in otherwise prohibitive environments. Examples of this can be found in the non-native enzymatic reactions within living cells.[246] Moreover, nanoreactors can be used to study catalytic reactions on the single molecule level.[247] The catalytic species within the confined volume are frequently enzymes. We have been studying two kinds of nanoreactors recently, polymersomes[248] and protein cages.[249]

---

[242] a) K. Renggli, P. Baumann, K. Langowska, O. Onaca, N. Bruns, W. Meier, *Adv. Funct. Mater.* **2011**, *21*, 1241–1259 b) K. T. Kim, S. A. Meeuwissen, R. J. M. Nolte, J. C. M. van Hest, *Nanoscale* **2010**, *2*, 844.

[243] a) D. M. Vriezema, M. Comellas Aragonès, J. A. A. W. Elemans, J. J. L. M. Cornelissen, A. E. Rowan, R. J. M. Nolte, *Chem. Rev.* **2005**, *105*, 1445–1490 b) M. Uchida, M. T. Klem, M. Allen, P. Suci, M. Flenniken, E. Gillitzer, Z. Varpness, L. O. Liepold, M. Young, T. Douglas, *Adv. Mater.* **2007**, *19*, 1025–1042 c) A. de la Escosura, R. J. M. Nolte, J. J. L. M. Cornelissen, *J. Mater. Chem.* **2009**, *19*, 2274 d) K. T. Kim, S. A. Meeuwissen, R. J. M. Nolte, J. C. M. van Hest, *Nanoscale* **2010**, *2*, 844 e) K. Renggli, P. Baumann, K. Langowska, O. Onaca, N. Bruns, W. Meier, *Adv. Funct. Mater.* **2011**, *21*, 1241–1259 f) M. Marguet, C. Bonduelle, S. Lecommandoux, *Chem. Soc. Rev.* **2012**, *42*, 512.

[244] T. Terashima, A. Nomura, M. Ouchi, M. Sawamoto, *Macromol. Rapid Commun.* **2012**, *33*, 833–841.

[245] K. Renggli, P. Baumann, K. Langowska, O. Onaca, N. Bruns, W. Meier, *Adv. Funct. Mater.* **2011**, *21*, 1241–1259.

[246] P. Tanner, V. Balasubramanian, C. G. Palivan, *Nano Lett.* **2013**, *13*, 2875–2883.

[247] a) M. Comellas Aragonès, H. Engelkamp, V. I. Claessen, N. A. J. M. Sommerdijk, A. E. Rowan, P. C. M. Christianen, J. C. Maan, B. J. M. Verduin, J. J. L. M. Cornelissen, R. J. M. Nolte, *Nat. Nanotechnol.* **2007**, *2*, 635–639 b) S.-H. Shin, H. Bayley, *J. Am. Chem. Soc.* **2005**, *127*, 10462–10463.

[248] M. Spulber, A. Najer, K. Winkelbach, O. Glaied, M. Waser, U. Pieles, W. Meier, N. Bruns, *J. Am. Chem. Soc.* **2013**, *135*, 9204–9212.

[249] K. Renggli, M. G. Nussbaumer, R. Urbani, T. Pfohl, N. Bruns, *Angew. Chem. Int. Ed.* **2014**, *53*, 1443–1447.

An intriguing possibility for responsive nanoreactors is the use of protein cages. Examples are ferritin,[250] viral capsids,[251] and bacterial microcompartments.[252] These hollow nanostructures self-assemble from various protein subunits, and range in diameter from < 10 nm to more than 500 nm. Some of them assemble or disassemble in response to changes in their environment[253] and others possess pores that open, widen or close in the presence of certain triggers.[254] We have explored the thermosome (THS), a chaperonin from the archea *Thermoplasma acidophilum*, as a functional nanostructure. For example, we have entrapped a pair of fluorescent proteins and used the thermosome as a scaffold that brings the proteins into defined proximity to enable fluorescence resonance energy transfer (FRET) between the two proteins.[255] As reported in chapter 7, we have focused on the possibility of using the thermosome as a nanoreactor for polymerization reactions, as it has pores that are large enough to allow macromolecules and synthetic polymers to enter and leave the protein cage. We have encapsulated a copper complex as catalysts for atom transfer radical polymerization (ATRP) into the cavity of THS and conducted ATRP of N-isopropyl-acrylamide (NiPAAm) and poly(ethylene glycol) methylacrylate (PEGA) within the cage.[256] The effect of the confined reaction space, as predicted by simulations,[257] manifested itself in smaller but more narrowly dispersed polymer products compared to polymers synthesized under comparable conditions with a catalyst conjugated to a globular protein.[256]

By combining the advantages of the THS nanoreactor with the functionalities of the ATRPases described in chapters 3 to 5, we aim to replace the copper catalyst with a more environmentally friendly catalyst, rendering the resulting polymers more compatible with biomedical, food grade and electronic device requirements. For this purpose we encapsulated horseradish peroxidase (HRP) into the thermosome with a similar approach as previously reported by Bruns et al.[255]

---

250 T. Ueno, M. Suzuki, T. Goto, T. Matsumoto, K. Nagayama, Y. Watanabe, *Angew. Chem. Int. Ed.* **2004**, *43*, 2527–2530.

251 a) M. Comellas Aragonès, H. Engelkamp, V. I. Claessen, N. A. J. M. Sommerdijk, A. E. Rowan, P. C. M. Christianen, J. C. Maan, B. J. M. Verduin, J. J. L. M. Cornelissen, R. J. M. Nolte, *Nat. Nanotechnol.* **2007**, *2*, 635–639 b) D. P. Patterson, P. E. Prevelige, T. Douglas, *ACS Nano* **2012**, *6*, 5000–5009.

252 T. O. Yeates, C. A. Kerfeld, S. Heinhorst, G. C. Cannon, J. M. Shively, *Nat. Rev. Microbiol.* **2008**, *6*, 681–691.

253 M. Comellas Aragonès, H. Engelkamp, V. I. Claessen, N. A. J. M. Sommerdijk, A. E. Rowan, P. C. M. Christianen, J. C. Maan, B. J. M. Verduin, J. J. L. M. Cornelissen, R. J. M. Nolte, *Nat. Nanotechnol.* **2007**, *2*, 635–639.

254 J. A. Speir, S. Munshi, G. Wang, T. S. Baker, J. E. Johnson, *Structure* **1995**, *3*, 63–78M. G. Bigotti, A. R. Clarke, *Arch. Biochem. Biophys.* **2008**, *474*, 331–339.

255 a) N. Bruns, K. Pustelny, L. M. Bergeron, T. A. Whitehead, D. S. Clark, *Angew. Chem. Int. Ed.* **2009**, *48*, 5666–5669 b) N. Bruns, D. S. Clark, *Chimia* **2011**, *65*, 245–249.

256 K. Renggli, M. G. Nussbaumer, R. Urbani, T. Pfohl, N. Bruns, *Angew. Chem. Int. Ed.* **2014**, *53*, 1443–1447.

257 P. B. Zetterlund, *Polym. Chem.* **2011**, *2*, 534–549.

## 8.2 Results & Discussion

### 8.2.1 Preparation of THS-HRP

To encapsulate horseradish peroxidase into the thermosome, specific chemical attachment points had to be engineered into the cavities of the THS complex. A mutation at K316C of the β-subunit introduced four cysteine residues into the inner cavity of each hemisphere, which enabled selective coupling of protein guests inside the THS. To avoid attachment of HRP on the outside of the THS, the surface exposed cysteines of each subunit on the native THS were replaced by alanines.[258] The mutated α- and β-subunit genes were co-expressed in *E. coli*, as described in section 7.2.1.

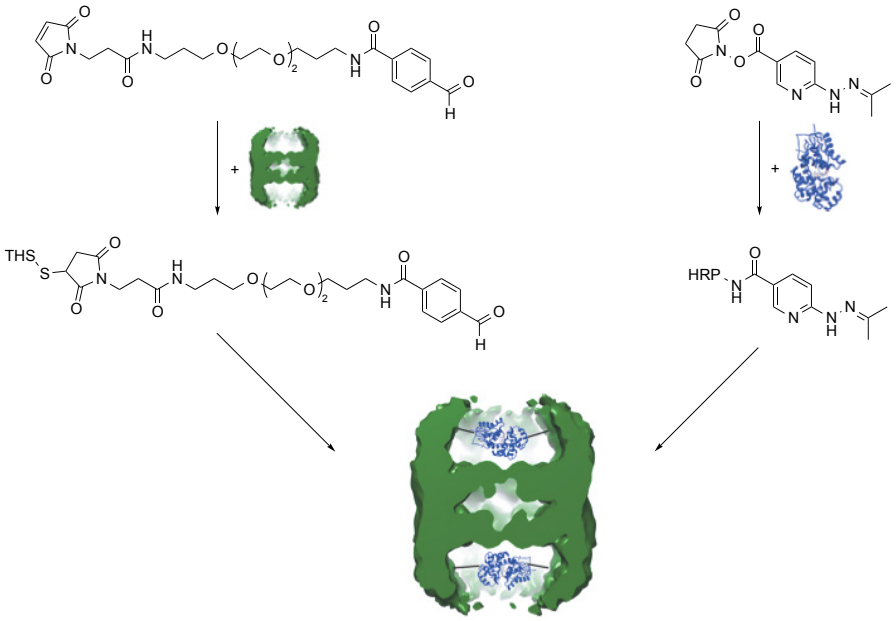


**Figure 8.1** Coupling strategy to covalently bind a HRP inside the cavities of THS. The free cysteins on the β-subunits of THS are modified with MTFB, using maleimide chemistry. The HRP is modified with HyNic which targets the lysine residues with succinimidyls. The resulting THS-HRP includes up to two HRP molecules into the cavities of one THS.

In Figure 8.1 the strategy to covalently enclose the guest enzyme HRP into the cavities of the THS is shown. In a first step, the four free cystein on the β-subunits in each cavity of the the THS were modified with the heterobifunctional linker maleimido trioxa-6-formyl benzamide (MTFB) to introduce an aromatic aldehyde by the means of maleimide chemistry. The HRP on the other hand was modified via its lysins with succinimidyl 6-hydrazinonicotinate acetone hydrazine (HyNic), a second heterobifunctional linker that introduced a hydrazine residue.

[258] N. Bruns, K. Pustelny, L. M. Bergeron, T. A. Whitehead, D. S. Clark, *Angew. Chem. Int. Ed.* **2009**, *48*, 5666–5669.

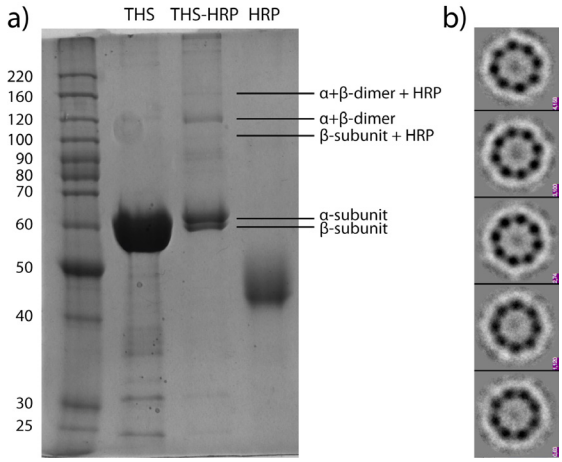


**Figure 8.2** Characterization of THS-HRP. a) SDS-PAGE of THS, THS-HRP and HRP. The presence of bands at approx. 100 kDa and 160 kDa indicate that THS can be functionlized with HRP (Subunit 58 kDa + HRP 44 kDa). b) Averaged cryo-electron microscopy images of THS-HRP display the typical hexadecameric structure of THS, indicating that the THS-HRP remains stable after formation. Furthermore, the enclosed HRP can be suspected in the center of the structure.

The modified THS protein cage and the modified enzyme HRP were conjugated in a simple incubation step. A 25-fold excess of HRP with respect to THS was used to couple the host and guest in buffer by mixing for 14 h at room temperature. The guest-host complex was purified by size-exclusion chromatography that separated the unreacted HRP from the THS-HRP. The SDS-PAGE in Figure 8.2a indicates that THS is functionlized with HRP by displaying bands at approx. 100 and 160 kDa for the β-subunit-HRP dimer and the α/β-subunit-HRP trimer. Cryo-electron microscopy images of THS-HRP (averaged over several hundred structures to increase the signal-to-noise ratio) display the typical hexadecameric structure of THS, indicating that the THS-HRP remains stable after formation (Figure 8.2b). Furthermore, the enclosed HRP can be suspected in the center of the structure. The complex was further confirmed by UV/Vis spectroscopy (Figure 8.3a) and showed three distinct bands corresponding to THS and HRP (280 nm), HyNic-MTFB (354 nm) and HRP (402 nm) allowing for calculation of the molecular substitution ratio of 0.3 ± 0.1 HRP per THS. In addition, small angle X-ray scattering (SAXS) confirms that the HRP is located inside the THS since the intensity is lower compared to an unfunctionalized and therefore empty THS (Figure 8.3b). This indicates that the former is a structure with higher electron density compared to THS-HRP, i.e. the empty THS contained in the cavities water molecules that possess a higher electron density than the encapulated HRP.

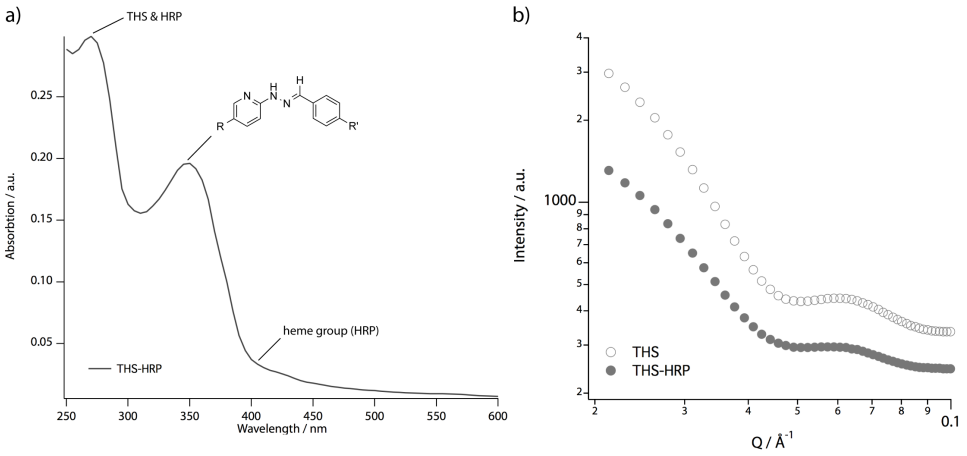


**Figure 8.3** Characterization of THS-HRP. a) UV/Vis spectrosopy of THS-HRP revealed a molecular substitution ratio of 0.3 ± 0.1 HRP per THS using the absorbtion of THS and HRP (280 nm), HyNic-MTFB (354 nm) and HRP (402 nm). b) SAXS measurements of empty THS and THS-HRP indicate an incorporation of HRP due to different electron density contrast.

### 8.2.1 Polymerization of PEGA with THS-HRP

As indicated by the results of THS-$L_x$Cu, addition of organic co-solvents to aqueous ATRP can result in better performance of a given catalyst. By adding organic co-solvent, side reactions tend to play a less domiant role and therefore the polymerization is better-controlled/living.[259] Therefore, a 7:3 *v*/*v* mixture of double distilled water (dd$H_2O$) and THF under argon atmosphere was used as reaction media to polymerize poly(ethylene glycol) methyl ether acrylate (PEGA) with a number average molecular weight of 480 g $mol^{-1}$. The polymerization under ARGET ATRP conditions with THS-HRP as catalyst and 2-hydroxyethyl-2-bromoisobutyrate (HEBIB) as initiator in molar ratios of [Monomer]:[Initiator]:[THS-HRP] 67:1:2 x $10^{-2}$ was performed with sodium ascorbate as reducing agent. GPC revealed pPEGA with a poly(styrene) apparent $M_n$ of 4400 g $mol^{-1}$ and a PDI of 1.08 (reaction scheme see Figure 8.4).

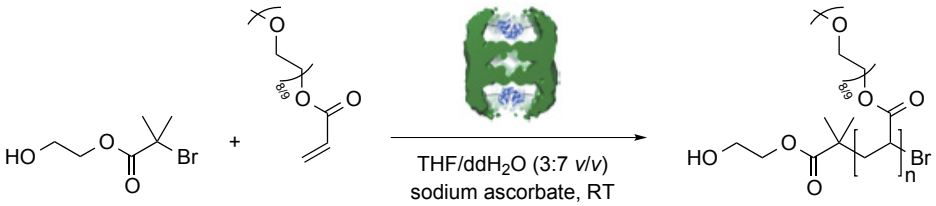


**Figure 8.4** Reaction scheme of the polymerization of PEGA using HEBIB as initiator, sodium ascorbate as reducing agent and THS-HRP as the catalyst under ARGET ATRP conditions in aqueous solution with 3:7 *v*/*v* THF/dd$H_2O$.

[259] N. V. Tsarevsky, K. Matyjaszewski, *Chem. Rev.* **2007**, *107*, 2270–2299.

To assess the effect of the confined space in the THS nanoreactor, polymerizations with free HRP were performed in comparison (HRP characterization see chapter 4). ARGET ATRP with HRP yielded pPEGA with an poly(styrene) apparent molecular weight $M_n$ of 5500 g mol$^{-1}$ and a PDI of 1.50 as determined by GPC (Figure 8.5). The comparison of the THS-HRP nanoreactor versus the free ATRPase indicates that the resulting polymers are about the same length and have a lower PDI if produced in the nanoreactor. This indicates that the synthesis of pPEGA benefits from the confined reaction space and exerts greater control over the polymerization, indicated by a narrower molecular weight distribution. A reason for the higher degree of control with THS-HRP may derive from the close proximity of the growing polymer chain to the ATRPase inside the nanoreactor. This indicates that THS-HRP also benefits from the confined space of the nanoreactor, as demonstrated for THS-$L_x$Cu,[260] when we incorporate HRP.

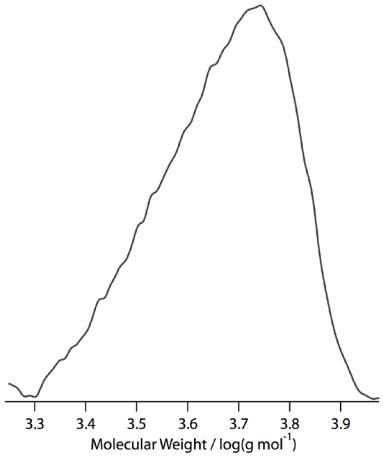


**Figure 8.5** GPC traces of pPEGA synthesized with THS-HRP in a dd$H_2O$/THF (7:3 *v*/*v*) mixture.

In comparison, the THS-conjugated catalyst THS-$L_x$Cu produced pPEGA with poly(ethylene oxide) apparent $M_n$ of 1400 g mol$^{-1}$ and a PDI of 1.06. In addition, the polymerization of PEGA with the BSA-conjugated catalyst produced pPEGA with apparent $M_n$ of 119400 g mol$^{-1}$ and a PDI of 3.12 (see chapter 7).

## 8.3 Conclusion

In a first experimental approach we demonstrated the incorporation of ATRPases, i.e. horseradish peroxidase, into the cavities of the chaperonin thermosome. The resulting nanoreactor was used to polymerize PEGA under ARGET ATRP conditions in a mixture of 7:3 *v*/*v* water and THF under argon atmosphere. The resulting polymers benefit from the confined space of the nanoreactor as demonstrated in chapter 7 by

[260] K. Renggli, M. G. Nussbaumer, R. Urbani, T. Pfohl, N. Bruns, *Angew. Chem. Int. Ed.* **2014**, *53*, 1443–1447.

THS-$L_x$Cu.[261] These results are consistent with simulations of other nanoreactor systems.[262] Such a positive effect on the polymerization in comparison to BSA-$L_x$Cu (chapter 2) but also to our data with free HRP ins solution,[263] as reported in chapter 4, is most probably due to the close proximity of the ATRP reagents. However, the scope of THS-HRP has to be extended in order to draw further conclusions, e.g. biological stability of the THS-HRP complex, different monomers, kinetic experiments.

Protein nanoreactors with incorporated ATRPases allow for environmentally friendly polymerization with enzymes. The study of single molecule ATRP experiments with THS-incorporated ATRPases could lead to a better understanding of the reaction mechanisms behind ATRPases. Moreover, the THS-HRP system could be used to investigate the influences of external triggers, e.g ATP that open and closes the cavities of the THS nanoreactor, on the polymer product.

Protein cages have been shown to be useful nanoreactors in many cases. Nevertheless, their full potential is merely starting to emerge, as many hollow protein structures have not been studied as nanoreactors. Moreover, the intrinsic gating properties of protein cages and viruses have only been exploited in a few cases. A further possibility to enhance their potential is their site-selective modification. Either naturally occurring points of modification, such as the termini of the peptide chains, can be used, or specific attachment points can be engineered into the protein structure by, e.g. site-directed mutagenesis. Using such methods, it might be possible to selectively modify both the exterior and interior surfaces of cages to create multifunctional nanosystems. Furthermore, the location of a modification can be selected, e.g. whether it is close to a pore in the shell, or spaced apart. No other nanoreactor system allows targeting attachment points with such spatial precision.

Many reactions in organic synthesis require solvents other than water as reaction media. For example, esterifications are commonly carried out in organic solvents in order to drive the equilibrium of the reaction towards the formation of the ester. Also, many synthetic targets are only soluble in non-polar media. Thus, making protein cages compatible with non-aqueous solvents will greatly enhance their applicability as synthetic tools. Promising first steps toward this goal are the solubilisation of a viral capsid in organic solvents,[264] and the genetic modification of the inner surface of DNA binding protein from starved cells (Dps) from hydrophilic to hydrophobic.[265]

---

[261] K. Renggli, M. G. Nussbaumer, R. Urbani, T. Pfohl, N. Bruns, *Angew. Chem. Int. Ed.* **2014**, *53*, 1443–1447.

[262] P. B. Zetterlund, *Polym. Chem.* **2011**, *2*, 534.

[263] S. J. Sigg, F. Seidi, K. Renggli, T. B. Silva, G. Kali, N. Bruns, *Macromol. Rapid Commun.* **2011**, *32*, 1710–1715.

[264] H. R. Johnson, J. M. Hooker, M. B. Francis, D. S. Clark, *Biotechnol. Bioeng.* **2007**, *97*, 224–234.

[265] J. Swift, W. A. Wehbi, B. D. Kelly, X. F. Stowell, J. G. Saven, I. J. Dmochowski, *J. Am. Chem. Soc.* **2006**, *128*, 6611–6619.

# 9 The Archaeal Chaperonin Thermosome as ATP Triggerable Protein Nanoreactor[266]

*Kasper Renggli, Martin G. Nussbaumer, Michael Walther, Blaise Tardy, Nora Sauter, Martina Garni, Douglas S. Clark, Martin U. Hegner and Nico Bruns*

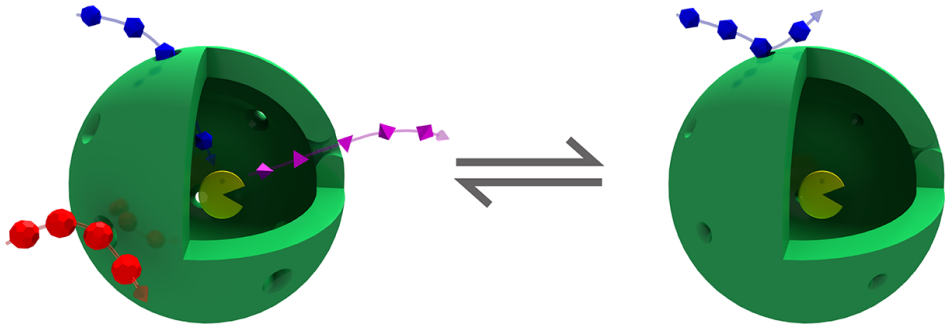

*Reaction compartments on the nanoscale effectively become nanoreactors when substrate and product are exchanged between bulk solution and the cavity. Nanoreactors exhibit responsiveness if access can be modulated by external triggers. In this chapter, natural nanoreactors that include protein-based bacterial microcompartments, protein cages, and viruses are discussed. The protein cage thermosome was assessed as an ATP triggerable nanoreactors by the means of biological and nanomechanical sensing techniques.*

[266] Parts of this chapter were published in: K. Renggli, P. Baumann, K. Langowska, O. Onaca, N. Bruns, W. Meier, *Adv. Funct. Mater.* **2011**, *21*, 1241–1259.

## 9.1 Introduction

Selective access by substrates to the interior of protein microcompartments is believed to be a key property responsible for resolving a paradox that is encountered in metabolic cascade reactions in cages:[267] On the one hand, a function of the cages is to retain small molecules, such as $CO_2$, acetaldehyde, or propionaldehyde within the cavities. On the other hand, larger substrates and cofactors must be able to enter the compartments through pores in the protein shell. A means to resolve this paradox is the provision of pores that control the selective movement of small molecules across the microcompartment shell. The protein structures of some carboxysome pores reveals a positive electrostatic potential in the pore, created by charged side chains.[268] This potential is proposed as a discriminator between charged and uncharged molecules, which could facilitate the diffusion of negatively charged substrates and products of carbon fixation (bicarbonate, 3-phosphoglycerate, and ribulose-1,5-bisphosphate) through the shell, while the uncharged intermediate $CO_2$ remains trapped inside the carboxysome. A spatial arrangement of certain enzymes around the pore on the inside of the shell has also been presented as a mechanistic solution to the paradox.[269] Recent crystallographic data on a carboxysome shell protein[270] and on the Eut microcompartment[271] point to an additional, active gating mechanism. In these studies shell subunits were found that assemble into pseudo hexamers or trimers, respectively, with a central pore that undergoes conformational changes. Most pores in carboxysomes appear to be constitutively open. However, the recently characterized carboxysome shell-protein forms a pore that is either open or closed, depending on the side chain conformation of two residues. The open pore is approximately 1.4 nm in diameter.[270] The open pore of the Eut microcompartment has a diameter of 0.8 nm at the narrowest point, large enough to allow penetration of cofactors, but it can also exists in a closed state.[271] Thus, these pores may be able to cycle between an open, presumably permeable state, and a closed, non-permeable state. One putative mechanism would then involve a coupling between cofactor binding and pore opening.

Although nature uses protein-based microcompartments efficiently as reactors, our understanding of the functioning, molecular structures, and mechanisms involved in these systems is still developing. For example, the conditions that favor an open or a closed pore configuration of the Eut microcompartments are not yet known.

---

267 S. Q. Cheng, Y. Liu, C. S. Crowley, T. O. Yeates, T. A. Bobik, *BioEssays* **2008**, *30*, 1084–1095.

268 a) C. A. Kerfeld, M. R. Sawaya, S. Tanaka, C. V. Nguyen, M. Phillips, M. Beeby, T. O. Yeates, *Science* **2005**, *309*, 936–938 b) Y. Tsai, M. R. Sawaya, G. C. Cannon, F. Cai, E. B. Williams, S. Heinhorst, C. A. Kerfeld, T. O. Yeates, *PLoS Biol.* **2007**, *5*, 1345–1354.

269 a) S. Q. Cheng, Y. Liu, C. S. Crowley, T. O. Yeates, T. A. Bobik, *BioEssays* **2008**, *30*, 1084–1095 b) G. D. Price, M. R. Badger, F. J. Woodger, B. M. Long, *J. Exp. Bot.* **2008**, *59*, 1441–1461 c) F. Cai, S. Heinhorst, J. M. Shively, G. C. Cannon, *Arch. Microbiol.* **2008**, *189*, 141–150.

270 M. G. Klein, P. Zwart, S. C. Bagby, F. Cai, S. W. Chisholm, S. Heinhorst, G. C. Cannon, C. A. Kerfeld, *J. Mol. Biol.* **2009**, *392*, 319–333.

271 S. Tanaka, M. R. Sawaya, T. O. Yeates, *Science* **2010**, *327*, 81–84.

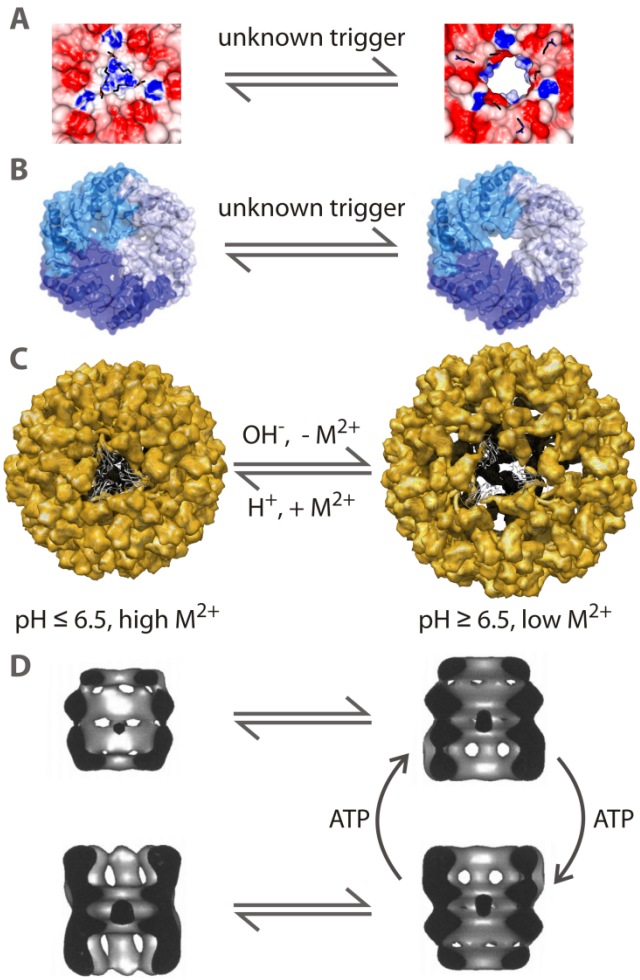


**Figure 9.1** Examples of gated pores in protein-based nanoreactors. A) Carboxysome, B) Eut microcompartment, C) cowpea chlorotic mottle virus, D) cut away models of a thermosome based on cryo-electron microscopy data. A: adapted from[272] with permission from Elsevier, B: adapted from[273] with permission from AAAS, C: rendered from X-Ray data (PDB: 1CWP) using the Chimera program and from a model fitted to cryo-electron microscopy data[274] (VIPER entry: CCMW_swln_1), D: adapted from[275] with permission from Elsevier.

Some pores in protein microcompartments have been crystallized in a closed and in an open conformation, although the trigger that induces the transition has not yet been identified (Figure 9.1a and b).[276] Some, but not all, viral capsids undergo pH- and metal-ion dependent reversible structural transitions that induce a "swelling" of the

[272] M. G. Klein, P. Zwart, S. C. Bagby, F. Cai, S. W. Chisholm, S. Heinhorst, G. C. Cannon, C. A. Kerfeld, *J. Mol. Biol.* **2009**, *392*, 319–333.
[273] S. Tanaka, M. R. Sawaya, T. O. Yeates, *Science* **2010**, *327*, 81–84.
[274] F. Tama, C. L. I. Brooks, *J. Mol. Biol.* **2002**, *318*, 733–747.
[275] G. Schoehn, M. Hayes, M. Cliff, A. R. Clarke, H. R. Saibil, *J. Mol. Biol.* **2000**, *301*, 323–332.
[276] a) M. G. Klein, P. Zwart, S. C. Bagby, F. Cai, S. W. Chisholm, S. Heinhorst, G. C. Cannon, C. A. Kerfeld, *J. Mol. Biol.* **2009**, *392*, 319–333 b) S. Tanaka, M. R. Sawaya, T. O. Yeates, *Science* **2010**, *327*, 81–84.

particle and an opening of the pores. When the pH of a solution of the Cowpea Chlorotic Mottle Virus (CCMV) is raised above pH 6.5 in the absence of metal ions, the capsid increases its diameter by 10% and 60 separate pores open to diameters of 2 nm each (Figure 9.1c).[277] The presence of metal ions such as $Ca^{2+}$ and $Tb^{3+}$ induces the closed conformation of the capsid by binding of the metal to coordination sites at the quasi-three-fold axis of CCMV, i.e. in the openings.[278] The pores in the swollen form allow the free exchange of molecules between the inside and the outside of the capsid. In contrast, there is no apparent exchange of large molecules in the non-swollen form.[279] Gated pores of much larger size are found in heat-shock protein (Hsp 60) molecular chaperones, the chaperonins. These are hollow, spherical or cylinder-like protein cages formed from two rings stacked back to back. They sequester denatured proteins from solution in order to assist in protein refolding. Group II chaperonins such as eukaryotic TRiC/CCT or archaeal thermosomes possess built-in lids that cover the central cavities (Figure 9.1d). The gated pore is large enough (up to approximately 10 nm in diameter) to allow the uptake of guest proteins into the cavity.[280] The lids are formed by helical protrusions at the tip of the apical domain of the subunits. Their opening and closing proceeds in a two stroke-cycle, in which one ring opens in a cooperative movement while the other ring closes.[281] The conformational changes are driven by the hydrolysis of adenosine triphosphate (ATP). Depending on the experimental conditions, fully closed or open conformations are obtained as well.[282] TRiC uses an iris-like conformational change, where apical and intermediate domains rotate in a coordinated manner to close off access to the central cavity.[283]

Here, we investigate the different conformations of thermosome (THS), a group II chaperonin from the archaea *Thermoplasma acidophilum* in response to ATP and its analogues. The THS in its closed conformation is a protein cage that self-assembles from eight α- and eight β-subunits into a spherical complex approx. 15.8 nm in diameter, comprising two stacked, eight-membered rings. Each ring encloses a cavity measuring between 8.6 and 5.4 nm in diameter and approx. 4.5 nm in height.[284] The native role of the THS is to refold unfolded or partially unfolded proteins, especially upon heat shock of a cell. To accomplish this, the THS can uptake proteins into its

---

277 a) J. A. Speir, S. Munshi, G. Wang, T. S. Baker, J. E. Johnson, *Structure* **1995**, *3*, 63–78 b) F. Tama, C. L. I. Brooks, *J. Mol. Biol.* **2002**, *318*, 733–747 c) L. O. Liepold, J. Revis, M. Allen, L. Oltrogge, M. Young, T. Douglas, *Phys. Biol.* **2005**, *2*, S166–S172.

278 G. Basu, M. Allen, D. Willits, M. Young, T. Douglas, *JBIC, J. Biol. Inorg. Chem.* **2003**, *8*, 721–725.

279 L. O. Liepold, J. Revis, M. Allen, L. Oltrogge, M. Young, T. Douglas, *Phys. Biol.* **2005**, *2*, S166–S172.

280 a) G. Schoehn, M. Hayes, M. Cliff, A. R. Clarke, H. R. Saibil, *J. Mol. Biol.* **2000**, *301*, 323–332 b) J. Zhang, M. L. Baker, G. F. Schröder, N. R. Douglas, S. Reissmann, J. Jakana, M. Dougherty, C. J. Fu, M. Levitt, S. J. Ludtke, et al., *Nature* **2010**, *463*, 379–383.

281 M. G. Bigotti, A. R. Clarke, *Arch. Biochem. Biophys.* **2008**, *474*, 331–339.

282 a) G. Schoehn, M. Hayes, M. Cliff, A. R. Clarke, H. R. Saibil, *J. Mol. Biol.* **2000**, *301*, 323–332 b) L. Ditzel, J. Lowe, D. Stock, K. O. Stetter, H. Huber, R. Huber, S. Steinbacher, *Cell* **1998**, *93*, 125–138.

283 C. R. Booth, A. S. Meyer, Y. Cong, M. Topf, A. Sali, S. J. Ludtke, W. Chiu, J. Frydman, *Nat. Struct. Mol. Biol.* **2008**, *15*, 746–753.

284 L. Ditzel, J. Lowe, D. Stock, K. O. Stetter, H. Huber, R. Huber, S. Steinbacher, *Cell* **1998**, *93*, 125–138.

cavities. The access of macromolecules to the THS is granted by two pores approx. 8-10 nm in diameter at the poles of the spherical THS.[285] These pores are gated by lids, which are formed by helical protrusions in the apical domains of the subunits. The built-in lids of chaperonins open and close in an iris-like movement, which is fueled by the hydrolysis of ATP.[286] The opening of the lid is accomplished by a concerted rotational movement of the apical and intermediate domains of the subunits in one ring. The crystal structure of the THS in its closed conformation reveals sixteen small pores in the wall of the THS that are formed by adjacent subunits. These irregular shaped windows, potentially allowing for water, ions and small molecular weight organic compounds to enter and leave the cavities. However, their exact permeability has still to be elucidated and may not only depend on the size of the permeating molecules.

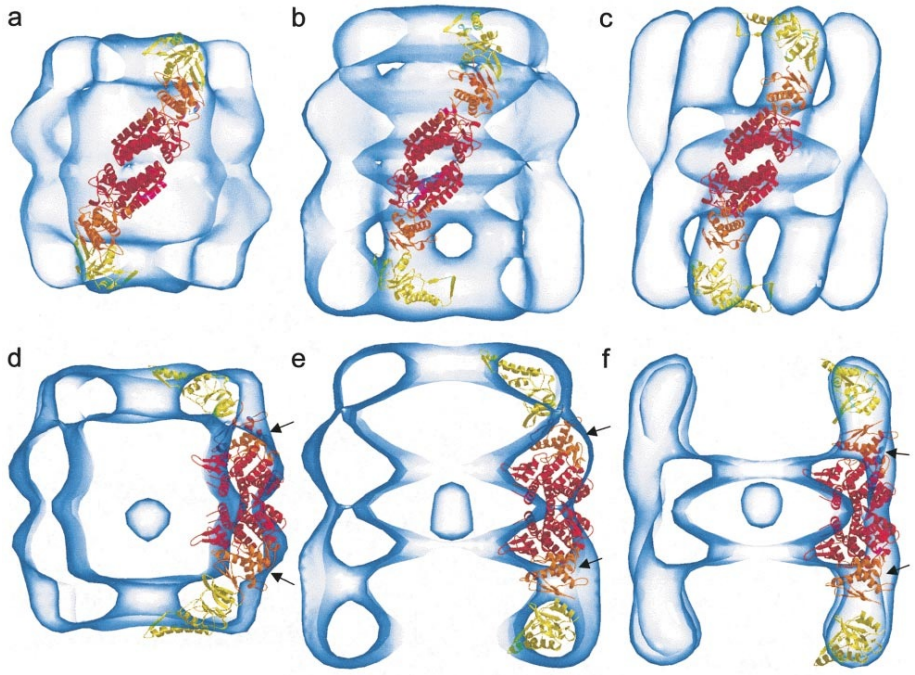


**Figure 9.2** Fits of the domain atomic structures to three cryo-EM maps of THS. a) and d) Closed form; b) and e) bullet form; c) and f) open form. a)-c) The front surfaces; d)-f) sections through the maps. The angle of the intermediate domain helix is indicated by arrows, showing the change in tilt relative to the equatorial domain (and thus nucleotide binding pocket) between open and closed rings. Figure reproduced from Schoehn et al.[287] with permission from Elsevier.

---

285 a) G. Schoehn, E. Quaite-Randall, J. L. Jiménez, A. Joachimiak, H. R. Saibil, *J. Mol. Biol.* **2000**, *296*, 813–819 b) C. R. Booth, A. S. Meyer, Y. Cong, M. Topf, A. Sali, S. J. Ludtke, W. Chiu, J. Frydman, *Nat. Struct. Mol. Biol.* **2008**, *15*, 746–753 c) J. Zhang, M. L. Baker, G. F. Schröder, N. R. Douglas, S. Reissmann, J. Jakana, M. Dougherty, C. J. Fu, M. Levitt, S. J. Ludtke, et al., *Nature* **2010**, *463*, 379–383.

286 a) G. Schoehn, E. Quaite-Randall, J. L. Jiménez, A. Joachimiak, H. R. Saibil, *J. Mol. Biol.* **2000**, *296*, 813–819 b) G. Schoehn, M. Hayes, M. Cliff, A. R. Clarke, H. R. Saibil, *J. Mol. Biol.* **2000**, *301*, 323–332.

287 G. Schoehn, M. Hayes, M. Cliff, A. R. Clarke, H. R. Saibil, *J. Mol. Biol.* **2000**, *301*, 323–332.

In the absence of nucleotides THS rests in the apo state, which is characterized by the two hemispheres being in an open conformation (Figure 9.2c and f). When ATP is added to a THS solution in the presence of $Mg^{2+}$ the protein starts its ATPase reaction cycle. This cycle is thought to be a two-stroke mechanism in which one ring closes upon hydrolysis of ATP to ADP and Pi, while the opposing ring binds ATP and opens (Figure 9.2b and e). Detailed studies with several group II chaperonins such as the eukaryotic TRiC/CCT and the archaeal *Methanococcus maripaludis* Chaperonin (Mm-cpn) have shown that ATP binding causes domain movements and the trigonal bipyramidal transition state of ATP hydrolysis triggers lid closure.[288] Thus, one or both lids can be closed by incubation of group II chaperonins with the transition state mimic ADP-$AlF_x$ or in the presence of ATP and $AlF_x$ which is converted *in situ* by the chaperonins to ADP-$AlF_x$ (Figure 9.2a and d). The non-hydrolysable ATP analogues adenosine 5'-[β,γ-imido]triphosphate (AMP-PNP) as well as adenosine 5'-[γ-thio] triphosphate (ATP-γ-S) failed to close TRiC/CCT, however other studies report lid closure of group II chaperonins with AMP-PNP. The discrepancy in these findings might be explained by hydrolyzed impurities in the nucleotide preparation used, but also due to structural differences between the chaperonins.

## 9.2 Characterization of Conformational Changes in Thermosome by Biological Methods

We characterized the effect of nucleotides and their transition state mimics on the thermosome from *Thermoplasma acidophilum*. To this end we encapsulated the enzyme horseradish peroxidase (HRP) into thermosome as described in section 8.2.1 and explored the activity of the biocatalyst in comparison to the free enzyme. The biocatalytic property of HRP was then used to assess the different conformational states of THS.

### 9.2.1 Enzymatic Activity and Half-Life of THS-HRP

In a first step we assessed the enzymatic activity of the encapsulated horseradish peroxidase and the half-life of the complex. We compared the activity of the encapsulated HRP with the activity of the native free enzyme with an UV/Vis spectroscopic activity assay. Horseradish peroxidase catalyzes the transformation of 2,2'-Azino-bis(3-ethylbenzothiazoline-6-sulfonic acid) diammonium salt (ABTS) to its radical, positively charged form in the presence of hydrogen peroxide.

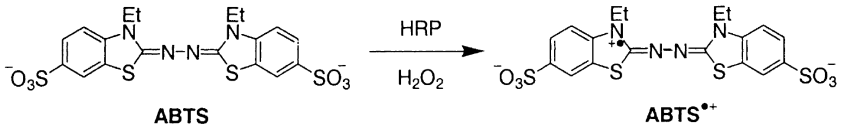


[288] a) C. R. Booth, A. S. Meyer, Y. Cong, M. Topf, A. Sali, S. J. Ludtke, W. Chiu, J. Frydman, *Nat. Struct. Mol. Biol.* **2008**, *15*, 746–753 b) J. Zhang, M. L. Baker, G. F. Schröder, N. R. Douglas, S. Reissmann, J. Jakana, M. Dougherty, C. J. Fu, M. Levitt, S. J. Ludtke, et al., *Nature* **2010**, *463*, 379–383.

The formation of product can be measured with colorimetric UV/Vis assay at an absorbance wavelength of 420 nm,[289] which allows for the calculation of the enzymatic activity. The temperature dependent activity of the free native form of HRP compared to the THS-HRP complex is shown in Figure 9.3.

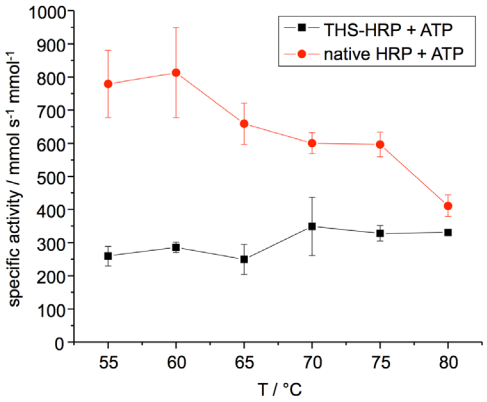


**Figure 9.3** Temperature dependent enzymatic activity in the presence of ATP of free native HRP in comparison to encapsulated HRP. The specific activity was determined by a colorimetric ABTS assay. THS-HRP shows lesser activity due to the shielding effect of the THS protein cage.

The graph shows a lesser activity of the THS-HRP complex compared to the native enzyme, which we excepted due to the fact that the encapsulated enzyme is significantly shielded by the protein cage and only accessible through the openings of the thermosome. This is an advantage in the case of the half-life of HRP (Figure 9.4), since the encapsulated enzyme can maintain its function also in the higher temperature regimes, similar to a PEGylated enzyme.[290] The activity plot is the confirmation that the enzymatic activity of the encapsulated HRP remains intact and the protein cage only has the effect of lowering the enzymatic activity.

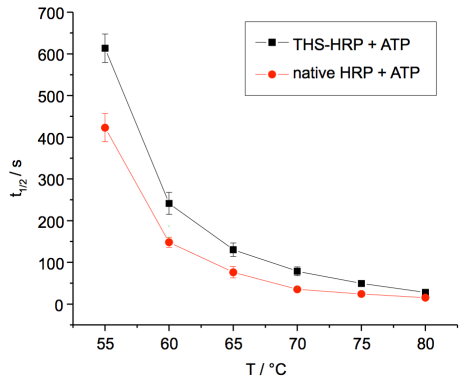


**Figure 9.4** Temperature dependent half-life of HRP in the presence of ATP. The free native HRP displays a shorter half-life compared to the encapsulated and therefore shielded HRP.

[289] J. Pütter, R. Becker (Eds.), *Peroxidases*, 3rd Edn., Verlag Chemie, Deerfield Beach, FL, **1983**.
[290] G. DeSantis, J. B. Jones, *Curr. Opin. Biotechnol.* **1999**, *10*, 324–330.

### 9.2.2 Effect of ATP Analogues on THS-HRP

Having proof of the successful encapsulation and enzymatic activity of the horseradish peroxidase we were able to assess the different conformations of the THS induced by nucleotides and their analogues. For our purpose we used the catalytic activity of HRP and measured the transformation of the non-fluorescent dihydro rhodamine 6G (dhRh6G) to the fluorescent form rhodamine 6G (Rh6G). DhRh6G is only transformed to Rh6G in the presence of HRP and hydrogen peroxide.[291] It therefore serves very well as a tool to assess the opening and closing of the lids of THS in presence of nucleotides. This can then be used to modulate the THS as a triggerable nanoreactor. As mentioned above, in the absence of nucleotides THS rests in the apo state, which is characterized by the two hemispheres being in an open conformation. Different studies with archaeal group II chaperonins showed that adenosine triphosphate (ATP) starts the ATPase reaction cycle in the presence of $Mg^{2+}$.[292]

For our purposes we studied the effect of no additive, ATP, ATP-γ-S and ATP/$AlF_x$ on the lid opening of thermosome. The guest molecule HRP is linked to THS and sits in the cavity of the thermosome. Thus, if the lids of the thermosome are open, HRP can efficiently catalyze $H_2O_2$ to $H_2O$ and transform DhRh6G to its fluorescent state Rh6G. If the lids are closed, HRP cannot catalyze any $H_2O_2$ and no fluorescence will be measured. Thermosome was incubated for 30 min with ATP or its analogon and the conversion of dhRh6G to Rh6G by $H_2O_2$ was assessed in the fluorescence cuvette for 30 min. In order to assess how much $H_2O_2$ can also degradate dhRh6G in the absence of HRP, a no-HRP control was performed and the resulting intensity deducted. Fluorescence measurements of Rh6G were performed at an excitation wavelength of 205 nm and an emission wavelength of 535 nm.

The fluorescence results (Figure 9.5) show the highest activity for HRP if the THS lies in its apo state. This native conformation of THS without any additives should result in an unimpeded catalyzing activity of the encapsulated enzymes since the two cavities are completely exposed to the surrounding media without any movement of the THS lids. These results confirm our hypothesis that THS is in a fully open state when no ATP derivatives are added.

---

[291] L. Edman, Z. Földes-Papp, S. Wennmalm, R. Rigler, *Chem, Phys.* **1999**, *247*, 11-22.

[292] a) C. R. Booth, A. S. Meyer, Y. Cong, M. Topf, A. Sali, S. J. Ludtke, W. Chiu, J. Frydman, *Nat. Struct. Mol. Biol.* **2008**, *15*, 746–753 b) G. Schoehn, M. Hayes, M. Cliff, A. R. Clarke, H. R. Saibil, *J. Mol. Biol.* **2000**, *301*, 323–332 c) J. Zhang, M. L. Baker, G. F. Schröder, N. R. Douglas, S. Reissmann, J. Jakana, M. Dougherty, C. J. Fu, M. Levitt, S. J. Ludtke, et al., *Nature* **2010**, *463*, 379–383.

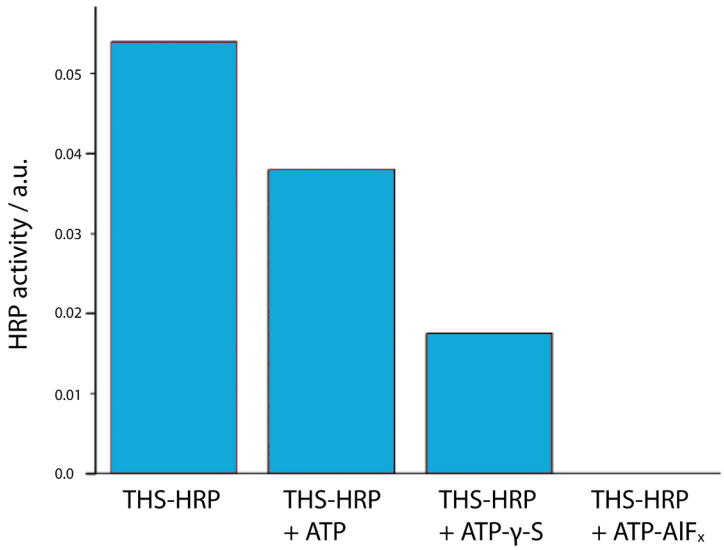


**Figure 9.5** Influence of ATP derivatives on thermosome activity. HRP is linked to the thermosome and catalyzes the degradation of $H_2O_2$, which then transforms DhRh6G to its fluorescent state Rh6G. HRP can only catalyze the degradation of $H_2O_2$ if the lids of the thermosome are open.

When ATP is added, it causes the thermosomes to alternately open and close its lid,[293] which can be seen by a reduced HRP activity in Figure 9.5. When ATP-$AlF_x$ is added, the lids are blocked and stay closed, displayed by no HRP activity (Figure 9.5). ATP-$AlF_x$ stabilizes the transition state, since $AlF_x$ forms a pentavalent structure that mimics the trigonal-bipyramidal conformation of the γ-phosphate undergoing hydrolysis.[294] If the non-hydrolysable ATP-γ-S is added to the THS-HRP system, we observe a lower HRP activity, compared to ATP (Figure 9.5). This indicates an increased duration of closed lids compared to ATP, hindering HRP activity more than with ATP as an additive.

These experiments indicate that THS can be modulated by the means of ATP analogues, i.e. that the opening and closing mechanism of THS can be controlled to a certain extent. Our results for ATP and ATP-$AlF_x$ are also in good agreement with results from THS[295] and Mm-cpn.[296] In the case of ATP-γ-S, small-angle neutron-scattering (SANS) studies have suggested that 5'-[β,γ-imido]triphosphate (p[NH]ppA), a similar ATP analogue, can effect the conformational changes in the THS, which were interpreted as an open-to-closed transition upon binding of ATP.[297] This phenomena was also described for the group II chaperonin Mm-cpn by the use of p[NH]ppA.[298] They describe a rhodanese enzymic activity of 70% for ATP and an activity of approx.

[293] G. Schoehn, M. Hayes, M. Cliff, A. R. Clarke, H. R. Saibil, *J. Mol. Biol.* **2000**, *301*, 323–332.
[294] A. M. Gulick, C. B. Bauer, J. B. Thoden, I. Rayment, *Biochemistry* **1997**, *36*, 11619–11628.
[295] L. Ditzel, J. Lowe, D. Stock, K. O. Stetter, H. Huber, R. Huber, S. Steinbacher, *Cell* **1998**, *93*, 125–138.
[296] J. Zhang, M. L. Baker, G. F. Schröder, N. R. Douglas, S. Reissmann, J. Jakana, M. Dougherty, C. J. Fu, M. Levitt, S. J. Ludtke, et al., *Nature* **2010**, *463*, 379–383.
[297] I. Gutsche, J. Holzinger, N. Rauh, W. Baumeister, R. P. May, *J. Struct. Biol.* **2001**, *135*, 139–146.
[298] A. Kusmierczyk, J. Martin, *Biochem. J.* **2003**, *371*, 669–673.

40% for p[NH]ppA in comparison to the apo state, which is comparable with our results for THS-HRP. In TRiC/CCT, cryo-electron-microscopic reconstruction in the presence of p[NH]ppA revealed the chaperonin to be in a closed conformation,[299] indicating ATP hydrolyzation differences between group II chaperonins. The ability of THS-HRP to maintain enzymic activity in the presence of the non-hydrolysable ATP-γ-S indicates that ATP-γ-S hydrolysis is blocking the THS in an intermediate state between open and closed conformations, as described by SANS experiments.[300] Another explanation could be that ATP-γ-S is slowing down the THS movement due to the non-hydrolysable part of the analogue, thus resulting in a lower HRP activity. Thus, to modulate the THS, ATP-γ-S is not an ideal choice.

We can conclude that the THS can be modulated with ATP analogues. The most interesting analogue ATP-$AlF_x$ has the potential to close the protein cages completely, indicated by no HRP activity. Further, the addition of ATP and ATP-γ-S lowers the catalytic activity of HRP, indicating that the THS cycles between an open and closed conformation. Moreover, the absence of additives allows for the highest catalytic activity of HRP, indicating that the THS lies in a completely open conformation.

[299] O. Llorca, J. Martín-Benito, J. Grantham, M. Ritco-Vonsovici, K. R. Willison, J. L. Carrascosa, J. M. Valpuesta, *EMBO J.* **2001**, *20*, 4065–4075.

[300] I. Gutsche, J. Holzinger, N. Rauh, W. Baumeister, R. P. May, *J. Struct. Biol.* **2001**, *135*, 139–146.

## 9.3 Nanomechanical Sensing of Conformational Changes in Thermosome

### 9.3.1 Introduction

A more recent approach of our group to assess the question of what mechanism lies behind the opening and closing of the protein involves the use of cantilever arrays. In collaboration with the group of Martin Hegner at Trinity College Dublin. An ideal biosensor should be able to measure label-free, in real-time and in parallel to avoid falsified results. Numerous label-free techniques were developed for biological, medical and chemical research to detect and characterize interactions between molecular partners, e.g. surface plasmon resonance,[301] ellipsometry,[302] and quartz micro balance (QCM).[303] These systems are only dependant on the immobilization of one of the partners on the transducer interface. Another promising technique involves the use of miniaturized silicon cantilevers that require no external probes or labeling and can operate autonomously.[304]

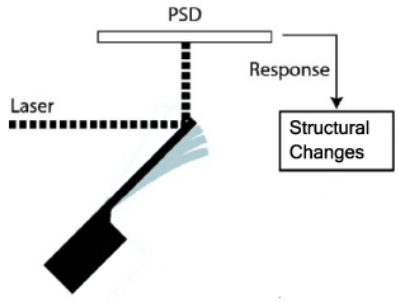


**Figure 9.6** Detailed scheme of the static system where structural changes are detected by the static bending of asymmetrical functionalized cantilevers. An optical readout is used where a laser beam is reflected on top of the cantilever and pointed towards a position sensitive detector (PSD). Adapted from Braun et al.[305] Copyright 2005 by the American Physical Society.

Applications with cantilever arrays range from antibody-antigen interactions[306] to the detection of gene mutation in total RNA.[307] In static mode, the cantilever is sensitive to surface stress differences between the two cantilever surface areas. If the upper and lower surface areas experience different stress the cantilever will bend. An asymmetric coating with a reactive layer on one surface of the cantilever favors

[301] C. E. Jordan, R. M. Corn, *Anal. Chem.* **1997**, *69*, 1449–1456.
[302] Z. H. Wang, G. Jin, *Anal. Chem.* **2003**, *75*, 6119–6123.
[303] K. A. Marx, *Biomacromolecules* **2003**, *4*, 1099–1120.
[304] J. Fritz, M. K. Baller, H. P. Lang, H. Rothuizen, P. Vettiger, E. Meyer, H.-J. Güntherodt, C. Gerber, J. K. Gimzewski, *Science* **2000**, *288*, 316–318.
[305] T. Braun, V. Barwich, M. K. Ghatkesar, A. H. Bredekamp, C. Gerber, M. Hegner, H. P. Lang, *Phys. Rev. E* **2005**, *72*, 031907.
[306] G. Wu, R. H. Datar, K. M. Hansen, T. Thundat, R. J. Cote, A. Majumdar, *Nat. Biotechnol.* **2001**, *19*, 856–860.
[307] F. Huber, H. P. Lang, N. Backmann, D. Rimoldi, C. Gerber, *Nat. Nanotechnol.* **2013**, *8*, 125–129.

preferential adsorption of molecules on this surface. In most cases, the intermolecular forces in the adsorbed molecule layer produce a compressive stress, i.e. the cantilever bends down if its reactive surface is its upper one. A more detailed scheme of our static system is shown in Figure 9.6. The group of Martin Hegner previously demonstrated the feasibility of nanomechanical sensing of conformation changes in proteins by the means of subunit loss in bacteriorhodopsin due to denaturation.[308]

### 9.3.2 Results & Discussion

We attached THS covalently to Si cantilever arrays with eight cantilevers from IBM Research Laboratory (Figure 9.7). The cantilevers had a pitch of 250 µm and were 500 µm long, 100 µm wide and 1 µm thick. They were coated on one side with a layer of 2 nm titan and on top a 20 nm thick layer of gold.

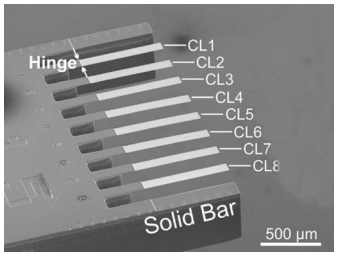


**Figure 9.7** Scanning electron microscope image of a typical cantilever array used for nanomechanical sensing. Adapted from Huber et al.[309] with permission from AIP Publishing LLC.

Dithio-bis-(succinimidyl undecanoate) (DSU)[310] was used to functionalize the gold surface of cantilever 2, 4, 6 and 8, enabling them to covalently attach THS via the amine groups of the lysine present on the surface of the protein (see Figure 9.8 and 9.9). As reference, an alternative thiol coating of gold on cantilever 1, 3, 5 and 7 was made with 11-mercapto-1-unedecanol, which is protein repellent.

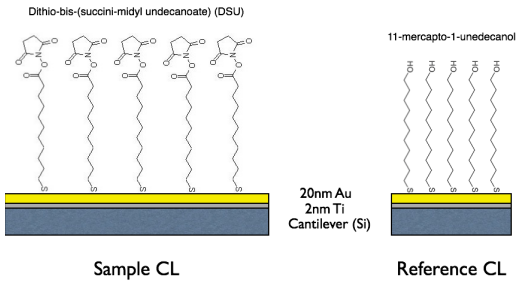


**Figure 9.8** the cantilevers were functionalized with 2 nm Ti and 20 nm Au. Sample cantilevers were functionalized with DSU and reference cantilever with 11-mercapto-1-unedecanol.

---

308 T. Braun, N. Backmann, M. Vögtli, A. Bietsch, A. Engel, H.-P. Lang, C. Gerber, M. Hegner, *Biophys. J.* **2006**, *90*, 2970–2977.

309 F. Huber, H.-P. Lang, M. Hegner, M. Despont, U. Drechsler, C. Gerber, *Rev. Sci. Instrum.* **2008**, *79*, 086110.

310 P. Wagner, P. Kernen, M. Hegner, E. Ungewickell, G. Semenza, *FEBS Lett.* **1994**, *356*, 267–271.

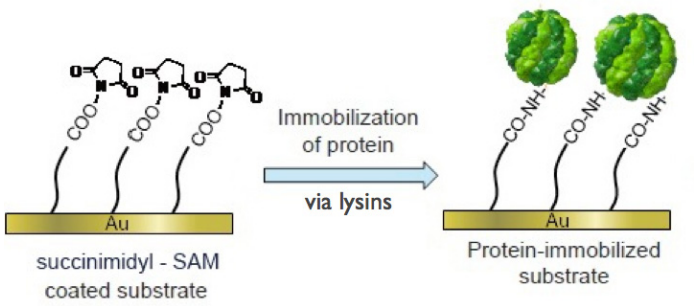


**Figure 9.9** Strategy to covalently attach THS via lysines to the DSU coated surface of the cantilever array. Adapted from [311] with permission from Dojindo Molecular Technologies.

The setup shown in Figure 9.10 was operated in static mode and all measurements were performed in the 7.5 µl fluid cell in MES buffer at pH 5.2 (100 mM MES, 150 mM NaCl, 20 mM $MgCl_2$). The induced bending of the cantilever was measured by reflecting a laser beam on top of the cantilever and pointing it towards a position sensitive detector (PSD).[312] Surface stress was induced by the conformation changes of the immobilized protein due to ATP or its analogues. Various forces such as intermolecular interactions, electrostatic forces as well as changes in the electronic density may contribute to the resulting surface stress.[313]

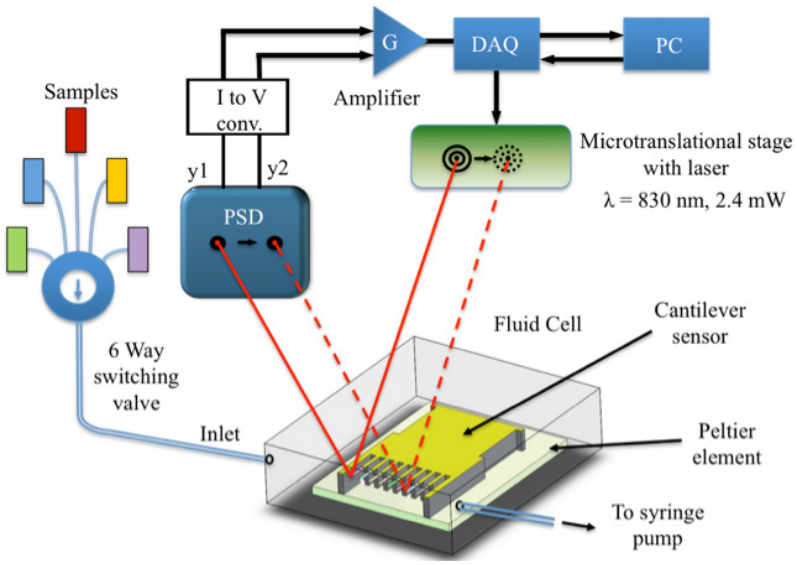


**Figure 9.10** Experimental setup for nanomechanical sensing with cantilever arrays.

---

311 Dojindo Molecular Technologies, *http://www.dojindo.com/store/p/795-Amine-Coupling-Kit.html*, accessed June 19, 2014.

312 H. P. Lang, R. Berger, C. Andreoli, J. Brugger, M. Despont, P. Vettiger, C. Gerber, J. K. Gimzewski, J. P. Ramseyer, E. Meyer, *Appl. Phys. Lett.* **1998**, *72*, 383–385.

313 M. Godin, V. Tabard-Cossa, Y. Miyahara, T. Monga, P. J. Williams, L. Y. Beaulieu, R. Bruce Lennox, P. Grutter, *Nanotechnology* **2010**, *21*, 075501.

We monitored the deflection signal of the fixed cantilever array with the immobilized THS. After reaching a stable signal we injected a solution of ATP in MES buffer (30 min under constant flow) into the fluid chamber where the cantilever array was placed. After this injection phase, the flow was stopped and the deflection signal was measured again. Our results show a clear change in surface stress due to the presence of ATP, which is expected to cycle the THS between open and closed conformations (Figure 9.11). The surface stress is measured in a bending of the cantilever by 50 nm. This value is the difference between the averaged signal of the four sample cantilevers and the averaged signal of the four reference cantilevers.

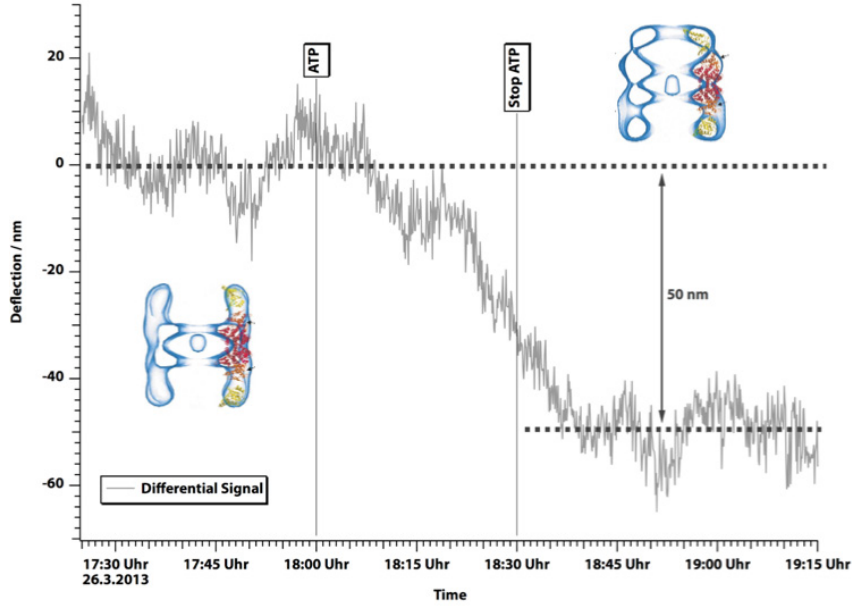


**Figure 9.11** Change in cantilever deflection of 50 nm induced by surface stress of THS as a reaction to the addition of ATP. This value is the difference between the averaged signal of the four sample cantilevers and the averaged signal of the four reference cantilevers.

The effect of ATP-$AlF_x$, which should close and block the THS completely, on the surface stress is shown in Figure 9.12 The same procedure described for ATP was adapted to the measurements with ATP-$AlF_x$. The surface stress resulted in a bending of the cantilever by 75 nm. This value is the difference between the averaged signal of the four sample cantilevers and the averaged signal of the four reference cantilevers.

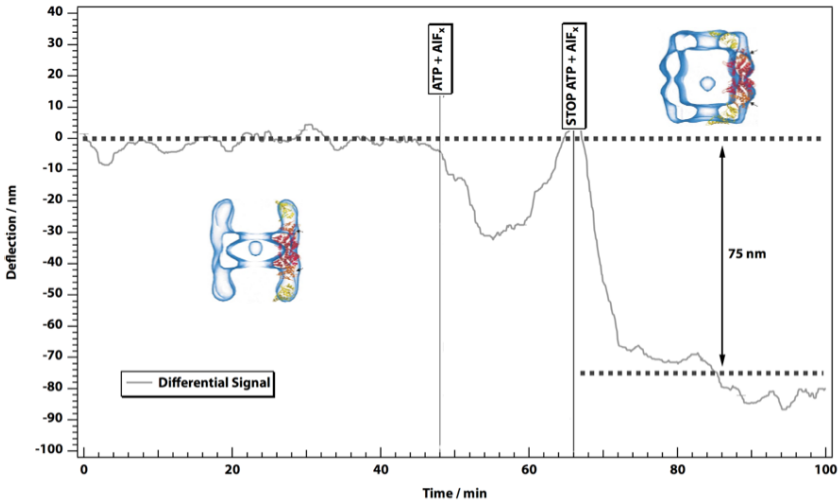


**Figure 9.12** Change in cantilever deflection of 75 nm induced by surface stress of THS as a reaction to the addition of ATP-AlF$_x$. This value is the difference between the averaged signal of the four sample cantilevers and the averaged signal of the four reference cantilevers.

The preliminary nanomechanical sensing results in a combination with the enzymatic assays of THS-HRP reported before allow the conclusion that a difference in surface stress induced by different ATP analogues can be seen. This might display the first results where conformation changes of a protein were nanomechanically measured. It is exciting to measure a difference in cantilever bending dependent on conformational changes of THS induced by the ATP analogue. However, we are still looking for an explanation of how the surface stress is induced by the different movements of the subunits. Further studies with established methods, i.e. digestion- and ATPase assays have to be performed in order to draw further conclusions.

## 9.4 Conclusions

By the means of nanomechanical sensing and enzymatic assays we demonstrated the effect of ATP analogues on the archaeal chaperonin THS. Whereas ATP displays typical cyclic movements between open and closed conformation for the group II chaperonin, the ATP-γ-S seems to slow down the cycling process or blocks the THS in an intermediate state. ATP-$AlF_x$ possesses the most interesting ability to close and block the THS completely. The use of ATP analogues renders the THS an ATP triggered protein cage or even nanoreactor.

Nanoreactors are ideal vessels for reactions within living tissue in the context of drug-delivery, or when immobilized on surfaces as e.g. sensors. However, the greatest challenge at the nanoscale is to control the influx of substrates and the release of products from the nanoreactor, as no conventional openings, valves or lids can be engineered into the reactors.

This chapter showed a way to render protein cages as gated nanoreactors. Nature leads the way, both in providing a multitude of reaction compartments, e.g. cells, lipid-based organelles, protein microcompartments and protein cages, and in the degree of control over accessibility to the compartments. Gated nanoreactors found in nature have pores that are determined by the structure of proteins. These can be dedicated membrane proteins that allow controlled access through a lipid bilayer, or pores between subunits of a multi-subunit protein assembly. Some pores act merely as size-selective openings, some discriminate between substances according to their charge or molecular identity, and some are actively gated, i.e. an external stimulus, like ATP leads to a change in conformation of the proteins and therefore to an opening or closing of the pore. Some of the microcompartments found in nature have been used in a non-biological context, e.g. chaperonins.[314]

Triggered nanoreactors show promising potential in applications in the areas of medicine, sensing, synthesis of drugs and other chemical products, and as analytical tools to study reaction mechanisms in confined volumes.

[314] N. Bruns, K. Pustelny, L. M. Bergeron, T. A. Whitehead, D. S. Clark, *Angew. Chem. Int. Ed.* **2009**, *48*, 5666–5669.

# 10 General Conclusion & Outlook

The present PhD thesis entitled *Protein Nanoreactors and Native Enzymes for Controlled/Living Radical Polymerization* began with the hypothesis that protein-catalyst conjugates are able to beneficially influence controlled/living radical polymerization, i.e. atom transfer radical polymerization (ATRP). The general motivation for this work is driven by problems that occur when transition metal catalyst are used for ATRP. These most commonly used catalyst are only biocompatible to a limited extend and the resulting polymers show unwanted coloration due to the remaining catalyst. Moreover, by conjugating the catalyst into the cavities of a protein cage, we could gain insights into the catalytic mechanism of ATRP as well as into effects of the confined space. Polymer chemistry in particular enables us to perform successful research with proteins since synthetic strategies in a biocompatible environment, i.e. aqueous solution are well established.

Inspired by problems addressed earlier in our research group, we developed a robust conjugation and purification method to attach transition metal catalysts to proteins or enclose them into protein cages using bis-aryl hydrazone linker chemistry. Successively, we determined good performing ATRP conditions that allowed for significant lower catalyst concentrations. Thus, activators regenerated by electron transfer (ARGET) ATRP was used to constantly regenerate the catalyst into its active form by the means of a reducing agent.

Chapter 2 described one of these protein-catalyst conjugates in full detail. The ATRP catalyst was conjugated to the globular protein bovine serum albumin (BSA) and the complex was extensively characterized using biological and physical methods. The resulting conjugate was used to polymerize N-isopropyl acrylamide (NiPAAm) and poly(ethylene glycol) methyl ether acrylate (PEGA) in aqueous solution and was subsequently analyzed upon its structural integrity after polymerization. The ARGET ATRP of NiPAAm and PEGA yielded polymers with a moderate control over the molecular weight and the polydispersity of the polymers. However, our focus was to reduce the residual copper in polymers. Thus, BSA that served as a functional handle was used to remove the copper containing catalyst effectively from solution. We showed a reduction of residual copper to ppb levels, either by precipitation or by Dynabead removal.

Chapters 3 to 5 dealed with our findings that some metalloproteins can mediate ATRP. Enzymes have been introduced into synthetic chemistry as green and very selective alternatives to conventional catalysts. In polymer chemistry enzymes have been used as catalysts for polycondensation, ring-opening polymerizations, free radical polymerizations of vinyl-type monomers and the polymerization of aromatic compounds by radical-induced oxidative coupling. However, controlled/living radical polymerizations catalyzed by enzymes have not been exploited. Our results and the ones from di Lena represent the first reports of biocatalytic, controlled/living radical polymerization. Bringing those enzymes into organic solution, e.g. by conjugation of end-group-reactive polymers such as PEG, poly(oxazolines) and amphiphilic blockcopolymers to the surface-exposed lysines or cysteins of the enzymes, could lead

to interesting new routes towards environmentally friendly catalysis, functional materials or functional nanosystems.

In Chapter 7 The group II chaperonin thermosome (THS) from the archaea *Thermoplasma acidophilum* is reported as protein nanoreactor for ATRP. For that purpose, a copper catalyst was entrapped into the THS. The confined space within the protein nanoreactor favorably influenced the polymerization of NiPAAm and PEGA under ARGET ATRP conditions in comparison to polymerizations carried out with the globular protein BSA. In chapter 8 this concept was adapted and instead of the copper-complex, we covalently entrapped an enzyme as ATRP catalyst. We demonstrated that the space constriction in the THS has similar effects on the final polymer product, as shown for THS-$L_x$Cu. Further studies of the polymerization, i.e. kinetic experiments, are needed to explore the compartmentalization effect and the mechanism behind it. In addition, the use of protein nanoreactors could enable mechanistic studies of ATRP on a single molecule level. Moreover, protein nanoreactors with encapsulated enzymes, i.e. ATRPases, could help to understand the reaction mechanisms behind ATRPases. In addition, the nanoreactor could be used as a template to synthesize polymer nanoparticles with defined shape and size.

Chapter 9 described a way to render protein cages, i.e. THS, gated nanoreactors. The gated behavior of THS driven by the hydrolysis of ATP and ATP analogues was shown by enzymatic assays. The incorporation of HRP into THS allowed to study the opening and closing of the cage by converting the non-fluorescent dihydro rhodamine 6G into its fluorescent form rhodamine 6G. In addition, nanomechanical sensing with cantilever arrays measured the surface stress induced by the opening and closing of the protein cage in response to ATP analogues. Additional experiments are needed, i.e. digestion- and ATPase assays to confirm the gated behavior of our system. Furthermore, cycle experiments with cantilever arrays could show that a polymerization can be temporary stopped, i.e. by closing the protein cage, and started again with the addition of the appropriate ATP analogue. The field of gated nanoreactors is still in its infancy and leaves plenty of room for new developments. Thus, gated nanoreactors could be used in the areas of medicine, sensing, synthesis of drugs and other chemical products, and as analytical tools to study reaction mechanisms in confined volumes.

# Acknowledgements

During my PhD time at the University of Basel I had the support of many dedicated scientists to whom I express my sincere thanks. First of all, I would like to thank Nico Bruns for letting me pursue this wonderful topic and for guiding me with enthusiasm through my time in his group. He has given me all the freedom I wanted to achieve my goals and for that I am very grateful.

Further, I would like to thank Wolfgang Meier, for all his support and advice. Also, I would like to thank Corinne Vebert for accepting the co-examination of my PhD thesis.

Furthermore, I like to thank Martin Hegner, Markus Zehringer, Thomas Pfohl, Jürg Jourdan, Cornelia Palivan and Thomas Braun for their support and advice.

I very grateful to my collaboration partners and friends Raphael Urbani, Benjamin Bircher and Michael Walther for their expertise and the way we discussed about science and life in general.

Moreover, I thank the Swiss Nanoscience Institute and especially Meret Hornstein and Tibor Gyalog.

Julia Razumovitch, Kelner Rodriguez de Franca, Karolina Langowska, Smahan Toughraï and Gabrielle Persy are thanked for the cosy atmosphere in our office (4.06).

Further, I like to thank all current and former members of the Meier labs for creating such a fruitful working atmosphere. Additionally, I would like to thank my subgroup mates Farzad Seidi, Gergo Kali, Katarzyna Makyla, Mariana Spulber, Martin Nussbaumer, Martin Rother, Marzena Kocik and Severin Sigg for sharing their knowledge and all their help in lab.

I am grateful to my gifted Master and blockcourse students Martina Garni, Nora Sauter, Rahel Hinkelmann, Simon Zihlmann, Tilana Silva and Yasemin Seker who enriched this thesis due to their motivation and hard work during their time in the group.

A special thank goes to Tom Eaton and Patrick Burch for their support and enthusiasm towards the postdoc level.

Further, I thank the administrative and technical staff Sven Kasper, Georg Holderied, Michael Devereux, Urs Buser, Ruth Pfaltzberger, Jean-Pierre Ramseyer, Daniel Sacker, Audrey Fischer, Daniela Tischhauser, Katrein Spieler, Beatrice Erismann and Maya Greuter of the departments of chemistry and physics for their continues support.

I gratefully acknowledge funding for my own position and financial support for projects from the University of Basel, the Marie Curie Actions of the European Commission, the Holcim Stiftung Wissen, the NCCR Nanosciences, the Swiss Nanoscience Institute, the Swiss Chemical Society and the Swiss National Science Foundation.

I am very grateful to my family, who was always there for me, loved, endured and supported me during my whole studies and this thesis.

# A Experimental Section

## A.1 Atom Transfer Radical Polymerization with Protein Conjugated Catalysts

### A.1.1 Materials

Commercially available chemicals were purchased from Sigma-Aldrich and used without further purification unless otherwise noted. The linker 3-N-maleimido-6-hydraziniumpyridine hydrochloride (MHPH) was obtained from SoluLink (San Diego, USA). NMR solvents were obtained from Cambridge Isotope Laboratories. Buffers were produced using double-distilled water. N-isopropyl acrylamide (NiPAAm) was recrystallized from a mixture of hexane and toluene (2:1 *v*/*v*). Poly(ethylene glycol) methylether acrylate (PEGA) with a number average molecular weight of 480 g $mol^{-1}$ was filtered over a neutral aluminium oxide column. 2-hydroxyethyl acrylate (HEA) and N,N,N',N'-tetraethyl-diethylenetriamine (TEDETA) were purified by vacuum distillation. Albumin from bovine serum (BSA) was purchased from Sigma-Aldrich (Switzerland) which was prepared using heat shock fractionation and may be referred to as Cohn Fraction V serum albumin.

### A.1.2 Methods

The $M_n$ and the PDI of the polymers were determined by gel permeation chromatography (GPC) unless otherwise noted. Samples for GPC (0.1 ml) were removed from the reaction mixture without separation of the protein and filtered over a small plug of basic aluminium oxide in order to remove salts and protein. The plug was washed with additional 0.2 ml of water and the filtrates were combined. Then the sample was lyophilized and redissolved in the appropriate GPC eluent to concentrations of 1 mg $ml^{-1}$. The measurements of pNiPAAm were performed on an Agilent 1100 Series instrument equipped with Viscotek I-columns (I-GUARD-0478 (40 mm x 7.8 mm), I-MBHMW-3078 (300 mm x 7.8 mm, exclusion limit > 10 $10^6$ g $mol^{-1}$), and I-MBMMW-3078 (300 mm x 7.8 mm, exclusion limit > 2 $10^5$ g $mol^{-1}$)) thermostated to 45°C and a refractive index detector maintained at 35°C. N,N-dimethylformamide (DMF) containing 20 mM lithium bromide was used as mobile phase with a flow rate of 1.0 ml $min^{-1}$. Poly(methyl methacrylate) standards (PSS, Mainz) were used for calibration. The measurements and analysis of pPEGA was performed on an Agilent 1100 Series instrument equipped with Agilent PL aquagel-OH columns (PL aquagel-OH Guard 8 μm (50 mm x 7.5 mm), and PL aquagel-OH MIXED-M 8 μm (300 mm x 7.5 mm, exclusion limit > 6 $10^5$ g $mol^{-1}$)) thermostated to 30°C and a refractive index detector maintained at 35°C. 100 mM $NaNO_3$ and 10 mM $NaH_2PO_4$ in aqueous solution at pH 7.0 containing 4:1 (*v*/*v*) MeOH was used as mobile phase with a flow rate of 1.0 ml $min^{-1}$. Polyethylene oxide ReadyCal standards (PSS, Mainz) were used for calibration. UV/Vis analyses were performed on a Lambda 35 spectrometer (Perkin Elmer) with 1 cm quartz cuvettes (Hellma, Germany) and on a

NanoDrop (Thermo Scientific). Protein concentrations were determined from the absorption at 280 nm, using an extinction coefficient of 43824 $M^{-1}$ $cm^{-1}$ for BSA.[315] $^1H$ NMR spectroscopy was carried out on a Bruker DPX-NMR (400 MHz) instrument. All experiments were performed at room temperature. Neutron activation analysis (NAA) was performed on a nuclear research reactor in the Department of Physics, University of Basel. Samples (1 ml) were activated by thermal neutrons at 2 kW for 15 min and measured with a Ge-detector. Qualitative analysis was performed using the $^{66}$Cu-Peak at 1039.2 keV. Quantitative analysis was performed in collaboration with the Kantonslabor Basel-Stadt using the $^{66}$Cu-Peak at 1039.2 keV with respect to an internal calibrated gold standard and validated against standard solutions of $CuBr_2$. The distinct gamma energy of the resulting nucleide was measured after 2 hours with a Ge-detector. Sodium dodecyl sulfate polyacrylamide gel electrophoresis (SDS-PAGE) was performed with self-casted 12% polyacrylamide gels and tris-HCl as running buffer in a Biorad Miniprotean 3 cell setup at 200 V for 70 min. Novex BenchMark Protein Ladder (Invitrogen) was used as molecular weight marker. Native gel electrophoresis was carried out using ready-casted 5% polyacrylamide gels (Biorad) and tris-glycine as running buffer. The gel was run for 180 min at 80 V. NativeMark Unstained Protein Standard (Invitrogen) was used as molecular weight marker. All gels were Coomassie stained with SimplyBlue SafeStain (Invitrogen). Gels were scanned on a Gel Doc EZ imager (Biorad).

### A.1.3 Synthesis of 2-((3-(bis(2-(diethylamino) ethyl)amino) propanoyl)oxy) ethyl 4-formylbenzoate

4-(dimethoxymethyl)benzoic acid was synthesized by refluxing a solution of 4-formyl benzoic acid in MeOH. After cooling to room temperature, crystals of the product were collected by filtration, washed with MeOH and dried under vacuum. 300 mg 4-(dimethoxymethyl)benzoic acid (1.53 mmol) and 910 mg 2-(6-chloro-1-H-benzotriazole-1-yl)-1,1,3,3-tetramethylaminium hexafluorophosphate (HCTU; 2.19 mmol, 1.43 equiv.) were dissolved in 40 ml acetonitrile (p.A.) in a 100 ml 2-neck round bottom flask under argon atmosphere. 557 µl triethylamine (404 mg, 4.00 mmol, 2.61 equiv.) was added and the solution was stirred for 5 min at room temperature. Freshly distilled 345 µl 2-hydroxyethylacrylate (HEA; 349 mg, 3.00 ml, 1.96 equiv.) was added and the reaction mixture was stirred at room temperature overnight. To the crude reaction mixture, 1.023 ml TEDETA (861.5 mg, 4.00 mmol, 2.61 equiv.) was added and the solution was stirred for 24 h at room temperature. 50 ml of water, 50 ml of saturated aqueous NaCl solution and 50 ml of 10% aqueous $Na_2CO_3$ were added, and the resulting solution was extracted with 3 x 100 ml dichloromethane. The combined organic phase was washed with 20 ml of 10% $Na_2CO_3$, dried over $Na_2SO_4$ and concentrated in vacuum to yield a brown oil. The crude product was purified by flash chromatography (basic $Al_2O_3$, eluent: $CH_2Cl_2$ with 1.75 vol.% EtOH). The acetal was cleaved by dissolving the product in 10 ml acetonitril/water (2:1 *v*/*v*) and acidification with a few drops of HCl. The solution was stirred 1 h at room

[315] K. Hirayama, S. Akashi, M. Furuya, K. Fukuhara, *Biochem. Biophys. Res. Commun.* **1990**, *173*, 639–646.

temperature. Then, 50 ml of water and 10 ml of 3N HCl were added and impurities/side products were extracted with $CH_2Cl_2$ (1 x 50 ml, 1 x 10 ml). The pH of the aqueous phase was adjusted to pH 9-10 by addition of 10% $Na_2CO_3$. Then, the aqueous phase was extracted with 3 x 100 ml $CH_2Cl_2$. The combined organic phase was dried over $Na_2SO_4$ and concentrated in vacuum. For the product (compound **1**) a yield of 85% was achieved.

### A.1.4 Preparation of BSA-$L_x$Cu

15 mg of BSA (220 nmol, 1 equiv.) was weighted into a falcon tube and dissolved in 15 ml modification buffer (100 mM $NaH_2PO_4$, 150 mM NaCl, pH 6.5). 163 µl of a 41.5 mM 3-N-maleimido-6-hydraziniumpyridine hydrochloride (MHPH) solution (1.6 mg, 6.6 µmol, 30 equiv.) in dimethyl sulfoxide (DMSO) was added and the reaction mixture was incubated at 37°C while shaking for 2 h. The sample was concentrated to 250 µl using 30k MWCO diafiltration devices at 4700 rpm. The supernatant was then diluted three times with 15 ml conjugation buffer (100 mM sodium phosphate, 150 mM NaCl, pH 6.0) and reconcentrated. 250 µl of the resulting BSA-MHPH solution (12.8 mg, 187.7 µmol, 1.0 equiv.) was diluted with 12 ml conjugation buffer. 90.0 µl of a 21.5 mM solution of compound **1** (see A.1.3) in DMSO (0.83 mg, 1.8 µmol, 10 equiv.) was added. The reaction mixture was shaken overnight at RT and concentrated with a 30k MWCO diafiltration device to 250 µl at 4700 rpm. Buffer was exchanged to complexation buffer (100 mM sodium acetate, pH 5.2) with three spun cycles. To nine parts of BSA-$L_x$ solution (9.8 mg, 143.7 nmol) one part of a 50 mM $CuBr_2$ solution in complexation buffer was added. The successful complexation of Cu could be seen by a change in color from light blue to yellow if high concentrations of protein were used. To remove non-complexed copper, the solution was concentrated with a 30k MWCO diafiltration device to 250 µl at 4700 rpm, three times diluted and reconcentrated with 15 ml reaction buffer (100 mM sodium acetate, 150 mM NaCl, 80 mM $MgCl_2$, pH 5.2) or $ddH_2O$. Finally, the BSA-$L_x$Cu solution was diluted with the corresponding solvent to a volume of 2.0 ml, yielding 5.5 mg (80.6 nmol) protein. The number of bis-aryl hydrazone linker groups formed was determined from the absorbance at 354 nm using an extinction coefficient of ($\varepsilon(\text{hydrazone})_{354\ nm}$ = 29000 $M^{-1}$ $cm^{-1}$).[316] According to UV/Vis data 0.21 ± 0.1 of the available cysteins in BSA carry a ligand and NAA yields a complexation of approx. 50% (see A.1.5) resulting in 95 ng copper per mg BSA.

### A.1.5 Quantitative Neutron Activation Analysis

Quantitative analysis with neutron activation analysis (NAA) of a 3.0 mg $ml^{-1}$ (45 nmol $ml^{-1}$) BSA-$L_x$Cu sample revealed a copper concentration of 270 ng $ml^{-1}$ copper which corresponds to 4.2 nmol $ml^{-1}$. With a TEDETA-ligand to BSA molar substitution ratio (MSR) of 0.21 ± 0.01, a $Cu^{II}$/ligand complexation efficiency of approx. 50% was calculated.

[316] SoluLink Company, *Catalog and Reference Manual* **2008**.

### A.1.6 MHPH Molar Substitution Ratio

The 6-hydraziniumpyridine molar substitution ratio (MSR) for BSA was determined by adding a 20 µl aliquot of a BSA-MHPH sample in conjugation buffer to 480 µl of a 0.5 mM 4-nitrobenzaldehyde solution in 100 mM sodium acetate buffer (pH 5.2). The solution was incubating at 37°C for 1 h and the absorbance at 390 nm ($\varepsilon(\text{hydrazone})_{390\ nm}$ = 24000 $M^{-1}$ $cm^{-1}$) was determined.[317] A blank value determined with 20 µl conjugation buffer was subtracted. The determination of MSR was carried out in triplicates and the mean values and standard deviations are reported. The MSR for BSA resulted in 0.22 ± 0.01 modified cysteins per BSA.

### A.1.7 ARGET ATRP of NiPAAm

25.0 mg NiPAAm (220 µmol, 66.7 equiv.) and 0.7 mg 2-hydroxyethyl-2-bromoisobutyrate (HEBIB; 3.3 µmol, 1.0 equiv.) were dissolved in 375 µl reaction buffer (100 mM sodium acetate, 150 mM NaCl, 80 mM $MgCl_2$, pH 5.2). 30.0 µl of BSA-$L_x$Cu in reaction buffer (50 µg, 0.8 nmol, 2.2 $10^{-4}$ equiv.) containing approx. 5 ng copper (0.08 nmol, 2.4 $10^{-5}$ equiv.) was added. The polymerizations were started by adding 200 µl of deoxygenized 4.25 mM L-ascorbic acid solution (0.15 mg, 0.85 µmol, 0.25 equiv.) in reaction buffer. The reactions were stirred for 20 h at room temperature and stopped by adding 605 µl non-deoxygenated reaction buffer and exposure to ambient air.

### A.1.8 ARGET ATRP of PEGA in Aqueous Solution

0.1 ml PEGA (220.0 µmol, 66.7 equiv.) and HEBIB (0.7 mg, 3.3 µmol, 1.0 equiv.) were dissolved in 375 µl reaction buffer. 30 µl of BSA-$L_x$Cu in reaction buffer (50.0 µg, 0.8 nmol, 2.2 $10^{-4}$ equiv.) containing approx. 5 ng copper (0.08 nmol, 2.4 $10^{-5}$ equiv.) was added. The polymerizations were started by adding 200 µl of deoxygenized 4.25 mM L-ascorbic acid solution (0.15 mg, 0.85 µmol, 0.25 equiv.) in reaction buffer. The reactions were stirred for 20 h at room temperature and stopped by adding 605 µl non-deoxygenated reaction buffer and exposure to ambient air.

### A.1.9 Precipitation Experiments

BSA or Hb were prepared in concentrations of 0.5 mg $ml^{-1}$, 1 mg $ml^{-1}$ and 2 mg $ml^{-1}$ in water. To these solution organic cosolvent (MeOH, EtOH and formamide) was added in vol.% of 5%, 10%, 15%, 20%, 30%, 40%, 50%, 60%, 70%, 80% and 90%. Subsequently, the protein absorbtion at 280 nm was measured with UV/Vis spectroscopy.

[317] SoluLink Company, *Catalog and Reference Manual* **2008**.

### A.1.10 Dynabead Removal

The procedure was performed according to the instruction manual.[318] BSA was bound over an antibody-antigen recognition to magnetic spheres via rabbit IgG anti-BSA antibody. The magnetic spheres were manipulated with a strong magnet to remove the BSA-catalyst complex from solution. Protein concentrations were determined from the UV/Vis absorption at 280 nm, using an extinction coefficient of 43824 $M^{-1}$ $cm^{-1}$ for BSA.[319]

[318] "Dynabead Manual," can be found under http://tools.lifetechnologies.com/content/sfs/manuals/ImmunoprecipitationKitDynalProteinA_man.pdf, **2013**.

[319] K. Hirayama, S. Akashi, M. Furuya, K. Fukuhara, *Biochem. Biophys. Res. Commun.* **1990**, *173*, 639–646.

## A.2 Horseradish Peroxidase as Catalyst for Atom Transfer Radical Polymerization

### A.2.1 Materials

N-isopropylacrylamide (NiPAAm, 97%, Sigma-Aldrich) was purified by recrystallization from a hexane/toluene (2:1) mixture. Horseradish peroxidase (HRP; highly stabilized, essential salt-free, lyophilized powder with an activity of 200-300 units per mg solid (using pyrogallol), P2088, Sigma-Aldrich), (+)-sodium L-ascorbate (Asc, ≥ 98%, Sigma-Aldrich), ethylene glycol (≥ 99%, Sigma-Aldrich), bromoisobutyryl bromide (98%, Sigma-Aldrich), pyridine (≥ 99.8%, Fluka) and dichloro methane (DCM, Baker) were used as received. NMR solvents were obtained from Cambridge Isotope Laboratories. The water soluble initiator 2-hydroxyethyl-2-bromoisobutyrate (HEBIB) was synthesized according to a published protocol by the overnight reaction of ethylene glycol and bromoisobutyryl bromide in the presence of pyridine in DCM.[320]

### A.2.2 Methods

The conversion of the reaction as well as the purity of the starting materials was determined by $^1$H NMR spectroscopy using a Bruker DPX-NMR (400 MHz) instrument. The solvents were $D_2O$ and $CDCl_3$. All the measurements were performed at room temperature. Conversion was calculated from the baseline corrected spectra using the integrals of the signal at 5.59 ppm, which corresponds to one proton of the residual monomer, and the overlapping signals at 3.85 and 3.77 ppm, which correspond to one proton of the monomer and one of the polymer. The endgroup determination by NMR ($^1$H COSY) and the $^1$H NMR spectrum was measured on a Bruker Ultrashield NMR (600 MHz) instrument with 7 mg of purified pNiPAAm dissolved in 0.5 ml of 100% deuterated $D_2O$.

Neutron activation analysis (NAA) was performed by activation of 14 mg purified pNiPAAm at 2 kW for 30 min by thermal neutrons in the nuclear reactor of the Department of Physics, University of Basel. The quantitative analysis was performed using the main peak of $^{82}$Br at 776.517 keV with respect to an internal calibrated gold standard and validated against a bromine doped curcuma reference. The distinct gamma energy of the resulting nuclide was measured after 3 days with a Ge-detector.

The number average molecular weight $M_n$ and the polydispersity index (PDI) of the polymers were determined by gel permeation chromatography (GPC). The measurements were performed on an Agilent 1100 Series instrument equipped with Viscotek I-columns (I-GUARD-0478 (40 mm x 7.8 mm), I-MBHMW-3078 (300 mm x 7.8 mm, exclusion limit > 10 $10^6$ g mol$^{-1}$), and I-MBMMW-3078 (300 mm x 7.8 mm, exclusion limit > 2 $10^5$ g mol$^{-1}$)) thermostated to 45°C and a refractive index detector maintained at 35°C. N,N-Dimethylformamide (DMF) containing 20 mM lithium

[320] W. Jakubowski, J.-F. Lutz, S. Slomkowski, K. Matyjaszewski, *J. Polym. Sci. A Polym. Chem.* **2005**, *43*, 1498–1510.

bromide was used as mobile phase with a flow rate of 1.0 ml $min^{-1}$. Polystyrene standards were used for calibration.

UV/Vis spectra were recorded on a Spectra Max M5e (Molecular Devices) in 1 cm quartz cuvettes. The step width was set to 1 nm. Circular dichroism (CD) spectroscopy was performed on a Chirascan CD spectrometer (Applied Photophysics) equipped with a thermostated cuvette holder (TC425, Quantum Northwest). The samples were measured at 22°C in 0.2 nm steps with a bandwidth of 1 nm and 1 s integration time using a 1 mm quartz cuvette. Spectra were averaged over five points. The protein concentration was adjusted to measure in a HT voltage range between 250 and 800 V in the far-UV region. Subsequently, the protein concentration was determined by UV/Vis spectroscopy using an extinction coefficient of 102 000 $M^{-1}$ $cm^{-1}$ at 403 nm.[321]

Matrix-assisted laser desorption/ionization with time of flight detector mass spectrometry (MALDI-ToF MS) was carried out with a Voyager DE PRO (Perseptive Biosystems) in the linear mode using delayed extraction (750 ns), positive polarity, an accelerating voltage of 25000 V, a grid voltage of 93% and a guide wire voltage of 0.15%. The mass spectra were averaged over a total of 1000 laser shots. Sinapic acid (Sigma-Aldrich) was used as matrix. 5 µl of aqueous sample solution was added to 10 µl of a 21 mg $ml^{-1}$ matrix solution in 50% acetonitrile and 0.1% trifluoroacetic acid. 2 µl of the mixture were applied to a 100-well stainless steel plate and allowed to dry at room temperature.

Sodium dodecyl sulfate polyacrylamide gel electrophoresis (SDS-PAGE) was performed with self-casted 12% tris-glycine gels in a Biorad Miniprotean 3 cell setup at 200 V for 80 min. Novex Sharp Pre-stained Protein Standard (Invitrogen) was used as molecular weight marker. Acidic native gel electrophoresis was carried out using self-casted 10% acetate-glycine gels and tris-glycine as running buffer. The gel was run for 180 min at 80 V. All gels were Coomassie stained.

### A.2.3 Polymerizations

Polymerizations were carried out in 100 mM sodium phosphate or 100 mM sodium carbonate buffers set to pH 5.2, 6.0, 6.5, 7.0, 7.5, 8.5, 9.5, and 10.5. Oxygen was removed from buffers by purging them with argon for 20 – 30 minutes. HEBIB (4.8 ml, 7.0 mg, 33 mmol) and NiPAAm (255.0 mg, 2.253 mmol) were weighed into a two-neck round bottom flask. HRP (5.0 mg, 0.11 mmol) and sodium ascorbate (9.0 mg, 45 mmol) were weighted into two 2-ml glass vial and the vials were placed into two 10 ml two-neck round bottom flask. Air was removed from all the flasks in three evacuation and Argon flushing cycles. The vials fulfilled two purposes: They prevented the powders from being blown around by the argon and the one with the protein served as small-volume reaction vessel for the polymerization. The monomer and the initiator were dissolved in 3.0 ml oxygen-free buffer, the HRP in 0.2 ml and ascorbate in 1.2 ml of the same buffer. 0.3 ml of initiator/monomer solution was syringed to the HRP solution, and then the reaction was started by transferring 0.1 ml of the reducing agent solution into the HRP/NiPAAm/HEBIB solution in the vial by means of a syringe. The

[321] L. M. Shannon, E. Kay, J. Y. Lew, *J. Biol. Chem.* **1966**, *241*, 2166–2172.

ratio of reactants in the reaction mixture was 1:68:1.1:0.034 (HEBIB:NiPAAm:Asc: HRP) unless otherwise noted. The reaction was stirred at room temperature and 0.1 ml samples were removed for analytical purposes in periodic intervals. The analytical samples were exposed to air, and filtered over a small plug of neutral aluminium oxide. The plug was washed with additional 0.2 ml of water and the filtrates were combined. 0.25 ml of filtrate was added to 0.25 ml of $D_2O$ and analyzed by $^1H$ NMR to determine the conversion. Then the sample was lyophilized, redissolved in THF and filtered through a plug of neutral aluminium oxide in order to remove salts and protein. The THF was evaporated using a rotary evaporator to yield a white solid containing that was analyzed by GPC.

For start- and end-group determination by NMR and NAA, a pNiPAAm sample was synthesized and purified to remove small molecules such as unreacted initiator, monomer, and salts. Polymerization was performed for 1.5 h with a ratio of 1:20:0.66:0.009 (HEBIB:NiPAAm:Asc:HRP). After filtration through aluminum oxide, the crude product was extensively dialyzed against double distilled water (MWCO 1000 g $mol^{-1}$). The product solution was lyophilized and the polymer ($M_n$ = 92500 g $mol^{-1}$, PDI = 2.6 (GPC)) was analyzed using a 600 MHz NMR ($^1H$, and $^1H$ COSY) and NAA.

HRP was purified at the end of typical polymerization reaction carried out at pH 6.0 for 16 h in order to analyze its structural integrity. The polymerization mixture was centrifuged at 40°C at relative centrifugation force of 20000 g in a Sigma 3-18k centrifuge to remove PNIPAAm. The pellet was colorless, indicating that it did not contain HRP. The brown supernatant was subsequently buffer-exchanged three times with water in an Amicon Ultra-15 spin centrifugal filter unit (MWCO 3000 g $mol^{-1}$), which removed small molecules like unreacted monomer and ascorbate.

## A.3 Hemoglobin and Red Blood Cells Catalyze Atom Transfer Radical Polymerization

### A.3.1 Materials

Hemoglobin from bovine blood (Hb; lyophilized powder, H2500), hemin from bovine (≥ 90%), L-ascorbic acid (AscA; ≥ 98%), sodium L-ascorbate (≥ 98%) N,N-dimethyl formamide (DMF; 99% (for synthesis) and Chromasolv plus (for gel permeation chromatography (GPC)), N-methyl-2-pyrrolidone (NMP; Chromasolv plus), lithium bromide (≥ 99%), copper bromide (≥ 98%,) 2-bromopropionitrile (BPN; 97%), and the reagents for the Ellman's test were purchased from Sigma-Aldrich, and used as received unless otherwise indicated. Ultraviolet/visible (UV/Vis) spectra of Hb solutions revealed that the commercial product was Hb in its iron(III) state, i.e., methemoglobin. N-isopropylacrylamide (NiPAAm; 97%, Sigma-Aldrich) was purified by recrystallization from a hexane/toluene (2:1) mixture. Poly(ethylene glycol) methyl ether acrylate (PEGA; $M_n$ = 480 g $mol^{-1}$, Sigma-Aldrich) and poly(ethylene glycol) methyl ether methacrylate (PEGMA; $M_n$ = 500 g $mol^{-1}$, Sigma-Aldrich) were passed over aluminum oxide prior to use in order to remove the inhibitor. N,N,N′,N′ Tetraethyldiethylenetriamine (TEDETA; 90%, Sigma-Aldrich) was distilled before use. N-(2-hydroxyethyl)maleimide (HEMI)[322] and 2-hydroxyethyl-2-bromoisobutyrate (HEBIB)[323] were synthesized according to published protocols. Polymerizations were carried out in double distilled water as the solvent unless otherwise stated. Oxygen was removed from water prior to polymerizations by purging it with argon for 30 min. NMR solvents were obtained from Cambridge Isotope Laboratories. Argon (99.998%, Carbagas) was used without further purification. Fresh human erythrocytes were obtained from the Corresponding Author by taking a 7.5 ml blood sample with a monovette EDTA KE blood collection system (Sarstedt), followed by centrifugation and removal of the blood plasma and of the buffy coat.

### A.3.2 Methods

$^1$H NMR spectroscopy was carried out with a Bruker DPX-NMR (400 MHz) instrument. All measurements were performed at room temperature. The purity of starting materials and the spectra of a purified pNiPAAm sample were determined using $CDCl_3$ as solvent. The conversion of polymerizations was measured using a mixture of $D_2O$ and water as solvent. Conversion of NIPAAm was calculated from baseline-corrected spectra using the integrals of the signal at 5.59 ppm, which corresponds to one proton of the residual monomer, and the overlapping signals at 3.85 and 3.77 ppm, which correspond to one proton of the monomer and one of the polymer. Conversion of PEGA was calculated accordingly from the integrals of the

[322] a) W. M. Gramlich, M. L. Robertson, M. A. Hillmyer, *Macromolecules* **2010**, *43*, 2313–2321 b) W. H. Heath, F. Palmieri, J. R. Adams, B. K. Long, J. Chute, T. W. Holcombe, S. Zieren, M. J. Truitt, J. L. White, C. G. Willson, *Macromolecules* **2008**, *41*, 719–726.

[323] W. Jakubowski, J.-F. Lutz, S. Slomkowski, K. Matyjaszewski, *J. Polym. Sci. A Polym. Chem.* **2005**, *43*, 1498–1510.

peaks at 6.48, 6.21, 6.00 ppm (3H of monomer) and at 3.37 ppm (3H of monomer and polymer). Conversion of PEGMA was calculated accordingly from the integrals of the peak at 5.73 ppm (3H of monomer) and at 3.37 ppm (3H of monomer and polymer). The apparent number average molecular weight ($M_n$) based on polystyrene (PS) standards and the polydispersity index (PDI) of the polymers were determined by GPC. Measurements of pNiPAAm were performed on an Agilent 1100 Series instrument equipped with a refractive index detector. Two different column setups were used. The samples synthesized using native Hb and Cys-blocked Hb as catalyst were measured with three Viscotek I-columns (I-GUARD-0478 (40 mm x 7.8 mm), I-MBHMW-3078 (300 mm x 7.8 mm, exclusion limit > 10 $10^6$ g $mol^{-1}$), and I-MBMMW-3078 (300 mm x 7.8 mm, exclusion limit > 2 $10^5$ g $mol^{-1}$)) thermostatted to 45°C, using DMF (with 20 mM lithium bromide) as the mobile phase with a flow rate of 1.0 ml $min^{-1}$. The samples obtained from polymerizations with erythrocytes were measured with a PLgel 5 µm MIXED-C (300 x 7.5 mm, Varian) column plus a PLgel 3 µm (50 x 7.5 mm, Varian) guard column thermostatted to 70°C. In this case, the mobile phase was NMP (with 50 mM lithium bromide) with a flow rate of 1.0 ml $min^{-1}$. PS standards were used for calibration of both setups. Control experiments with poly(methyl methacrylate) (PMMA) standards on the I-column setup showed the calibration curves to be similar: PMMA calibration results in apparent molecular weights 3-11% lower than PS calibration. Measurements of pPEGA were performed on a Viscotek GPCmax system using a refractive index detector, with Agilent PLgel columns (10 µm guard + 2 x 5 µm mixed C, or 10 µm guard + mixed C + 10 µm 100 Å + 5 µm $10^3$ Å) thermostatted to 30°C and THF as mobile phase at a flow rate of 1 ml $min^{-1}$. Calibration was carried out with PS standards. For GPC analysis of PEGA and PEGMA polymerization kinetics, the polymer was not separated from the monomer during sample work (see above). As the peaks of residual monomer and polymer were not baseline-separated, a lower molecular weight limit was set to the polymer peak for $M_n$ and PDI determination (PEGA polymerization with Cys-blocked Hb: log M = 3.08, PEGMA polymerization with Cys-blocked Hb: log M = 3.2, erythrocyte-catalyzed polymerization of PEGA: log M = 3.2). The limit was kept constant throughout the analysis of each kinetic run. NAA was performed by activation of 8 mg purified pNiPAAm at 2 kW for 30 min by thermal neutrons in the nuclear research reactor of the Department of Physics, University of Basel. The quantitative analysis was performed using the main peak of $^{82}$Br at 776.517 keV with respect to an internal calibrated gold standard and validated against a bromine doped curcuma reference. The distinct gamma energy of the resulting nuclide was measured after 3 days with a Ge-detector. UV/Vis spectra were recorded on a Specord 210 Plus (Analytik Jena) in 1 cm quartz cuvettes. The spectra are reported as millimolar absorptivity (referring to one heme group and one globin subunit). To this end, heme concentration of samples were determined as cyanmethemoglobin:[324] A dilution series of each sample was prepared using a solution that contained 200 mg $l^{-1}$ $K_3Fe(CN)_6$, 50 mg $l^{-1}$ KCN, and 1.0 g $l^{-1}$ $NaHCO_3$. After at least 20 min of incubation at room temperature, the absorbance at 540 nm of each

[324] W. G. Zijlstra, A. Buursma, *Comp. Biochem. Physiol., Part B: Biochem. Mol. Biol.* **1997**, *118*, 743–749.

solution was measured. The sample's heme concentration was calculated from this data by linear regression, using an extinction coefficient of 11.0 $mM^{-1}$ $cm^{-1.52}$ CD spectroscopy was performed on a Chirascan CD spectrometer (Applied Photophysics) equipped with a thermostatted cuvette holder (TC425, Quantum Northwest). The samples were measured at 22°C in 0.2 nm steps with a bandwidth of 1 nm and 1 s integration time using a 1 mm quartz cuvette. Spectra were averaged from two consecutive scans and smoothed over five data points. The protein concentration was adjusted so as to be able to measure within an HAT voltage range between 250 and 900 V in the far-UV region. The protein concentration was determined by UV/Vis spectroscopy of cyanmethemoglobin complexes as described above. Ellipticities are reported on a molar heme basis. Sodium dodecyl sulfate (SDS) polyacrylamide gel electrophoresis was performed with self-casted 12% tris-glycine gels in a Biorad Miniprotean 3-cell setup at 200 V for 40 min. Novex Sharp Prestained Protein Standard or BenchMark Protein Ladder (Invitrogen) were used as molecular weight markers. Samples from polymerization reactions analyzed by SDS gel electrophoresiswere taken directly from the reaction mixture, and analyzed without prior filtration through aluminum oxide.

### A.3.3 Synthesis of Cys-Blocked Hb

To eliminate the possibility of chain transfer reactions, the accessible cysteine groups of bovine Hb were modified with N-(2-hydroxyethyl)maleimide (HEMI). To this end, Hb (300 mg, 4.65 μmol) and HEMI (20.0 mg, 0.140 mmol) were incubated in 300 ml of 100 mM sodium phosphate buffer (pH 6.5, 150 mM NaCl) for 2 h at 37°C. The protein was then desalted by spin diafiltration against 100 mM sodium phosphate buffer (pH 6.0, 150 mM NaCl) (2x) and against water (3x) using Amicon Ultra-15 spin centrifugal filter unit (molecular weight cutoff (MWCO) 10 000 g $mol^{-1}$, Millipore). The degree of modification was analyzed by measuring the concentration of Hb's accessible cysteines before and after modification with the Ellman's test.

### A.3.4 NiPAAm Polymerization with Native Hb or Cys-Blocked Hb

HEBIB (24 mg, 0.11 mmol) and NiPAAm (1016 mg, 8.978 mmol) were weighed into a two-neck round-bottom flask and dissolved in 15 ml water in an argon atmosphere. Solutions of native Hb and AscA were prepared by dissolving Hb (70.0 mg, 1.09 μmol Hb tetramer) in 5 ml water and AscA (30.0 mg, 0.170 mmol) in 3 ml water in two-neck round-bottom flasks under an argon atmosphere. Cys-blocked Hb was obtained as stock solution from the modification step, and its concentration was measured by UV/Vis spectroscopy. The solution was diluted with water to obtain the same protein concentration as with native Hb. This solution was deprived of oxygen by purging with argon for 30 min. A polymerization was started by transferring 2 ml of AscA solution and 4.3 ml of either native Hb or Cys-blocked Hb solution to the initiator/monomer flask. The ratio of reactants in the reaction mixture was 1:79:1:0.008 (HEBIB:NiPAAm:AscA:Hb; Hb refers to the full protein consisting of 4 heme groups and 4 globins) unless otherwise noted. The reaction was stirred at room temperature, and 1 ml samples were removed for analytical purposes at periodic intervals. The

analytical samples were exposed to air and filtered over a small plug of neutral aluminum oxide. The plug was washed with an additional 2 ml of nondeoxygenated water, and the filtrates were combined. The filtrate (0.4 ml) was added to 0.4 ml of $D_2O$ and analyzed by $^1H$ NMR to determine the conversion. The remaining analytical sample was lyophilized to yield a solid that was redissolved in DMF (with 20 mM lithium bromide) and analyzed by GPC.

pH-dependent reactions were carried out for 24 h in 100 mM KCl solution (set to pH = 1.5 with HCl), 100 mM sodium citrate buffer (pH = 3.2 after addition of ascorbate), 100 mM sodium acetate buffers (4.0, and 4.5 after addition of ascorbate) or 100 mM sodium phosphate buffers (pH 5.0, 5.8, and 7.6 after addition of ascorbate), replacing AscA with sodium ascorbate as the reducing agent.

Hb was purified at the end of a typical 24 h polymerization reaction in order to characterize the recovered protein with circular dichroism (CD) and UV/Vis spectroscopy. To this end, the polymerization mixture was centrifuged at 40°C at a relative centrifugation force of 15000 g in a Sigma 3-18k centrifuge to remove pNiPAAm. The supernatant was subsequently buffer-exchanged three times with water in an Amicon Ultra-15 spin centrifugal filter unit (MWCO 10000 g $mol^{-1}$), which removed small molecules such as unreacted monomer and AscA.

For bromine quantification by neutron activation analysis (NAA) and a chain extension experiment, a polymerization was stopped after 45 min (10% conversion). The polymer was purified as described above, followed by extensive dialysis against water (Spectra/Por 7 dialysis membrane, MWCO 1000; Spectrum Laboratories). Part of the sample solution was lyophilized and analyzed by NAA. The rest of the polymer was used as macroinitiator for conventional ATRP. To this end, NiPAAm (625 mg, 5.52 mmol) was dissolved in 20 ml of the dialyzed polymer solution (3.53 mg $ml^{-1}$ pNiPAAm). The resulting mixture was purged with argon for 30 min. Solutions of CuBr (31.5 mg, 0.219 mmol) in 1 ml DMF and of TEDETA (22.6 µl, 88.0 µmol) in 200 µl DMF were prepared. Both solutions were purged with argon. Then, 200 µl of the CuBr solution was transferred to the TEDETA solution. To start the polymerization, all of this catalyst solution was transferred to the flask that contained the macroinitiator/monomer solution. The reaction was stirred at room temperature for 3 h under argon. It was stopped by exposing it to air and by adding 10 ml of nondeoxygenated water. The copper was removed by filtration over a basic aluminum oxide column. The nonreacted monomer was removed by extensive dialysis against water (Spectra/Por 7 dialysis membrane, MWCO 1000; Spectrum Laboratories). Finally, the solution was lyophilized to obtain a white solid.

A control reaction with hemin instead of Hb was carried out overnight under argon atmosphere with deoxygenated reagent solutions. HEBIB (24 mg, 0.11 mmol) and NiPAAm (1044 mg, 9.226 mmol) were dissolved in 20 ml water. Hemin (4.0 mg, 6.1 mmol) was dissolved in 4 ml DMSO. AscA (12.0 mg, 68 µmol) was dissolved in 2 ml water. The hemin solution (0.8 ml) and 1 ml of the AscA solution were transferred into the monomer/initiator solution. The reaction was stirred at room temperature overnight.

To follow the polymerization in situ with UV/Vis spectroscopy, the reaction was downscaled to the volume of a standard cuvette. HEBIB (2.4 mg, 0.011 mmol) and

NiPAAm (100 mg, 0.884 mmol) were weighed into a sealable cuvette and dissolved in 1.5 ml water. AscA (20.3 mg, 0.115 mmol) was dissolved in 2 ml water in a two-neck round-bottom flask. A solution of Cys-blocked Hb was diluted with water to a concentration of 12.4 mg $ml^{-1}$ (0.193 μmol $ml^{-1}$). All solutions were purged for 30 min with argon. The polymerization was started by transferring 0.5 ml of Hb solution and 0.2 ml of AscA solution to the cuvette. The reaction was run at room temperature. The first spectrum was recorded directly after the addition of the AscA solution. Thereafter, spectra were recorded every 45 s, or every 4 min.

### A.3.5 PEGA and PEGMA Polymerization with Cys-Blocked Hb

HEBIB (12 mg, 0.057 mmol) and monomer (PEGA: 2120 mg, 4.42 mmol; PEGMA: 2120 mg, 4.24 mmol) were weighed into a two-neck round-bottom flask and dissolved in 6 ml water in an argon atmosphere. Cys-blocked Hb stock solution was diluted with water to a concentration of 12.5 mg $ml^{-1}$ and deprived of oxygen by purging with argon for 30 min. Polymerization was started by transferring 2 ml of AscA solution (30 mg $ml^{-1}$ in the PEGA polymerization, 15 mg $ml^{-1}$ in the PEGMA polymerization) and 2 ml of Cys-blocked Hb solution to the initiator/monomer flask. The ratios of reactants in the reaction mixture were 1:78:3:0.007 (HEBIB:PEGA:AscA:Hb) and 1:75:1.5:0.008 (HEBIB:PEGMA:AscA:Hb). (Hb refers to the full protein consisting of 4 heme groups and 4 globins.) The reaction was stirred at room temperature, and 1 ml samples were removed for analytical purposes at periodic intervals and exposed to air. The analytical sample (0.5 ml) was diluted with 0.5 ml of $D_2O$ and filtered over a small plug of neutral aluminum oxide. The filtrate was analyzed by $^1H$ NMR to determine the conversion. The remaining analytical sample was mixed with 2 ml of tetrahydrofuran (THF). $MgSO_4$ was added to remove the water, the sample was filtered through a Millex-LCR syringe filter (hydrophilic PTFE, 0.45 μm; Milipore), and the THF solution was analyzed by GPC.

### A.3.6 Polymerization with Erythrocytes

Polymerizations with fresh human erythrocytes were carried out on the same day on which the blood sample was taken. NiPAAm polymerization: HEBIB (24 mg, 0.11 mmol) and NiPAAm (1008 mg, 8.908 mmol) were weighed into a two-neck round-bottom flask and dissolved in 15 ml water. The solution was purged for 30 min with argon. AscA (120 mg, 0.681 mmol) was dissolved in 3 ml deoxygenated water in a two-neck round-bottom flask under an argon atmosphere. Two milliliters of erythrocytes was purged with argon for 30 min and then diluted with 3 ml of deoxygenated water under an argon atmosphere. The polymerization was started by transferring 1.5 ml of AscA solution and 4 ml of erythrocyte suspension to the initiator/monomer flask. The reaction was stirred at room temperature for 24 h. Samples for $^1H$ NMR and GPC analysis were prepared as described above. PEGA polymerization: HEBIB (12 mg, 0.057 mmol), and PEGA (2120 mg, 4.42 mmol) were weighed into a two-neck round-bottom flask and dissolved in 5 ml water. The solution was purged for 30 min with argon. AscA (60 mg, 0.34 mmol) was dissolved in 2 ml deoxygenated water in a two-neck round-bottom flask under an argon atmosphere.

Two ml of erythrocytes were purged with argon for 30 min. The polymerization was started by transferring 1 ml of AscA solution and 2 ml of erythrocyte suspension to the initiator/monomer flask. The reaction was stirred at room temperature. Samples for $^{1}H$ NMR and GPC analysis were taken every hour and prepared for analysis as described above.

## A.4 A Chaperonin as Protein Nanoreactor for Atom Transfer Radical Polymerization

### A.4.1 Materials

Commercially available chemicals were purchased from Sigma-Aldrich and used without further purification unless otherwise noted. The linker 3-N-maleimido-6-hydraziniumpyridine hydrochloride (MHPH) was obtained from SoluLink (San Diego, USA). NMR solvents were obtained from Cambridge Isotope Laboratories. Buffers were produced using double-distilled water. N-isopropyl acrylamide (NiPAAm) was recrystallized from a mixture of hexane and toluene (2:1 *v*/*v*). Poly(ethylene glycol) methylether acrylate (PEGA) with a number average molecular weight of 480 g $mol^{-1}$ was filtered over an neutral aluminium oxide column. 2-hydroxyethyl acrylate (HEA) and N,N,N',N'-tetraethyl-diethylenetriamine (TEDETA) were purified by vacuum distillation.

Albumin from bovine serum (BSA) was purchased from Sigma-Aldrich (Switzerland) which was prepared using heat shock fractionation and may be referred to as Cohn Fraction V serum albumin. To encapsulate an ATRP catalyst into the thermosome (THS), a THS with three point mutations C363A (α-subunit), K316C (β-subunit) and C364A (β-subunit) was used. The mutant was described previously.[325] The fermentation and purification of this THS was carried out as reported previously.[323] In brief, the mutated α- and β-subunit genes were co-expressed in E. coli BL21 (DE3) Codon Plus-RIL. Fermentations were carried out in Terrific Broth medium at 30°C. Purification of THS was performed in three chromatography steps. An anion-exchange chromatography (column: HiPrep 16/10 Q FF, GE Healthcare) to capture the THS from the cell lysate was followed by size-exclusion chromatography (two columns in series: first a Superose 6 prep grade and second a HiPrep 16/60 Sephacryl S-200 high resolution, GE Healthcare) to remove low molecular mass assemblies and single subunits. The sample was further purified by high-resolution anion-exchange chromatography (column: Mono Q 10/100 GL, GE Healthcare) to yield fully assembled THS with a α- to β-subunit ratio of 8:8.[326] The corresponding fractions were identified by sodium dodecyl sulfate polyacrylamide gel electrophoresis (SDS-PAGE) and native PAGE.

### A.4.2 Methods

Matrix-assisted laser desorption/ionization with time of flight detector mass spectrometry (MALDI-ToF MS) was carried out with a Voyager DE PRO (Perseptive Biosystems) in the linear mode using delayed extraction (750 ns), positive polarity, an accelerating voltage of 25000 V, a grid voltage of 93% and a guide wire voltage of 0.15%. The mass spectra were averaged over a total of 1000 laser shots. pNiPAAm was separated from the protein cage by size exclusion spin centrifugation using 100k

[325] N. Bruns, K. Pustelny, L. M. Bergeron, T. A. Whitehead, D. S. Clark, *Angew. Chem. Int. Ed.* **2009**, *48*, 5666–5669.
[326] M. G. Bigotti, A. R. Clarke, *J. Mol. Biol.* **2005**, *348*, 13–26.

MWCO diafiltration devices (Amicon Ultra, Millipore, MA, USA) at 13600 rpm leaving the THS in the supernatant while the polymer could be collected from the flow-through. 5 μl of the flow-through was added to 10 μl of a 21 mg $ml^{-1}$ sinapinic acid solution in 50% acetonitrile and 0.1% trifluoroacetic acid. 2 μl of the mixture were applied to a 100-well stainless steel plate and allowed to dry at room temperature. Data Explorer Software (Applied Biosystems) was used to calculate the number average molecular weight ($M_n$) and the polydispersity index (PDI) from the mass-spectra.

The $M_n$ and the PDI of the polymers were determined by gel permeation chromatography (GPC) unless otherwise noted. Samples for GPC (0.1 ml) were removed from the reaction mixture without separation of the protein and filtered over a small plug of basic aluminium oxide in order to remove salts and protein. The plug was washed with additional 0.2 ml of water and the filtrates were combined. Then the sample was lyophilized and redissolved in the appropriate GPC eluent to concentrations of 1 mg $ml^{-1}$. The measurements of pNiPAAm were performed on an Agilent 1100 Series instrument equipped with Viscotek I-columns (I-GUARD-0478 (40 mm x 7.8 mm), I-MBHMW-3078 (300 mm x 7.8 mm, exclusion limit > 10 $10^6$ g $mol^{-1}$), and I-MBMMW-3078 (300 mm x 7.8 mm, exclusion limit > 2 $10^5$ g $mol^{-1}$)) thermostated to 45°C and a refractive index detector maintained at 35°C. N,N-dimethylformamide (DMF) containing 20 mM lithium bromide was used as mobile phase with a flow rate of 1.0 ml $min^{-1}$. Poly(methyl methacrylate) standards (PSS, Mainz) were used for calibration. The measurements of Analysis of pPEGA was performed on an Agilent 1100 Series instrument equipped with Agilent PL aquagel-OH columns (PL aquagel-OH Guard 8 μm (50 mm x 7.5 mm), and PL aquagel-OH MIXED-M 8 μm (300 mm x 7.5 mm, exclusion limit > 6 $10^5$ g $mol^{-1}$)) thermostated to 30°C and a refractive index detector maintained at 35°C. 100 mM $NaNO_3$ and 10 mM $NaH_2PO_4$ in aqueous solution at pH 7.0 containing 4:1 (*v*/*v*) MeOH was used as mobile phase with a flow rate of 1.0 ml $min^{-1}$. Polyethylene oxide ReadyCal standards (PSS, Mainz) were used for calibration. Small angle X-ray scattering (SAXS) was performed on a Bruker AXS Nanostar with an Incoatec Cu - IμS Microfocus X-ray source (λ = 0.154 nm), and a VANTEC 2000 2D detector. The measurements were done with 45 kV and 650 μA and the integration time was 12 h. About 20 μl of sample with the concentration of 1.5 mg $ml^{-1}$ was loaded into a glass capillary (d = 1 mm, thickness of the wall = 0.01 mm), the capillary was closed by melting the top of the capillary, the closed capillary was put into the Nanostar, vacuum was applied and the measurement was started. The data were azimuthally averaged with SAXS v.4.1.36 Bruker software and fitted with BrukerAXS Nanofit software (version 1.2.1.1). UV/Vis analyses were performed on a Lambda 35 spectrometer (Perkin Elmer) with 1 cm quartz cuvettes (Hellma, Germany) and on a NanoDrop (Thermo Scientific). Protein concentrations were determined from the absorption at 280 nm, using an extinction coefficient of 210880 $M^{-1}$ $cm^{-1}$ for the hexadecameric THS complex[327] and of 43824 $M^{-1}$ $cm^{-1}$ for

[327] N. Bruns, K. Pustelny, L. M. Bergeron, T. A. Whitehead, D. S. Clark, *Angew. Chem. Int. Ed.* **2009**, *48*, 5666–5669.

BSA.[328] $^1$H NMR spectroscopy was carried out on a Bruker DPX-NMR (400 MHz) instrument. All experiments were performed at room temperature. Sodium dodecyl sulfate polyacrylamide gel electrophoresis (SDS-PAGE) was performed with self-casted 12% polyacrylamide gels and tris-HCl as running buffer in a Biorad Miniprotean 3 cell setup at 200 V for 70 min. Novex BenchMark Protein Ladder (Invitrogen) was used as molecular weight marker. Native gel electrophoresis was carried out using ready-casted 5% polyacrylamide gels (Biorad) and tris-glycine as running buffer. The gel was run for 180 min at 80 V. NativeMark Unstained Protein Standard (Invitrogen) was used as molecular weight marker. All gels were Coomassie stained with SimplyBlue SafeStain (Invitrogen). Gels were scanned on a Gel Doc EZ imager (Biorad). Graphical images of THS were produced with the UCSF Chimera package[329] from the Resource for Biocomputing, Visualization and Informatics at the University of California, San Francisco.

### A.4.3 Preparation of THS-$L_x$Cu

0.2 mg of THS (0.2 nmol, 1 equiv.) was diluted in 200 µl modification buffer (100 mM $NaH_2PO_4$, 150 mM NaCl, pH 6.5). 1.5 µl of a 41.5 mM 3-N-maleimido-6-hydraziniumpyridine hydrochloride (MHPH) solution (14.9 µg, 60.0 nmol, 270 equiv.) in dimethyl sulfoxide (DMSO) and 2 µl of a 100 mM phenylmethylsulfonylfluorid (PMSF) aqueous solution were added. The reaction mixture was incubated under shaking at 37°C for 2 h. Excess of reagents were removed and the buffer of the sample was changed using 100k MWCO diafiltration devices at 13600 rpm. The sample was first concentrated to 25 µl and the supernatant was then diluted three times with 0.5 ml conjugation buffer (100 mM sodium phosphate, 150 mM NaCl, pH 6.0) and reconcentrated. 50 µl of the resulting THS-MHPH solution (0.18 mg, 0.18 nmol, 1 equiv.) was diluted in 350 µl conjugation buffer and 0.8 µl of a 21.5 mM solution of compound 1 (synthesis see A.1.3) in DMSO (6.5 µg, 14 nmol, 80 equiv.). 4 µl of the PMSF solution was added. The reaction mixture was shaken overnight at RT and concentrated with a 100k MWCO diafiltration device to 25 µl at 13600 rpm. Excess of reagents was removed and the buffer was exchanged to complexation buffer (100 mM sodium acetate, pH 5.2) with three spun cycles. To nine parts of THS-$L_x$ solution (0.15 mg, 0.16 nmol) one part of a 50 mM $CuBr_2$ solution in complexation buffer was added. To remove non-complexed copper, the solution was concentrated to 25 µl with a 100k MWCO diafiltration device at 13600 rpm, three times diluted and reconcentrated with 0.5 ml reaction buffer (100 mM sodium acetate, 150 mM NaCl, 80 mM $MgCl_2$, pH 5.2) or dd$H_2O$. Finally, the THS-$L_x$Cu solution was diluted with the corresponding solvent to a volume of 2.0 ml, yielding 0.1 mg (0.1 nmol) protein. The number of bis-aryl hydrazone linker groups that had formed was determined from the absorbance at 354 nm using an extinction coefficient of ($\varepsilon(\text{hydrazone})_{354\ nm}$ = 29000 $M^{-1}$ $cm^{-1}$).[330] UV/Vis

[328] K. Hirayama, S. Akashi, M. Furuya, K. Fukuhara, *Biochem. Biophys. Res. Commun.* **1990**, *173*, 639–646.
[329] E. F. Pettersen, T. D. Goddard, C. C. Huang, G. S. Couch, D. M. Greenblatt, E. C. Meng, T. E. Ferrin, *J. Comput. Chem.* **2004**, *25*, 1605–1612.
[330] SoluLink Company, *Catalog and Reference Manual* **2008**.

data revealed that 3.9 ± 0.1 of the available 8 cysteins per THS carry a ligand. The $Cu^{II}$ content of the THS-$L_x$Cu sample was estimated from the complexation efficiency of the ligand in BSA-$L_x$Cu (see A.1.5). If 3.9 ± 0.1 cysteins carry a ligand and 50% of the ligands in THS-$L_x$Cu complex $Cu^{II}$, a copper concentration of 135 ng per mg THS would be achieved.

### A.4.4 Preparation of BSA-4FB

15 mg of BSA (220 nmol, 1 equiv.) was weighted into a falcon tube and dissolved in 15 ml modification buffer. 163 µl of a 41.5 mM MHPH solution (1.6 mg, 6.6 µmol, 30.0 equiv.) in DMSO was added and the reaction mixture was incubated at 37°C while shaking for 2 h. The sample was concentrated to 250 µl using 30k MWCO diafiltration devices at 4700 rpm. The supernatant was then diluted three times with 15 ml conjugation buffer and reconcentrated. 250 µl of the resulting BSA-MHPH solution (11.5 mg, 168.7 nmol, 1.0 equiv.) was diluted with 12 ml conjugation buffer. 90.0 µl of a 21.5 mM methyl 4-formylbenzoate (4FB) solution in DMSO (0.82 mg, 1.73 µmol, 10.00 equiv.) was added. The reaction mixture was shaken overnight at RT and concentrated with a 30k MWCO diafiltration device to 250 µl at 4700 rpm. Buffer was exchanged to compexation buffer with three spun cycles. To nine parts of BSA-4FB solution (9.1 mg, 133.5 nmol) one part of a 50 mM $CuBr_2$ solution in complexation buffer was added. To remove non-complexed copper, the solution was concentrated with a 30k MWCO diafiltration device to 250 µl at 4700 rpm, three times diluted and reconcentrated with 15 ml reaction buffer. Finally, the solution was diluted to a volume of 2.0 ml, yielding 5.8 mg (85.1 nmol) BSA-4FB

### A.4.5 MHPH Molar Substitution Ratio

The 6-hydraziniumpyridine molar substitution ratio (MSR) for THS was determined by adding a 20 µl aliquot of a THS-MHPH or BSA-MHPH sample in conjugation buffer to 480 µl of a 0.5 mM 4-nitrobenzaldehyde solution in 100 mM sodium acetate buffer (pH 5.2). The solution was incubating at 37°C for 1 h and the absorbance at 390 nm ($\varepsilon(\text{hydrazone})_{390\ nm}$ = 24000 $M^{-1}$ $cm^{-1}$) was determined.[331] A blank value determined with 20 µl conjugation buffer was subtracted. The determination of MSR was carried out in triplicates and the mean values and standard deviations are reported. The MSR for THS resulted in 7.7 ± 0.4 modified cysteins per THS, i.e. all eight thiol groups present in the THS could be modified.

### A.4.6 ARGET ATRP of NiPAAm

25.0 mg NiPAAm (220 µmol, 66.7 equiv.) and 0.7 mg 2-hydroxyethyl-2-bromoisobutyrate (HEBIB; 3.3 µmol, 1.0 equiv.) were dissolved in 375 µl reaction buffer (100 mM sodium acetate, 150 mM NaCl, 80 mM $MgCl_2$, pH 5.2). 30.0 µl of THS-$L_x$Cu in reaction buffer (50.0 µg, 0.05 nmol, 1.5 $10^{-5}$ equiv.) containing approx. 7 ng copper (0.1 nmol, 3 $10^{-5}$ equiv.) was added and the solution was deoxygenated by

[331] SoluLink Company, *Catalog and Reference Manual* **2008**.

bubbling with argon for 20 min. The polymerizations were started by adding 200 µl of deoxygenized 4.25 mM L-ascorbic acid solution (0.15 mg, 0.85 µmol, 0.25 equiv.) in reaction buffer. The reactions were stirred for 20 h at room temperature and stopped by adding 605 µl non-deoxygenated reaction buffer and exposure to aµbient air. The control reactions were performed accordingly but with 30.0 µl of native THS in reaction buffer (incubated with $CuBr_2$ solution. Size exclusion spin centrifugation was used to remove the unbound copper; 50.0 µg, 0.05 nmol, 1.5 $10^{-5}$ equiv.) or with 30.0 µl of BSA-4FB in reaction buffer (50.0 µg, 0.8 nmol, 2.2 $10^{-4}$ equiv.).

### A.4.7 ARGET ATRP of PEGA in Aqueous Solution

0.1 ml PEGA (220.0 µmol, 66.7 equiv.) and HEBIB (0.7 mg, 3.3 µmol, 1.0 equiv.) were dissolved in 375 µl reaction buffer. 30 µl of THS-$L_x$Cu in reaction buffer (50 µg, 0.05 nmol, 1.5 $10^{-5}$ equiv.) containing approx. 7 ng copper (0.1 nmol, 3 $10^{-5}$ equiv.) was added. Argon was bubbled trough the solution for 20 min. The polymerizations were started by adding 200 µl of deoxygenized 4.25 mM L-ascorbic acid solution (0.15 mg, 0.85 µmol, 0.25 equiv.) in reaction buffer. The reactions were stirred for 20 h at room temperature and stopped by adding 605 µl non-deoxygenated reaction buffer and exposure to ambient air. The control reactions were performed accordingly but with 30.0 µl of native THS in reaction buffer (incubated with $CuBr_2$ solution. Size exclusion spin centrifugation was used to remove the unbound copper; 50.0 µg, 0.05 nmol, 1.5 $10^{-5}$ equiv.).

### A.4.8 ARGET ATRP of PEGA in the Presence of ATP

0.1 ml PEGA (220 µmol, 66.7 equiv.), HEBIB (0.7 mg, 3.3 µmol, 1.0 equiv.) and 170 µg adenosine 5'-diphosphate sodium salt (ATP; 395 nmol, 0.1 equiv.) were dissolved in 375 µl reaction buffer. 30 µl of THS-$L_x$Cu in reaction buffer (50 µg, 0.05 nmol, 1.5 $10^{-5}$ equiv.) containing approx. 7 ng copper (0.1 nmol, 3 $10^{-5}$ equiv.) was added. Argon was bubbled trough the solution for 20 min. The polymerizations were started by adding 200 µl of deoxygenized 4.25 mM L-ascorbic acid solution (0.15 mg, 0.85 µmol, 0.25 equiv.) in reaction buffer. The reactions were stirred for 20 h at room temperature and stopped by adding 605 µl non-deoxygenated reaction buffer and exposure to ambient air.

### A.4.9 ARGET ATRP of PEGA in a $ddH_2O$/THF Mixture

0.1 ml PEGA (220 µmol, 66.7 equiv.) and 0.7 mg HEBIB (3.3 µmol, 1.0 equiv.) were dissolved in 300 µl of a $ddH_2O$/THF (7:3 *v*/*v*) mixture. 1500 µl of THS-$L_x$Cu in $ddH_2O$ (50 µg, 0.05 nmol, 1.5 $10^{-5}$ equiv.) containing approx. 7 ng copper (0.1 nmol, 3 $10^{-5}$ equiv.) was added. Argon was bubbled through the solution for 20 min. For the reactions with BSA 150 µl of BSA-$L_x$Cu in $ddH_2O$ (50 µg, 0.8 nmol, 2.2 $10^{-4}$ equiv.) containing approx. 5 ng copper (0.08 nmol, 2.4 $10^{-5}$ equiv.) was added. The polymerizations were started by adding 100 µl of 3.15 mM sodium ascorbate solution

(0.75 mg, 3.75 μmol, 0.12 equiv.) in a $ddH_2O$/THF (7:3 *v*/*v*) mixture. The reactions were stirred for 20 h and stopped by adding 550 μl non-deoxygenated $ddH_2O$ and exposure to ambient air. The control reactions were performed accordingly but with 30 μl of native THS (incubated with $CuBr_2$ solution. Size exclusion spin centrifugation was used to remove the unbound copper in $ddH_2O$; 50.0 μg, 0.05 nmol, 1.5 $10^{-5}$ equiv.)

## A.5 Incorporation of ATRPases into Protein Nanoreactors

### A.5.1 Materials

Commercially available chemicals were purchased from Sigma-Aldrich and used without further purification unless otherwise noted. The linkers maleimido trioxa-6-formyl benzamide (MTFB) and succinimidyl 6-hydrazinonicotinate acetone hydrazine (HyNic) were obtained from SoluLink (San Diego, USA). Buffers were produced using double-distilled water. Poly(ethylene glycol) methylether acrylate (PEGA) with a number average molecular weight of 480 g $mol^{-1}$ was filtered over a neutral aluminium oxide column. THS was expressed in *E. coli* as described above.

### A.5.2 Methods

The $M_n$ and the PDI of the polymers were determined by gel permeation chromatography (GPC) unless otherwise noted. Samples for GPC (0.1 ml) were removed from the reaction mixture without separation of the protein and filtered over a small plug of basic aluminium oxide in order to remove salts and protein. The plug was washed with additional 0.2 ml of water and the filtrates were combined. Then the sample was lyophilized and redissolved in the GPC eluent to concentrations of 1 mg $ml^{-1}$. Measurements of pPEGA were performed on a Viscotek GPCmax system using a refractive index detector, with Agilent PLgel columns (10 µm guard + 2 x 5 µm mixed C, or 10 µm guard + mixed C + 10 µm 100 Å + 5 µm $10^3$ Å) thermostatted to 30°C and THF as mobile phase at a flow rate of 1 ml $min^{-1}$. Calibration was carried out with PS standards. Small angle X-ray scattering (SAXS) experiments were performed with a Bruker AXS Metaljet Nanostar. The X-ray are generated by focusing electrons onto a micro-size liquid metal jet of an allow consisting of 95% Ga and 5% In. This setup allows for a power load of > 100 kW $mm^2$. The scattering patterns are detected by a Vantec 2000 2D detector. Exposure time were 3600 s. About 20 µl of sample with the concentration of 1.5 mg $ml^{-1}$ was loaded into a glass capillary (d = 1 mm, thickness of the wall = 0.01 mm), the capillary was closed by melting the top of the capillary, the closed capillary was put into the Nanostar, vacuum was applied and the measurement was started. The data were azimuthally averaged with SAXS v.4.1.36 Bruker software and fitted with BrukerAXS Nanofit software (version 1.2.1.1). UV/Vis analyses were performed on a NanoDrop (Thermo Scientific). Protein concentrations were determined from the absorption at 280 nm, using an extinction coefficient of 210880 $M^{-1}$ $cm^{-1}$ for the hexadecameric THS complex[332] and of 102 000 $M^{-1}$ $cm^{-1}$ at 403 nm for HRP. Sodium dodecyl sulfate polyacrylamide gel electrophoresis (SDS-PAGE) was performed with self-casted 12% polyacrylamide gels and tris-HCl as running buffer in a Biorad Miniprotean 3 cell setup at 200 V for 70 min. Novex BenchMark Protein Ladder (Invitrogen) was used as molecular weight marker. All gels were Coomassie stained with SimplyBlue SafeStain (Invitrogen). Gels were scanned on a Gel Doc EZ imager (Biorad). Graphical images of THS were produced with the UCSF Chimera

[332] N. Bruns, K. Pustelny, L. M. Bergeron, T. A. Whitehead, D. S. Clark, *Angew. Chem. Int. Ed.* **2009**, *48*, 5666–5669.

package[333] from the Resource for Biocomputing, Visualization and Informatics at the University of California, San Francisco.

### A.5.3 THS-MTFB Modification

8.1 µl of 35.7 mM MTFB in DMSO was diluted in 41.9 µl modification buffer, which lead to 50 µl 5.78 mM MTFB. 100 µl of 10 µM THS was added to the 50 µl 5.78 µM MTFB (150 µl 6.4 µM THS, 1.93 mM MTFB, > 25 fold excess of MTFB to cysteins in THS) and incubated under gentle shaking at 37°C for 2.5 h. The sample was centrifuged 4 times for 5 min at 13000 rpm and refilled every time with conjugation buffer at pH 6.0. The final sample was filled up to 200 µl with conjugation buffer and reversely centrifuged for 3 min at 3800 rpm to retrieve the sample.

### A.5.4 HRP-HyNic Modification

HyNic stock solution: 20 µl 100 mM HyNic + 80 µl modification buffer = 100 µl 20 mM HyNic. HRP stock solution: 1.76 mg HRP + 100 µl modification buffer = 100 µl 400 µM HRP. 100 µl 400 µM HRP + 30 µl modification buffer + 20 µl 20 mM HyNic (150 µl 266.67 µM HRP, 2.67 mM HyNic, 10 fold excess of HyNic) were incubated for 1.5 h at room temperature and shaked. The sample was centrifuged 4 times for 5 min at 13400 rpm and refilled every time with conjugation buffer at pH 6.0. The final sample was filled up to 200 µl with conjugation buffer and reversely centrifuged for 3 min at 3800 rpm to retrieve the sample.

### A.5.5 THS-HRP Conjugation

200 µl THS-MTFB + 200 µl HRP-HyNic were incubated at room temperature under shaking for 14 h. The sample was then purified with HiPrep 16/60 Sephacryl S-200 column in modification buffer. The method used was MN HiPrep Sephacryl S200 THSHRP. A SDS-gel electrophoresis was performed and tubes were filtered with 0.22 µm filters and centrifuged (Amicon 5 ml 100 kDa, 5000 g, 3 min) to a final volume of 200 µl and an approx. amount of 1 mg THS-HRP. The successful conjugation was confirmed by SDS PAGE. The molecular substitution ratio (MSR) was calculated by determining the number of HRP molecules using the absorption at 403 nm. This value was deducted from the 280 nm signal, which is an overlay signal of THS and HRP.

[333] E. F. Pettersen, T. D. Goddard, C. C. Huang, G. S. Couch, D. M. Greenblatt, E. C. Meng, T. E. Ferrin, *J. Comput. Chem.* **2004**, *25*, 1605–1612.

### A.5.6 ARGET ATRP of PEGA in a ddH2O/THF Mixture

0.1 ml PEGA (220 μmol, 66.7 equiv.) and 0.7 mg HEBIB (3.3 μmol, 1.0 equiv.) were dissolved in 300 μl of a $ddH_2O$/THF (7:3 *v*/*v*) mixture. 1500 μl of THS-HRP in $ddH_2O$ (50 μg, 0.05 nmol, 1.5 $10^{-5}$ equiv.) was added. Argon was bubbled through the solution for 20 min. The polymerizations were started by adding 100 μl of 3.15 mM sodium ascorbate solution (0.75 mg, 3.75 μmol, 0.12 equiv.) in a $ddH_2O$/THF (7:3 *v*/*v*) mixture. The reactions were stirred for 20 h and stopped by adding 550 μl non-deoxygenated $ddH_2O$ and exposure to ambient air.

## A.6 The Archaeal Chaperonin Thermosome as ATP Triggerable Protein Nanoreactor

### A.6.1 Materials

Commercially available chemicals were purchased from Sigma-Aldrich and used without further purification unless otherwise noted. Dithio-bis-(succinimidyl undecanoate) (DSU) was produced according to protocol.[334] Expression of Thermosome in *E. coli* is described above. The conjugation of THS-HRP is reported in sections A.5.3 to A.5.5.

### A.6.2 Methods

Kinetic experiments were performed on a SpectraMax M5$^e$ machine with following method: FL-Kinetic, excitation = 505 nm, emission = 535 nm, autocutoff. The measurement was done for 30 min with an intervall of 10 seconds and 6 readings. PMT was medium.

### A.6.3 Kinetic Experiments

0.5 µl (2.25 mM) of dihydro Rhodamine 6G (dhRh6G) were added to 400 µl MES buffer (100 mM MES, 150 mM NaCl, 20 mM $MgCl_2$). 200 µl of this solution was transferred into a FCS cuvette and 1 µl of the incubated (30 min, 37°C) ATP solutions listed in Table A.6.1 was added (3.5 µl for the ATP-AlFx solution). First, the cuvette was blanked, then 10 µl freshly prepared $H_2O_2$ (0.6%) was added and the FCS measurement was started. In order to assess how much $H_2O_2$ can also degrade dhRh6G in the absence of HRP, a no-HRP control was performed. The following SpectraMax method was used for all experiments: FL-Kinetic, excitation = 505 nm, emission = 535 nm, autocutoff. The measurement was done for 30 min with an intervall of 10 seconds and 6 readings. PMT was medium.

| ATPs | THS-HRP | HRP |
|---|---|---|
| Without additive | 5 $\mu$l THS-HRP + 10 $\mu$l MES | 5 $\mu$l HRP + 10 $\mu$l MES |
| ATP | 2 $\mu$l THS-HRP + 4 $\mu$l ATP | 2 $\mu$l HRP + 4 $\mu$l ATP |
| ATP-$\gamma$S | 2 $\mu$l THS-HRP + 4 $\mu$l ATP-$\gamma$S | 2 $\mu$l HRP + 4 $\mu$l ATP-$\gamma$S |
| ATP-$AlF_x$ | 2 $\mu$l ATP + 6 $\mu$l 10 mM $Al(NO_3)_3$ + 1$\mu$l THS-HRP + 6 $\mu$l 60 mM NaF | 2 $\mu$l ATP + 6 $\mu$l 10 mM $Al(NO_3)_3$ + 1$\mu$l HRP + 6 $\mu$l 60 mM NaF |

**Table A.6.1** ATP solutions for kinetic experiments.

### A.6.4 Cantilever Array Coating

Gold coated cantilevers (2 nm Ti and 20 nm Au, IBM Rüschlikon) were rinsed in EtOH, 5 min UV cleaning and again rinsed in EtOH. In a next step, reference

[334] P. Wagner, P. Kernen, M. Hegner, E. Ungewickell, G. Semenza, *FEBS Lett.* **1994**, *356*, 267–271.

cantilevers 1,3,5,7 with 11-mercapto-1-unedecanol and sample cantilevers 2,4,6,8 were functionalized with DSU. The functionalization was performed with a self-build apparatus for 45min at RT. Subsequently, the cantilevers were rinse 3x in EtOH and 6x in MES buffer (100 mM MES, 150 mM NaCl, 20 mM $MgCl_2$). Finally, 25 µl THS in 20 mM phosphate at pH 7.4 (520 nM) was added on the cantilevers and incubation for 30 min. The functionalized cantilever array was then rinsed in MES buffer twice and assembled into the measuring chamber.

### A.6.5 Nanomechanical Sensing of Conformation Changes in THS

Measurements were performed in static mode at 31°C with a constant flow of 1 µl $min^{-1}$. After equilibration of the system with MES buffer the different ATP solutions according to Table A.6.1 were injected onto the cantilever array. The experiments were monitored with the NOSEtool software. The individual deflection curves of the sample and reference cantilevers were averaged and the difference is plotted.

# B List of Publication and Impact of the Work

## B.1 Publications

**Renggli, K.**; Nussbaumer, M. G.; Urbani, R.; Pfohl, T.; Bruns, N.: A Chaperonin as Protein Nanoreactor for Atom Transfer Radical Polymerization. *Angew. Chem. Int. Ed.* **2014***, 53*, 1443–1447, DOI: 10.1002/anie.201306798.

**Renggli, K.**; Nussbaumer, M. G.; Urbani, R.; Pfohl, T.; Bruns, N.: Ein Chaperonin als Protein-Nanoreaktor für die radikalische Atomtransferpolymerisation. *Angew. Chem.* **2014***, 126*, 1467–1472, DOI: 10.1002/ange.201306798.

Bruns, N.; **Renggli, K.**; Lörcher, S.; Pollard, J.; Spulber, M.: Combining Polymers with the Functionality of Proteins. ATRPases, Nanoreactors and Damage Self-Reporting Materials. *Chimia* **2013**, *67*, 777–781, DOI: 10.2533/chimia.2013.777.

**Renggli, K.**; Spulber, M.; Pollard, J.; Rother, M.; Bruns, N.: Biocatalytic ATRP: Controlled Radical Polymerizations Mediated by Enzymes. *ACS Symp. Ser.* **2013**, *1144*, 163–171, DOI: 10.1021/bk-2013-1144.ch012.

Bircher, B. A.; Duempelmann, L.; **Renggli, K.**; Lang, H. P.; Gerber, C.; Bruns, N.; Braun, T.: Real-Time Viscosity and Mass Density Sensors Requiring Microliter Sample Volume Based on Nanomechanical Resonators. *Anal. Chem.* **2013**, *85*, 8676–8683, DOI: 10.1021/ac4014918.

Silva T. B.; Spulber, M.; Kocik, M. K.; Seidi, F.; Charan, H.; Rother, M.; Sigg, S.; **Renggli, K.**; Kali, G.; Bruns, N.: Hemoglobin and Red Blood Cells Catalyze Atom Transfer Radical Polymerization. *Biomacromolecules* **2013**, *14*, 2703–2712, DOI: 10.1021/bm400556x.

**Renggli, K.**; Walther, M.; Nussbaumer, M.; Hegner, M. U.; Bruns, N.: Nanomechanical Sensing of Conformation Changes in the Group II Chaperonin Thermosome from the Archaea Thermoplasma Acidophilum. *Proceedings of the 10$^{th}$ International Nanomechanical Sensing Workshop*. **2013**.

**Renggli, K.**; Nussbaumer, M.; Bruns, N.: Controlled Radical Polymerization in Protein Nanoreactors: Protein-Conjugates as Green Alternatives to Conventional Catalysts. *Polym. Prepr. (Am. Chem. Soc., Div. Polym. Chem.)* **2012**, *53*, 294–295.

Bruns, N.; Silva, T. B.; Kocik, M. K.; Sigg, S. J.; Seidi, F.; **Renggli, K.**; Charan, H.; Kali, G.: ATRPases: Enzymes as Catalysts for Atom Transfer Radical Polymerization. *Polym. Prepr. (Am. Chem. Soc., Div. Polym. Chem.)* **2012**, *53*, 292–293.

Kali, G.; Silva, T. B.; Sigg, S. J.; Seidi, F.; **Renggli, K.**; Bruns, N.: ATRPases: Using Nature's Catalysts in Atom Transfer Radical Polymerizations. *ACS Symp. Ser.* **2012**, *1100*, 171–181, DOI: 10.1021/bk-2012-1100.ch011.

Sigg, S. J.; Seidi, F.; **Renggli, K.**; Silva, T. B.; Kali, G.; Bruns, N.: ATRPases: Enzymes as Catalysts for Atom Transfer Radical Polymerization *Chimia* **2012**, *66 (1–2)*, 66, DOI: 10.2533/chimia.2012.66.

Braun, J.; **Renggli, K.**; Razumovitch, J.; Vebert, C.: Dynamic Light Scattering in Supramolecular Materials Chemistry. In Steed, J. W.; Gale, P. A.: *Supramolecular Chemistry: From Molecules to Nanomaterials* **2012**, *2*, 411–424. John Wiley & Sons, Ltd. ISBN: 978-0-470-74640-0, DOI: 10.1002/ 9780470661345.smc039.

Bruns, N.; **Renggli, K.**; Seidi, F.; Kali, G.: Atom Transfer Radical Polymerization with Protein-Conjugated Catalysts: Easy Removal of Copper Traces and Controlled Radical Polymerizations in Protein Nanoreactors. *Polym. Prepr. (Am. Chem. Soc., Div. Polym. Chem.)* **2011**, *52*, 521–522.

Sigg, S. J.; Seidi, F.; **Renggli, K.**; Silva, T. B.; Kali, G.; Bruns, N.: Horseradish Peroxidase as a Catalyst for Atom Transfer Radical Polymerization. *Macromol. Rapid Commun.* **2011**, *32*, 1710–1715, DOI: 10.1002/marc.201100349.

**Renggli, K.**; Baumann, P.; Langowska, K.; Onaca, O.; Bruns, N.; Meier, W.: Selective and Responsive Nanoreactors. *Adv. Funct. Mater.* **2011**, *21*, 1241–1259, DOI: 10.1002/adfm.201001563.

**Renggli, K.**; Bruns, N.: Solid or Swollen Polymer-Protein Hybrid Materials. *ACS Symp. Ser.* **2010**, *1043*, 17–34, DOI: 10.1021/bk-2010-1043.ch002.

## B.2 Oral Presentations

INAScon 2013 - 7$^{th}$ International Nanoscience Student Conference, University College London and Imperial College London, 19.08.2013–22.08.2013, Title: A Chaperonin as Protein Nanoreactor for Atom Transfer Radical Polymerization, **K. Renggli**, M. Nussbaumer, R. Urabni, T. Pfohl, N. Bruns.

NMC 2013 - 10$^{th}$ International Workshop on Nanomechanical Sensing, Stanford University, CA, USA, 01.05.2013–03.05.2013, Title: Nanomechanical Sensing of Conformation Changes in the Group II Chaperonin Thermosome from the Archaea Thermoplasma Acidophilum, **K. Renggli**, M. Walther, M. Nussbaumer, M. Hegner, N. Bruns.

11th Greta Pifat Mrzljak International School of Biophysics 2012, Primošten, Croatia, 29.09.2012–09.10.2012, Title: Controlled Radical Polymerization in Protein Nanoreactors and with Native Enzymes, **K. Renggli**, T.B. Silva, M. Kocik, M. Spulber, M. Nussbaumer, N. Bruns.

244th ACS National Meeting, Philadelphia, PA, USA, 19.08.2012–23.08.2012, Title: Controlled Radical Polymerization in Protein Nanoreactors: Protein-Conjugates as Green Alternatives to Conventional Catalysts, **K. Renggli**, M. Nussbaumer, N. Bruns.

8th Swiss Soft Days, University of Geneva, Geneva, Switzerland, 01.06.2012, Title: Controlled Polymerization in Protein Nanoreactors and with Native Enzymes, **K. Renggli**, N. Bruns.

## B.3 Poster Presentations

Fall Meeting of the Swiss Chemical Society 2013, EPFL, Lausanne, Switzerland, 06.09.2013, Title: Protein Nanoreactors and Native Enzymes for Controlled Radical Polymerization in Aqueous Solution, **K. Renggli**, M. Spulber, M. Nussbaumer, N. Bruns.

PolyColl 2013 – Annual Meeting of the Division of Polymer, Colloids and Interfaces, Universität Basel, Basel, Switzerland, 07.06.2013, Title: Protein Nanoreactors and Native Enzymes for Controlled Radical Polymerization in Aqueous Solution, **K. Renggli**, M. Spulber, R. Urbani, M. Nussbaumer, T. Pfohl, N. Bruns.

Swiss NanoConvention, Basel, Switzerland, 23.05.2013–24.05.2013, Title: Controlled Radical Polymerization in Protein Nanoreactors and with Native Enzymes, **K. Renggli**, M. Spulber, M. Nussbaumer, N. Bruns.

11th Greta Pifat Mrzljak International School of Biophysics 2012, Primošten, Croatia, 29.09.2012–09.10.2012, Title: Controlled Radical Polymerization in Protein Nanoreactors and with Native Enzymes, **K. Renggli**, T.B. Silva, M. Kocik, M. Spulber, M. Nussbaumer, N. Bruns.

Fall Meeting of the Swiss Chemical Society 2012, ETH Zürich, Zürich, Switzerland, 13.09.2012, Title: Controlled Radical Polymerization in Protein Nanoreactors, **K. Renggli**, M. Nussbaumer, N. Bruns.

EPF 2011 – European Polymer Congress, Granada, Spain, 26.06.2011–01.07.2011, Title: Protein Nanoreactors for Atom Transfer Radical Polymerization, **K. Renggli**, G. Kali, N. Bruns.

Fall Meeting of the Swiss Chemical Society 2010, ETH Zürich, Zürich, Switzerland, 16.09.2010, Title: Protein Coupled Copper-Catalysts for Atom Transfer Radical Polymerization, **K. Renggli**, F. Seidi, N. Bruns.

SPS Annual Meeting and Polycoll 2010, University of Basel, Switzerland, 21.06.2010–22.06.2010, Title: Protein Coupled Copper-Catalysts for Atom Transfer Radical Polymerization in Pure Water, **K. Renggli**, F. Seidi, N. Bruns.

Swiss Snow Symposium 2010, Parpan GR, Switzerland, 19.02.2010–21.02.2010, Title: Protein Coupled Copper-Catalysts for Atom Transfer Radical Polymerization, **K. Renggli**, N. Bruns.

## B.4 Summer Schools and Workshops

INAScon 2013, London, England, 19.08.2013–22.08.2013 7$^{th}$ International Nanoscience Student Workshop.

NMC 2013 Stanford University, CA, USA, 01.05.2013–03.05.2013, 10$^{th}$ International Workshop on Nanomechanical Sensing.

11$^{th}$ Greta Pifat Mrzljak International School of Biophysics 2012, Primošten, Croatia, 29.09.2012–09.10.2012, Biomolecular Complexes and Assemblies.

SNI Doctorate School 2012, Bad Ramsach, Switzerland, 11.09.2012–12.09.2012, PhD Workshop: A Career in Industry.

7$^{th}$ Nanoscience in the Snow 2012, Riederalp, Switzerland, 25.01.2012-27.01.2012, Workshop in the Framework of the Swiss NCCR Nanoscale Science.

NMC 2011 Dublin, Ireland, 11.05.2011–13.05.2011, 8$^{th}$ International Workshop on Nanomechanical Sensing.

INAScon 2007, Silkeborg, Denmark, 07.07.2007–10.07.2007, 1$^{st}$ International Nanoscience Student Workshop.